University of Alberta

# Feasibility of Cone Penetration Test Applied to Horizontal Directional Drilling in Continuous Boreholes

by

©

**Renato Viana Clementino**

A thesis submitted to the Faculty of Graduate Studies and Research in
partial fulfillment of requirements for the degree of Doctor of Philosophy

in

Geoenvironmental Engineering

Department of Civil and Environmental Engineering

Edmonton, Alberta

Spring 2002

National Library
of Canada

Acquisitions and
Bibliographic Services

395 Wellington Street
Ottawa ON K1A 0N4
Canada

Bibliothèque nationale
du Canada

Acquisitions et
services bibliographiques

395, rue Wellington
Ottawa ON K1A 0N4
Canada

Your file Votre référence

Our file Notre référence

The author has granted a non-exclusive licence allowing the National Library of Canada to reproduce, loan, distribute or sell copies of this thesis in microform, paper or electronic formats.

L'auteur a accordé une licence non exclusive permettant à la Bibliothèque nationale du Canada de reproduire, prêter, distribuer ou vendre des copies de cette thèse sous la forme de microfiche/film, de reproduction sur papier ou sur format électronique.

The author retains ownership of the copyright in this thesis. Neither the thesis nor substantial extracts from it may be printed or otherwise reproduced without the author's permission.

L'auteur conserve la propriété du droit d'auteur qui protège cette thèse. Ni la thèse ni des extraits substantiels de celle-ci ne doivent être imprimés ou autrement reproduits sans son autorisation.

0-612-68555-1

Canada

**University of Alberta**

**Library Release Form**

**Name of Author:** Renato Viana Clementino

**Title of Thesis:** Feasibility of Cone Penetration Test Applied to Horizontal Directional Drilling in Continuous Boreholes

**Degree:** Doctor of Philosophy

**Year this Degree Granted:** 2002

Permission is hereby granted to the University of Alberta Library to reproduce single copies of this thesis and to lend or sell such copies for private, scholarly or scientific research purposes only.

The author reserves all publication and other rights in association with the copyright in the thesis, and except as herein before provided, neither the thesis nor any substantial portion thereof may be printed or otherwise reproduced in any material form whatever without the author's prior written permission.

2012-108B Street
Edmonton, Alberta
Canada – T6J 5T8

January 29, 2002

Date submitted to the Faculty of Graduate Studies and Research

**University of Alberta**

**Faculty of Graduate Studies and Research**

The undersigned certify that they have read, and recommend to the Faculty of Graduate Studies and Research for acceptance, a thesis entitled **Feasibility of Cone Penetration Test Applied to Horizontal Directional Drilling in Continuous Borehole** submitted by **Renato Viana Clementino** in partial fulfillment of the requirements for the degree of **Doctor of Philosophy in Geoenvironmental Engineering**.

Dr. Peter K. Robertson

Dr. Kevin W. Biggar

Dr. Richard Chalaturnyk

Dr. D. Rogowsky

Dr. D. Schmitt

Dr. John A. Howie

Dec. 17, 2001

Date approved

**To Vania , Anna Cláudia and Fernanda**

# Abstract

Sand pockets or lenses are a great concern for tunnel construction. The increasing use of mechanized tunnel boring has made it even more important for the designer to know in advance the location and characteristics of sand pockets along the tunnel alignment. Geoenvironmental site assessments are normally conducted by using vertical boreholes; however, groundwater contamination plumes and pools are usually much longer and wider than they are thick. Therefore, assessing the extent of contamination plumes and pools may be accomplished more efficiently by following a horizontal rather than a vertical testing path. Furthermore, assessing soil contamination beneath existing surface or subsurface obstructions such as storage tanks and buildings can be very difficult, if not impossible, to perform by means of vertical boreholes. In these contexts, horizontal site characterization is extremely desirable. A probe with the ability to obtain soil lithology and parameters in a horizontal path and at the same time delineate the lateral extent of contamination, in a cost-effective way, may be a great aid to tunneling and remediation designs.

Horizontal Directional Drilling (HDD) Technique has a unique characteristic of providing a horizontal borehole with an entry and an exit point. This feature, brought about the idea of developing a logging device based on Cone Penetration Testing (CPT) technology where the penetrometer is pulled back through the borehole rather than pushed ahead of the drill stem. The main objective of this research was to study the feasibility of developing such a logging device and to design, build and field test this novel probe, called the Horizontal Directional Pre-Bored Cone Penetration Test (HD-PB-CPT).

Because of the boundary conditions of the problem, the principal of cavity expansion theory was used to provide a first concept of the ideal probe dimensions. A pilot test with similar boundary condition of the study problem was conducted to validate the theoretical assumptions made. Prototype 1 was then design, constructed and field tested at the University of Alberta field experimental site. To better understand the soil deformation pattern and to eliminate some design problems identified during Prototype1 field tests, small scale laboratory physical modeling tests were performed. Prototype 2 was then constructed and an electrical resistivity module was also added to the probe to improve identification of soil lithology change and to allow the probe to screen for soil contamination. The field tests of these two prototypes have shown that this new tool has good potential application in geotechnical and geoenvironmental site assessment where conventional vertical logging is not suitable. However, tip and sleeve friction resistance values were lower than those obtained from standard vertical CPT's performed in the same soil. Either further probe modification will be necessary to obtain a closer data match with the standard vertical CPT, or when more HD-PB-CPT data are available changes in existing vertical CPT classification charts can be proposed to better suit the HD-PB-CPT test results.

# Acknowledgements

I would like to express my gratitude to the enthusiastic interest, guidance, friendship, and valuable ideas provided by my supervisors, Dr. Peter K. Robertson and Dr. Kevin W. Biggar throughout this research.

I am gratefully thanked to ConeTec Investigation Ltd, SubTerra Corporation and Commercial Trenching Ltd. for their cooperation during this research.

I would like to acknowledge the financial support from CAPES – Brazilian Government Agency, UERJ – Rio de Janeiro State University (Brazil) and NSERC - Natural Sciences and Engineering Research Council (Canada).

Special thanks to Gerry Cyre for his excellent ideas, and effort helping in the development and construction the HD-PB-CPT. I also wish to thank him for the help and companionship during the field testing. He was always there for me even during the weekends. Special thanks also, to Steve Gamble for the friendship and help with laboratory testing and fieldwork. Without the help of these two skillful geotechnical technologists this research would never have been accomplished.

I wish to express my gratitude to Dr. Marcus P. Pacheco, for his encouragement and making up my mind to take this challenge of doing my doctoral program in a foreign country, something I was not very keen to do, but I really don't regret it now. If I had stayed in Brazil life may have been easier, but I would not have learned as much, both, technically and in life experience.

I would like to thank this friendly country, specially the nice and friendly people of Edmonton who know how to welcome a foreigner and make adaptation problems much easier to handle.

My friend Dr. Marvin Silva, many thanks for his friendship and helping me to decode Dr. Morgenstern blackboard hand writing during his lectures.

Dimitri Papanicolas, for his insistence in having me finished my thesis. Without having him stressing me out all the time the completion of this work would have taken longer.

I would also like to thank Prof. Eduardo B. Cordeiro for all his advice during my professional life and for making me interested in the geotechnical and geoenvironmental field of engineering.

My thanks to my dad Marcelo for his support and handling all my business in Brazil. My deepest gratitude to my dear mom Cecy for her lack of selfishness. When we left to Canada in 1995, she knew she was not going to be alive to see hers granddaughters again and she never said a word discouraging us to come.

I wish to thank Spot (my dog) for his companionship late at night when everybody was asleep he was always there laying on top of my feet beneath the computer desk.

My special thanks to my dear daughters Anna Cláudia and Fernanda for their love and understanding the absence of their dad in some important events of their lives.

Finally, my very special thanks to my wife Vania for her love and encouragement for us to come to Canada. She had no doubt that this new experience was worthwhile. During our first two years, while I was taking my courses, she took out of my hands any housework so I could totally dedicate to my study, and at that time she still had to carry on her own research at the UofA for her M.Sc. She knew well how to manager my bad mood and stress during those years, for all that I am really thankful. I hope I will have the chance to do the same for her during the final stage of her doctoral program.

# Table of contents

**CHAPTER 1**

**Introduction** .......... **1**
**1.1 Problem Definition and Research Objectives** .......... **1**
**1.2 Thesis Content** .......... **5**
**1.3 Potential Geotechnical Application** .......... **5**
**1.4 Potential Geoenvironmental Application** .......... **8**
1.4.1 Surface/Subsurface Obstacles .......... 8
1.4.2 Boundaries of Contamination Plumes .......... 9
1.4.3 Screening for Dense Non-Aqueous Phase Liquids (DNAPLs) .......... 11
**1.5 Summary** .......... **16**

**CHAPTER 2**

**Horizontal Directional Drilling (HDD) Technology** .......... **17**
**2.1 Introduction** .......... **17**
**2.2 HDD Operational Procedure** .......... **20**
2.2.1 The Power System .......... 20
2.2.2 Special Drilling Component .......... 23
2.2.3 The Guidance System .......... 24
**2.3 Summary** .......... **28**

**CHAPTER 3**

**Cone Penetration Test (CPT) Technology** .......... **29**
**3.1 Introduction** .......... **29**
**3.2 CPT Principles** .......... **31**
3.2.1 Equipment and Test Description .......... 32
3.2.2 Pushing Rigs .......... 37
**3.3 A Brief History of the Evolution of the CPT** .......... **39**

**3.4 Geotechnical Applications** ........ **41**
3.4.1 Soil Stratigraphy and Classification ........ 42
3.4.2 Geotechnical Parameters ........ 49
**3.5 Geoenvironmental Applications** ........ **56**
**3.6 Summary** ........ **62**

**CHAPTER 4**

**Horizontal Directional Pre-Bored Cone Penetration Test HD-PB-CPT (Prototype 1 Development)** ........ **63**
**4.1 Introduction** ........ **63**
**4.2 Concept and Issues** ........ **65**
4.2.1 Probe First Idealization ........ 65
4.2.2 Soil Disturbance ........ 66
4.2.3 Cavity Strain ........ 68
4.2.4 Initial State of Stresses ........ 70
**4.3 Pilot Test** ........ **72**
4.3.1 Site Location and Geology ........ 72
4.3.2 Pilot Test Procedure ........ 78
4.3.3 Pilot Test Results ........ 79
**4.4 Probe Development** ........ **82**
4.4.1 Design ........ 82
4.4.2 Material Selection ........ 88
4.4.3 HDD Stem and HD-PB-CPT Connection ........ 90
4.4.4 Load Cell Design and Calibration ........ 92
4.4.5 Data Acquisition System ........ 95
**4.5 Summary** ........ **99**

**CHAPTER 5**

**Prototype 1 – Field Tests** ........ **101**
**5.1 Introduction** ........ **101**
**5.2 First Series of Field Tests** ........ **106**

5.2.1 Results and Data Analysis of Test 1 .......................................... 109
5.2.2 Results and Data Analysis of Test 2 .......................................... 111
**5.3 Second Series of Field Tests ............................................ 120**
5.3.1 Results and Data Analysis of Test 3 .......................................... 123
5.3.2 Results and Data Analysis of Test 4 .......................................... 126
5.3.3 Results and Data Analysis of Test 5 .......................................... 129
**5.4 Final Considerations .................................................. 132**
**5.5 Summary .............................................................. 135**

**CHAPTER 6**

**Laboratory Modeling ..................................................... 136**
**6.1 Introduction .......................................................... 136**
**6.2 Laboratory Modeling Set Up ............................................ 143**
6.2.1 Sample Preparation ............................................................ 144
6.2.2 Consolidation Chamber ........................................................ 145
6.2.3 Load System and Consolidation ................................................ 148
6.2.4 Test Assembly ................................................................. 152
**6.3 Penetration Test ...................................................... 156**
6.3.1 60° Apex Angle Cone ........................................................... 157
6.3.2 30° Apex Angle Cone ........................................................... 162
**6.4 Borehole Constraint Device ............................................ 164**
6.4.1 Length of the Constraint Device ............................................... 164
6.4.2 Analysis of the Results ....................................................... 166
**6.5 Summary .............................................................. 170**

**CHAPTER 7**

**Soil Electrical Resistivity Measurements for Environmental Application ..... 172**
**7.1 Introduction .......................................................... 172**
**7.2 A Brief Background .................................................... 172**

**7.3 Electrical Resistivity (Conductivity) Measurements Principle** ........ **174**
7.3.1 Propagation of Electric Current ........ 174
7.3.2 Methods Used to Measured Soil Electrical Resistivity (Conductivity) ........ 175
7.3.3 Principles and Units ........ 175
**7.4 Resistivity Cone Penetration Test (RCPT) for Environmental Applications** ........ **179**
**7.5 Summary** ........ **184**

**CHAPTER 8**
**Horizontal Directional Pre-Bored Resistivity Cone Penetration Test HD-PB-RCPT (Prototype 2 Development)** ........ **186**
**8.1 Introduction** ........ **186**
**8.2 Modifications to Improve Cone and Friction Sleeve Results** ........ **188**
**8.3 Electrical Resistivity Module (ERM)** ........ **191**
8.3.1 Excitation Source and Resistivity Calculation ........ 191
8.3.2 Number of Electrodes ........ 193
8.3.3 ERM and Data Acquisition System Description ........ 195
8.3.4 ERM Calibration ........ 196
**8.4 Summary** ........ **200**

**CHAPTER 9**
**Prototype 2 – Field Tests** ........ **202**
**9.1 Introduction** ........ **202**
**9.2 First Series of HD-PB-RCPT Tests (November 1999)** ........ **205**
9.2.1 HD-PB-RCPT Tests with 60° Apex Angle Cone ........ 206
9.2.2 HD-PB-RCPT Tests with 30° Apex Angle Cone ........ 210
**9.3 Second Series of HD-PB-RCPT Testes (January, 2000)** ........ **214**
9.3.1 HD-PB-RCPT Tests with 60° Apex Angle Cone ........ 215

9.3.1 HD-PB-RCPT Tests with 60° Apex Angle Cone .............................. 215
9.3.2 HD-PB-RCPT Tests with 30° Apex Angle Cone .............................. 223
**9.4 Complementary Data Analysis** .............................. **232**
9.4.1 Average Values and Standard Deviation .............................. 232
9.4.2 Standard Cone and Pre-Bored Cone Resistance Relationship........ 238
**9.5 Summary** .............................. **245**

**CHAPTER 10**

**Summary and Conclusions** .............................. **247**
**10.1 Introduction** .............................. **247**
**10.2 Conclusions** .............................. **248**
**10.3 Further Research** .............................. **249**
10.3.1 Development of a Special Reamer .............................. 249
10.3.2 Pore Pressure Measurement .............................. 252
10.3.3 Environmental Sensors .............................. 253
**10.4 Final Considerations** .............................. **254**

**References** .............................. **256**

**Appendix 1**

**CPTU Profiles (University of Alberta Field Laboratory)** .............................. **269**

**Appendix 2**

**Laboratory Index Tests** .............................. **274**

**Appendix 3**

**HD-PB-CPT Drawings** .............................. **278**

**Appendix 4**

**HD-PB-RCPT Drawings** .............................. **286**

**Appendix 5**

**Equation Development** .............................. **294**

# List of Tables

TABLE 1.1 – Some of the most common dnapl chlorinated solvents and their nomenclature (modified from Pankow and Cherry 1996). ........ 11
TABLE 1.2 – Principal uses of the four major chlorinated solvent products (modified from Pankow and Cherry 1996). ........ 12
TABLE 2.1 – Directional drill rigs groups (modified from CMW 1996). ........ 21
TABLE 3.1 – Comparison of applicability and usefulness of in situtests (modified from Robertson 1986). ........ 30
TABLE 3.2 – Evaluation of soil hydraulic conductivity based on a normalized soil behavior type classification chart by Robertson (1990). ........ 51
TABLE 5.1 - Estimated pulling forces. ........ 102
TABLE 6.1 – Characteristics of the clay ........ 145
TABLE 7.1 – Typical resistivity and conductivity values for bulk soil mixtures and pore fluids (modified from Campanella et al. 1994b and Lunne et al. 1997). ........ 178
TABLE 9.1 – Data comparison between the HD-PB-CPT and HD-PB-RCPT tests. Only the horizontal sections of the tests were considered. the sand pit section was not included. ........ 233
TABLE 9.2 – Average cone and friction sleeve resistance and a verage force acting on the cone load cell and on the friction sleeve load cell. ........ 237
TABLE 9.3 – Factored normalized cone resistance. ........ 244

# List of Figures

Figure 1.1 – CPT test being performed horizontally inside a tunnel. ....... 3
Figure 1.2 – Horizontal directional drilling pulling a CPT based probe (modified from CMW 1996)............................ 4
Figure 1.3 – Presence of sand pockets in the tunnel alignment of Edmonton's South LRT extension (modified from Eisenstein and Sorensen 1986)................................. 6
Figure 1.4 – Tunnel roof failure due to the presence of sand pockets (modified from Matheson 1970). ....................................... 7
Figure 1.5 – Extent of a brine contaminated plume screened by electrical conductivity CPT (modified from Horsnell 1988).......................................... 10
Figure 1.6 – Vertical logging increases the potential for the development of new pathways of continued vertical DNAPL migration (modified from Fetter 1993). ................ 14
Figure 1.7 – Laser induced fluorescence (LIF) sensor coupled with an HDD for hydrocarbon/DNAPL detection (modified from Nielsen 1997). ...................................................... 15
Figure 1.8 – Schematic of the multiple-port soil sampler (modified from Ariaratnam et al. 2000). .......................................... 15
Figure 2.1 – HDD typical borehole configurations. ............................ 18
Figure 2.2 – HDD drill rig components............................................ 21
Figure 2.3 – Horizontal Directional Drill rigs. ..................................... 22
Figure 2.4 – Directional drilling steering. .......................................... 23
Figure 2.5 – Compaction type drilling bit. .......................................... 24
Figure 2.6 – Downhole mud motor (modified from CMW 1996)............ 24
Figure 2.7 – Transmitter unit............................................................. 26
Figure 2.8 – Walkover receiver (DigiTrak). ......................................... 26

Figure 2.9 – Guidance system by walkover method. .............................. 27
Figure 3.1 – Electrical cone penetrometer sketch. ................................ 33
Figure 3.2 – Different load cells designs for CPTs (modified from Lunne et al. 1997). ...................................... 35
Figure 3.3 – Examples of truck-mounted CPT rigs (courtesy of ConeTec Ltd.). .............................................. 38
Figure 3.4 – Inside the CPT enclosure: adding a rod to advance the test with the hydraulic jack system. ........................... 39
Figure 3.5 – Former cone penetration test (modified from Barentsen 1936). ........................................................ 40
Figure 3.6 – CPT repeatability: average, and average plus and minus one standard deviation from 6 CPT tests performed at a uniform site (modified from Douglas and Olsen 1981). ............................................ 43
Figure 3.7 – CPT soil behavior type classification chart (modified from Douglas and Olsen 1981). ........................ 44
Figure 3.8 – Soil behavior type classification chart based on excess pore water pressure and cone resistance (modified from Jones and Rust 1982). ............................ 46
Figure 3.9 – Soil behavior type classification charts. ............................ 47
Figure 3.10 – Normalized soil behavior type classification charts. ........ 48
Figure 3.11 – Chart for the estimation of horizontal hydraulic conductivity from CPTU dissipation tests (Modified from Robertson et al. 1992). .................... 52
Figure 3.12 – Prediction of sand's friction angle from CPT (modified from Robertson and Campanella 1983). ........... 53
Figure 3.13 – Density Index estimation from CPT data: a) for normally consolidated sand, and b) for overconsolidated sand (modified from Lunne et al. 1997). ....................................................... 55
Figure 3.14 – Laser Induced Fluorescence CPT .................................... 58

Figure 3.15 – Schematic view of the UV probes. .................................. 60
Figure 3.16 – Profile from UV induced fluorescence. ............................ 61
Figure 4.1 – Sketch of the sharp cone and typical pressuremeter like curve obtained from a sharp cone test (modified from Ladanyi 1994). ........................................ 64
Figure 4.2 – Schematic view of the first idealization of the HD-PB-CPT. ................................................................ 66
Figure 4.3 – Idealized pressuremeter test curves (modified from Ferreira, 1992). ...................................... 68
Figure 4.4 – Elastic and Plastic zones. ................................................ 69
Figure 4.5– Initial state of stresses around a vertical and a horizontal CPT (modified from Broere and van Tol 1998)................................................................... 71
Figure 4.6 – University of Alberta field laboratory location (modified from Bhanot 1968). ........................................ 75
Figure 4.7 – Typical CPTU soil profile from University of Alberta field laboratory. ........................................................... 76
Figure 4.8 – Undrained shear strength profile estimated from CPTU tests. ............................................................... 77
Figure 4.9 – Pilot tests (vertical pre-bored CPTs). ................................ 81
Figure 4.10 – Sketch of the HD-PB-CPT prototype 1............................ 85
Figure 4.11 – HD-PB-CPT prototype 1................................................. 86
Figure 4.12 – Detailed view of the front of the HD-PB-CPT. ................. 86
Figure 4.13 – Front part of the HD-PB-CPT disassembled. ................... 87
Figure 4.14 – HD-PB-CPT rear view. .................................................. 87
Figure 4.15 – Cone resistance as a function of the effective overburden stress and sand density (modified from Baldi et al. 1982)............................................................. 89
Figure 4.16 – Connector tool and load safety pin. ........... 91
Figure 4.17 – Cone and friction sleeve calibration curves. ..................... 93

Figure 4.18 – View of the load cells calibration in the Universal Testing Machine. .......... 94
Figure 4.19 – HD-PB-CPT electronics. .......... 96
Figure 4.20 – Data acquisition control and monitoring panel. .......... 96
Figure 4.21 – Data acquisition system van and position measurement device. .......... 98
Figure 6.1 – Axial strain contours around a 60° penetrometer. Positive signs are compression strains (modified from Teh and Houlsby 1991). .......... 137
Figure 6.2 – Strain path due to cone penetration in clay with different apex angles. (modified from Teh and Houlsby, 1991). .......... 139
Figure 6.3 – Octahedral strains for 18° and 60° apex angle cones. (modified from Acar and Tumay, 1986) .......... 140
Figure 6.4 – Location of the elasto-plastic boundary in cone penetration (modified from Teh and Houlsby, 1991). .......... 142
Figure 6.5 – Possible plastic zones around a penetrometer (modified from Teh and Houlsby, 1991). .......... 142
Figure 6.6 – Consolidation chamber diagram. .......... 147
Figure 6.7 – Top view of the consolidation chamber. .......... 148
Figure 6.8 – Consolidation load system. .......... 149
Figure 6.9 – Consolidation curves of specimens from chamber A and B. .......... 151
Figure 6.10 – Chamber's side cut and chamber's top cut. .......... 153
Figure 6.11 – View of a half specimen after being cut. .......... 154
Figure 6.12 – Half pipe preparation (borehole modeling). .......... 155
Figure 6.13 – Final test assembly closer view of grid lines (60° half cone ready to penetrate the borehole). .......... 156
Figure 6.14– Soil's deformation pattern of a 2.25 cm in diameter cone with an apex angle of 60° being pushed through a 1.5 cm borehole in soft clay

and longitudinal view of penetration.............................158
Figure 6.15 – Octahedral strain contours for a standard 60° cone (Acar and Tumay, 1986). And octahedral strain contours for a pre-bored 60° cone, and strain mesh with the octahedral strain (%) of each node. .........161
Figure 6.16 – 30° cone penetration, beginning of soil accumulation after 11.8 cm of penetration. And after 30 cm of penetration, soil accumulation ahead of the cone's tip was only about 0.6 cm and remains around this magnitude during the whole test...............................................................163
Figure 6.17 – Diagram of the penetrometers, with the constraint device used in the modeling test. .................................165
Figure 6.18 – Deformation pattern of the 60° cone with the borehole constraint device. And deformation pattern of the 30° cone with the borehole constraint device........168
Figure 6.19 – Octahedral strain contours for a standard 60° cone (Acar and Tumay, 1986). And octahedral strain contours for a pre-bored 60° cone with borehole constraint device, and strain mesh with the octahedral strain (%) of each node. ..........................169
Figure 7.1 – RCPT from a waste disposal (inorganic compound) site (modified from Zuidberg et al. 1988). .............................181
Figure 7.2 – RCPT of a DNAPL spill site (modified from Woeller et al. 1991).......................................................182
Figure 7.3 – RCPT profile from a creosote contaminated site (modified from Campanella et al. 1994b).........................183
Figure 8.1 – HD-PB-RCPT with a 60° apex angle cone tip and with a 30°.................................................................190
Figure 8.2 – HD-PB-RCPT assembled with the 30° cone. .....................191
Figure 8.3 – HD-PB-RCPT ERM circuit...............................................193

Figure 8.4 – Effect of polarization in a two and four electrodes configuration probe (modified from Weemees 1990). .......195
Figure 8.5 – Electrical resistivity calibration tank.................................197
Figure 8.6 – Influence in $K$ value as a function of $d_s/d_c$ and $d_e/d_c$ (modified from Yeung and Akhtar 1995)..........................198
Figure 8.7 – Electrical Resistivity Module calibration curve. ................199
Figure 9.1 – HDD drill rig Ditch Witch JT 1720..................................203
Figure 9.2 – Drill stem and HD-PB-RCPT hook-up and beginning of penetration................................................204
Figure 9.3 – HD-PB-RCPT Test 6 with the 60° apex angle cone............208
Figure 9.4 – HD-PB-RCPT Test 7 with the 60° apex angle cone............209
Figure 9.5 - HD-PB-RCPT Test 8 with the 30° apex angle cone. ...........212
Figure 9.6 - HD-PB-RCPT Test 9 with the 30° apex angle cone. ...........213
Figure 9.7 – Load cell calibration curves using the new DC adapter. ...214
Figure 9.8 – HD-PB-RCPT Test 10, with 60° apex angle cone...............217
Figure 9.9 – HD-PB-RCPT Test 10, with 60° apex angle cone, normalized data.....................................................218
Figure 9.10 - HD-PB-RCPT Test 11, with 60° apex angle cone. ............219
Figure 9.11 - HD-PB-RCPT Test 11, with 60° apex angle cone, normalized data. .....................................................220
Figure 9.12 – Soil Behavior type classification chart, results from prototype 1 Tests, except Test 1 (modified from Robertson, 1990)...........................................221
Figure 9.13 - Soil Behavior type classification chart, results from prototype 1 Tests, except Test 1 and prototype 2 Tests 10 and 11(modified from Robertson, 1990). ..........222
Figure 9.14 - HD-PB-RCPT Test 12, with 30° apex angle cone. ............226
Figure 9.15 - HD-PB-RCPT Test 12, with 30° apex angle cone, normalized data. .....................................................227
Figure 9.16 – Arrival of the drilling bit; connection of the probe; penetration and probe completely

inside the soil.......................................................229
Figure 9.17 - HD-PB-RCPT Test 13, with 30° apex angle cone............230
Figure 9.18 - HD-PB-RCPT Test 13, with 30° apex angle cone, normalized data. .......................................................231
Figure 9.19 – Model of cone penetration into a perfectly plastic medium (modified from Van Wieringen 1982). ...............239
Figure 9.20 – Frequency distribution of cone resistance/limit pressure ratio from 170 measurements on clay. ............241
Figure 9.21 – Model of a pre-bored cone penetration into a perfectly plastic medium. ............................................242
Figure 10.1 – Difference in borehole shape. ......................................251
Figure 10.2 – Soil accumulation in front of the HD-PB-RCPT. .............251
Figure 10.3 – Example of pore pressure versus depth diagram during penetration (modified from Torstensson 1975).......................................................252

# List of Symbols:

## Latin Symbols

| | |
|---|---|
| $a$ | cone area ratio |
| $a$ | cone radius |
| $A$ | area |
| $a$ | constant |
| $B_q$ | normalized pore pressure parameter ratio |
| $C_0$ | constant |
| $C_1$ | constant |
| $C_2$ | constant |
| $d_c$ | diameter of the probe |
| $DC$ | direct current |
| $d_e$ | distance between electrodes |
| $d_s$ | chamber diameter |
| $e$ | void ratio |
| $E$ | Young's modulus |
| $E$ | electrical field |
| $E_1$ | strain invariant (triaxial compression) |
| $E_2$ | strain invariant (pressuremeter) |
| $E_3$ | strain invariant (simple shear) |
| $e_{max}$ | maximum void ratio |
| $e_{min}$ | minimum void ratio |
| $F$ | formation factor |
| $F_r$ | normalized friction ratio |
| $f_s$ | friction sleeve resistance |
| $F_s$ | force acting on the friction sleeve |
| $F_T$ | total CPT force |
| $G$ | shear modulus |
| $G_s$ | relative density (former specific gravity) |
| $I_D$ | density index (former relative density) |
| $I_r$ | rigidity index |
| $J$ | current density |
| $k$ | constant factor |
| $K$ | earth pressure coefficient |
| $K$ | calibration factor |
| $k_h$ | horizontal coefficient of permeability |
| $L$ | length |
| $m$ | constant |
| $n$ | soil porosity |
| $N_{kt}$ | cone factor |
| $N_s$ | constant |
| $N_{\Delta u}$ | pore pressure based cone factor |

| | |
|---|---|
| $OCR$ | overconsolidation ratio |
| $p_o$ | effective overburden stress |
| $p_l$ | limit pressure |
| $p_l^*$ | corrected limit pressure |
| $p_{max}$ | practical limit pressure |
| $q_c$ | cone resistance |
| $Q_c$ | cone resistance force |
| $q_{cH}$ | horizontal cone resistance |
| $q_{Cm}$ | cone resistance from a pre-bored penetration test |
| $q_{cV}$ | vertical cone resistance |
| $q_t$ | corrected total cone resistance |
| $Q_t$ | normalized cone resistance |
| $R$ | resistance |
| $r$ | cone radius |
| $R_f$ | friction ratio |
| $R_o$ | initial radius |
| $r_p$ | radial distance of plastic boundary |
| $R_{PE}$ | radius of the plastic-elastic transition |
| $s$ | shape factor |
| $S_t$ | clay sensitivity |
| $S_u$ | undrained shear strength |
| $t_{50}$ | time for 50% soil consolidation |
| $u_1$ | pore pressure measurement position on the CPTU |
| $u_2$ | pore pressure measurement position on the CPTU |
| $u_3$ | pore pressure measurement position on the CPTU |
| $u_o$ | equilibrium or hydrostatic pore water pressure |
| $V_1$ | velocity 1 |
| $V_2$ | velocity 2 |
| $V_3$ | velocity 3 |
| $V_4$ | velocity 4 |
| $V_s$ | shear wave velocity |
| $W_H$ | work performed by a horizontal CPT expanding a cavity |
| $W_V$ | work performed by a vertical CPT expanding a cavity |
| $z_p$ | distance between the cone tip and the plastic boundary |

## Greek Symbols

| | |
|---|---|
| $\beta$ | apex angle |
| $\Delta_u$ | excess or dynamic pore water pressure |
| $\Delta R$ | difference between cavity expanded radius and initial radius |
| $\varepsilon$ | cavity strain |
| $\varepsilon_{rr}$ | radial strain |
| $\varepsilon_{rz}$ | shear strain |
| $\varepsilon_{zz}$ | axial strain |

| | |
|---|---|
| $\varepsilon_{zz'}$ | axial strain along $z'$ axis |
| $\varepsilon_{\theta\theta}$ | circunferential strain |
| $\gamma_{oct}$ | octahedral strain |
| $\nu$ | Poisson's ratio |
| $\theta$ | angle between $z$ and $z'$ axis |
| $\rho$ | resistivity |
| $\rho$ | soil density |
| $\sigma$ | electrical conductivity |
| $\sigma'$ | vertical or mean effective stress |
| $\sigma'_H$ | effective horizontal stress |
| $\sigma'_v$ | effective vertical stress |
| $\sigma_{vo}$ | total overburden stress |
| $\sigma'_{vo}$ | effective initial vertical stress |

# List of Abbreviations:

| | |
|---|---|
| AC | - Alternate current |
| AFRL/MQL | - U.S. Air Force Research Laboratory |
| ASTM | - American Society for Testing Materials |
| CEC | - Cation exchange capacity |
| CPT | - Cone penetration test |
| CPTU | - Cone penetration test with pore pressure measurement |
| DBA-AG | - Depth bridge amplifier with adjustable gain |
| DC | - Direct current |
| DCM | - Dichloromethane |
| DNAPL | - Dense non-aqueous phase liquid |
| ERM | - Electrical resistivity module |
| FDPT | - Full displacement pressuremeter test |
| HDD | - Horizontal directional drilling |
| HD-PB-CPT | - Horizontal directional pre-bored cone penetration test |
| HD-PB-RCPT | - Horizontal directional pre-bored resitivity cone penetration test |
| ISSMFE | - International Society of Soil Mechanics and Foundation Engineering |
| IRTP | - International Reference Test Procedure |
| LIF | - Laser induced fluorescence |
| LRT | - Light Rail Transit |
| LVDT | - Linear variable differential transformer |
| MAC | - Maximum acceptable concentration |
| PBPT | - Pre-bored pressuremeter test |
| PCE | - Perchloroethylene |
| PVC | - Polyvinyl chloride |
| RCPT | - Resistivity cone penetration test |
| RMS | - Root mean square |
| SBPT | - Self boring pressuremeter test |
| SBTC | - Soil behavior type classification |
| SCT | - Sharp cone test |
| SI | - Système International d'unités |
| SPT | - Standard penetration test |
| TDS | - Total dissolved solids |
| TCE | - Trichloroethylene |
| UV | - Ultra violet |
| UVIF | - Ultra violet induced fluorescence |

# CHAPTER 1

# Introduction

## 1.1 PROBLEM DEFINITION AND RESEARCH OBJECTIVES

A geotechnical and/or geoenvironmental site investigation program has the following objectives, according to Lunne et al. (1997):

- to determine the nature and sequence of the subsurface strata (geological regime);
- to determine the groundwater conditions (hydrogeological regime);
- to determine the physical and mechanical properties of the subsurface strata; and
- to determine the distribution, composition and concentration of contaminants (geoenvironmental application).

Currently, there are many techniques available to accomplish the above objectives, which include in situ and laboratory testing. The main focus of this research is with in situ testing which can be further divided into surface and subsurface testing methods.

Surface methods of investigation, usually involving geophysical techniques, allow evaluation of large areas of essentially all of the material involved. They lack ground-truthing capability, however, thus making results difficult to interpret (Campanella et al. 1994a). Interpretation of geophysical data is generally not straightforward and relies on subjective human judgement; two experts may not even agree on the meaning of the data (CCME 1994; Greenhouse et al. 1997). In urban areas with many surface obstacles such as buildings and busy highways, surface geophysical testing techniques may not be suitable to use.

Subsurface testing typically employs vertical methods, such as vertical drilling and vertical probes. As with surface methods, their use may be impaired by surface or subsurface obstacles. Furthermore, subsurface characterization only allows an appraisal of a fraction of a percent of the subsoil because of its pinpoint characteristic (Campanella et al. 1994a).

Based on the above there is need for a tool that would be able to characterize a soil's subsurface by following a horizontal path rather than a vertical one. With regards to geoenvironmental applications, groundwater contamination plumes and pools are usually much longer and wider than they are thick. Therefore, assessing the extent of contamination plumes and pools could be accomplished much more efficiently by following a horizontal rather than a vertical testing path. With respect to geotechnical applications, the use of mechanized tunnel boring has brought about an increasing need for obtaining soil data along the alignment of the tunnel (Broere and van Tol 1998). Due to normal soil variation and irregularities, an extensive soil survey would be necessary in order to obtain enough information from vertical measurements. Using a horizontal testing path along the tunnel crown or centerline, on the other hand, would be a much more rational way to obtain these data. This is the case not only for tunnels but also for any other linear structures such pipelines, for instance.

As shown in Figure 1.1, it is feasible to perform the cone penetration test (CPT) horizontally (ConeTec 1989); however, the potential for rod buckling and the necessity of opening a large pit to perform the test renders this option unattractive particularly for long test sections.

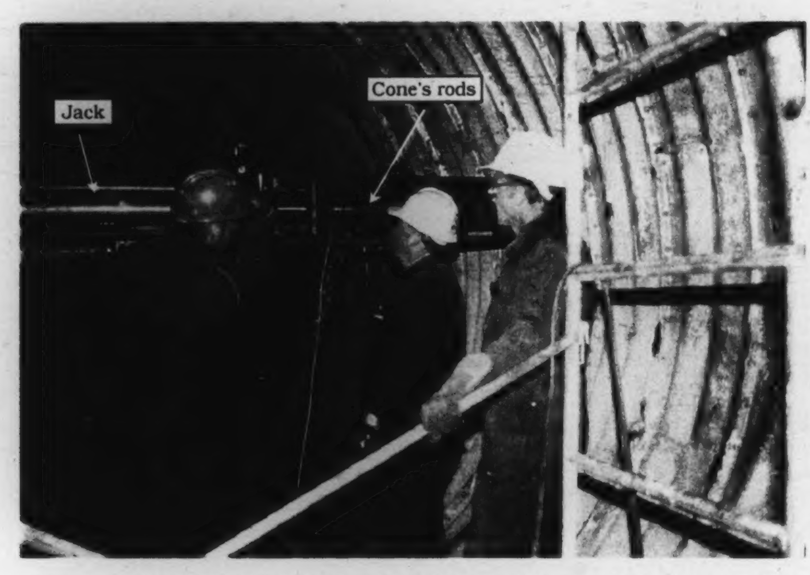

Figure 1.1 – CPT test being performed horizontally inside a tunnel (ConeTec 1989).

In this context, the objectives of the present research were to study the feasibility of developing a horizontal logging device capable of detecting soil lithology changes and simultaneously screen for soil contamination, followed by the design, construction and field testing of this novel probe.

The unique characteristic of horizontal directional drilling (HDD) of drilling a borehole with an entry and an exit point initiated the idea of developing the horizontal logging probe, based on CPT technology, where the penetrometer is pulled back through the pre-borehole rather than pushed ahead of the drill stem, as illustrated in Figure 1.2. Because the probe will be pulled, not pushed, the potential problem of rod buckling is eliminated. Furthermore because the HDD rig will be used to pull the probe, there will be no need to open an access pit to perform the test.

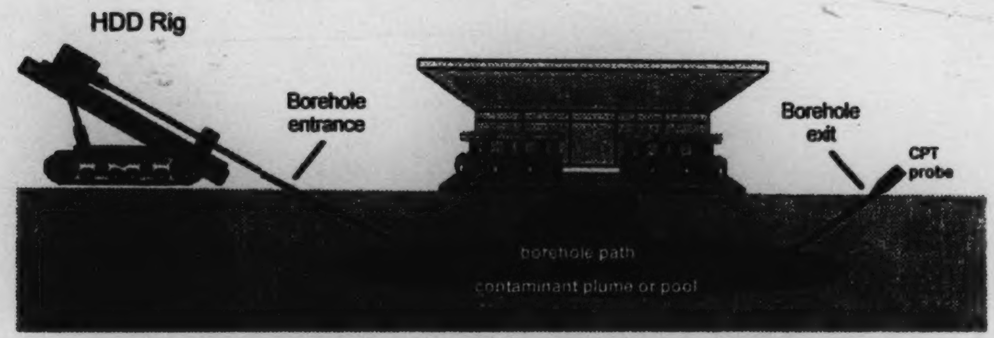

**Figure 1.2 – Horizontal directional drilling pulling a CPT based probe. (modified from CMW 1996)**

As the probe is being pulled through the pre-borehole, it expands the hole and measures cone and friction sleeve resistance in the same manner as a standard CPT. The boundary condition of the problem is similar to cavity expansion; therefore, cavity expansion theory was used to perform a preliminary assessment of the new probe's ideal dimensions. A pilot test was conducted to validate the assumptions made. Prototype 1 was then built and field tested in Lake Edmonton clay at the University of Alberta field laboratory. The results from these first prototype tests showed that further improvement was necessary. Therefore, small scale laboratory physical modeling tests were conducted to gain a better understanding of the soil deformation pattern. A second prototype was then constructed and field tested in the same soil and location as Prototype 1. This time, an electrical resistivity module was added to Prototype 2 to improve identification of soil lithology change and to allow the probe to screen for soil contamination. Because the test was performed in a pre-opened borehole drilled by an HDD rig, this new horizontal logging probe was called the Horizontal Directional Pre-Bored Cone Penetration Test (HD-PB-CPT).

## 1.2 THESIS CONTENT

Chapter 2 provides a brief introduction to HDD technology and operation methodology. Though CPT is a well known, well established, and broadly used tool in the geotechnical/geoenvironmental fields, Chapter 3 nevertheless presents an overview of this versatile technology for the benefit of those readers from other fields of study, but who have closely related interests in the environmental, soil, and geophysical sciences. Chapter 4 describes the concept design and development of the HD-PB-CPT (Prototype 1). Prototype 1 field test results are presented and discussed in Chapter 5. Chapter 6 describes and presents the results of the small scale physical modeling tests. The development of Prototype 2 is described in Chapter 8 followed by the field test results and discussion in Chapter 9. Because an electrical resistivity module was added to Prototype 2 a background of soil electrical resistivity measurement is presented in Chapter 7. Finally, summary, conclusion and suggestions for future research are presented in Chapter 10. The following sections of this chapter provide more detail on the potential application of this new probe for geotechnical and geoenvironmental site investigation.

## 1.3 POTENTIAL GEOTECHNICAL APPLICATION

A main concern in tunneling design in soil beneath the water table is sand pockets or lenses (May and Thomson 1979; Tweedie et al. 1992). When tunnel boring reaches a sand pocket there is a great risk of having the tunnel flood or even a collapse due to the higher permeability of the sand and its lack of cohesion. A collapse could produce a sink hole at the surface, which could create a great material and human hazard and increase the cost of the tunneling by millions of dollars.

Eisenstein (1999) stated that sand pockets are always a concern for tunneling design. For instance, during the construction of Edmonton's Light Rail Transit (LRT) there was a great deal of concern about sand pockets under Jasper Avenue. In an effort to track these pockets, even with vertical boreholes made every 20 meters along the tunnel alignment, it was not possible to locate all of them. The presence of sand pockets in the LRT tunnel alignment can be seen in Figure 1.3.

Glacial till formation is favorable for tunneling, (Eisenstein and Sorensen 1987), so it was convenient to have the tunnel placed in this kind of formation; nevertheless, sand pockets still pose a problem and their localization by means of vertical boreholes is neither efficient nor economical.

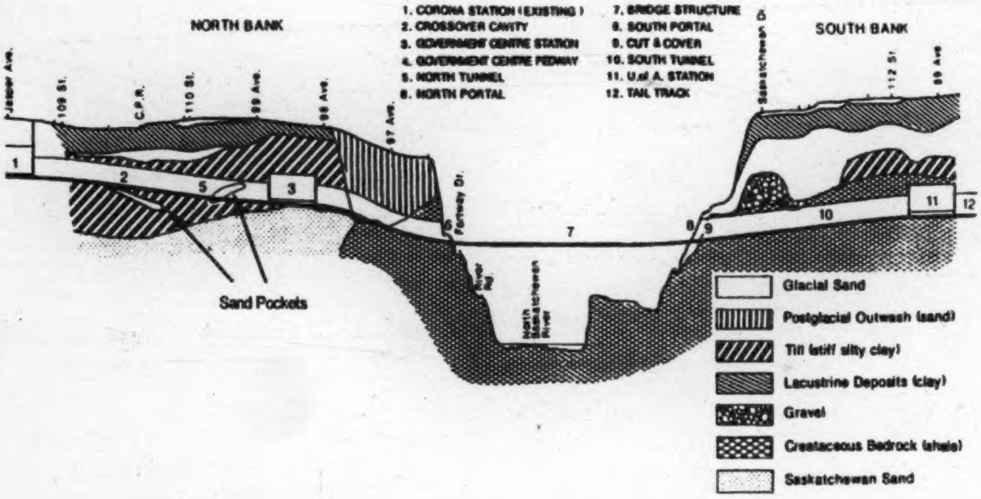
NORTH BANK
SOUTH BANK
1. CORONA STATION (EXISTING)
2. CROSSOVER CAVITY
3. GOVERNMENT CENTRE STATION
4. GOVERNMENT CENTRE PEDWAY
5. NORTH TUNNEL
6. NORTH PORTAL
7. BRIDGE STRUCTURE
8. SOUTH PORTAL
9. CUT & COVER
10. SOUTH TUNNEL
11. U.of A. STATION
12. TAIL TRACK
Jasper Ave.
109 St.
C.P.R.
110 St.
99 Ave.
98 Ave.
97 Ave.
Fortway Dr.
River Rd
North Saskatchewan River
Saskatchewan Dr.
112 St.
89 Ave.
Sand Pockets
1
2
3
5
6
7
8
9
10
11
12
Glacial Sand
Postglacial Outwash (sand)
Till (stiff silty clay)
Lacustrine Deposits (clay)
Gravel
Creataceous Bedrock (shale)
Saskatchewan Sand

Figure 1.3 – Presence of sand pockets in the tunnel alignment of Edmonton's South LRT extension (modified from Eisenstein and Sorensen 1986).

To better illustrate the problem of sand pockets for tunneling, Figure 1.4 (a) - (c) shows a failure of an unsupported section of a tunnel's roof during construction. Analysis of the failure has shown that the presence of sand pockets adversely affected the roof's stability (Matheson 1970). The tunnel was excavated in clay till and the tunnel invert was at a depth of 26.4 m. It is worth noting that new advancements in tracking devices allow a HDD to bore to approximately 30 m in depth. Beyond this limit a wire line magnetometer-accelerometer navigation system must be used. However this increases the cost significantly (Allouche et al. 1998a).

Figure 1.4 – Tunnel roof failure due to the presence of sand pockets. (a) Block of clay till falling; (b) View of roof damage and (c) Debris on the floor after roof failure (modified from Matheson 1970).

A tool that could identify and characterize sand pockets or sand lenses horizontally along the tunnel alignment would be extremely useful.

## 1.4 POTENTIAL GEOENVIRONMENTAL APPLICATION

CPT's or CPTU's (if pore pressures are measured), are excellent logging devices that provide near continuous soil profiles of mechanical properties, soil types and detailed soil stratigraphies (Robertson et al. 1998). This information is crucial for a sound hydrogeological idealization of the subsurface, thus essential for good geoenvironmental site characterization. CPT's or CPTU's are capable of detecting sand layers as thin as 1 or 2 cm, layers that are detected with difficulty with conventional drilling and sampling techniques (Horsnell 1988). Such layers, if continuous, are of great concern because they permit significant contaminant migration. The features of the CPT have made it an attractive device to enhance with the development of new sensors for geoenvironmental site characterization. The most common sensors used measure temperature, pH, resistivity, density and moisture using gamma and neutron rays, and also hydrocarbon presence using laser induced fluorescence (LIF) and UV fluorescence. These sensors can be easily incorporated to the HD-PB-CPT, making it an excellent alternative tool for screening soil contamination along a horizontal profile as will be described next.

### 1.4.1 SURFACE/SUBSURFACE OBSTACLES

Currently, the most common methods used to assess potential soil and groundwater contamination use conventional drilling and sampling, and direct push devices deployed vertically from the soil surface. Vertical tools, however, are limited in their capability to sample the soil below any surface/subsurface obstacles such as buildings, highways, storage tanks and rivers (Allouche et al. 1998b). For these situations the HD-PB-CPT test can be easily performed to screen for contamination beneath the obstacle, as illustrated in Figure 1.2.

### 1.4.2 BOUNDARIES OF CONTAMINATION PLUMES

The transport of dissolved solute contamination in groundwater is governed by advection, dispersion, diffusion and retardation (Fetter 1993). Usually, due to both stratigraphy and advective transport contamination plumes are much longer and wider than they are thick. Therefore, to delineate the extent of a contamination plume, horizontal logging rather than vertical logging may be much more effective. Figure 1.5 shows the application of a vertical conductivity CPT to identify the vertical (Figure 1.5a) and lateral (Figure 1.5b) extent of a brine plume (Horsnell 1988). The plan view of the site (Figure 1.5b) shows that it was necessary to perform 18 CPT tests to completely delineate the plume contours. The same result could have been achieved by performing only 4 horizontal logging tests along the alignment, shown by the gray lines in Figure 1.5(b), and only 3 or 4 CPTs to define contamination depths.

It is worth noting that the maximum thickness of the plume was about 8.5 m (27.5 feet) whereas its length and width were approximately 180 m and 120 m respectively, distances easily covered by a midsize HDD rig. Furthermore, performing horizontal logging would have no data loss beneath the source of the contamination, i. e., beneath the brine disposal pond, once horizontal logging probe can go easily under the pond whereas vertical logging device cannot.

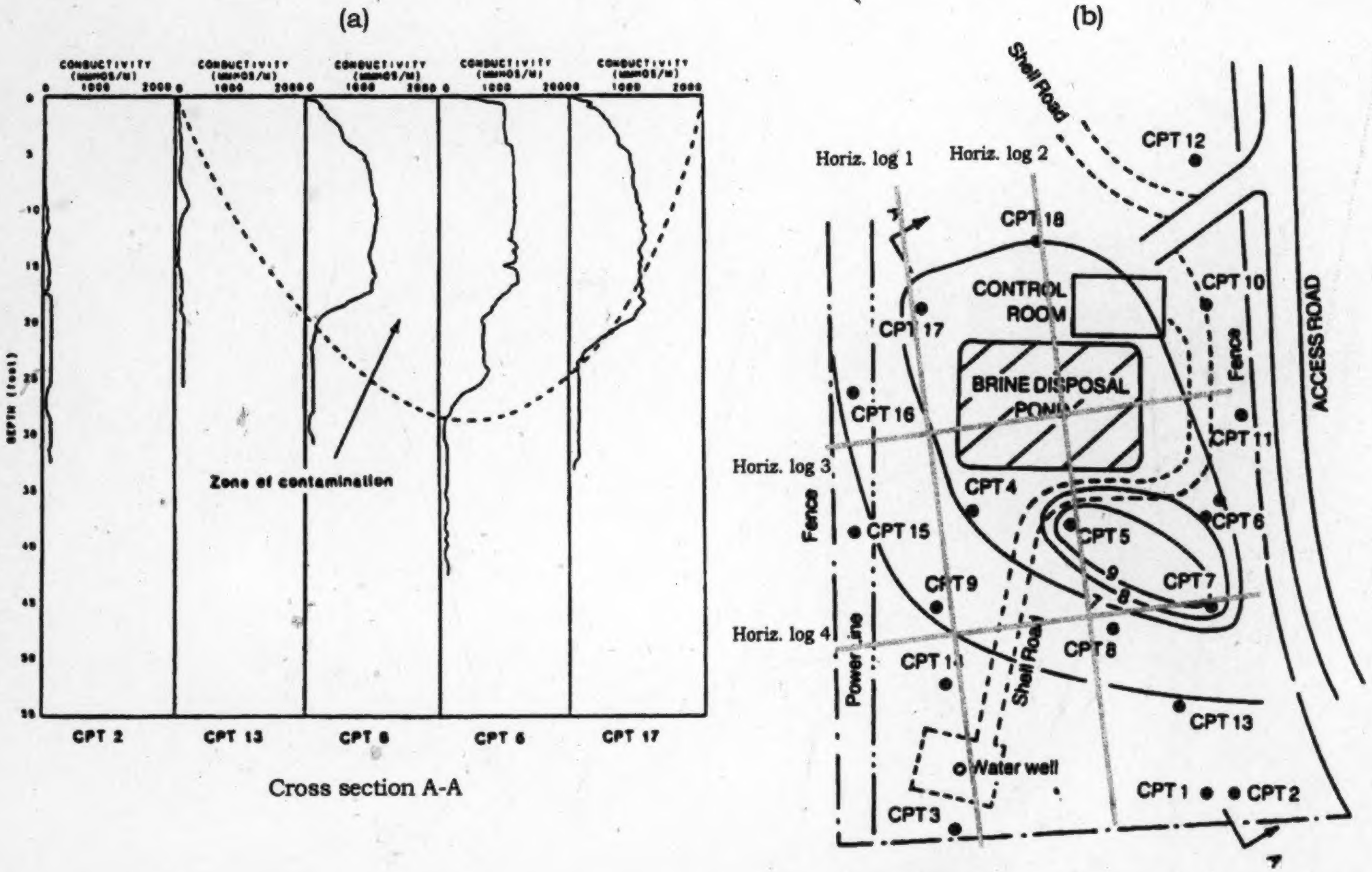

Figure 1.5 – (a) Vertical and (b) lateral extent of a brine contaminated plume screened by electrical conductivity CPT. (modified from Horsnell 1988)

### 1.4.3 SCREENING FOR DENSE NON-AQUEOUS PHASE LIQUIDS (DNAPLs)

Dense non-aqueous phase liquids (DNAPLs) are separate-phase hydrocarbon liquids that are denser than water. These include chlorinated solvents, halogenated benzenes, wood preservative wastes, coal tar wastes, and pesticides (EPA 1998). Among these chemicals, the chlorinated solvents are of greatest concern. The other DNAPLs have not been used in as many industrial applications or in as large quantities. Some compounds are also much less soluble than chlorinated solvents, making them much less mobile. Furthermore, important soluble components of creosote and coal tar are more degradable in the groundwater than are most chlorinated solvents (Pankow and Cherry 1996).

Table 1.1 presents the chemical names, acronyms and commercial names of the four most common DNAPL chlorinated solvents. The principal uses of these compounds are shown in Table 1.2.

Table 1.1 – Some of the most common DNAPL chlorinated solvents and their nomenclature (modified from Pankow and Cherry 1996).

| CHEMICAL NAME | ACRONYMS/COMMERCIAL NAMES |
|---|---|
| Perchloroethylene | PCE, tetrachloroethylene, ethylene tetrachloride, Nema, Tetracap, Tetropil, Perclene, Ankilostin, Didakene, PerSec |
| Trichloroethylene | TCE, ethinyl trichoride, Tri-Clene, Trielene, Trichloran, Trichloren, Algylen, Triline, Tri, Trethylene, Westrosol, Chlorylen, Gemalgene, Germalgene |
| 1,1,1-Trichloroethane | TCA, methyl chlorothene, Solvent 111, TRI-ETHANE, |
| Dichloromethane | DCM, methylene chloride, methylene dichloride, methylene bichloride |

Table 1.2 – Principal uses of the four major chlorinated solvent products (modified from Pankow and Cherry 1996).

| APPLICATION | PERCENTAGE USE | | | |
|---|---|---|---|---|
| | TCA | DCM | PCE | TCE |
| Adhesives | 9 | - | - | 1 |
| Aerosol | 11 | 29 | - | - |
| Chemical intermediate | - | - | 29 | - |
| Cold cleaning | 20 | - | - | - |
| Dry cleaning/textile production | - | - | 56 | - |
| Electronics | 6 | 8 | - | - |
| Metal cleaning/degreasing | 44 | 9 | 11 | 85 |
| Paint removal/stripping | - | 27 | - | 1 |
| Urethane foam | - | 10 | - | - |
| Miscellaneous | 3 | 8 | 4 | 6 |

Chlorinated organic solvent contamination levels (in dissolved form) are very low, usually in the μg/L (ppb) or mg/L (ppm) ranges. For example, the maximum acceptable concentration (MAC) for PCE is 30 μg/L, for TCE and DCM is 50 μg/L (CCME 1999) and for TCA is 200 μg/L (Fetter 1993). The reasons for such low limits are that these chemicals are suspected carcinogens and there is also evidence that excessive exposure may result in kidney and liver damage (Pankow and Cherry 1996).

Chlorinated solvents have low absolute solubilities but high solubility/MAC ratios, hence the contamination produced by a pool will typically be in excess of its MAC. Thus, even small pools can cause high levels of groundwater contamination that could last for decades or even centuries (Pankow and Cherry 1996).

Unlike petroleum products, chlorinated solvents are not detectable by taste or odor at typical contamination levels. When released on the surface in free phase form in quantities sufficient to overcome the entry pressure, they do not stop at the water table like petroleum products do. Instead, they will continue to migrate downwards until stopped by a less permeable layer where they will accumulate and form a pool of free product and leaving behind a trail of residual product as shown in Figure 1.6.

Free product pools of DNAPLs can be small in volume and thus extremely difficult to locate. A large number of boreholes may be necessary to locate small to medium sized pools using conventional vertical drilling and sampling, which is usually not very practical (Pankow and Cherry 1996). There is a low probability of detecting such pools due to the pinpoint characteristics of vertical logging. Horizontal logging, on the other hand, provides a much longer contact area within the target zone, increasing the chance of detection of at least the residual phase.

Furthermore, searching for DNAPL by vertically drilling into a subsurface can result in the creation of new pathways for continued vertical migration of the free phase to previously uncontaminated strata (CCME 1994; Greenhouse et al. 1997; EPA 1998), as illustrated in Figure 1.6.

According to Nielsen et al. (1997) survey data suggest that more than 80% of DNAPL contamination is within 21 meters of the surface, which would make it easy to reach using the horizontal directional drill technique.

The above information shows that HDD may be an attractive tool to use when searching for DNAPLs. In fact, the U.S. Air Force Research Laboratory (AFRL/MLQ) is also developing a probe that uses HDD to deliver a downhole laser induced fluorescence (LIF) sensor to locate free phase DNAPL and petroleum contamination (Nielsen 1997), as shown in Figure 1.7. Despite LIF being a very good sensor for hydrocarbon/DNAPL detection, however, it is a very expensive technology and its application is also limited to contaminants that fluoresce. In addition, this particular probe does not provide any information regarding soil lithology, whereas the HD-PB-CPT can.

Nevertheless, the AFRL/MLQ research does show there is increasing interest in this new approach for geotechnical and geoenvironmental site investigation, namely, the development of new tools for horizontal soil/contamination screening and characterization. Recently, in this same line of research, Ariaratnam et al. (2000) have developed a horizontal multiple-port soil sampler device that would be an excellent tool to use in combination with the HD-PB-CPT to obtain multiple soil samples in critical zones identified by the HD-PB-CPT. A schematic sketch of the multiple-port soil sampler is shown in Figure 1.8.

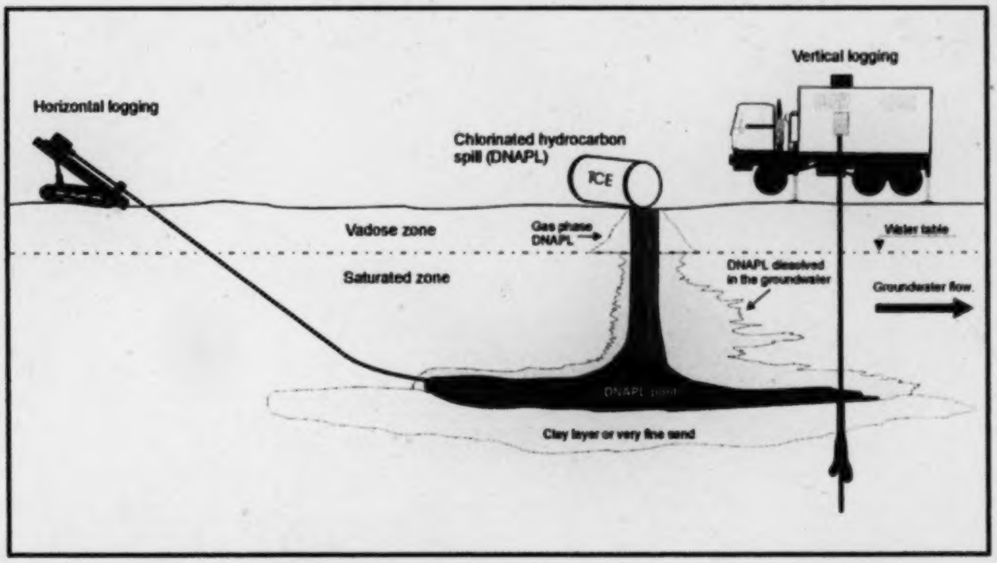
Vertical logging
Horizontal logging
Chlorinated hydrocarbon spill (DNAPL)
TCE
Vadose zone
Gas phase DNAPL
Water table
Saturated zone
DNAPL dissolved in the groundwater
Groundwater flow
DNAPL pool
Clay layer or very fine sand

Figure 1.6 – Vertical logging increases the potential for the development of new pathways of continued vertical DNAPL migration (modified from Fetter 1993).

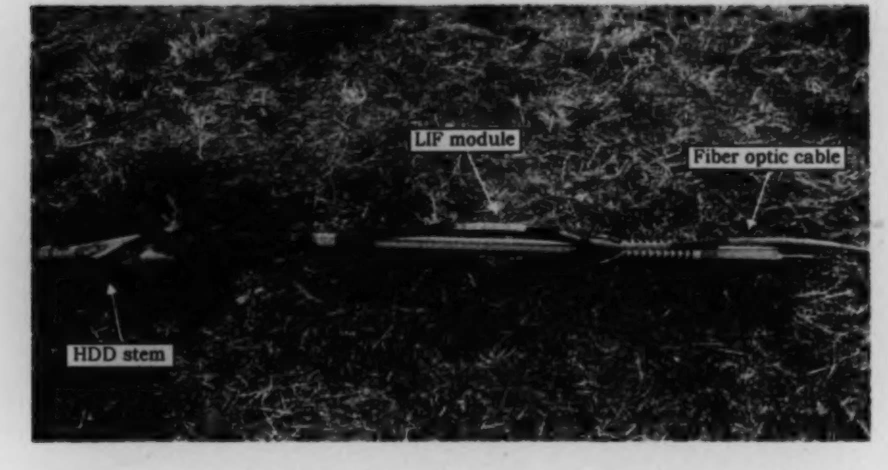
LIF module
Fiber optic cable
HDD stem

Figure 1.7 – Laser induced fluorescence (LIF) sensor coupled with an HDD for hydrocarbon/DNAPL detection (modified from Nielsen 1997).

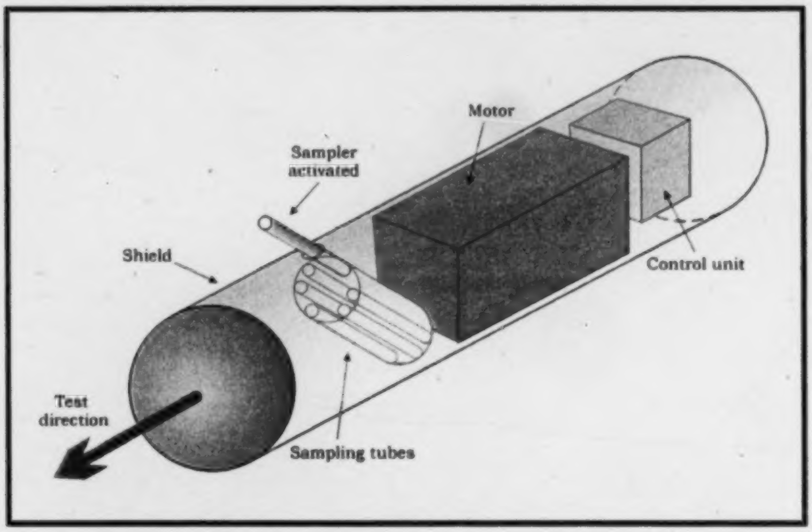
Motor
Sampler activated
Shield
Control unit
Test direction
Sampling tubes

Figure 1.8 – Schematic of the multiple-port soil sampler (modified from Ariaratnam et al. 2000).

## 1.5 SUMMARY

In some special situations, the use of vertical boreholes and vertical logging and sampling tools for geotechnical/geoenvironmental site investigation are not optimal, practical or are even impossible. Examples of such situations are:

- target zones located under surface/subsurface obstacles;
- along linear structures such as tunnels for which a large number of vertical boreholes would be necessary to obtain enough information to characterize the subsoil or to locate sand pockets along a tunnel alignment;
- contaminant plums, which are usually much longer and wider than they are thick; it may be much more effective to delineate the lateral extent of contamination plumes or pools by following a horizontal path rather than multiple vertical ones, and
- when searching for DNAPLs using vertical devices it increases the potential for the development of new pathways of continued vertical DNAPL migration.

The above examples show that there is a place for a device to obtain subsoil information via a horizontal path rather than a vertical one. Horizontal Directional Drilling (HDD) technology with its ability to create a borehole with an entry and an exit point has opened the possibility to develop such a device.

The scope of this research is to study the feasibility and develop a new probe using Cone Penetration Test (CPT) technology coupled with HDD technology for horizontal soil/contamination site investigation.

# CHAPTER 2

# Horizontal Directional Drilling (HDD) Technology

## 2.1 INTRODUCTION

Horizontal Directional Drilling (HDD) technology was developed by the oil and gas industry and driven by the particular needs of the industry. The technology has been developed to intersect multiple fracture systems within a reservoir and to prevent premature water or gas intrusion which would interfere with oil production. Another attractive feature of HDD technology for the oil and gas industry is that the horizontal well provides a significantly greater contact surface area of exposure to the reservoir than a conventional vertical well (DOE 1993). This feature is significant because generally oil and gas reservoirs are much wider than they are thick. This technology has since been downsized to be a less costly operation to attend to the needs of the utility installation industry (Kramer et al. 1992; Kaback and Oakley 1996).

HDD technology uses specialized bits and drilling procedures to curve the borehole, while electronic sensors are used to monitor and adjust the borehole path. The bore is initiated at a relatively shallow angle from the ground surface (typically < 30°) and is gradually curved into a horizontal trajectory. There are two types of HDD boreholes. Blind boreholes terminate within the subsurface. Continuous boreholes return to the ground surface, making it accessible from both ends; Figure 2.1.

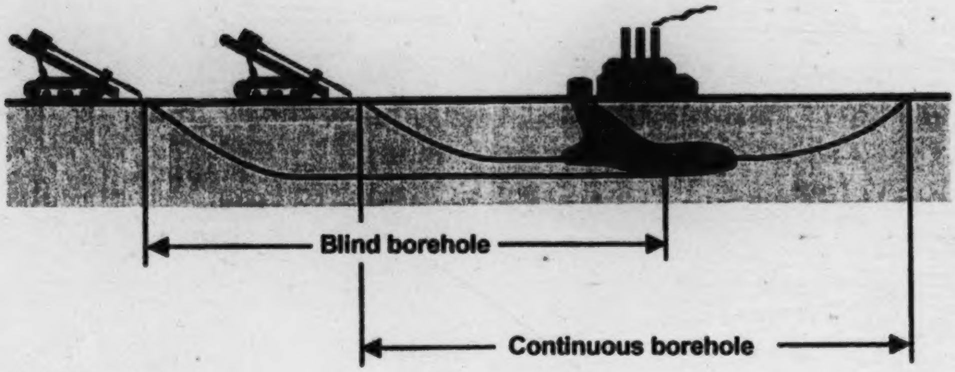

Figure 2.1 – HDD typical borehole configurations

The borehole path is defined by establishing the appropriate approach angle, the radius of curvatures and the step-off distance. Defining two of these criteria will automatically establish the third. The approach angle is the angle between the drill stem and the ground surface at the entry point. This angle may be between 7 and 90 degrees depending on the type of drill rig (Kaback and Oakley 1996); however, the most common approach angle used is between 7 and 25 degrees (CWM 1996). The curvature radius is classified in short (less than 45 m), medium (45 to 245 m) and long (greater than 245 m), with medium and long curvature radii being the most commonly used (CWM 1996). The distance between the borehole entry point and beginning of the horizontal section is the step-off distance and is usually a site specific condition due to surface obstacles or site boundary limitations.

HDD technology can create two basic types of bores, wellbores and boreholes. Wellbores are used when the main concern is to preserve the hydraulic conductivity of the host formation. This requires a special procedure to minimize or restore permeability damage caused by the drilling. Boreholes on the other hand have no concern for preserving the host formation's hydraulic conductivity. Wellbores are typically used in oil and gas recovery and currently also in environment applications. Boreholes are mainly used for pipe and utility installation.

Both applications start by drilling a pilot hole. Once the drill string emerges at the exit point, the drill bit is replaced by a back reamer. The pilot hole is then enlarged to the desired diameter while simultaneously pulling the product pipe back behind the reamer. Multiple reams may be required, sequentially enlarging the hole diameter. Currently HDD is able to install products up to 91 cm (36") in diameter (Allouche et al. 1998a).

Since the late 1980s HDD technology has successfully been applied to environmental remediation projects (Kaback and Oakley 1996). Horizontal wellbore applications for the remediation of soil contamination are attractive because soil contamination plumes or pools are usually much wider and longer than they are thick. Horizontal wellbores allow a higher screen-contamination contact area than do vertical wells. According to Parmentier and Klemivich (1996) one horizontal wellbore may replace up to ten vertical wells. Contamination plumes or pools beneath surface obstacles can easily be reached with a horizontal well, whereas using vertical wells could make the remediation process very difficult and expensive. The environmental remediation methods that have most benefited from horizontal wellbores are those used in ground water extraction for pumping and treatment, soil vapor extraction, air sparging, and other projects such as low air flow, for enhanced bioremediation, and free product recovery (Kaback and Oakley 1996).

A more recent and promising application of HDD technology is for soil sampling and logging for geoenvironmental and geotechnical site investigation (Ariaratnam et al. 2000). The first sampler used, coupled with HDD, was probably developed in the early 1990's (Cohen and Allouche 1998). Since then, several new areas of research, including the present one, have concentrated on the development of new, more advanced sampling and geophysical tools (Ariaratnam et al. 2000; Nielsen 1997).

A brief overview of HDD operational procedures and the equipment commonly used by the utility installation industry is given in the following section.

## 2.2 HDD OPERATIONAL PROCEDURE

Horizontal directional drilling can be divided into three main components:

- the power system;
- a special drilling component, and
- the guidance system.

The features and operational principles of each of these components are discussed below.

### 2.2.1 THE POWER SYSTEM

HDD is powered by a directional drill rig. The basic components of a HDD drill rig are shown in Figure 2.2. Though not shown in this Figure, the drill rig also has a pump for the injection of drilling fluid. Drill rigs are usually classified into three groups according to their thrust/pullback capability as shown in Table 2.1.

Presently there are 17 HDD rig and accessories manufacturers in North America (Allouche et al. 1998). Charles Machine Works Inc. and the Vermeer Manufacturing Company are the biggest manufacturers in this field. During the course of this research, it was possible to conduct the HD-PB-CPT test using drill rigs manufactured by both of these companies. Prototype 1 of the HD-PB-CPT was field tested using a Vermeer Navigator D24x40 (Figure 2.3a). Prototype 2 used a Charles Machine Works Inc. Ditch Witch Jet Trac JT1720 (Figure 2.3b). Both drills are classified as midi size rigs.

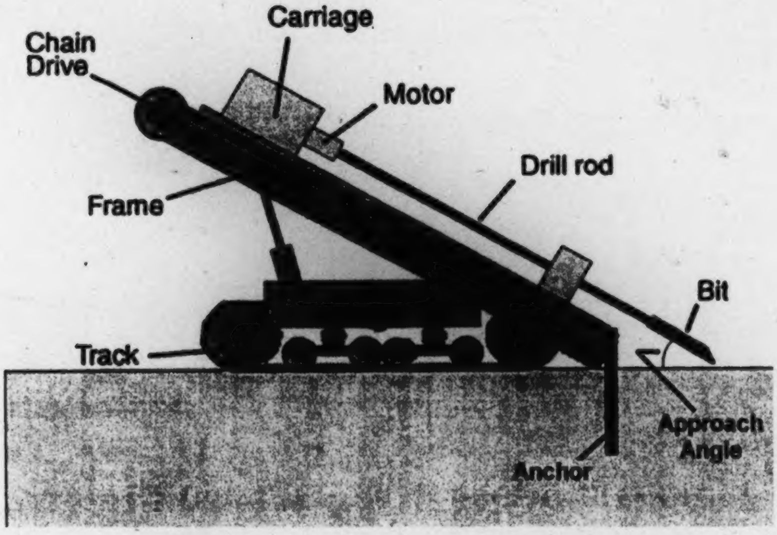

Figure 2.2 – HDD drill rig components

Table 2.1 – Directional Drill Rigs Groups (modified from CMW 1996)

| | **Mini Rigs** | **Midi Rigs** | **Maxi Rigs** |
|---|---|---|---|
| Thrust/pullback | <66.7 kN | 66.7 to 444 kN | > 444 kN |
| Maximum torque | 2.7 kN·m | 2.7 to 27 kN·m | 27 kN·m |
| Drill distance* | < 200 m | 200 to 600 m | > 600 m |

* Assuming a nominal 30.48 cm (12") diameter borehole

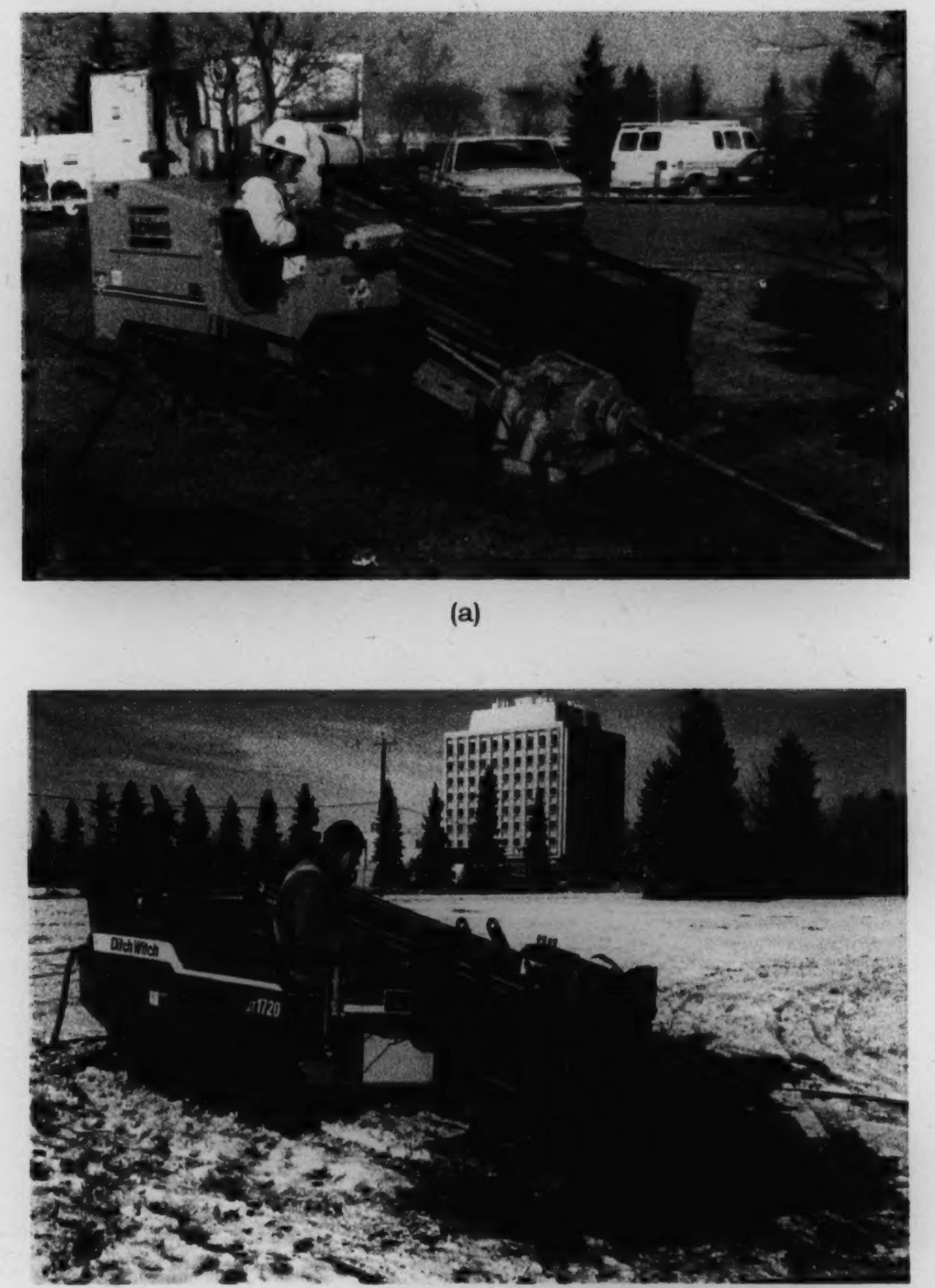
Ditch Witch
JT1720

(a)

(b)

Figure 2.3 – Horizontal Directional Drill rigs: a) Vermeer Navigator D 24x40 and b) Ditch Witch JT 1720.

### 2.2.2 SPECIAL DRILLING COMPONENT

Horizontal directional drilling uses a downhole assembly that creates a borehole and induces a curved trajectory. The trajectory is curved using a special tool that is eccentric with respect to the axis of the drill stem. To drill a straight borehole the drill string is rotated and pushed forwards simultaneously, as shown in Figure 2.4. To change the borehole direction, the rotation is stopped and the drill bit is positioned in the new target direction. The drill bit is then pushed against the soil, and because of the drill bit eccentricity the entire assembly is deflected towards the target direction (Figure 2.4). Once the new direction is achieved, drill string rotation is resumed.

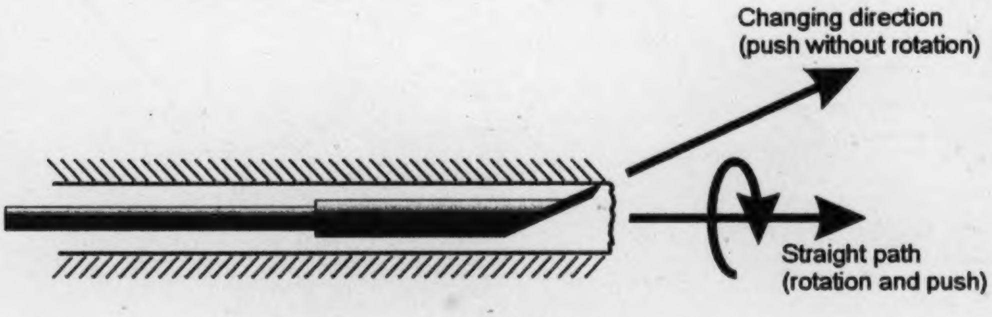

Figure 2.4 – Directional drilling steering.

The most common types of downhole steering tools used in HDD in utility installation are compaction drilling tools and mud motors (Allouche et al. 1998). Compaction drilling tools are used to drill through unconsolidated and soft to medium consolidated soils such as sand, silt, clay and soft sandstone. Figure 2.5 shows an example of a compaction drilling tool. Mud motors are used in hard soils to medium rocks. The mud motor uses a pressurized drilling fluid to rotate the cutting bit. The main advantage of the mud motor is that it reduces drill stem rotation and allows for drilling of boreholes with a short radius. A small bend in the drill string makes steering possible just behind the cutting head, which creates the eccentricity needed to deflect the tool when it is not being rotated (Figure 2.6).

Figure 2.5 – Compaction type drilling bit

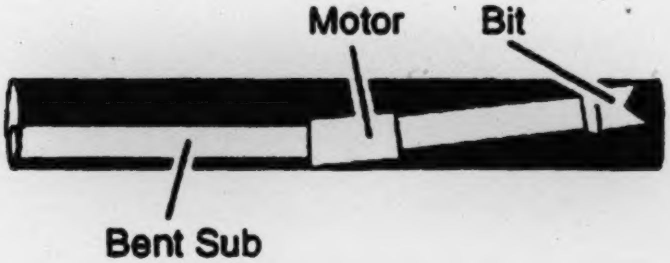

Figure 2.6 – Downhole mud motor (modified from CMW 1996).

### 2.2.3 THE GUIDANCE SYSTEM

There are two basic guidance systems or tracking methods used to locate the position, depth, and orientation of the drilling head during an HDD operation. These systems are known as the Electronic Beacon system (walkover method) and the Magnetometer and Accelerometer system (wire-line method).

The Electronic Beacon system is a battery operated transmitter that is housed behind the drill bit as shown in Figure 2.7. The transmitter sends a radio signal from the bottom of the borehole that is read by a hand-held receiver unit at the surface. The receiver displays four types of information to the operator: the *radio signal strength*; the *drill head depth*; the *inclination or pitch* (in the vertical plane) and the *drill face orientation*. The *radio signal strength* defines the drill head position. Once the receiver operator is approximately on top of the drill head, he swings the receiver across the borehole trajectory and monitors the radio signal strength. The maximum signal strength means that the receiver is right on top of the drilling head. The *drill head depth* can be displayed in inches or meters. The *Inclination or pitch* is expressed in percentage in relation to the drill rod length. The *drill face orientation*, is referenced to a 12 hour clock, i.e. if the indicator shows 6 o'clock the slant on the drill head is pointing down. Figure 2.8 shows a view of the information displayed by a receiver during an operation. At the drill rig, in front of the operator, there is also a remote monitor that receives and displays the same information obtained from the receiver unit. With the information displayed on the remote monitor, associated with that furnished by the receiver operator, the rig operator is able to navigate the drilling head. This method is often called the walkover method because the receiver operator at the surface keeps track of the drill head by walking over the transmitter. Figure 2.9 (a) and (b) show a view of the drilling head tracking using the walkover method, using a DigiTrak unit and a Subsite unit respectively. The accuracy of the walkover method is within at least 5% of the vertical distance (CMW 1996). Currently there are transmitters available that allow a maximum operational depth of 30 meters (Allouche et al. 1998a).

Figure 2.7 – Transmitter unit.

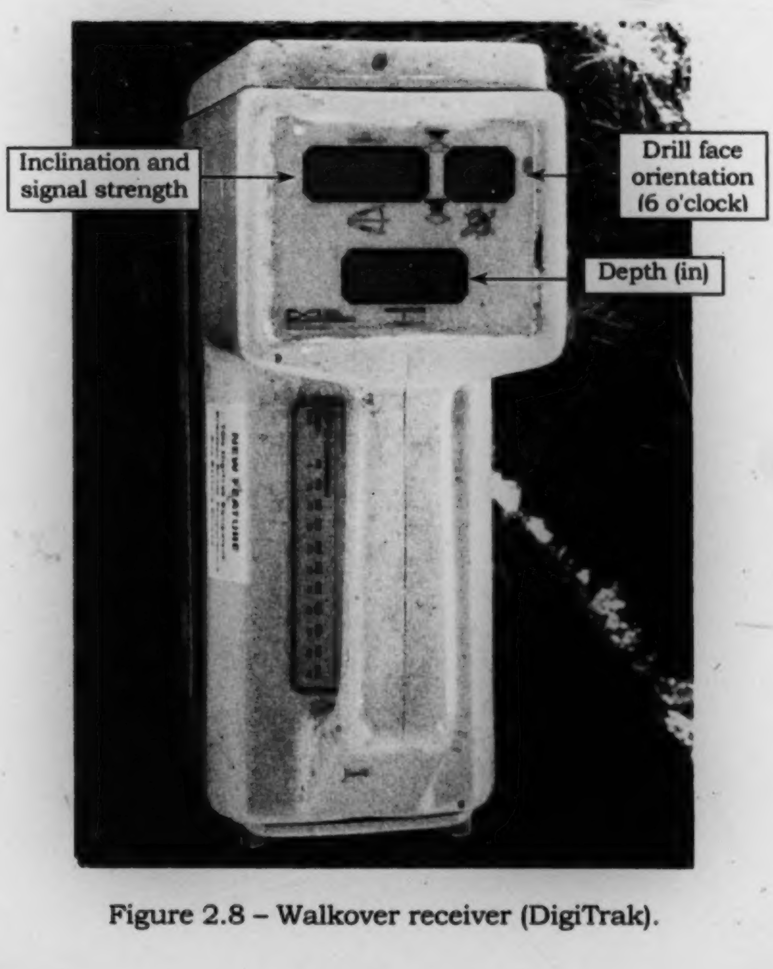
Inclination and signal strength
Drill face orientation (6 o'clock)
Depth (in)

Figure 2.8 – Walkover receiver (DigiTrak).

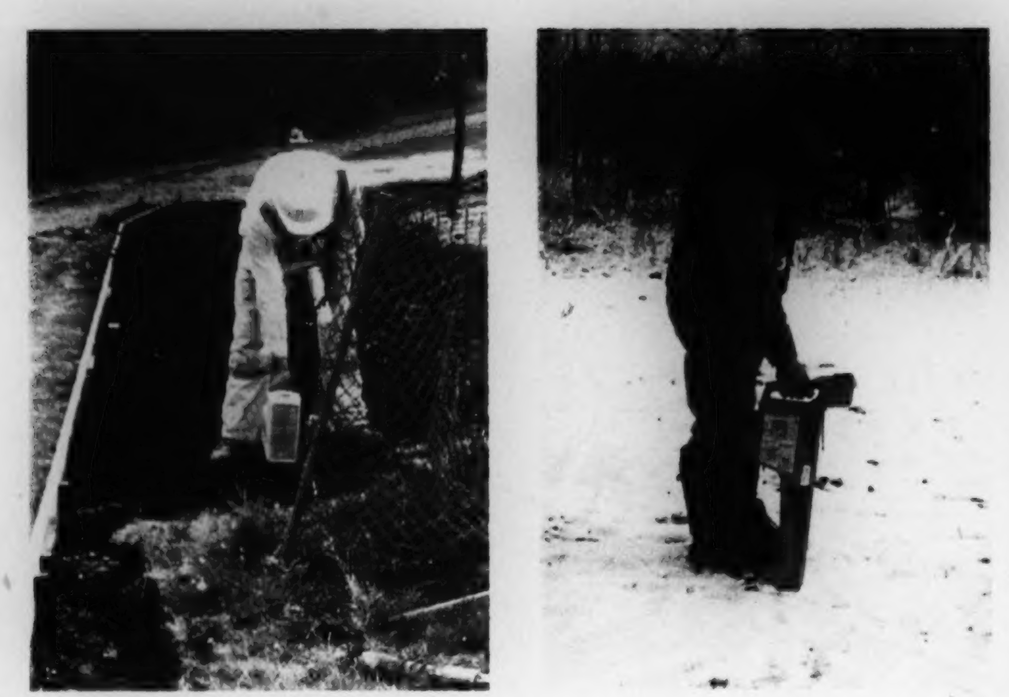

(a) (b)

Figure 2.9 – Guidance system by walkover method:
a) DigiTrak unit and b) Subsite unit.

In some situations when it is not possible to use the walkover method or when working at depths greater than 30 meters is required, a Magnetometer and Accelerometer wire-line system can be employed (Allouche et al. 1998). This system uses three magnetometers to measure the azimuth (the rotation about the horizontal plane) of the drill head in the earth's magnetic field, and three accelerometers to measure the pitch of the drill head in the earth's gravitational field. This guidance system sends the information gathered downhole by wire line to a computer on the surface which then calculates and displays the drilling head azimuth, pitch and drill face orientation. This system is considered to be the most accurate (2 % of the vertical depth); however, it is expensive and needs skilled operators. It is required when surface obstacles prevent walkover method or when drilling boreholes deeper than 30 m.

## 2.3 SUMMARY

The Horizontal Directional Drilling (HDD) technique, developed primarily by the oil and gas industries and later down-scaled to fit the needs of the utility industries, has the unique characteristic of providing a borehole with an entry and an exit point. HDD uses specialized drill tools and a guidance system to steer the borehole. The borehole starts from the surface at an angle (usually between 7° to 25°) from which the path of the borehole may be gradually steered into horizontal position as it reaches a desired depth. When the horizontal portion of the borehole is completed the bit is steered up again on a curved path to the predefined exit point.

The application of the HDD technique is expanding rapidly into other fields, such as for environmental soil remediation and geotechnical/geoenvironmental site investigation, rather than only utility installation.

# CHAPTER 3

# Cone Penetration Test (CPT) Technology

## 3.1 INTRODUCTION

A great number of publications are available regarding the Cone Penetration Test (CPT), (e.g., Sanglerat 1972; Schmertmann 1978; de Ruiter 1982; Meigh 1987; Robertson and Campanella 1988; Miran and Briaud 1990; Lunne et al. 1997; Robertson 1998). In 1995 an international symposium exclusively dedicated to cone penetration testing CPT'95 was held in Linköping, Sweden, generating a three volume set of proceedings. The most recent and comprehensive publication about the CPT is given in a book by Lunne et al. (1997). This publication has the added advantage of having an exclusive chapter dedicated to the geoenvironmental applications of penetration testing.

Presently, there are also several standards available about CPT test procedures. Some of these are: the International Reference Test Procedure (IRTP) developed by the International Society of Soil Mechanics and Foundation Engineering (ISSMFE 1999); The Swedish Standard for Cone Testing, developed by the Swedish Geotechnical Society (1992) and the American Society for Testing Materials - ASTM standards D 3441 (1994) and D 5778 (1995).

The main scope of this chapter is not to provide a comprehensive review of the state of the art of CPT technology, but rather to provide some basic information about its principles and applications. This chapter is intended to make it easier for those who are unfamiliar with this technology to understand the versatility of the CPT, and to understand why this technology was chosen to be coupled with HDD to produce a new logging device.

A brief comprehensive illustration of CPT versatility is shown in Table 3.1. This table, assembled by Robertson (1986) and adjusted by Lunne et al. (1997), shows a comparison of a partial list of the major in situ test methods and their applicability to obtain geotechnical information. An appraisal of this table shows that CPT methods present the highest rating, followed closely by the Self-boring pressuremeter (SBPT). However, the SBPT does not provide a continuous soil profile and it uses much more expensive technology.

Table 3.1 – Comparison of applicability and usefulness of in situ tests (modified from Robertson 1986).

| Test Method | Geotechnical information | | | | | | | | | | | | | Ground conditions | | | | | | |
|---|---|---|---|---|---|---|---|---|---|---|---|---|---|---|---|---|---|---|---|---|
| | Soil type | Profile | Piezometric pressure | Angle of friction | Undr. shear strength | Density | Compressibility ($m_v$, $C_c$) | Rate of consol. $C_h$, $C_v$) | Permeability ($k$) | Shear & Young Mod. | In situ stress ($K_0$) | Stress history (OCR) | Stress-strain curve | Hard rock | Soft rock – till, etc. | Gravel | Sand | Silt | Clay | Peat - organic |
| Dynamic cone (DCPT) | C | B | – | C | C | C | – | – | – | C | – | C | – | – | C | B | A | B | B | B |
| Mechanical cone | B | A/B | – | C | C | B | C | – | – | C | C | C | – | – | C | C | A | A | A | A |
| Electric cone (CPT) | B | A | – | C | B | A/B | C | – | – | B | B/C | B | – | – | C | C | A | A | A | A |
| Electric piezocone (CPTU) | A | A | A | B | B | A/B | B | A/B | B | B | B/C | B | C | – | C | – | A | A | A | A |
| Electric seismic piezocone (SCPTU) | A | A | A | B | A/B | A/B | B | A/B | B | A | B | B | B | – | C | – | A | A | A | A |
| Acoustic probe | B | B | – | C | C | C | C | – | – | C | – | C | – | – | C | – | A | A | A | A |
| Flat plate dilatometer (DMT) | B | A | C | B | B | C | B | – | – | B | B | B | C | C | C | – | A | A | A | A |
| Field vane shear test (VST) | B | C | – | – | A | – | – | – | – | – | – | B/C | B | – | – | – | – | | A | B |
| Standard penetration test (SPT) | A | B | – | C | C | B | – | – | – | C | – | C | – | – | C | B | A | A | A | A |
| Resistivity probe | B | B | – | B | C | A | C | – | – | – | – | – | – | – | C | – | A | A | A | A |
| Total stress cell | – | – | – | – | – | – | – | – | – | – | B | B | – | – | – | – | – | C | A | A |
| $K_0$ stepped blade | – | – | – | – | – | – | – | – | – | – | B | B | – | – | – | – | B | A | A | B |
| Plate load | C | – | – | C | B | B | B | C | C | A | C | B | B | B | A | B | B | A | A | A |
| Screw plate | C | C | – | C | B | B | B | C | C | A | C | B | – | – | – | – | A | A | A | A |
| Borehole permeability | C | – | A | – | – | – | – | B | A | – | – | – | – | A | A | A | A | A | A | B |
| Hydraulic fracture | – | – | B | – | – | – | – | C | C | – | B | – | – | B | B | – | – | C | A | C |
| Borehole shear | C | C | – | B | C | – | – | – | – | C | – | C | – | B | B | C | B | B | C | C |
| Pre-bored pressuremeter (PBPT) | B | B | – | C | B | C | B | C | – | B | C | C | C | A | A | B | B | B | A | B |
| Self-boring pressuremeter (SBPT) | B | B | A | B | B | B | B | A | B | A | A/B | B | A/B | – | B | – | B | B | A | B |
| Full displacement pressuremeter (FDPT) | B | B | – | C | B | C | C | C | – | A | C | C | C | – | C | – | B | B | A | A |
| Crosshole/downhole/surface seismic | C | C | – | – | – | – | – | – | – | A | – | B | – | A | A | A | A | A | A | A |

Note: A = high applicability, B = moderate applicability, C = limited applicability, – = not applicable.

The other sections of this chapter provide further details about CPT technology and its use in geotechnical and geoenvironmental site investigation.

## 3.2 CPT PRINCIPLES

The cone penetration test is also known as the Static Cone Penetration Test, the Quasi-Static Penetration Test, the Dutch Sounding Test and as Dutch Deep Sounding Test. If pore pressure is measured during penetration, the test is usually called the Piezocone Test whose acronym is CPTU.

The CPT can be divided in two main cone groups: the mechanical and the electrical. The mechanical cone has a double-rod system and works in a way similar to that of the first cone developed in the 1930's in the Netherlands. Details of this first CPT will be given in the next section.

Mechanical cones are still used today because of their low cost and operative simplicity. However, the rapid decrease in the cost of electronic devices and the advantages presented by electric cones has made the use of mechanical cone less attractive. Electrical cones have the following advantages over the mechanical cone:

- more rapid testing procedure;
- continuous data recording;
- higher accuracy and repeatability;
- real time plotting of the results and;
- capability of incorporating additional sensors.

This section, therefore, will concentrate on providing information and describing the electrical CPT/CPTU.

### 3.2.1 EQUIPMENT AND TEST DESCRIPTION

The standard CPT or CPTU test consists of pushing a 60° apex angle cone into the ground at a constant rate of 2 cm/sec. The cone is usually made of stainless steel and has a cross section area of 10 $cm^2$ (3.57 cm in diameter). Right above the cone there is a cylindrical sleeve known as the friction sleeve, also made of stainless steel with the same diameter as the cone and an outside surface area of 150 $cm^2$ and 13.37 cm in length. When performing a CPTU test the pore water pressure is usually measured behind the cone ($u_2$), but it can also be measured in two other positions, on the cone ($u_1$) and behind the friction sleeve ($u_3$), as illustrated in Figure 3.1. The position of the porous element influences the pore pressure values (Lunne et al. 1997); therefore, when performing a CPTU test it is important to indicate in the test report the porous element location, i.e., $u_1$, $u_2$ or $u_3$.

CPTs with larger and smaller diameters than the standard ones described are also available. Larger diameter cones such as those with cross sections of 15 $cm^2$ are usually used when there is a need to incorporate additional sensors or in very soft materials. Smaller diameter cones are usually used when there is a need to detect the presence of very thin layers or to perform pore pressure dissipation tests in very low permeability clay.

Three parameters are measured during the CPT penetration: cone resistance ($q_c$), also called tip resistance, sleeve friction resistance ($f_s$), sometimes referred to as side or skin resistance, and cone penetration depth. The total bearing force by the cone ($Q_c$) during penetration, divided by the cross section area of the cone, gives $q_c$; the total force acting on the friction sleeve ($F_s$), divided by the friction sleeve area, gives $f_s$. Despite not being directly measured, the friction ratio ($R_f$), expressed by Equation 3.1, is an important parameter that aids in soil identification in CPT/CPTU tests. Generally clayey soils have high friction ratios $R_f > 2\%$, while sandy soils have low friction ratios $R_f < 1\%$, (Robertson 1986).

$$R_f = \frac{f_s}{q_c} \times 100\% \qquad [3.1]$$

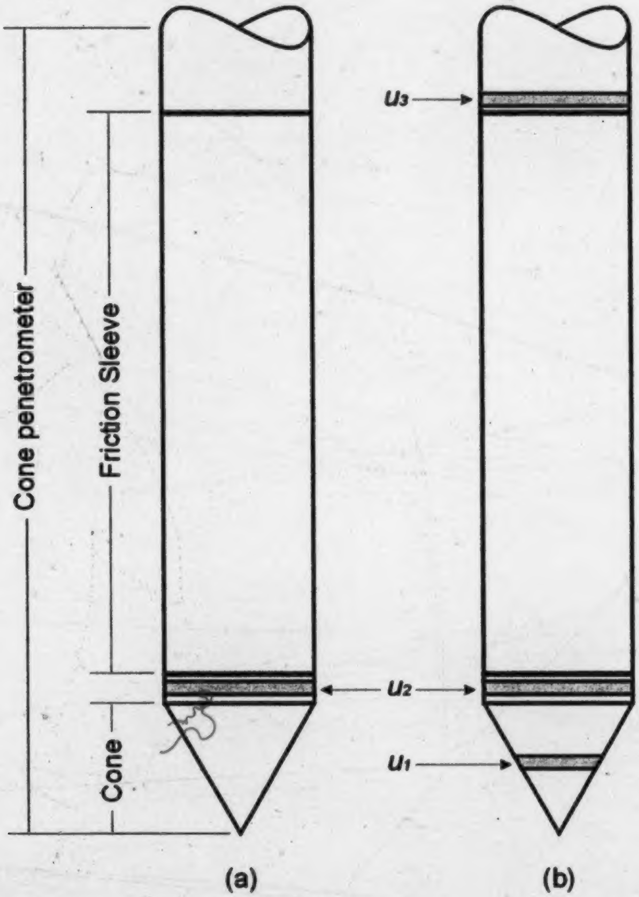
Cone penetrometer
Friction Sleeve
Cone
u3
u2
u1
(a)
(b)

Figure 3.1 – Electrical cone penetrometer sketch: a) standard CPTU, and b) other typical locations of pore pressure measurement points.

A fourth parameter, pore water pressure, is also measured when performing a CPTU test during penetration. The pore water pressure ($u_1$, $u_2$ or $u_3$) measured during the CPTU test is the result of the sum of the hydrostatic or equilibrium pore water pressure ($u_0$) and the excess or dynamic pore water pressure ($\Delta u$) that is being generated by the penetration of the cone, which is a function of the type and properties of the soil (de Rutier 1982). Soil identification, especially that of partially drained soils like fine sands, silts, and clayey silts, and also the detection of thin permeable layers embedded in clay can greatly be improved by measuring the pore water pressure during penetration (Robertson 1986). The equilibrium pore water pressure can also be monitored after a stop in penetration and dissipation of the dynamic pore water pressure has occurred.

The load acting on the cone ($Q_c$) and acting on the friction sleeve ($F_s$) is measured by electrical strain gage load cells located inside the probe. There are many different types of load cell configurations depending on the manufacture. They can be divided in two principal types:

- independent load cells, for which the cone resistance and the friction sleeve resistance are measured by two separated load cells, and
- dependent load cells, also called subtractive type load cells; for these cells the friction sleeve load cell measures the summation load from both the cone and the friction sleeve; the load, acting only on the friction sleeve, is obtained by subtracting the value of the cone load cell.

The subtractive type load cell is the simplest and easiest to build; this type was, therefore, the one selected to be used in the HD-PB-CPT. The three most commonly used load cell design types for use in CPTs are illustrated in Figure 3.2.

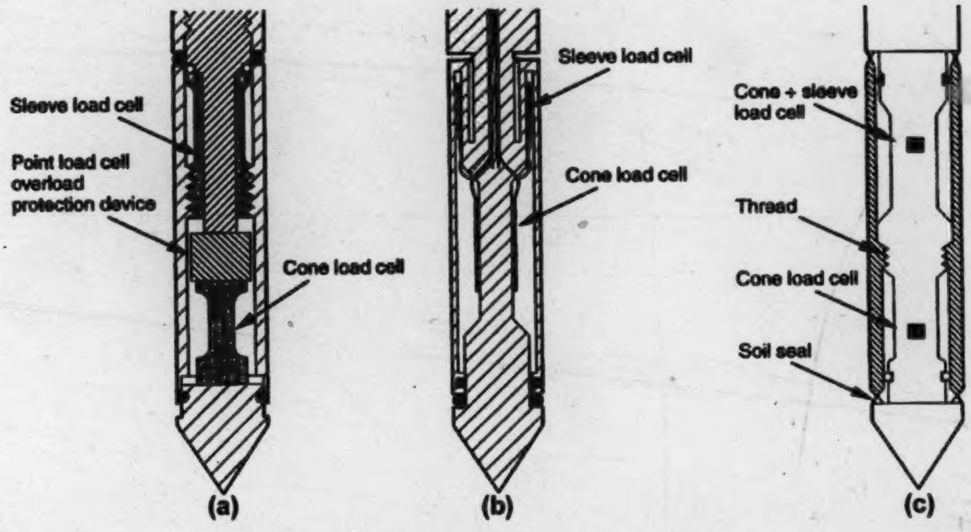
Sleeve load cell
Point load cell overload protection device
Cone load cell
Sleeve load cell
Cone load cell
Cone + sleeve load cell
Thread
Cone load cell
Soil seal
(a)
(b)
(c)

Figure 3.2 – Different load cells designs for CPTs: a) independent load cell where the cone and friction sleeve load cells are in compression; b) independent load cell where the cone load cell is in compression and friction sleeve load cell is in tension; c) dependent load cell, the subtractive type (modified from Lunne et al. 1997).

As mentioned previously one of the greatest advantages of the electric CPT is its capability of incorporating additional sensors. Thus, inclinometers (slope sensors) have also been included to monitor the test alignment (de Rutier 1982). It is advisable that for a penetration depth in excess of 15 m, slope sensors should be used to allow for any correction to be made to the depth of penetration (Lunne et al. 1997). A very useful addition was the incorporation of a velocity seismometer by Campanella and Robertson (1984). The seismometer allows the measurement of the shear wave velocity ($V_s$) during pauses in penetration. Once $V_s$ is known, the soil shear modulus ($G$) can be estimated by the Equation 3.2:

$$G = \rho V_s^2 \qquad [3.2]$$

where $\rho$ is the soil bulk density.

The seismic CPTU is a very powerful tool for site investigation since it provides an extremely rapid, reliable, and economic means of determining and evaluating the soil stratigraphy, strength, and modulus in one sounding test (Robertson 1986).

The CPT/CPTU test results are generally presented in real time by means of graphs. Cone resistance, sleeve friction resistance, friction ratio, and pore water pressure are all plotted versus depth for the CPTU. Sometimes a soil type profile is also plotted in real time. Of course, depending on which kind of sensors the CPT/CPTU is carrying, other plots are also possible, such as shear wave velocity, inclination, temperature, and pH. Examples of CPTU test results performed at the University of Alberta field laboratory site can be seen in Appendix 1.

The types of soil to which CPT/CPTU tests are mainly applied are soft to firm-stiff clays and sands. Gravel layers and boulders, heavily cemented zones and dense sand layers can restrict penetration (Robertson 1986). However, the development of heavy weight systems (300-400 kN) have allowed penetration depths to an average of 46 m in gravelly soils (Bratton et al. 1995). In soft soils penetration depth in excess of 100 m may be achieved (Robertson 1986).

### 3.2.2 PUSHING RIGS

The cone penetrometer driving equipment consists of hollow push rods; a thrust mechanism, usually a hydraulic jack; and a reaction system. This whole apparatus can be mounted on a light trailer or a truck. Using the light trailer has a disadvantage in that it requires earth anchors as a reaction system but for sites difficult to access, it might be the only way of performing the test. Presently, the most common system mounts the penetrometer rig on a truck or a tracked vehicle as shown in Figure 3.4 (a) and (b) respectively. The boxed enclosure also provides comfort for the crew, and it is ideal for the installation of the data acquisition system. An additional advantage is, when testing sites contaminated with hazardous materials, the rods can be decontaminated prior to entering the enclosure, thereby reducing the possibility of the crew being exposed to any hazardous material.

Typically, a hydraulic jack pushes 1 m long rod segments into the ground at 2 cm/second, pausing at the end of each stroke. Rods are then manually screwed together, as illustrated in Figure 3.4. The weight of the truck works as the reaction system and the truck's engine supplies the energy to run all the equipment. The thrust capability of a CPT truck is usually 200 kN because exceeding this load may cause the buckling of the standard 35.7 mm diameter push rods in softer upper soil layers (de Rutier 1982; Lunne et al. 1997). However, there are already heavy weight systems which use cones and rods of larger diameter (44.5 mm diameter). These cones and rods allow a total thrust of up to 400 kN (Bratton et al. 1995) to penetrate difficult soils such as gravels.

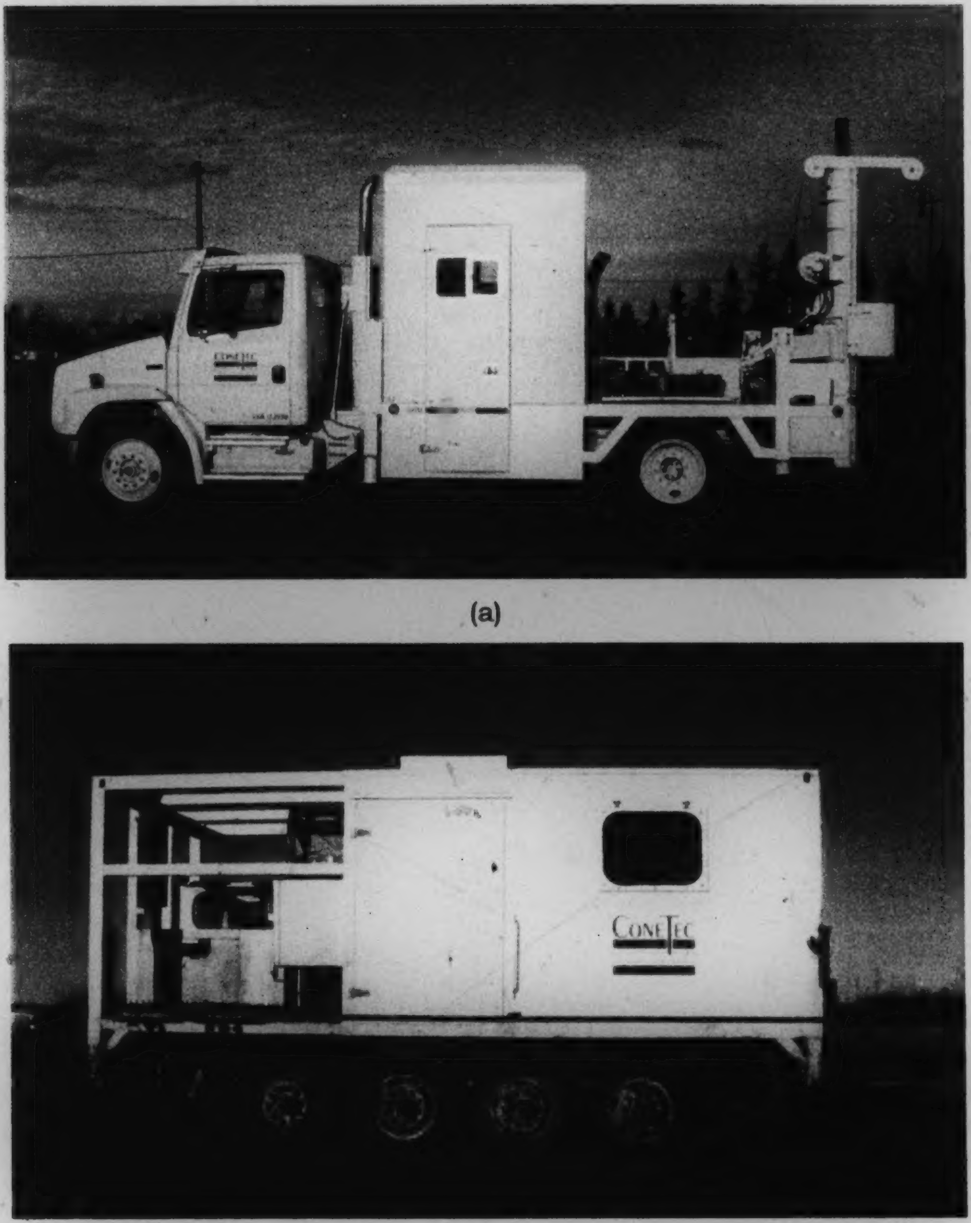
ConeTec
ConeTec

(a)

(b)

Figure 3.3 – Examples of truck-mounted CPT rigs: a) Wheel truck with rear auger and b) track CPT vehicle (courtesy of ConeTec Ltd.)

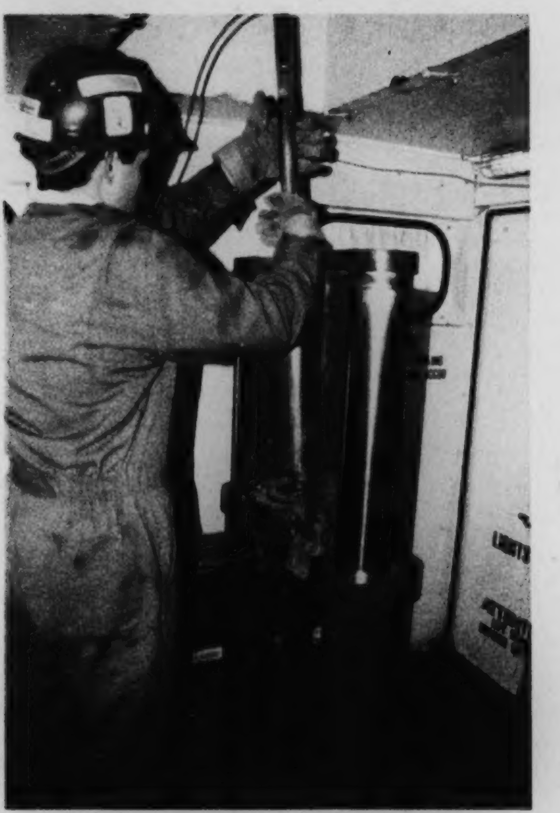

Figure 3.4 – Inside the CPT enclosure: adding a rod to advance the test with the hydraulic jack system.

## 3.3 A BRIEF HISTORY OF THE EVOLUTION OF THE CPT

New road development in the early 1930s in Holland created the need for a quick and inexpensive method of soil investigation to provide information about the consistency of alluvial soils. P. Barentsen (1936) an engineer at the Rijkswaterstaat (Department of Public Works), developed the first version of cone penetration test used today. Barentsen's cone apparatus consisted of a gas pipe of 19 mm (3/4") inside diameter that had a 15 mm diameter inner steel rod that could move up and down freely. At the end of this rod there was a 60° apex angle cone with cross section area of 10 $cm^2$ (35.7 mm in diameter), the same angle and area of today's standard CPT. Both the inner rod and the outer pipe were pushed down by hand and to the desired test depth, usually at each 50 cm, the outer pipe was held and the inner rod was pushed down 15 cm. A manometer placed on the top of the inner rod, as shown in Figure 3.51, was used to measure the soil resistance. The rate of penetration was 1 cm/sec, half of the rate used today. The test was advanced by screwing successive pieces of pipe 1 m in length to one another and repeating the testing procedure. Today the test is still being advanced by adding 1 m segments of rods. A similar test procedure is also used today by the mechanical cone penetrometer.

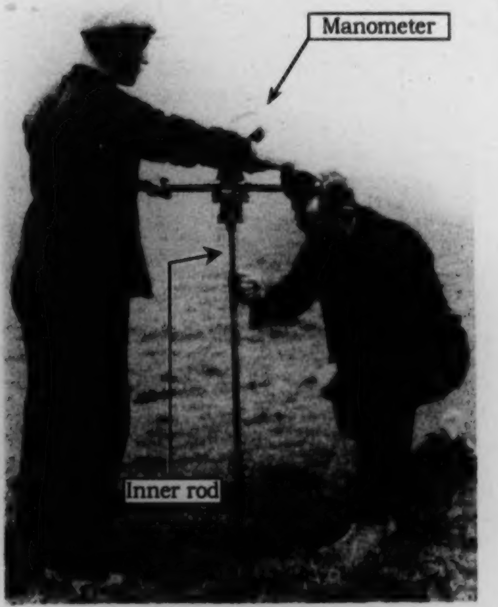

Figure 3.5 – Former cone penetration test (modified from Barentsen 1936).

The friction sleeve element was introduced by Begemann (1953, 1965) and he was also the first one to introduce the concept of friction ratio and how to use it to aid soil type classification. Penetrometers with pore pressure measurement devices started to be developed around the mid 1970s (Janbu and Senneset 1974; Schmertmann 1974; Torstensson 1975; Wissa et al. 1975). The first electrical cone was probably developed in the Second World War in Berlin (Broms and Flodin 1988). The first electric cone in Holland was developed in 1948 (Lunne et al. 1997). The first electrical cone that could measure local side friction was developed in 1957 by the Delft Soil Mechanics Laboratory (Lunne et al. 1997). Fugro and the Dutch State Research Institute together developed an electrical friction cone in 1965, whose shape and dimensions became the basis for the present International Reference Testing Procedure (Lunne et al. 1997).

More information about the historical background of penetrometer technology can be found in the comprehensive work by Sanglerat (1972) and Broms and Flodin (1988).

## 3.4 GEOTECHNICAL APPLICATIONS

Geotechnical in situ test methods can be divided into:

- specific test methods, and
- logging or stratigraphic profiling methods.

The former is used for measuring a soil's physical and mechanical properties at a specific point; these methods are usually expensive and time consuming. The latter are generally for stratigraphic profiling, but often they can also provide a preliminary evaluation of soil parameters based on empirical and semi-empirical correlations. Furthermore, when the site geology is uniform and well understood direct information from logging methods are commonly used for geotechnical design. Logging methods are usually faster and more economical than the specific test methods.

The CPT/CPTU is part of the logging test group. Currently there is no better tool to provide stratigraphic soil profiling where penetration is possible. The following section provides information about the three main applications of CPT/CPTU in site investigation. These applications are (Robertson 1998):

- to define soil stratigraphy and identify materials present,
- to provide a preliminary assessment of geotechnical parameters, and
- to provide information for direct geotechnical design.

The CPT/CPTU is not a tool to be used alone in site investigation, but rather should be complemented by boreholes and other tests. The CPT/CPTU results will provide information about the nature of the ground and where additional investigations should be carried out. In circumstances where the geology is well understood and uniform, and predictions of soil behavior based on CPT results have been confirmed, CPT data could be used alone for design. However, if a budget allows, it is always helpful to have some boreholes, sampling and testing to confirm the results.

### 3.4.1 SOIL STRATIGRAPHY AND CLASSIFICATION

There are three reasons why the electrical CPT/CPTU is such an excellent logging tool. First is its ability to obtain continuous or quasi-continuous logging data. Second is its remarkable repeatability. To better illustrate the CPT repeatability Figure 3.6 shows the average results and the average plus and minus one standard deviation from 6 CPT soundings performed at a uniform site. Figure 3.6 clearly shows that the deviation from the average is very small. The third reason is that the typical results of $q_c$ are high in sandy soils and low in clayey soils, whereas the value $R_f$ is low in sandy soils and high in clayey soils. This pattern has allowed researchers to develop several soil classification charts using both cone resistance and friction ratio.

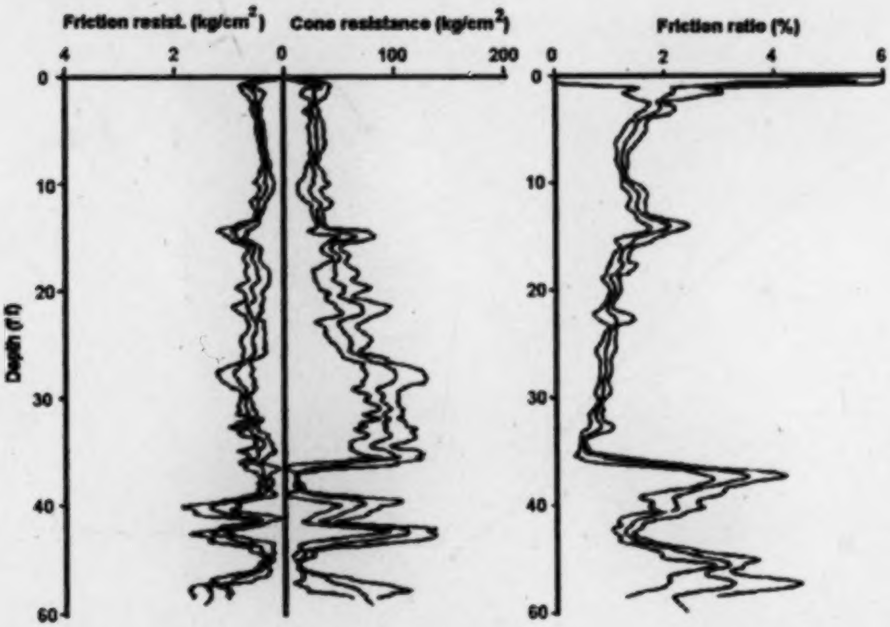

Figure 3.6 – CPT repeatability: average, and average plus and minus one standard deviation from 6 CPT tests performed at a uniform site (modified from Douglas and Olsen 1981).

Douglas and Olsen (1981) presented a comprehensive study of soil classification using CPT data. In their study they emphasize that CPTs are only able to provide a repeatable index of the soil aggregate behavior, CPT classification charts should not be used to provide an accurate prediction of soil classification based on grain size distribution, but rather as a reference to soil behavior type. Hence, soil classifications based on CPT data are usually referred to as soil behavior type classifications (SBTC). After extensive CPT data collection from several sites in California, Oklahoma, Utah, Arizona, and Nevada, Douglas and Olsen (1981) came up with the SBTC chart shown in Figure 3.7.

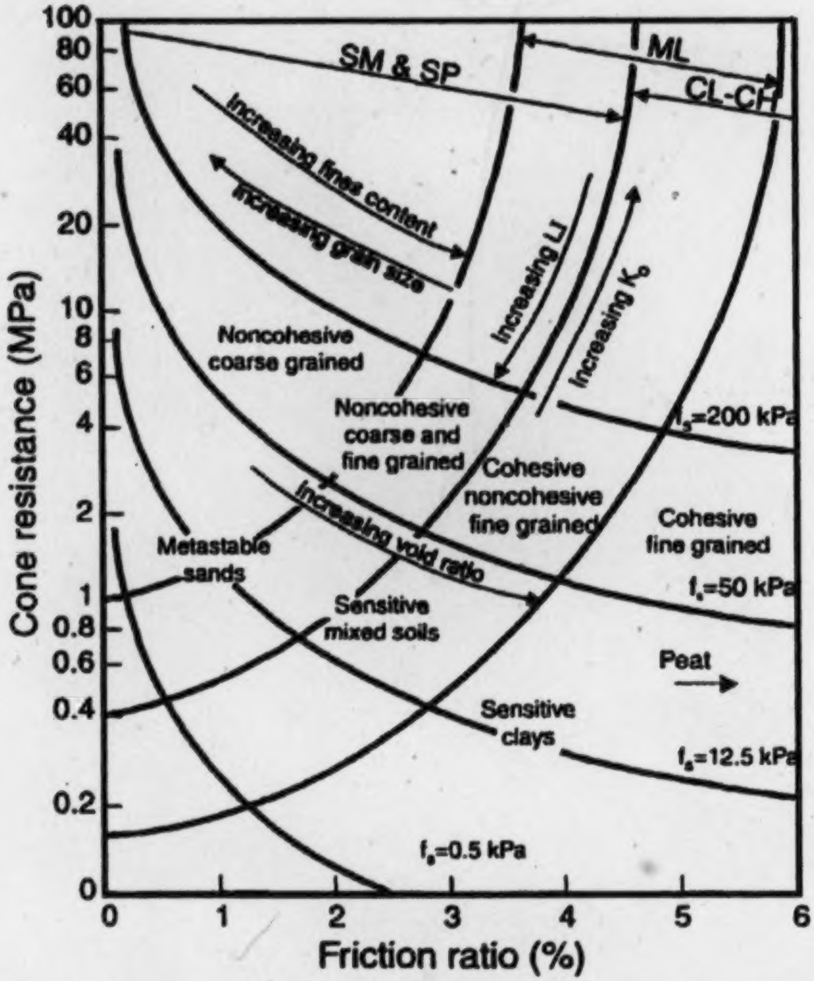

Figure 3.7 – CPT soil behavior type classification chart (modified from Douglas and Olsen 1981).

Usually sleeve friction measurement is not as accurate as pore water pressure measurements; therefore, some researchers such as Jones and Rust (1982) have proposed a soil classification chart for CPTU data using only the results of excess pore pressure and cone resistance. The chart proposed by Jones and Rust (1982) is reproduced in Figure 3.8. Robertson et al. (1986) have proposed an improved soil behavior type classification chart that uses all three measured parameters from the CPTU test, i.e., $q_c$, $f_s$ and $u_2$, (Figure 3.9). Robertson et al.'s (1986) chart also takes into account the water pressure effect on the measured cone resistance due to unequal end areas. Therefore, instead of using $q_c$ as input data it uses the corrected total cone resistance ($q_t$) as given by Equation 3.1. These charts also use as input data the normalized pore pressure parameter ratio, $B_q$, as shown in Equation 3.2.

$$q_t = q_c + u_2(1 - a) \qquad [3.1]$$

$$B_q = \frac{\Delta u}{q_t - \sigma_{vo}} \qquad [3.2]$$

where: $a$ is the cone area ratio that is approximately equal to the ratio of the cross-sectional area of the cone's shaft, divided by the cross section area of the base of the cone, $\Delta u$ is the excess pore pressure, and $\sigma_{vo}$ is the total overburden stress. For more information about water pressure effects on measuring CPTU data readers are referred to Lunne et al. (1997).

Cone and sleeve friction resistance values are affected by the overburden stress. Therefore, Robertson (1990) proposed normalized charts (Figure 3.10) to minimize overburden stress influence in the soil classification. For depths less than 20 m the charts in Figure 3.9 can still provide reasonable results (Robertson 1998).

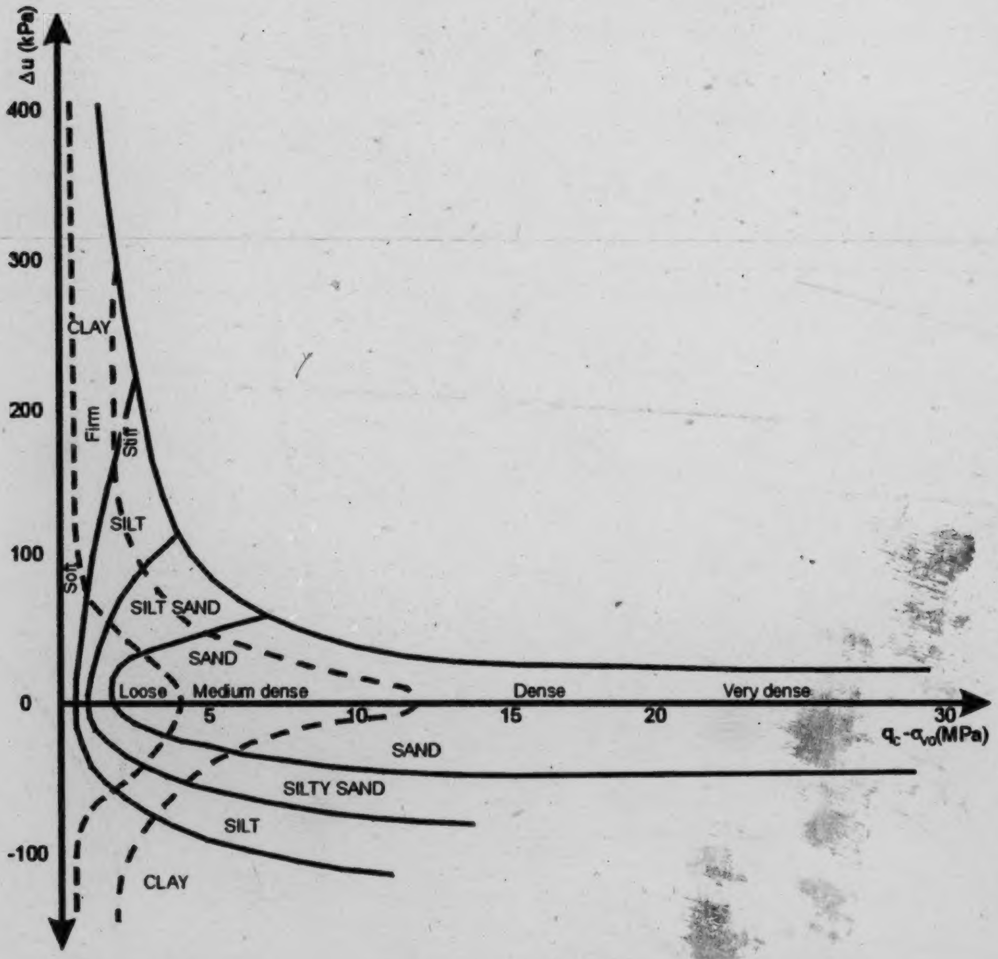

Figure 3.8 – Soil behavior type classification chart based on excess pore water pressure and cone resistance (modified from Jones and Rust 1982).

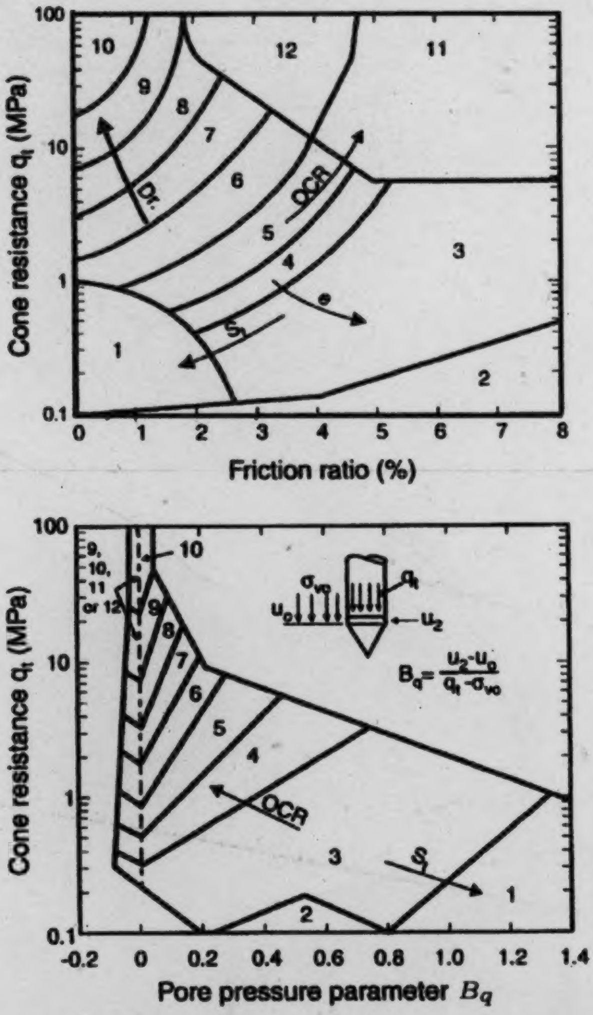

| Zone | Soil behavior type | Zone | Soil behavior type |
|---|---|---|---|
| 1 | Sensitive fine grained | 7 | Silty sand to sandy silt |
| 2 | Organic material | 8 | Sand to silty sand |
| 3 | Clay | 9 | Sand |
| 4 | Silty clay to clay | 10 | Gravelly sand to sand |
| 5 | Clayey silt to silty clay | 11 | Very stiff fine grained* |
| 6 | Sandy silt to clayey silt | 12 | Sand to clayey sand* |

* Overconsolidated or cemented

Figure 3.9 – Soil behavior type classification charts (after Robertson et al. 1986).

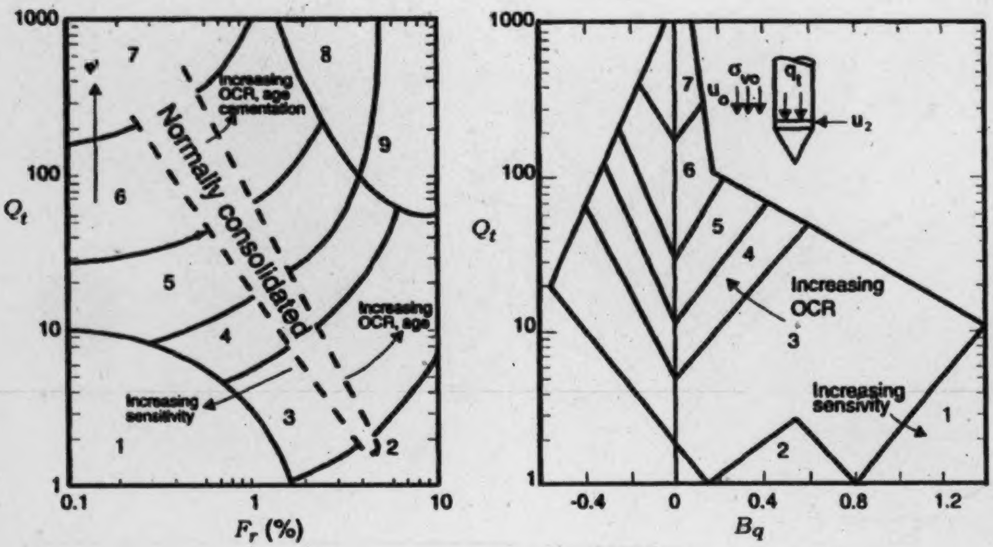

| Zone | Soil behavior type |
|---|---|
| 1 | - Sensitive, fine grained |
| 2 | - Organic soils-peats |
| 3 | - Clays-clay to silty clay |
| 4 | - Silty mixtures clayey silt to silty clay |
| 5 | - Sand mixtures; silty sand to sandy silt |
| 6 | - Sand; clean sands to silty sands |
| 7 | - Gravelly sand to sand |
| 8 | - Very stiff sand to clayey sand* |
| 9 | - Very stiff fine grained* |

* Heavily overconsolidated or cemented

$$Q_t = \frac{q_t - \sigma_{vo}}{\sigma'_{vo}}$$

$$F_r = \frac{f_s}{q_t - \sigma_{vo}} \times 100\%$$

$$B_q = \frac{\Delta u}{q_t - \sigma_{vo}}$$

$\sigma'_{vo}$ = overburden effective stress

Figure 3.10 – Normalized soil behavior type classification charts

(after Robertson 1990).

### 3.4.2 GEOTECHNICAL PARAMETERS

The cone penetration test induces complex changes in stress and strain around the cone tip. Due to the complexity of this problem, empirical and semi-empirical correlations are generally used to obtain geotechnical parameters from cone results for engineering design.

Analyses of cone penetration interpretations have also been performed by several authors based on bearing capacity theory, cavity expansion theory, flow models, and numerical models. Each of these approaches has its advantages and disadvantages (van den Berg 1994).

This section will briefly present some of the most common correlations used to obtain geotechnical parameters from CPT/CPTU tests. More detail and more in depth discussion regarding geotechnical parameters from cone penetration test is given by Schmertmann (1978), Robertson and Campanella (1983a and 1983b), Robertson and Campanella (1988), Lunne et al. (1997), and Robertson (1998).

It is worth mentioning that unless previous experience on the same geological formation exists and predictions based on CPT/CPTU results have been locally verified, these correlations should be used with caution and only as a guide or for preliminary assessment.

- Undrained Shear Strength ($S_u$)

Undrained shear strength from CPT/CPTU data can be estimated by means of Equation 3.3 (Robertson 1998).

$$S_u = \frac{q_t - \sigma_{vo}}{N_{kt}} \qquad [3.3]$$

where: $N_{kt}$ varies between 10 and 20, with 15 as an average. If pore pressure is not measured $q_c$ can be use instead of $q_t$.

Shear strength can also be estimated by using the excess pore water pressure (*Δu*) measured behind the cone by means of Equation 3.4 (Robertson 1998).

$$S_u = \frac{\Delta u}{N_{\Delta u}} \tag{3.4}$$

where: $N_{\Delta u}$ varies from 7 to 10.

- Overconsolidation ratio (*OCR*)

According to Robertson (1998) the easiest and the most reliable method to estimate *OCR* is by means of Equation 3.5.

$$OCR = k\frac{q_t - \sigma_{vo}}{\sigma'_{vo}} \tag{3.5}$$

where: *k* varies from 0.2 to 0.5 with an average of 0.3. For aged and heavily overconsolidated clays a higher value of *k* should be used.

- Hydraulic conductivity

An estimate of the formation's hydraulic conductivity (*k*) can be formulated as a function of the soil behavior type classification as shown in Table 3.2. A rough estimation of the horizontal hydraulic conductivity can be obtained from the chart proposed by Robertson et al. (1992) reproduced in Figure 3.11. This chart uses as input data the $t_{50}$, time for 50% dissipation of excess pore water pressure, obtained from CPTU dissipation test.

Table 3.2 – Evaluation of soil hydraulic conductivity based on a normalized soil behavior type classification chart by Robertson (1990).

| **Zone** | **Soil behavior type** | **Range of soil hydraulic conductivity (m/s)** |
|---|---|---|
| 1 | Sensitive fine grained | $3\text{x}10^{-9}$ to $3\text{x}10^{-8}$ |
| 2 | Organic soils | $1\text{x}10^{-8}$ to $1\text{x}10^{-6}$ |
| 3 | Clay | $1\text{x}10^{-10}$ to $1\text{x}10^{-9}$ |
| 4 | Silt mixtures | $3\text{x}10^{-9}$ to $1\text{x}10^{-7}$ |
| 5 | Sand mixtures | $1\text{x}10^{-7}$ to $1\text{x}10^{-5}$ |
| 6 | Sands | $1\text{x}10^{-5}$ to $1\text{x}10^{-3}$ |
| 7 | Gravelly sand to sand | $1\text{x}10^{-3}$ to 1 |
| 8 | Very stiff sand to clayey sand* | $1\text{x}10^{-8}$ to $1\text{x}10^{-6}$ |
| 9 | Very stiff fine-grained soil* | $1\text{x}10^{-9}$ to $1\text{x}10^{-7}$ |

*Overconsolidated or cemented

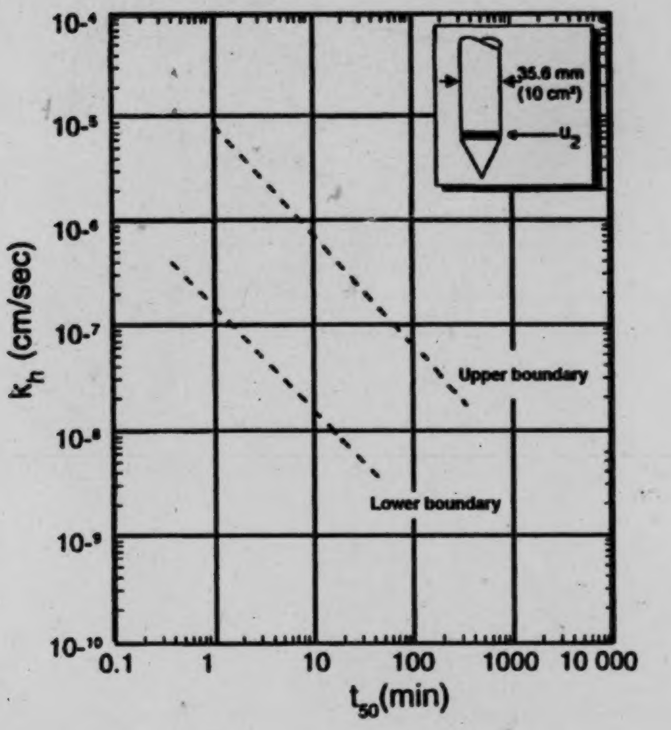

Figure 3.11 – Chart for the estimation of horizontal hydraulic conductivity from CPTU dissipation tests (Modified from Robertson et al. 1992)

- Friction angle ($\emptyset'$)

Based on the review of calibration chamber tests, Robertson and Campanella (1983) have proposed the chart shown in Figure 3.12 to estimate the drained friction angle ($\emptyset'$) of uncemented, unaged, moderately compressible and predominately quartz sand. Sand drained shear strength estimated from the CPT is affected by sand compressibility, among other factors; therefore, according to Robertson and Campanella (1983) the chart in Figure 3.12 will tend to predict a low friction angle for highly compressible sands.

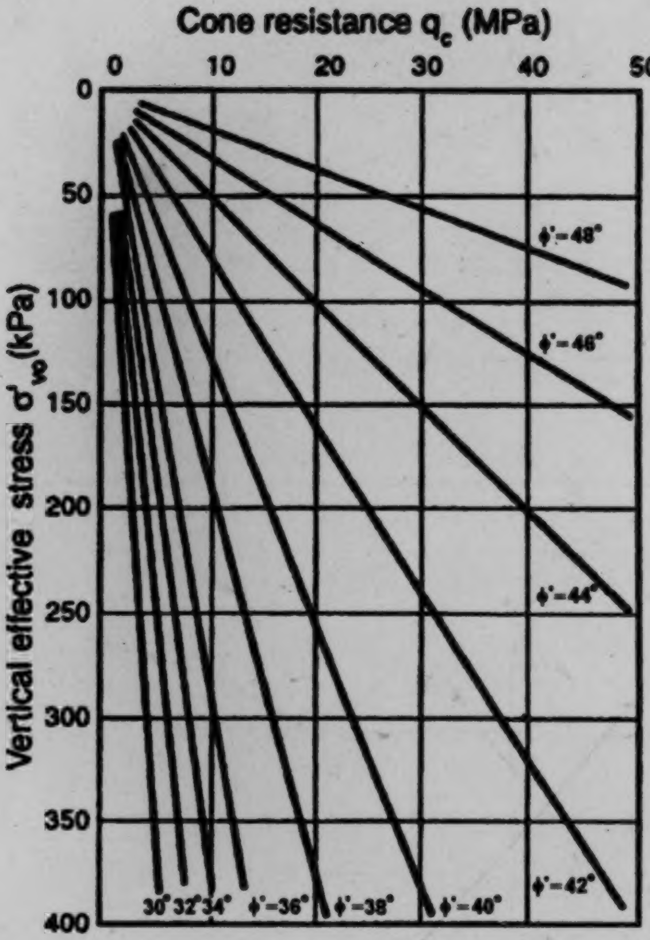

Figure 3.12 – Prediction of sand's friction angle from CPT (modified from Robertson and Campanella 1983)

- Density Index ($I_D$)

The density index, former relative density, is often used by geotechnical engineers to describe sand deposits; its value is given by Equation 3.6:

$$I_D = \frac{e_{max} - e}{e_{max} - e_{min}} \qquad [3.6]$$

where:

$e_{max}$ and $e_{min}$ are the maximum and minimum void ratio obtained in the laboratory by using standard test methods and $e$ is the natural soil void ratio measured in situ.

Density Index can be estimated from CPT data using the charts shown in Figure 3.13 (Lunne et al. 1997). Theses charts were based on the Equation [3.7] proposed by Baldi et al. (1986) developed from extensive calibration testing on Ticino sand.

$$I_D = \frac{1}{C_2} \ln\left[\frac{q_c}{C_0(\sigma')^{C_1}}\right] \qquad [3.7]$$

where:

$C_0$, $C_1$ and $C_2$ are constants from the soil;

$\sigma'$ = vertical or mean effective stress in kPa; and

$q_c$ = cone penetration resistance in kPa.

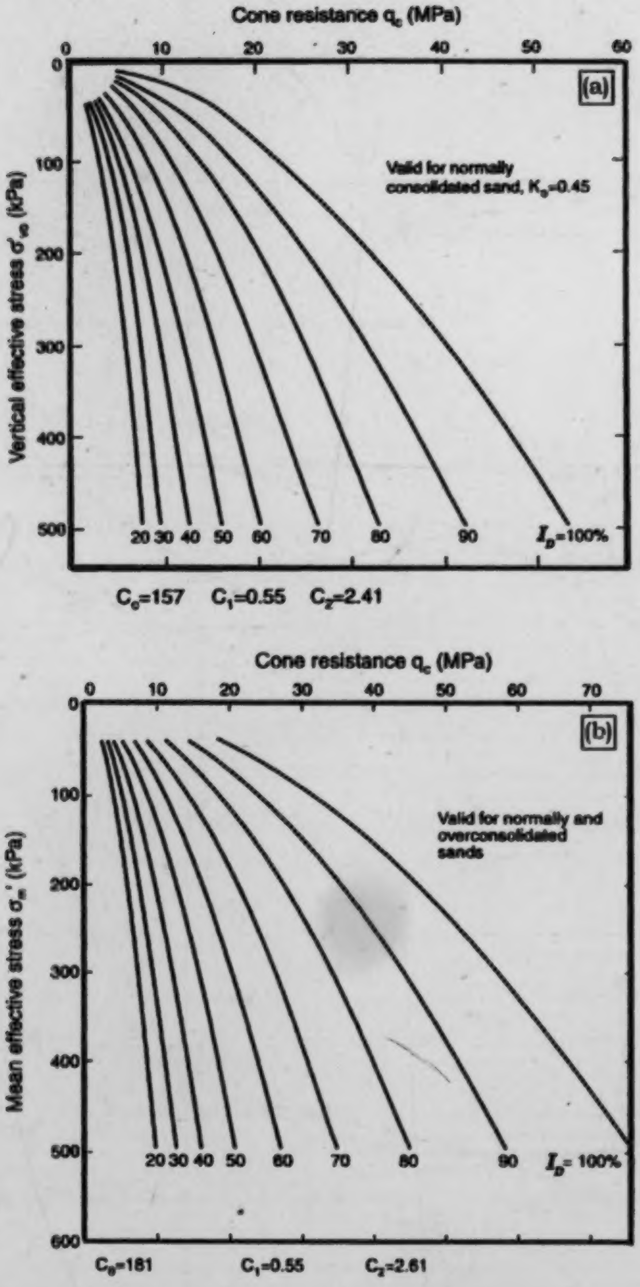

**Figure 3.13 – Density Index estimation from CPT data: a) for normally consolidated sand, and b) for overconsolidated sand (modified from Lunne et al. 1997).**

As recommended by Lunne et al. (1997) correlations for the density index from a CPT are approximate and are sensitive to variation in soil compressibility, horizontal stress and aging; the value obtained should be seen as a nominal value of $I_D$.

## 3.5 GEOENVIRONMENTAL APPLICATIONS

A geoenvironmental site investigation usually requires an extensive drilling program. As a result, a significant amount of potentially contaminated soil and water are produced during drilling. The drilling waste may require special handling and disposal adding significantly to the overall cost and time needed for the process. Currently in the US there are regulations in many states that require proper storage or disposal of the drill cuttings from environmental sites. This can increase the daily drilling cost by as much as US $1000.00 (Robertson et al. 1998). According to Bratton et al. (1995), site investigation programs using CPTs carried out at Tinker U.S. Air Force Base have shown that by eliminating the necessity of collecting, testing, and disposing the drill cuttings there has been a reduction in the total investigation program cost of 25%. Therefore, there is a clear incentive to develop techniques that do not produce cuttings from the subsurface. One of these techniques includes the use of direct push devices, which includes the CPT/CPTU. New sensors and devices have also been developed and added to the CPT/CPTU to enable its use in geoenvironmental projects.

The most common sensors incorporated in the CPT/CPTU include the electrical resistivity/conductivity measurement and special fiber optic devices for fluorescence measurements. A comprehensive description and application of direct push devices used for geoenvironmental site investigation is presented in Lunne et al. (1997).

Because the electrical resistivity/conductivity sensor was incorporated in the HD-PB-CPT as part of this study, this technology is discussed in more detail in Chapter 7. It is the author's opinion that fluorescence technologies have the potential to be added to the HD-PB-CPT making it an excellent tool for screening hydrocarbon contamination. A brief overview of laser and Ultra-Violet (UV) induced fluorescence are presented here.

- Laser Induced Fluorescence (LIF)

The polyaromatic constituents present in most hydrocarbons produce fluorescence when irradiated with various forms of light (Lunne et al. 1997). This feature was the key characteristic for the development of the Laser Induced Fluorescence (LIF) sensor. In 1987 the U.S. Navy introduced a sensor for detection of petroleum hydrocarbons based on LIF (DOE 1996). Two years earlier, the U.S. Army Corps of Engineers, Waterways Experiment Station developed a program to use the cone penetrometer for screening ground contamination, and created the SCAPS: Site Characterization and Analysis Penetrometer System. In 1989 a coordinated program involving the U.S. Army, U.S. Navy, U.S. Air Force, the Environmental Protection Agency (EPA) and the Department of Energy (DOE) incorporated the LIF and the CPT/CPTU technology together to create the LIF CPT (DOE 1996).

The LIF CPT consists of a cone that has a sapphire window placed about 60 cm above the cone tip. A pulse nitrogen laser light is sent down by a fiber optic cable to the window and the fluorescence generated, when the laser light reaches the hydrocarbon, is carried back to the surface by another fiber optic cable. From there it is dispersed by a spectrograph and the intensity of the fluorescence is quantified. A microcomputer with a data acquisition system collects, stores and plots the data, in real time, as a vertical profile on the computer screen. A schematic view of the LIF CPT is presented in Figure 3.14. It is worth noting in Figure 3.14, the grout system incorporated to this CPT, which allows for the grouting of the hole after testing.

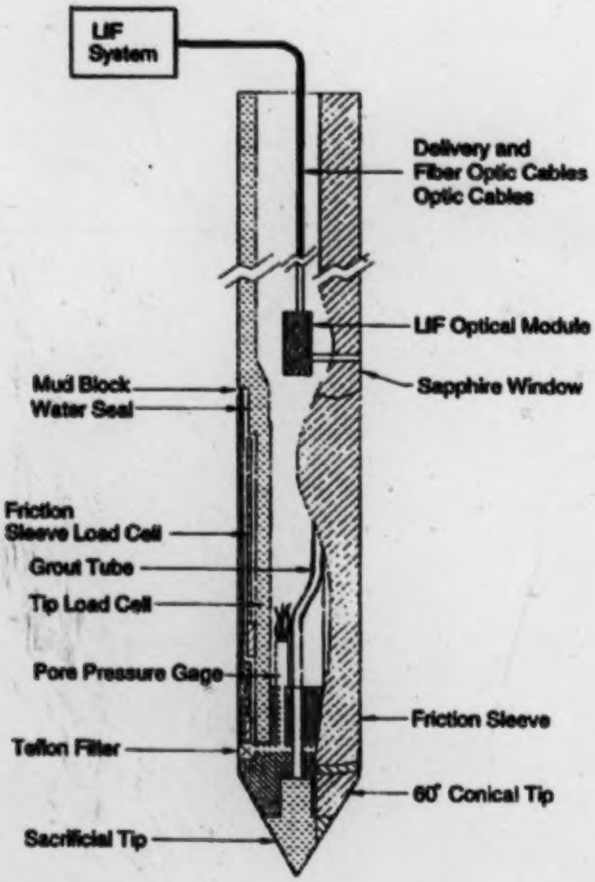
LIF System
Delivery and Fiber Optic Cables Optic Cables
LIF Optical Module
Sapphire Window
Mud Block
Water Seal
Friction Sleeve Load Cell
Grout Tube
Tip Load Cell
Pore Pressure Gage
Friction Sleeve
Teflon Filter
60° Conical Tip
Sacrificial Tip

Figure 3.14 – Laser Induced Fluorescence CPT

(modified from DOE 1996).

- Ultra Violet (UV) Fluorescence Probe

LIF probes are expensive and there is concern regarding the long term durability and maintenance of its fiber optic cables (Robertson et al. 1998). Researchers (Van Ree and Olie 1993; Haas and Forney 1995); therefore developed a ultra violet (UV) fluorescence CPT probe that either uses a small piece of fiber optic cable or no fiber optic cable at all. The probes contain a UV light source as well as the fluorescence detection system. Because the complete sensing system is located in the probe there is no need for fiber optic cables, or only the need of a small length of fiber optic cable as shown in Figure 3.15 (a) and (b). During penetration a small mercury lamp placed behind a clear window produces the UV light source that illuminates the soil in contact with the window on the probe. The fluorescence by the hydrocarbons is detected inside the probe by a small photomultiplicator tube. The signal is then conducted through the electrical CPT cable up to the ground surface where it is collected by a data acquisition system. A detection limit of 50 ppm dry weight for free phase light NAPLs has been reported by Lunne et al. 1997. The intensity of the fluorescence emitted by the contaminant is a function of the concentration of the contamination in the soil, but specific calibration is also required. This detection system can also use filters to control the excitation wavelength for identification of other contaminants; however, the filters must be installed prior to testing. Figure 3.16 shows an example profile from a UV induced fluorescence probe. Clear, sharp peaks in the fluorescence signal response indicate the depths of the contamination.

The UV sensoring system would appear to be a very promising one to add to the HD-PB-CPT for two reasons. It has a reasonable cost/benefit ratio and because of the large physical dimensions of the HD-PB-CPT, a significant amount of room is available inside the probe to easily accommodate the UV induced fluorescence apparatus.

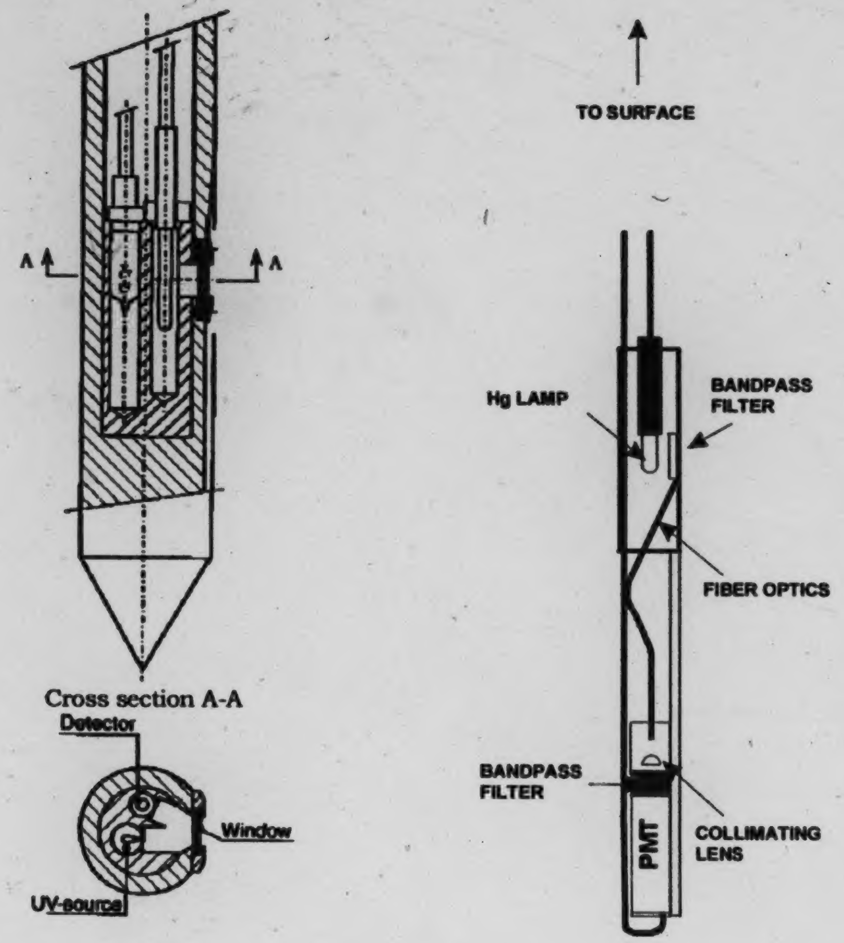
A
A
Cross section A-A
Detector
Window
UV-source
TO SURFACE
Hg LAMP
BANDPASS FILTER
FIBER OPTICS
BANDPASS FILTER
COLLIMATING LENS
PMT

(a)

(b)

Figure 3.15 – Schematic view of the UV probe developed by: a) Van Ree and Olie (1993) and b) Haas and Funy (1993).

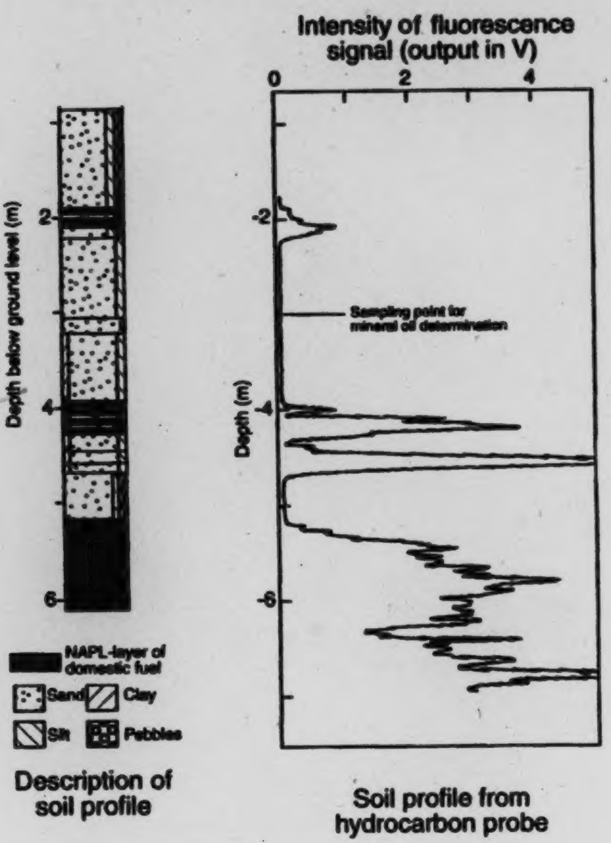

Description of soil profile

Soil profile from hydrocarbon probe

Figure 3.16 – Profile from UV induced fluorescence

(modified from Lunne et al. 1997)

## 3.6 SUMMARY

The electrical cone penetration test is one of the most versatile tools for geotechnical site investigation, and there is no other existing tool that provides better soil stratigraphy than the CPT/CPTU. The addition of new sensors to the CPT, its characteristic of generating no cuttings during logging, and its ability to generate a continuous soil profile have made the CPT a very attractive tool for geoenvironmental site investigation. Use of the CPT/CPTU for screening soil contamination plumes and pools is growing rapidly, as well as the confidence in its results. Therefore, CPT technology would appear to be a very good option to consider in the development of new horizontal directional logging devices.

# CHAPTER 4

# Horizontal Directional Pre-Bored Cone Penetration Test

# HD-PB-CPT

# (Prototype 1 Development)

## 4.1 INTRODUCTION

The soil reaction caused by pulling a probe through a smaller diameter pre-drilled borehole is analogous to that of a pre-bored pressuremeter test (PBPT), although it differs in principle. The former test is a near continuous test and it measures cone and sleeve friction resistance, whereas the PBPT test is performed at discrete intervals and measures the cavity (borehole) strain as a function of an applied stress.

Nevertheless, the geometry of the problem for both tests is similar. Each test starts with a pre-opened cavity that is expanded until the surrounding soil fails or it reaches its limit pressure ($p_l$). Therefore, issues relating to the influence of soil disturbance due to borehole drilling and to the total cavity strain necessary to achieve the natural soil $p_l$ can be analyzed based on the experience from the pressuremeter test results. This particular approach will be further discussed in the next section.

The concept of pushing (or pulling) a cone like probe through a pre-opened borehole to obtain soil parameters is not new. Ladanyi (1994) developed a probe, which he called the Sharp Cone Test (SCT). The SCT consisted of a low-angle cone (semi-angle varying from 1° to 10° depending on the soil deformability) that was pushed into a pre-drilled hole (Figure 4.1a). The cone had three pressure transducers along its lateral surface and as it was being pushed into the ground it was possible to record the stress and the cavity strain at each pressure transducer position. The data was then utilized to plot a pressuremeter like curve (Figure 4.1b) that was then used to obtain the mechanical properties of the soil.

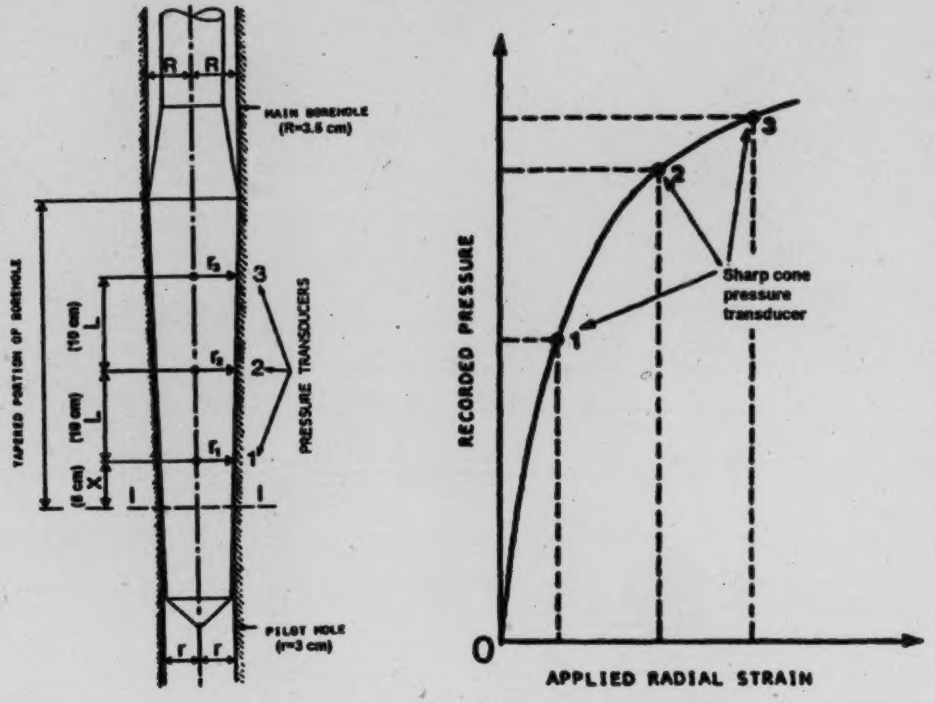
R
R
MAIN BOREHOLE
(R=3.5 cm)
TAPERED PORTION OF BOREHOLE
$r_3$
$r_2$
$r_1$
3
2
1
PRESSURE TRANSDUCERS
L
(10 cm)
L
(10 cm)
X
(5 cm)
I
I
PILOT HOLE
(r=3 cm)
r
r
RECORDED PRESSURE
APPLIED RADIAL STRAIN
0
1
2
3
Sharp cone pressure transducer

(a) (b)

Figure 4.1 – (a) Sketch of the sharp cone and (b) typical pressuremeter like curve obtained from a sharp cone test (modified from Ladanyi 1994).

Despite the SCT furnishing more complete rheological information of the soil than a standard CPT, three measuring points do not seem to be enough to obtain a well defined stress-strain curve. Increasing the number of pressure transducers adversely compromises the probe's length. In addition, what is wanted is a probe that is capable of providing soil lithology in real time just like a CPT does or at least one that is capable of distinguishing clay from sand along a horizontal path. Thus, the SCT approach is not suitable for this purpose.

Issues and concepts relating to the development of the first prototype of the HD-PB-CPT are discussed in the following sections.

## 4.2 CONCEPT AND ISSUES

### 4.2.1 PROBE FIRST IDEALIZATION

Like a conventional CPT, the HD-PB-CPT has two load cells; one for the cone resistance (*qc*) and the other for friction sleeve resistance (*fs*). A key difference between the CPT and HD-PB-CPT is that the cone resistance is calculated using only the soil annulus area (the cross-section of the probe minus the cross-section of the borehole) resulting from the expansion of the pre-bored hole, rather than the total cross-section of the cone as is used in conventional CPT test.

Because the cone-soil contact area is a function of the borehole diameter, the first idealization of the HD-PB-CPT had a caliper placed between the cone and the reamer to allow soil-cone contact area correction during the test, as shown schematically in Figure 4.2.

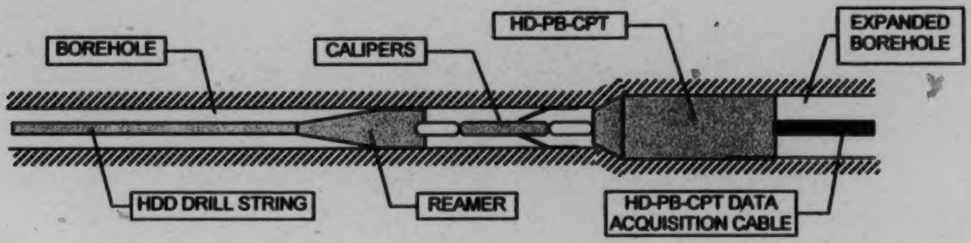

Figure 4.2 – Schematic view of the first idealization of the HD-PB-CPT.

Due to economic and time constraints, the first prototype was built without the caliper; instead a bullet-shaped device was placed on the front of the probe to assure a constant borehole diameter.

Later on, field tests (Chapter 5) and laboratory modeling tests (Chapter 6) showed that the caliper would not have worked properly. The soil deformation pattern which developed ahead of the cone during the test would have prevented the caliper from making a correct borehole diameter measurement.

### 4.2.2 SOIL DISTURBANCE

When conducting a test like the HD-PB-CPT, soil disturbance during drilling is an important concern. It does not matter how carefully pre-drilling is performed it will always cause soil unloading, and will inevitably change the initial stress conditions (Palmer 1972). Consequently, some degree of soil disturbance will always be generated.

The effects of soil disturbance on the test results can be mitigated by generating sufficient soil strain around the probe, overcoming the disturbed zone and achieving the limit pressure of the natural soil away from the borhole. Experience with pressuremeter tests has shown that if disturbance during drilling is small, as occurs in a Self-Boring Pressuremeter Test (SBPT), a cavity expansion of 10 to 15% may be adequate to capture the natural soil response (Carter et al. 1986; Ferreira 1992). If however, the disturbed zone is large the cavity expansion has to be larger. In other words, when drilling a pilot hole an annulus of perturbed soil is formed and large deformations during the subsequent expansion of the pilot hole are required until the natural soil response can be recorded. The above statement can easily be visualized by looking at idealized pressuremeter test curves as shown in Figure 4.3.

Among the different types of pressuremeter tests the SBPT is known to cause the least soil disturbance. The Full-Displacement Pressuremeter Test (FDPT), also called the Cone Pressuremeter, is the one that causes the most soil disturbance because the installation process highly overstresses the surrounding soil.

Figure 4.3 shows that a cavity strain of about 10 – 20% is enough to achieve the soil limit pressure by means of SBPT. The same limit pressure is reached by the FDPT, but with a higher cavity strain (40 – 50%). The PBPT causes a soil disturbance somewhat between the SBPT and the FDPT, consequently, the cavity strain necessary to achieve $p_l$ is in between the SBPT, and the FDPT (Figure 4.3). From this example it can be seen that the problem with soil disturbance during drilling can be overcome by inducing adequate cavity strain. It was anticipated that the behavior of the HD-PB-CPT would be similar to the PBPT.

Theoretically the limit pressure can only be reached at an infinite soil strain, thus the pressuremeter curves shown in Figure 4.3 are only going up to $p_{max}$, which is the practical limit pressure. According to Ferreira (1992) when the ratio $p_{max}/p_l$ is greater than 90%, the value of $p_{max}$ is close enough to the value of the limit pressure for practical purposes.

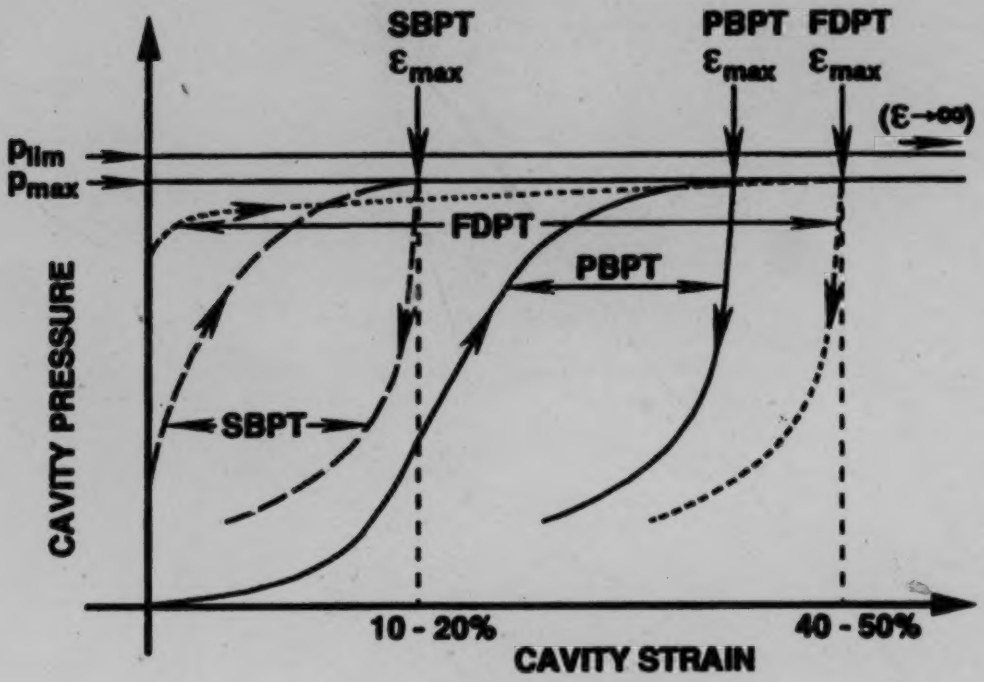

Figure 4.3 – Idealized pressuremeter test curves (modified from Ferreira 1992).

### 4.2.3 CAVITY STRAIN

A critical issue in the design of the HD-PB-CPT was to define the correct probe diameter. The probe diameter must produce a displacement large enough to reach the limit pressure of the natural soil and yet also assure that the drill rig would have enough capacity to pull the probe back through the borehole.

An assessment of the necessary strain to be imposed on the soil was performed by means of Equation 4.1(Ferreira 1992).

$$\frac{R_{PE}}{R_0} = \sqrt{\varepsilon . I_r(2+\varepsilon)} \qquad [4.1]$$

where:

$R_{PE}$ = radius of the plastic-elastic transition (disturbed zone)

$R_0$ = initial radius (borehole radius)

$\varepsilon$ = cavity strain = $\Delta R/R_0$ (where, $\Delta R$ is the difference between the expanded radius and the initial radius $R_0$)

$I_r$ = rigidity index = $G/S_u$ → $G$ = shear modulus

$S_u$ = undrained shear strength

Figure 4.4 provides an illustration of $R_{PE}$ and $R_0$.

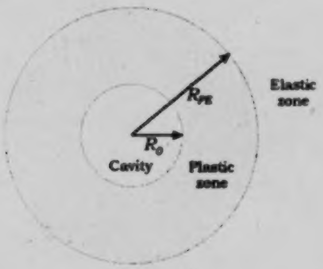

Figure 4.4 – Elastic and Plastic zones.

The $I_r$ of the soil, introduced by Vesic (1972), has a direct relationship with the amount of soil disturbance caused by pressuremeter installation (Ferreira 1992), and its value for most clay soils lies within the limited range from about 100 to 500, for soft and stiff clays respectively.

The higher the value of $I_r$ the larger the disturbed soil zone will be due to drilling. For example, according to Equation 4.1, if drilling causes a cavity strain of 1%, the plastic (disturbed) zone produced will be approximately

1.4 x $R_0$ for $I_r$ = 100 and 3.2 x $R_0$ for $I_r$ = 500. Therefore, the stiffer the soil the larger the resulting disturbed zone.

Now, assuming a disturbed zone 10 times larger than $R_0$ for soil with $I_r$ = 500 (stiff soils), and assuming that the limit pressure ($p_l$) in the natural soil would be achieved by inducing a soil deformation that would be two times larger than the disturbed zone radius, a cavity strain of 34 % can be calculated by means of Equation 4.1. On the other hand, for soft soils, $I_r$ = 100, a smaller disturbed zone can be expected. Thus, assuming in this case that the disturbed zone is 5 times $R_0$, and also assuming that by doubling this zone the limit pressure will be reached, the necessary cavity strain in this case would be $\varepsilon = 41$ %.

In order to validate the above strain calculations, field pilot tests were performed in Lake Edmonton clay soil at the University of Alberta field laboratory. The results of these pilot tests are presented and further discussed in section 4.3.

### 4.2.4 INITIAL STATE OF STRESSES

The initial state of stress around a vertical and a horizontal cone test may differ radically. The former test is subjected to a uniform all-round horizontal stress. The latter is subjected to a vertical overburden stress in the vertical direction, and a different horizontal stress in the horizontal direction, as shown schematically in Figure 4.5.

Because the effective horizontal stress has a key influence on the cone resistance for vertical CPT results (Houlsby and Hitchman 1988; Teh and Houlsby 1991), this difference in stress state may affect the HD-PB-CPT results.

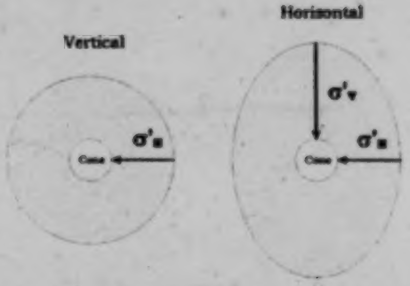

Figure 4.5– Initial state of stresses around a vertical and a horizontal CPT (modified from Broere and van Tol 1998).

In fact, results presented by Broere and van Tol (1998) from vertical and horizontal CPT tests in sand, conducted in a large diameter rigid wall calibration chamber, have shown that for normally consolidated sand at intermediate relative densities, the mean horizontal cone resistance ($q_{cH}$) is approximately 20% higher than the vertical cone resistance ($q_{cV}$). However, the horizontal friction ratio was 24% smaller, on average, than the vertical friction ratio. If the HD-PB-CPT follows this same trend, a recalibration of existing soil behavior type charts will have to be performed to adjust its use for horizontal CPT data.

By calculating the work done in order to expand the cavity for a vertical and a horizontal CPT, Broere and van Tol (1998) came up with the relationship shown by Equation 4.2.

$$\frac{q_{cH}}{q_{cV}} = \frac{W_H}{W_V} = \frac{1+K}{2K} \qquad [4.2]$$

where:

$W_H$ = work performed by the horizontal CPT in expanding the cavity.

$W_V$ = work performed by the vertical CPT in expanding the cavity.

$K$ = earth pressure coefficient.

If necessary, a relationship such as Equation 4.2 could also be applied to the HD-PB-CPT test results to obtain a closer match with the standard vertical CPT and improve soil classification, instead of recalibrating existing CPT soil classification charts.

It is worth mentioning that despite the large size of the chamber used (1.9 m in diameter and 3m in height) by Broere and van Tol (1998), the influence of the boundary condition may have affected both tests (the horizontal and the vertical) differently, making the comparison of the data more difficult to interpret.

## 4.3 PILOT TEST

As mentioned previously, a key issue in the development of the HD-PB-CPT was to determine the correct probe diameter necessary to induce a cavity expansion large enough to achieve the $p_l$ in the natural soil without compromising the drill rig pullback capability. In order to address this issue and validate the borehole strain calculations performed in section 4.2.3, two pilot field tests were performed at the University of Alberta field laboratory.

These pilot tests consisted of pre-bored CPT tests in which a, large diameter CPT (50.8 mm), was pushed through a pre-opened hole 37 mm in diameter. For the sake of simplicity, the pilot tests were performed in a vertical instead of horizontal direction. Further details on the pilot test procedures are given in section 4.3.2.

### 4.3.1 SITE LOCATION AND GEOLOGY

The University of Alberta field laboratory has been an ideal and very convenient site to perform the pilot, and later the HD-PB-CPT, prototype tests. It is close to the main University campus and there is easy access to test equipment. This site is located in central Edmonton, near 115 Street and 58 Avenue, as shown in Figure 4.6.

The soil at this location originates from Lake Edmonton deposit. Lake Edmonton was a proglacial lake which formed during deglaciation about 10 000 years ago, and it covered most of the Edmonton area. The lake was then drained by the North Saskatchewan River in postglacial times (Bhanot 1968). The lake sediments, generally, consist of varved silts and clays with scattered pebbles. The uppermost part of the lake deposit is more clayey and the lower part consists of fine sand and till-like lenses of clay with scattered pebbles (Bhanot 1968).

Four standard vertical CPTU tests (cone penetration tests with pore-pressure measurements), were carried out by ConeTec Investigation Ltd. at this site and are presented in Appendix 1. Three of the CPTU tests were conducted to a depth of 8 m to check the site soil profile, and one was carried out to a depth of only 3 m and was used as a reference for the pilot test. The results furnished by all the CPTU tests were very consistent with each other and are in agreement with the ones obtained by Bhanot (1968) from borehole logs.

The soil profile at the University field laboratory is essentially Lake Edmonton clay, about 4 to 7 meters in depth, overlying glacial till (Bhanot, 1968). According to the CPTU profiles at the specific location of the pilot tests, the upper 4 meters are predominantly clayey. Below this depth the soil consists of interbedded layers of silty clay and clayey silt, to a depth of 7 m. Beyond this depth the soil becomes more silty and sandy. Figure 4.7 presents a typical CPTU soil profile from the site.

The undrained shear strength ($S_U$) profile estimated from the CPTU tests is presented in Figure 4.8. The $S_U$ values were calculated by means of Equation 3.3. Because of the shallow depths of the CPTU tests $q_c$ was used in the equation instead of $q_t$, and the value of $N_{kt}$ was assumed to be 15. The average $S_U$ value at the depth of interest (3 to 4 m) is approximate 100 kPa.

According to Head (1988) this clay can be classified as firm to stiff according to its $S_U$ value which raised some concern about the capability of the HDD rig to pullback the HD-PB-CPT. This issue will be more thoroughly discussed in section 4.4.1. It is worth mentioning the good repeatability presented by the CPTU tests as it can be seen in Figure 4.8

Appendix 2 contains the lab indices and the gradation curve performed in the University of Alberta geotechnical laboratory of the Lake Edmonton clay of the test site

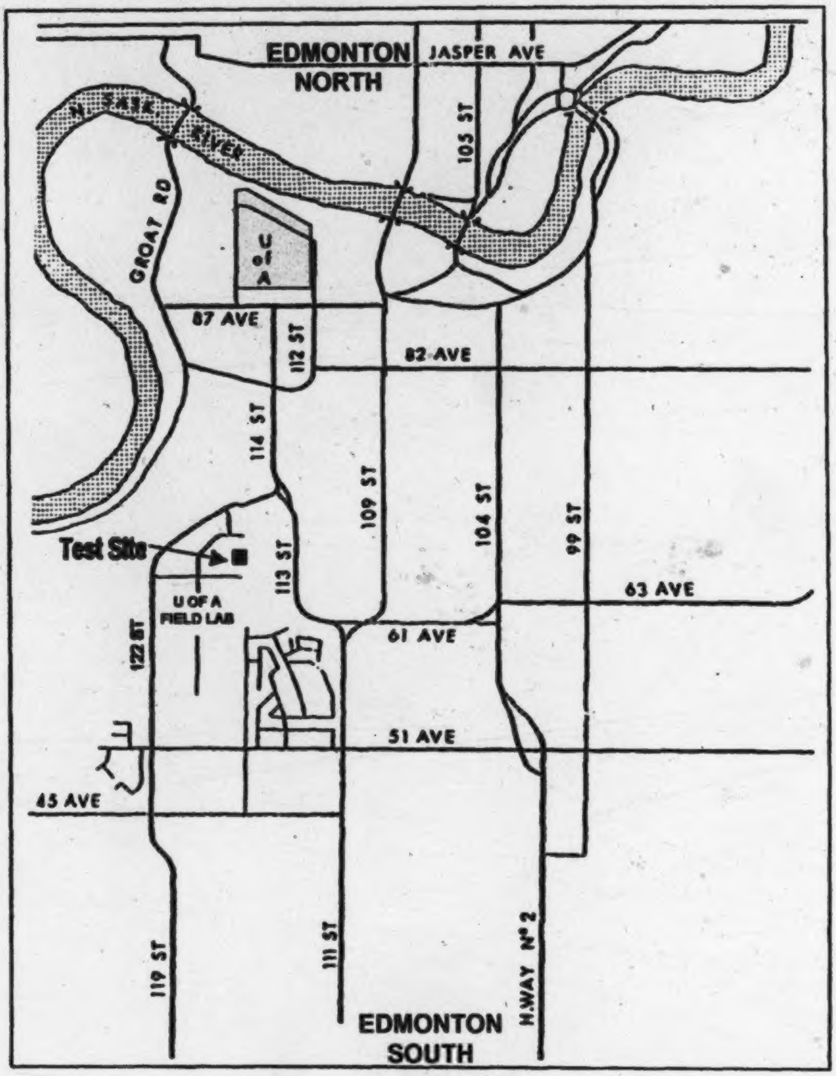
EDMONTON NORTH
JASPER AVE
N. SASK. RIVER
103 ST
GROAT RD
U of A
87 AVE
112 ST
82 AVE
114 ST
109 ST
104 ST
99 ST
Test Site
113 ST
63 AVE
U OF A FIELD LAB
61 AVE
122 ST
51 AVE
45 AVE
119 ST
111 ST
H.WAY N°2
EDMONTON SOUTH

Figure 4.6 – University of Alberta field laboratory location (modified from Bhanot 1968).

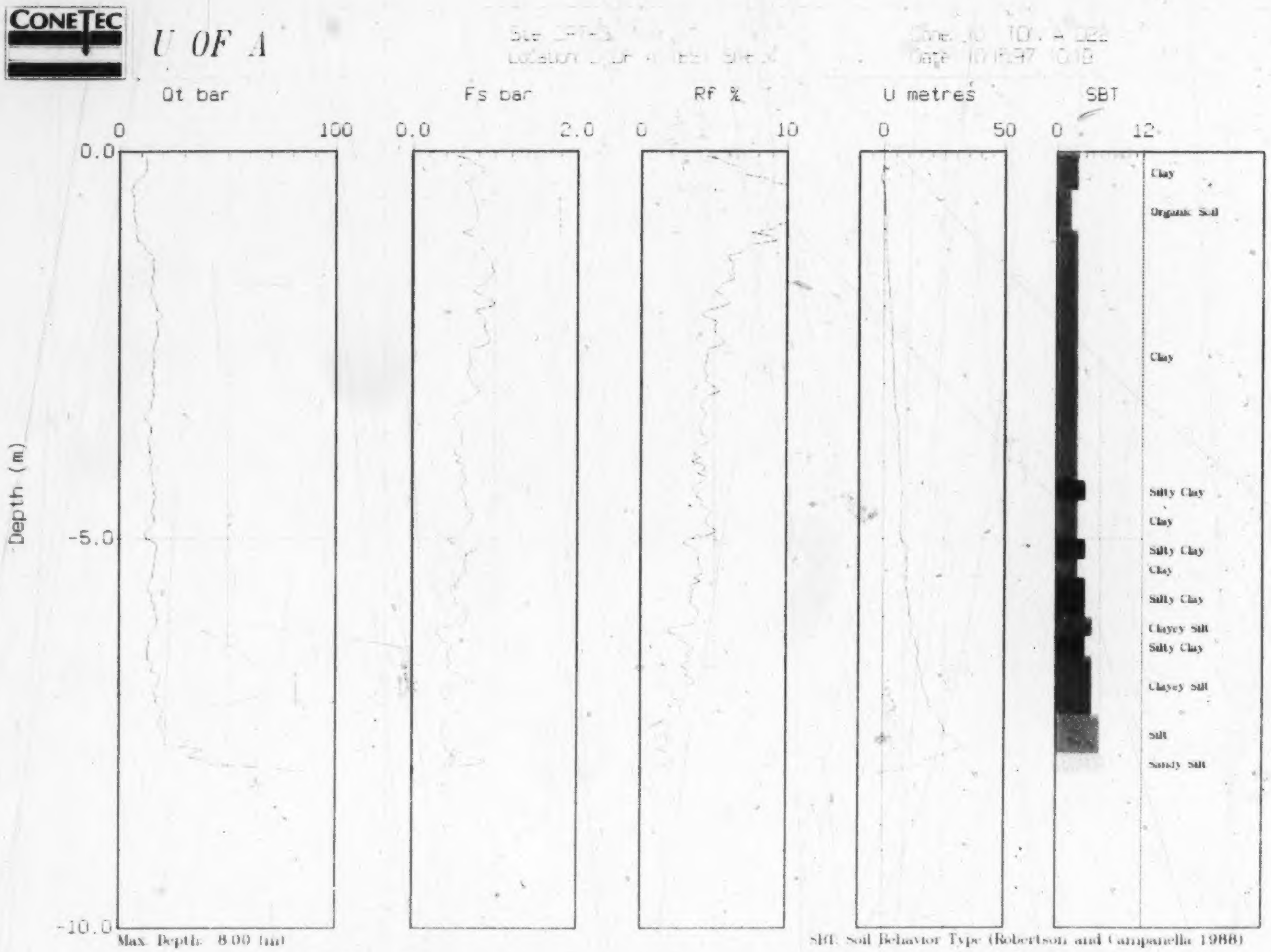

Figure 4.7 – Typical CPTU soil profile from University of Alberta field laboratory.

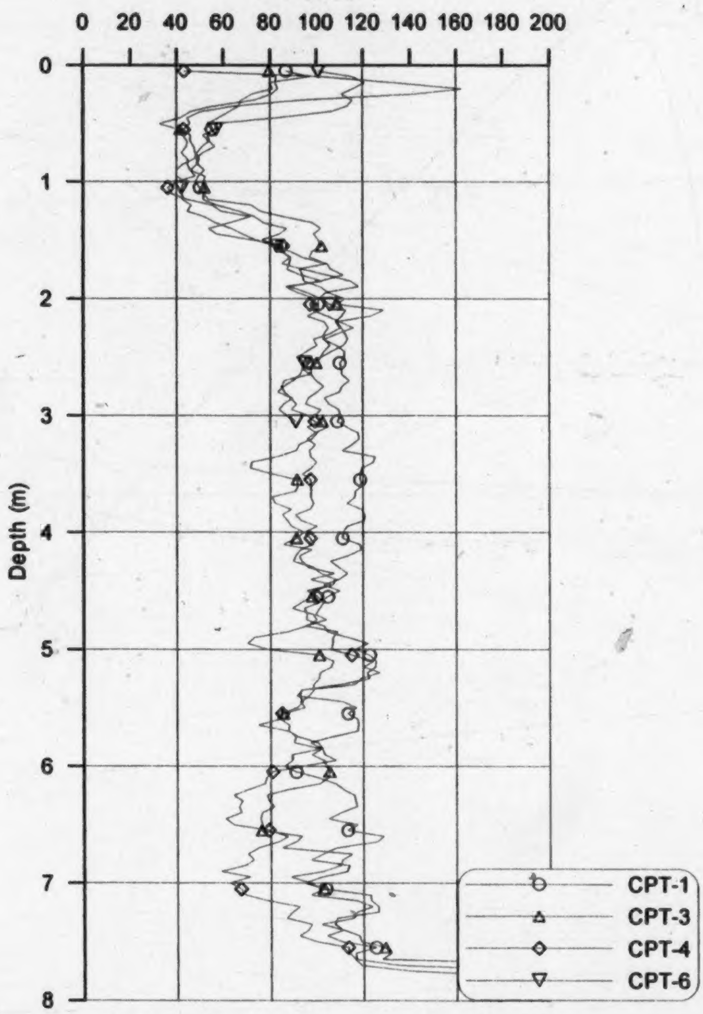

Figure 4.8 – Undrained shear strength profile estimated from CPTU tests.

### 4.3.2 PILOT TEST PROCEDURE

The initial plan was to perform the HD-PB-CPT tests at depths not greater than 3 m to allow an easy retrieval of the probe by excavation, if necessary. Therefore, the two pilot tests were performed to a depth of only 3 m.

A standard vertical CPT profile was obtained to use as a reference for the pilot tests. To minimize the influence of soil lithology changes, the two pre-bored vertical CPT tests were performed within 2 m of the standard CPT.

The pre-bored CPTs were performed by first pushing a 37 mm diameter rod with a venting device into the ground. The venting device allowed air to pass through the hollow rods, thus avoiding the formation of any vacuum that could reduce the borehole diameter when withdrawing the rods. To check the final borehole diameter resulting from this process, an extra 37mm borehole was pushed to a depth of 3 m, and filled with water. The total volume of water to fill this borehole was 3.1 liters, rendering an average borehole diameter of 36.3 mm; a difference of less than 2% when compared to the rods diameter. This difference was considered negligible.

After opening the borehole a 50.8 mm diameter cone was attached to the end of the rods and pushed again through the pre-opened hole. To minimize any misalignment between borehole and the CPT, the drill rig was not moved during the test procedure. The total soil cavity strain produced by the pilot test was $\varepsilon = \frac{50.8 - 37}{37} \times 100 = 37\%$. It was not possible to achieve a larger cavity strain due to the availability of equipment.

### 4.3.3 PILOT TEST RESULTS

Despite not moving the drill rig between the process of opening the borehole and performing the CPT test, it was difficult to ensure that a perfect alignment was obtained. As explained earlier, the $q_c$ of a pre-bored CPT is calculated based on the annulus area, i.e., the area difference between the cone area and the borehole area, therefore a misalignment of the cone with the borehole or an oversize borehole will affect the annulus area, consequently affecting the $q_c$ result.

As shown by the test results, Figure 4.9, the pre-bored CPT pilot test followed the same trend as those of the standard CPT, except for the first 50 cm of penetration.

In examining the cone resistance graph from Figure 4.9, the average $q_c$ value for the vertical pre-bored CPTs was about 50% smaller than the standard CPT for the first 50 cm of penetration. Cone resistance is influenced by the material ahead and behind the penetrating cone and the depth of this influence is a function of the cone diameter (Schmertmann 1978; Lunne et al. 1997). Using a larger 50.8 mm diameter cone, to expand the hole may have caused the surface boundary influence to be a little deeper than that for a standard cone, 35.7 mm in diameter. An oversizing of the borehole to this depth may have also been caused by the development of a soil plug ahead of the flat-ended rods.

As the test hole went beyond 50 cm, the cone resistance for both pre-bored CPTs followed a similar signature as the standard CPT, but with slightly higher $q_c$ values. These higher values may be a function of a decrease in the borehole diameter with depth or, as mentioned before, a deviation from the borehole alignment. Probably these results are not due to soil disturbance because if they were, the cone resistance would be expected to decrease or at least remain the same due to the clay sensitivity.

A constant, annulus, soil-cone contact area was used to calculate the cone resistance. If this contact area increased with depth, the calculated $q_c$ values showed in Figure 4.9, would be lower than shown. If it were possible to measure the borehole diameter variation with depth and correct for the contact area, a better agreement of $q_c$ values may have been obtained. On the other hand, the pre-bored CPT sleeve friction response shows a very good agreement compared with the standard CPT and only at shallow depths (up to 1m) were the results smaller. But once again, this seems to be due to an oversizing of the borehole and surface influence, even though the second pre-bored CPT was able to capture the same increase and decrease of friction presented by the standard CPT on the top 50 cm of the soil profile.

If the $q_c$ values were calculated by measuring the true value of the contact area, the friction ratio curves may have presented a better match with the standard CPT than those shown in Figure 4.9.

It can be seen from the test results that soil disturbance seems not to be an issue with respect to pre-bored CPT once the strain induced in the soil is large enough to capture the natural soil response. At least for Lake Edmonton clay, 37 % cavity strain appears to be enough to obtain a reasonable result.

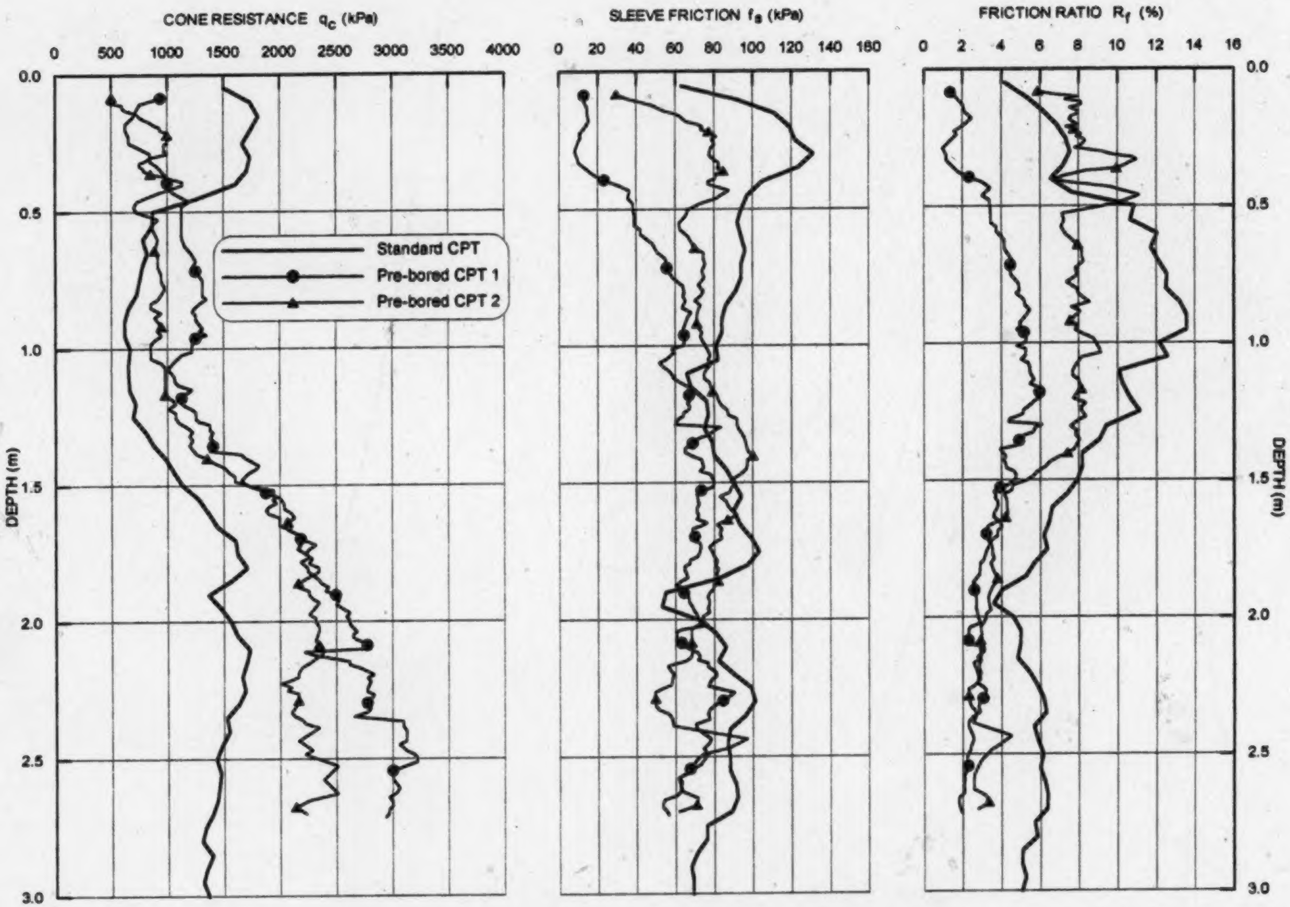

Figure 4.9 – Pilot tests (vertical pre-bored CPTs)

## 4.4 PROBE DEVELOPMENT

### 4.4.1 DESIGN

Concerns about the capability of the HDD rig to pull back the probe through soils like dense sands were a restraining factor in the HD-PB-CPT design. What was wanted was a drill rig that was capable of drilling a small pilot hole but also had a large pullback capability. Among the available drill rigs, the Vermeer Navigator D24x40 was the one with the best pullback/borehole diameter ratio. This rig has a pullback force of 105.9 kN (23,800 lbs.) and can drill a borehole as small as 10.16 cm (4") in diameter (Vermeer 1998).

The results from the previous vertical pilot test showed that a cavity strain of 37% would be enough to achieve the limit pressure of the natural soil, at least for Lake Edmonton clay. It was therefore, decided that a cavity strain of 50 % should be enough to produce sufficient soil displacement to achieve the limit pressure in the natural soil for a greater number of different soil types. Such a level of strain would also be within the HDD rig pulling capability for most soil types, depending on the test depth. Because the pilot borehole would be drilled with 10.16 cm (4") in diameter the first HD-PB-CPT prototype was built with a diameter of 15.24 cm (6").

Once the new probe's diameter was defined, a proportionality factor between the HD-PB-CPT cross section area (182.4 $cm^2$) and the standard CPT cross section area (10 $cm^2$) was used to define the sleeve friction dimensions. A standard CPT has a sleeve friction area of 150 $cm^2$, hence the sleeve friction area of the HD-PB-CPT was of 2736 $cm^2$, rendering a sleeve friction length of 57 cm.

The design of the HD-PB-CPT was based, as much as possible, on the recommendation and tolerances specified by the International Reference Test Procedure (IRTP) issued by the International Society of Soil Mechanics and Foundation Engineering (ISSMFE 1999) and the ASTM (1995a) standard test method D 5778-95.

Because the HD-PB-CPT is pulled and not pushed, the pulling force from the HDD drill stem had to be transferred from the front of the probe to the back of the probe so the load cells could work by compression. This transference of force was performed by using a shaft passing longitudinally through the middle of the tool and fastened at the back by a single nut that is secured to the shaft (Figure 4.10). The entire pulling force is carried by the nut and transferred to the shaft. The nut's threads and length were designed according to the ASME Screw and Thread Manual (1953). To avoid the possibility of the nut loosening during the test, a safety pin was used across the nut to anchor it to the shaft.

In the case of deep testing, it was possible that drilling fluid pressure ahead of the probe could interfere in the cone resistance data. Therefore, to allow the drilling fluid to pass through the probe and promote pressure equilibrium in front of the tool a hollowed shaft was used. Using a hollowed shaft was interesting because had the decision been to perform the test using a reamer ahead of the probe to obtain a more uniform pilot hole (Figure 4.2), the hollowed shaft would have prevented the formation of a vacuum in the region between the reamer and the probe's tip, which could adversely affect the test results. Due to the extensive weight and length of the probe it was decided to use two sets of "O" rings in the front and at the back of the probe to better protect the load cells against any ground water leakage.

Figure 4.10 shows a sketch with a plan view and the cross section of prototype 1; detailed pictures of the HD-PB-CPT are presented in Figure 4.11 through 4.14. It is worth mentioning that the probe's position was measured during the test with the help of the data acquisition cable. The cable was placed on top of a wheel that was connected to a precision multi-turn potentiometer. As the probe was being pulled, the cable continuously rotated the wheel which promoted a voltage variation output that was read and converted to distance (meters) by a data acquisition system.

The detailed designing drawings of the HD-PB-CPT with dimensions and material used in each element of the probe are presented in Appendix 3.

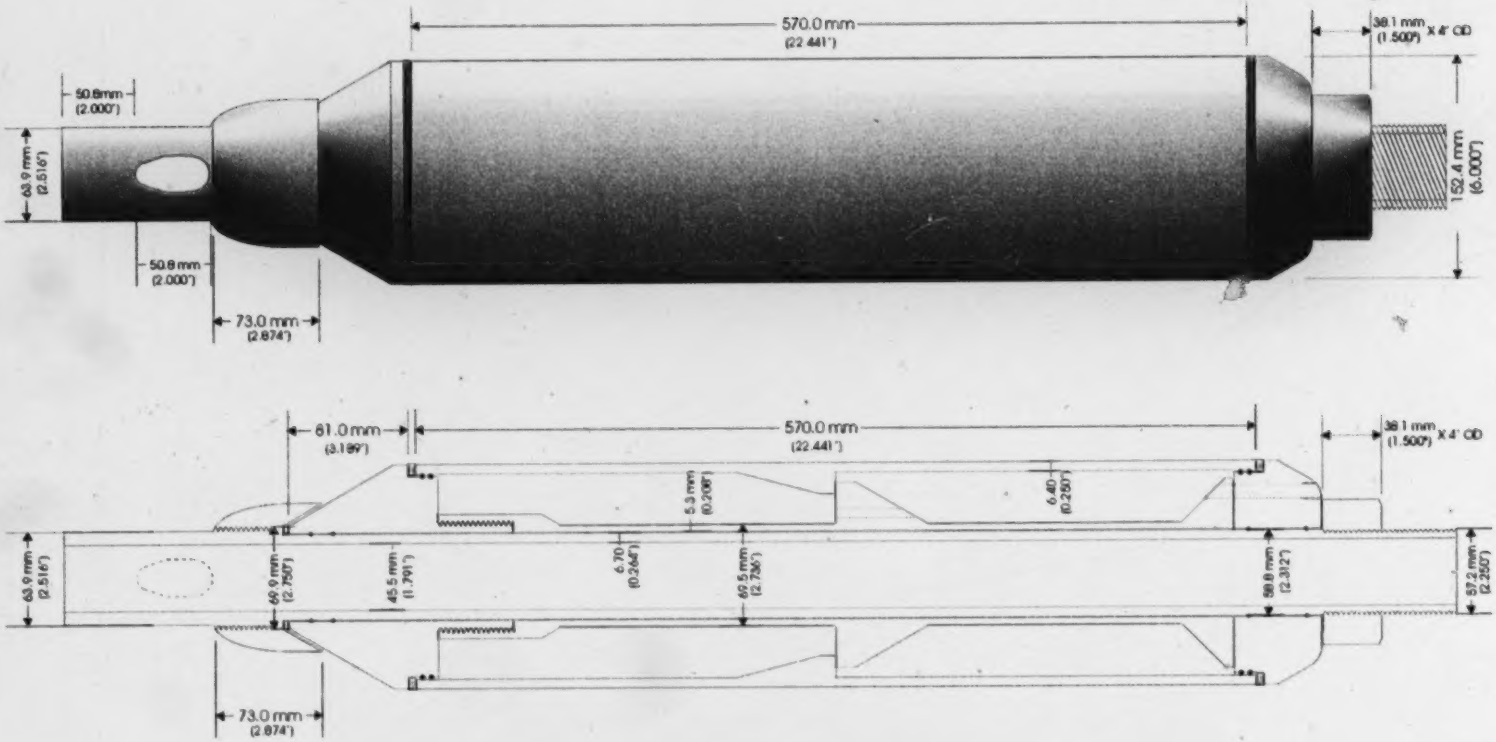
570.0 mm
(22.441")
38.1 mm (1.500") X 4' OD
152.4 mm
(6.000")
50.8mm
(2.000")
63.9 mm
(2.516")
50.8 mm
(2.000")
73.0 mm
(2.874")
81.0 mm
(3.189")
570.0 mm
(22.441")
38.1 mm (1.500") X 4' OD
5.3 mm
(0.208")
6.40
(0.250")
63.9 mm
(2.516")
69.9 mm
(2.750")
45.5 mm
(1.791")
6.70
(0.264")
69.5 mm
(2.736")
58.8 mm
(2.312")
57.2 mm
(2.250")
73.0 mm
(2.874")

Figure 4.10 – Sketch of the HD-PB-CPT prototype 1.

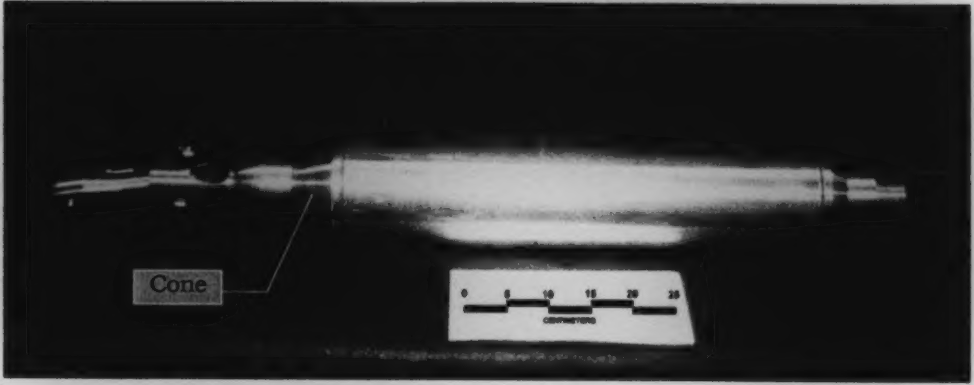
Cone
0
5
10
15
20
25
CENTIMETERS

Figure 4.11 – HD-PB-CPT prototype 1

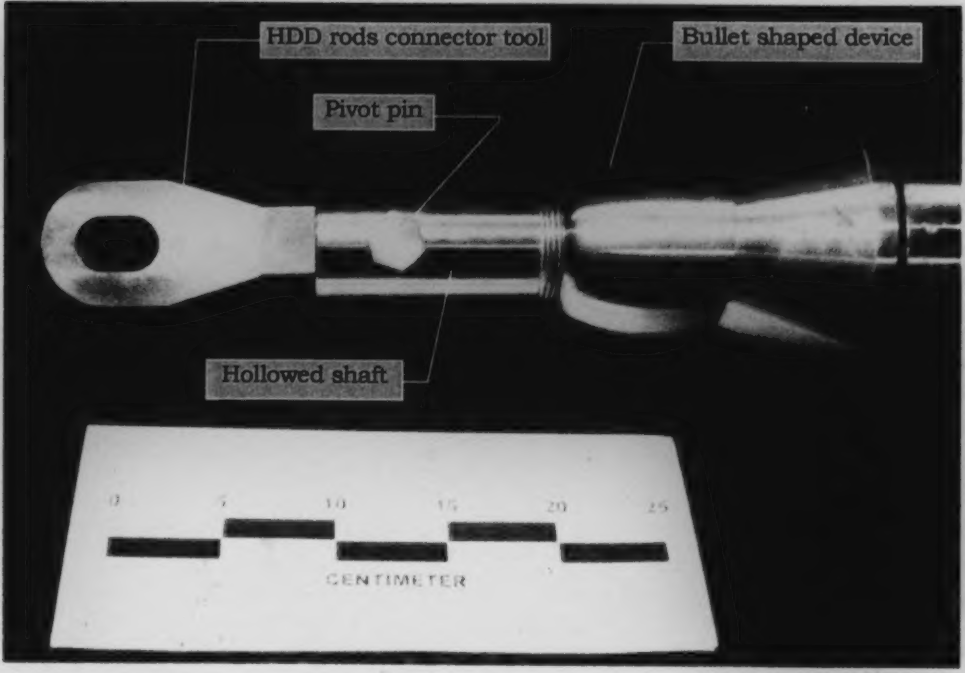
HDD rods connector tool
Bullet shaped device
Pivot pin
Hollowed shaft
0
5
10
15
20
25
CENTIMETER

Figure 4.12 – Detailed view of the front of the HD-PB-CPT

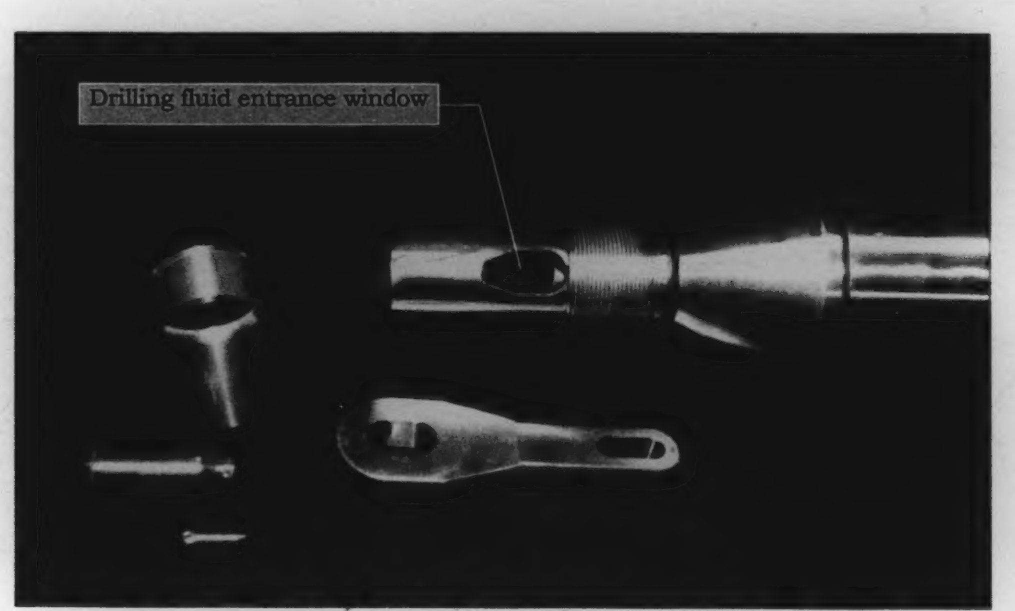
Drilling fluid entrance window

Figure 4.13 – Front part of the HD-PB-CPT disassembled.

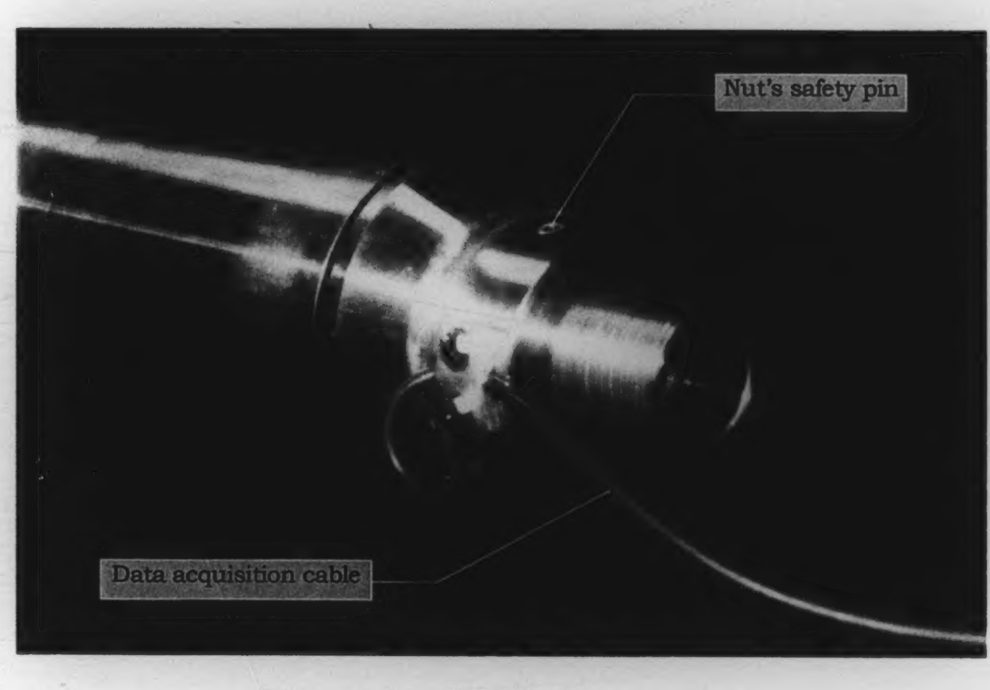
Nut's safety pin
Data acquisition cable

Figure 4.14 – HD-PB-CPT rear view.

### 4.4.2 MATERIAL SELECTION

The maximum pullback capability of the Vermeer Navigator D24x40 drill rig is 105.9 kN. This load would likely not be enough to pull the probe through deposits such as dense sands. In situations involving dense sands it might be necessary to use special hydraulic jacks with higher pulling capability than that delivered by the drill rig. The drawback of using these special jacks is that they usually have a smaller stroke length than the HDD rig, and the removal of the rods has to be done manually, which would cause a considerable delay in the testing time.

Nevertheless, the probe was designed with the consideration of the possibility of having to use these special jacks. An evaluation of the total force necessary to pull the HD-PB-CPT through dense sand deposits was made with the help of the chart proposed by Baldi et al. (1982) and reproduced here in Figure 4.15. Assuming a sand deposit with density index ($I_D$) of 75%, a unit weight of 20 kN/m$^3$ at a depth of 10 m (with a water table deeper than 10 m) a cone resistance of 22500 kPa was obtained from the chart in Figure 4.15. By using a typical friction ratio of 0.5% for this kind of deposit (Robertson and Campanella 1983), it was possible to estimate a total pulling force of 432 kN. Therefore, prototype 1 of the HD-PB-CPT was designed to withstand a total load of up to 450 kN.

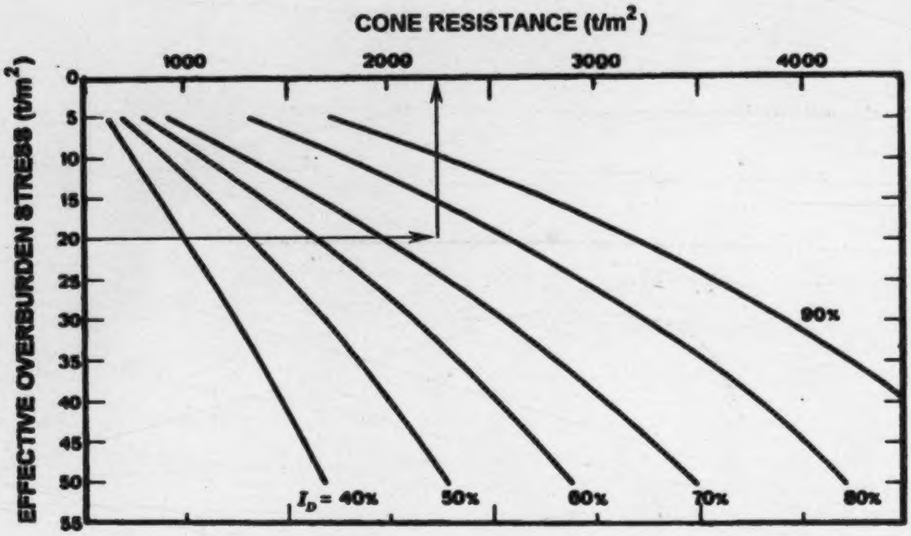

Figure 4.15 – Cone resistance as a function of the effective overburden stress and sand density (modified from Baldi et al. 1982).

A key part of the design was to define the ideal cross section of the hollowed shaft. During the test, the shaft is submitted to tensile stresses, and what was desired for this part of the probe was to have as large a hollowed shaft as possible, to facilitate drilling fluid flow and still have enough material thickness to resist the design load. This part of the probe was therefore built with alloyed steel AISI 4140 which has a yield strength of 655 MPa (Oberg et al. 1989). This was capable of resisting the design load but required a relatively small area of material. It also has the extra advantage of being easy to machine.

During the probe construction there was no mechanical tube available that closely approached the load cell's dimensions. The AISI 4140 mechanical tubes available would have required excessive machining time. Therefore, it was decided to use alloy steel AISI 4340 because it was possible to find a mechanical tube in this material with dimensions close to those desired. Despite being a more expensive material, the final product was cheaper due to lower machining costs.

The cone and the friction sleeve as well as the back part of the probe and the nut were built of stainless steel AISI 304, the conventional material for a standard CPT probe.

### 4.4.3 HDD STEM AND HD-PB-CPT CONNECTION

To reduce adverse bending forces acting on the probe during the curved section of the test, the connection between the HDD drilling stem and the probe could not be a rigid one. A special connector was built that was fastened to the probe's shaft by a pivot pin which would allow some degree of freedom in all directions. This connector was hooked to the HDD rods by means of a shackle.

When performing HD-PB-CPT tests at greater depths (10 to 30 m) there is a possibility the HDD rig may not have enough power to pull the probe through some stiffer or denser formations and the probe could get stuck. At these depths it is not feasible to retrieve the probe by excavation, therefore not only the probe will be lost in but also the drilling rods.

To avoid losing the drilling rod in particular, a safety pin was incorporated into the connector which would break when the pulling force reached approximately 80% of the HDD pullback capability, i. e. 84.7 kN. Figure 4.16(a) shows a view of the connector and the safety pin. Note that the middle section of the safety pin was designed to make the cross section weaker and allow it to fail with the desired load. Figure 4.16(b) shows a view of the connector and the safety pin after a tensile test. The total load withstood by the pin was 77.5 kN, 8.5% lower than the planned failure load. Because prototype 1 was to be tested in shallow depths (up to 5 m) and in clay, the safety pin failure load was considered satisfactory.

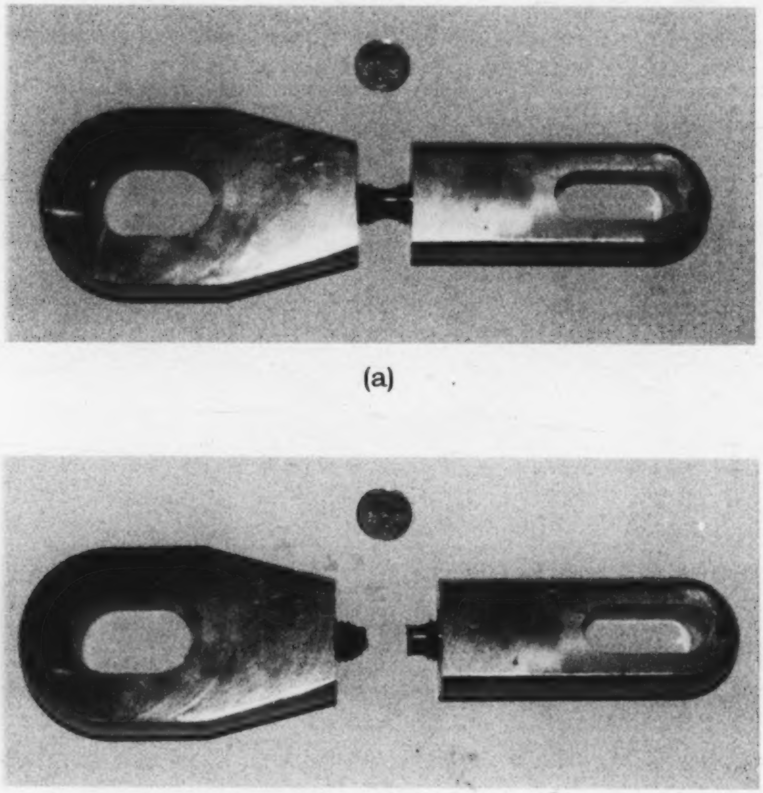

(a)

(b)

Figure 4.16 – Connector tool and load safety pin: (a) before tensile test and (b) after tensile test, failure load = 77.5 kN.

### 4.4.4 LOAD CELL DESIGN AND CALIBRATION

Two load cells of the subtractive type measure the cone resistance and the friction sleeve forces during penetration. With this type of device the two load cells are joined together in such a way that the cell closest to the cone measures the compressive forces generated by the cone while the second load cell measures both the compressive forces from the cone and from the friction sleeve; the friction sleeve forces are thus obtained by subtraction.

Each load cell has a full Wheatstone bridge circuit with two strain gages in each arm of the bridge so that any unwanted bending strain is canceled. The strain gages used to build the Wheatstone bridge circuit were a CEA-06-062UT-350 with a resistance of 350 ohm and gage factor of 2.080 ± 0.5 % manufactured by Measurements Group, Inc. A depth bridge amplifier with adjustable gain (DBA-AG) and a 5 volt regulator was used in each load cell to amplify the output signal. The amplifiers required an excitation voltage of 9 volts, which was then reduced to 5 volts in the DBA-AG to feed the Wheatstone bridge circuit. A circuit diagram of the load cells is presented in the next section.

The load cells were calibrated using a Universal Testing Machine with a total load capacity of 1000 kN. The maximum calibration load was only up to 100 kN to be compatible with the maximum pull capability of the HDD rig. These load cells can nevertheless withstand higher loads. Figure 4.17 shows the cone and friction sleeve calibration curve and Figure 4.18 shows a view of the load cell being calibrated in the Universal Testing Machine.

It is interesting to note in Figure 4.17 that the output signal for the friction sleeve load cell is lower than the output signal for the cone load cell. The reason being that the friction sleeve load cell amplifier was set to a smaller signal gain because this load cell is submitted to a higher load (cone plus friction sleeve load). Furthermore, the friction sleeve load cell was loaded with the friction sleeve in place, i.e., the load was being applied on the wing (top) of the friction sleeve load cell.

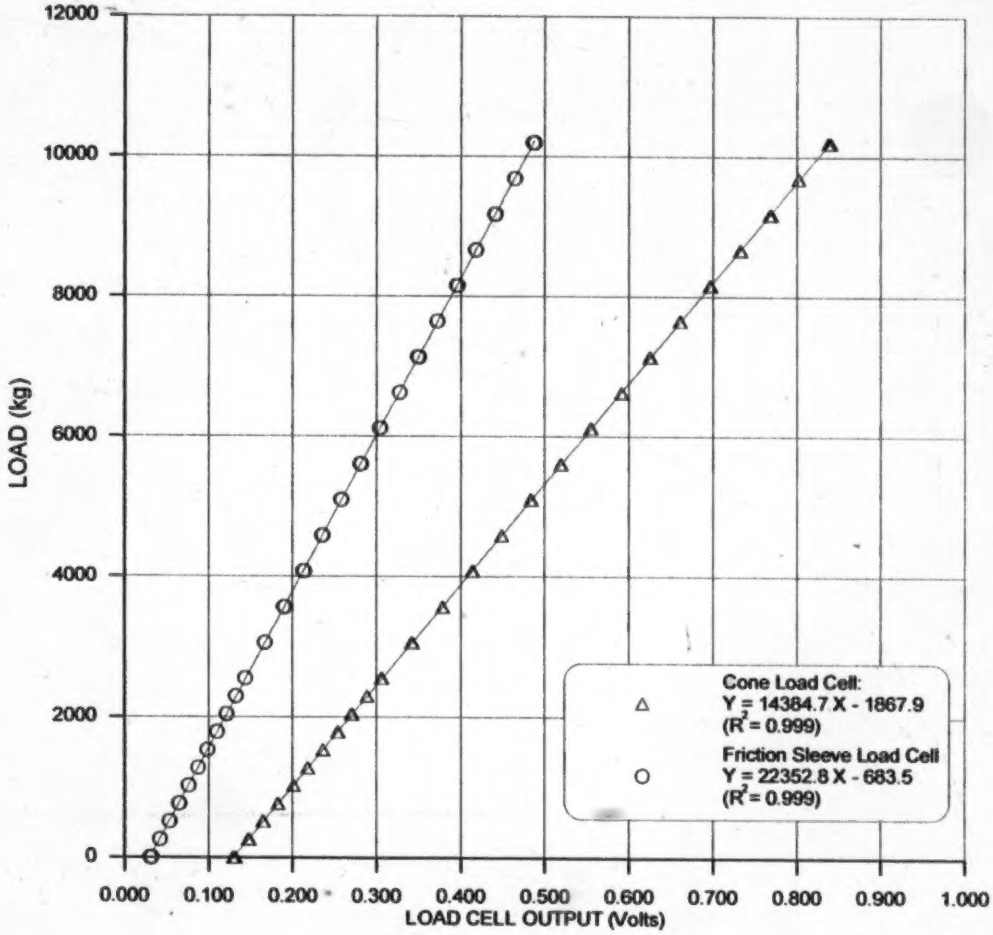

Figure 4.17 – Cone and friction sleeve calibration curves

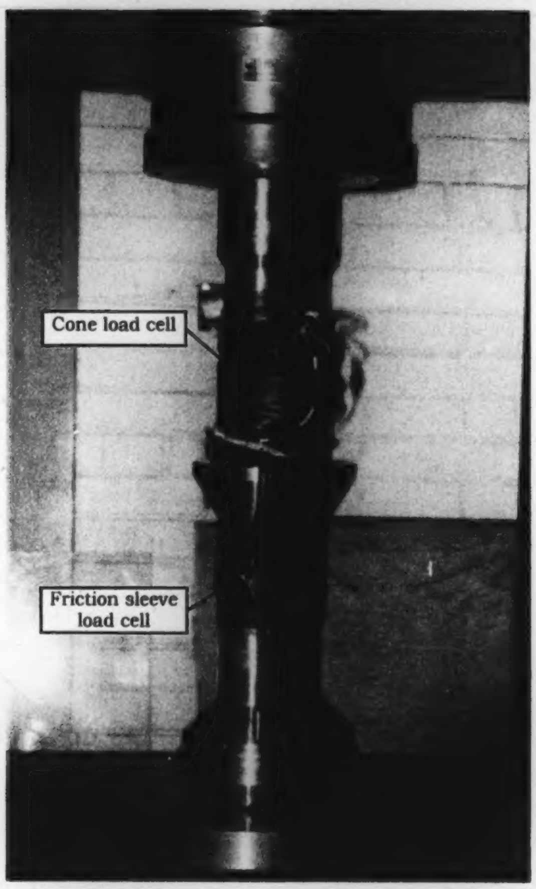
Cone load cell
Friction sleeve load cell

Figure 4.18 – View of the load cells calibration in the Universal Testing Machine.

### 4.4.5 DATA ACQUISITION SYSTEM

The data acquisition system was composed of a multi-turn precision potentiometer, which measures the probe's position during the test, two load cells, an analog-digital converter card DAQCard 700 manufactured by National Instruments and a laptop computer. The system was housed inside a van and powered by a gasoline generator. Figure 4.19 shows a schematic diagram of the electronics used in the HD-PB-CPT.

LabVIEW was used to develop a special program to control and monitor the HD-PB-CPT test. LabVIEW is a general-purpose programming system, but it also has libraries of functions and development tools designed specifically for data acquisition and instrument control which makes it a very powerful tool for the development of data acquisition software (LabVIEW 1998). LabVIEW also allows one to build a virtual instrument that consists of a front panel, and a dataflow diagram, written in *G* programming language, which serves as the source code.

Figure 4.20 shows the front panel displayed on the laptop screen, which allows one to control and monitor the HD-PB-CPT test. The test results, i. e., the cone resistance (MPa), the friction sleeve resistance (MPa) and the friction ratio (%) versus position (m) charts are displayed in real time, in 10 m segments. At any time during the test, it is possible to scroll the charts backward and forward to analyze any specific segments of the test.

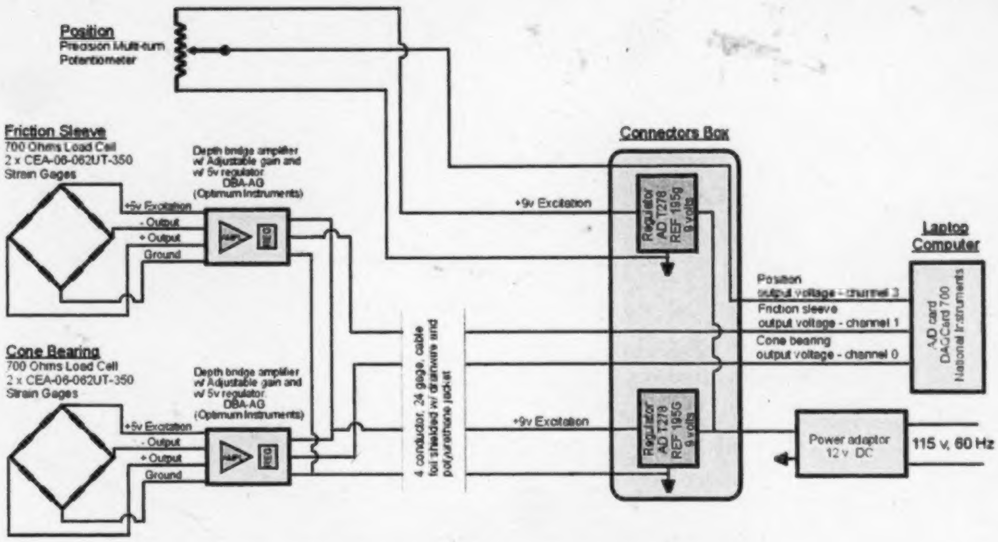
Position
Precision Multi-turn Potentiometer
Friction Sleeve
700 Ohms Load Cell
2 x CEA-06-062UT-350 Strain Gages
Depth bridge amplifier w/ Adjustable gain and w/ 5v regulator DBA-AG (Optimum Instruments)
+5v Excitation
- Output
+ Output
Ground
Cone Bearing
700 Ohms Load Cell
2 x CEA-06-062UT-350 Strain Gages
Depth bridge amplifier w/ Adjustable gain and w/ 5v regulator DBA-AG (Optimum Instruments)
+5v Excitation
- Output
+ Output
Ground
4 conductor, 24 gage, cable foil shielded w/ drainwire and polyurethane jacket
+9v Excitation
+9v Excitation
Connectors Box
Regulator AD T278 REF 195g 9 volts
Regulator AD T278 REF 195G 9 volts
Position output voltage - channel 3
Friction sleeve output voltage - channel 1
Cone bearing output voltage - channel 0
Laptop Computer
A/D card DAQCard 700 National Instruments
Power adaptor 12 v DC
115 v, 60 Hz

Figure 4.19 – HD-PB-CPT electronics.

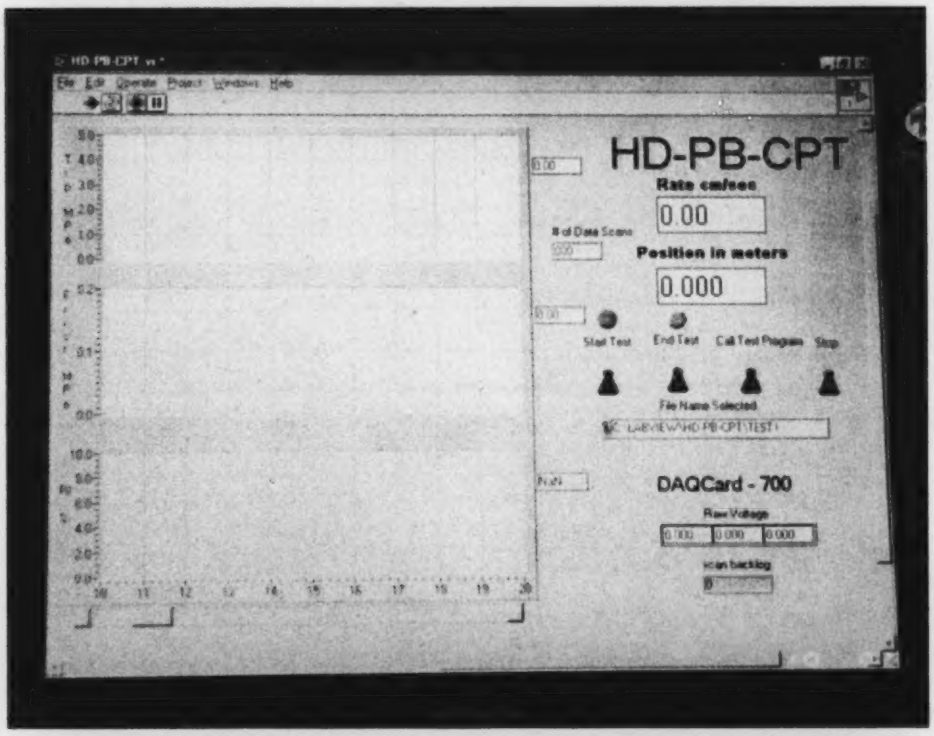
HD-PB-CPT.vi *
File Edit Operate Project Windows Help
50
40
30
20
10
0.0
0.2
0.1
0.0
10.0
8.0
6.0
4.0
2.0
0.0
10
11
12
13
14
15
16
17
18
19
20
HD-PB-CPT
Start Test
End Test
Call Test Program
Stop
DAQCard - 700

Rate cm/sec
0.00

# of Data Scans
0.00

Position in meters
0.000

File Name Selected
C:\LABVIEW\HD-PB-CPT\TEST1

Raw Voltage
0.000 0.000 0.000

scan backlog
0

Figure 4.20 – Data acquisition control and monitoring panel

The data is collected at each 5 cm of penetration and plotted on the screen charts. The actual calculated value is also shown in a small window on the top right side of each chart. The data value remains in this window until the next reading when it is replaced by the new values. Not only the calculated data are displayed but also the raw data (volts) are shown in three small windows on the bottom right corner of the screen. This feature helps to check if the sensors are working properly, since it is possible to monitor the output voltage of each instrument (load cells and position device) during the test.

The raw data (volts) and the calculated data are saved at each reading and the file can be accessed at any time via Excel. The analog-digital card scans the data at a rate of 100 scans/second and back averages the last 10 previously scanned data, saving and plotting it, hence minimizing any signal noise effect.

As recommended by the IRTP and ASTM (1995a) standard D 5778, the zero load reading has to be recorded before and after each test. Before the test, the zero load reading is performed by toggling the "Start Test" switch on the front panel screen, once the test is finished and the probe is free of any load, the "End Test" switch is toggled to record the end of test zero reading.

Also displayed on the front panel screen is the rate of penetration, in cm/seconds, and the probe's position in meters. If the probe is being pulled too quickly or too slowly it is possible, via radio communication, to give instructions to the HDD rig operator to adjust the probe's speed. Field tests have shown that the penetration rate must be closely monitored during the beginning of the test. It does not take the rig operator too long to get used to the of penetration rate of 2 cm/sec and to keep it reasonably constant. The HDD rig used in this field test uses 3 m long drilling rod, therefore, the test was conducted in strokes of 3 m.

Figure 4.21(a) shows a view of the van where the data acquisition was controlled as well as a view of the position measuring device and the HD-PB-CPT probe. Figure 4.21(b) shows a closer view of the position measuring device where the probe's cable can be seen placed on top of the multi-turn precision potentiometer.

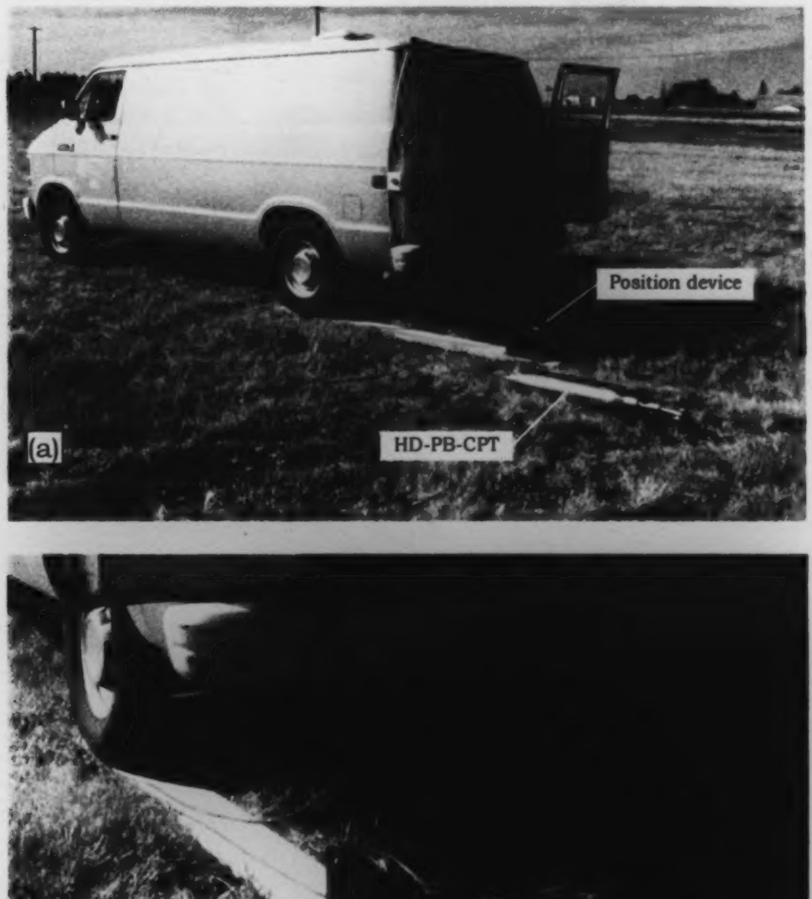

Figure 4.21 – (a) Data acquisition system van and (b) Position measurement device.

## 4.5 SUMMARY

A primary concern when performing a test in a pre-drilled borehole is soil disturbance. Nevertheless, experience with pressuremeter tests has shown that soil disturbance can be overcome by creating large enough cavity strain that extends well beyond the disturbed region and reaches the limit pressure in the natural soil. Pilot tests performed in Lake Edmonton clay at the University of Alberta field laboratory indicated that a cavity strain of 37 % seems to be sufficient to achieve the limit pressure in the natural soil for this kind of deposit. Therefore, the first prototype of the HD-PB-CPT was designed to create a soil cavity strain of 50 %, which was expected to be sufficient to achieve the limit pressure in the natural soil for most kinds of soils.

Despite its large dimensions, the design of the HD-PB-CPT is analogous to a standard CPT with subtractive type load cells. A key difference is that the HD-PB-CPT has a hollow shaft along its longitudinal axis that transfers the pulling force from the front of the probe to its back and also allows drilling fluid to pass through the tool promoting pressure equilibrium in front of the probe.

A special program, using LabVIEW, was developed to control and monitor the entire HD-PB-CPT test. The data acquisition system plots the test results on a laptop computer screen in real time. The data can also be retrieved via Excel for later analysis. The HD-PB-CPT position during the test is measured by a multi-turn precision potentiometer. The probe's data acquisition cable is placed on top of a wheel which rotates as the probe is being pulled. This sends a voltage variation signal to the analog-digital card which reads the signal and converts its value to a position in meters.

The data is collected at each 5 cm intervals and is saved and plotted on the charts on the laptop screen. The acquisition system scans the data at a rate of 100 scans/second back averaging the last 10 scans, hence, minimizing any signal noise effects.

# CHAPTER 5

# Prototype 1 – Field Tests

## 5.1 INTRODUCTION

Once prototype 1 was built, several tests were performed at the University of Alberta field laboratory at the same location of the previous vertical pilot tests and within 50 m of the four standard CPTU tests performed by ConeTec (Appendix 1).

The drill rig used to perform the field test of prototype 1 was the Vermeer Navigator D24/40 owned and operated by SubTerra Corporation. This rig has a pullback force of 105.9 kN (23 800 lbs) and can drill a 10.16cm (4") diameter borehole or a 8.9cm (3.5") diameter borehole if using a customized drill bit.

To be certain that the drill rig's pullback capability would not be exceeded a brief calculation of the total force required to pull the HD-PB-CPT through the pre-opened hole was conducted using the data from the CPTU tests (Appendix 1) performed previously at this site (Chapter 4). As shown in Table 5.1, for this kind of soil, the force required to pullback prototype 1 was much smaller than the capacity of the Vermeer Navigator D24/40 drill rig.

To minimize the frequency of drill rig relocation and reduce mobilization time, it was decided to perform two tests at the same horizontal alignment, but at different depths. One, was performed at approximately 2 meters depth and to assure a separation distance between the two tests of more than 10 times the probe's diameter, the other test was performed at a depth of about 4 meters, as shown in the sketch in Figure 5.1. This represents one meter increase in the test depth from what was originally planned. This depth was considered acceptable to retrieve the probe by excavation if something went wrong.

Table 5.1 - Estimated pulling forces.

| Depth 2.5m | $q_c$ (kPa) | $f_s$ (kPa) | $R_f$ (%) | Soil Type | $Q_c$ (kN) | $F_s$ (kN) | $F_T$ (kN) |
|---|---|---|---|---|---|---|---|
| CPT 1 | 1750 | 85 | 5 | Clay | 17.4 | 22.8 | 40.2 |
| CPT 3 | 1500 | 85 | 6 | Clay | 14.9 | 22.8 | 37.7 |
| CPT 4 | 1600 | 95 | 6 | Clay | 15.9 | 25.4 | 41.3 |
| Average | 1617 | 88 | 5.7 | - | 16.1 | 23.6 | 39.7 |
| **Depth 4.0m** | **$q_c$ (kPa)** | **$f_s$ (kPa)** | **$R_f$ (%)** | **Soil Type** | **$Q_c$ (kN)** | **$F_s$ (kN)** | **$F_T$ (kN)** |
| CPT 1 | 1750 | 60 | 3 | Silty Clay | 17.4 | 16.1 | 33.5 |
| CPT 3 | 1500 | 50 | 3 | Silty Clay | 14.9 | 13.4 | 28.3 |
| CPT 4 | 1550 | 60 | 4 | Clay | 15.4 | 16.1 | 31.5 |
| Average | 1600 | 57 | 3.3 | - | 15.9 | 15.2 | 31.1 |

Cone contact area ($A_C$) = 101.3 cm$^2$ Friction Sleeve area ($A_{FS}$) = 2729.0 cm$^2$

$q_c$ = cone stress resistance, $f_s$ = friction sleeve stress resistance, $R_f$ = friction ratio, $Q_c$ = cone force resistance, $F_s$ = friction sleeve force resistance and $F_T$ = total force

At these depths the soil is mainly a constant layer of Lake Edmonton clay; therefore, to create a well defined contrast between two soil zones, a 3.5 m x 3.5 m x 3.75 m deep pit was excavated along the proposed test alignment and filled with clean sand. Appendix 2 contains the gradation curve, maximum and minimum densities and the relative density $G_s$ (former specific gravity) of the sand.

The sand was dumped into the pit without any compaction rendering the sand to be in a very loose state. Figure 5.2 (a) shows the pit being opened. The walls of the pit show that the soil is a homogeneous clay. Figure 5.2 (b) shows the sand being dumped into the pit. A steel pipe was placed in the corner of the sandpit to allow measurement of the ground water table depth.

Later, in the second series of field tests the sand was totally removed from the pit and the pit was re-filled with sand, compacted in layers using the bucket of the backhoe. Due to the variability of the compaction process it was not possible to obtain a homogeneous increase of density throughout the whole sandpit.

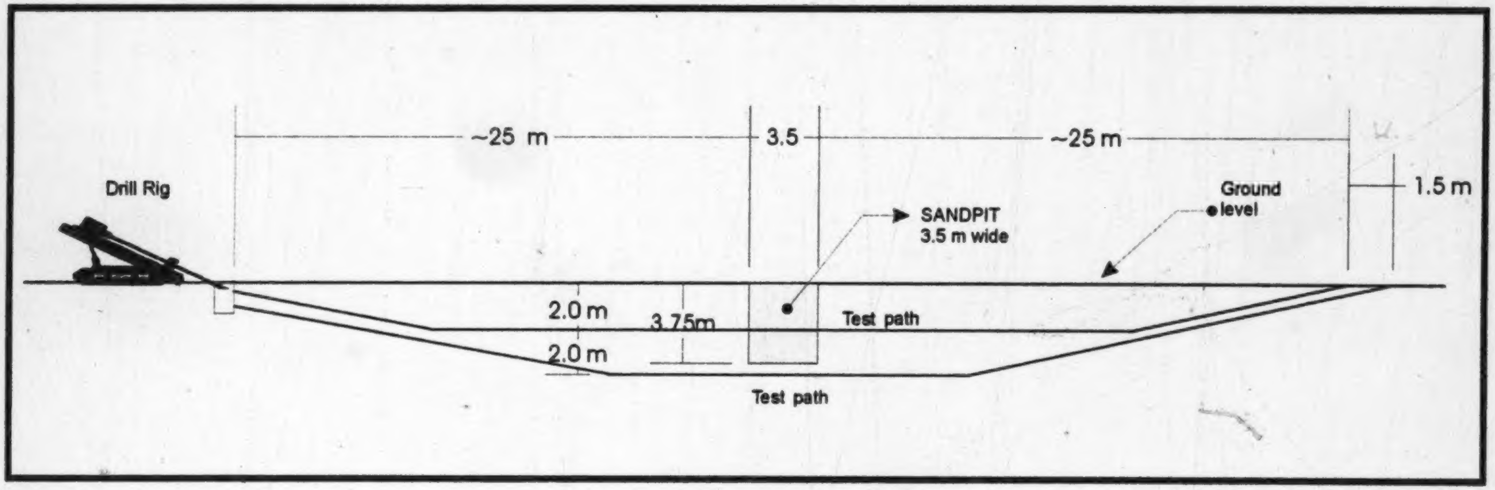
~25 m
3.5
~25 m
Drill Rig
Ground
level
1.5 m
SANDPIT
3.5 m wide
2.0 m
3.75m
Test path
2.0 m
Test path

Figure 5.1 - – Field test profile.

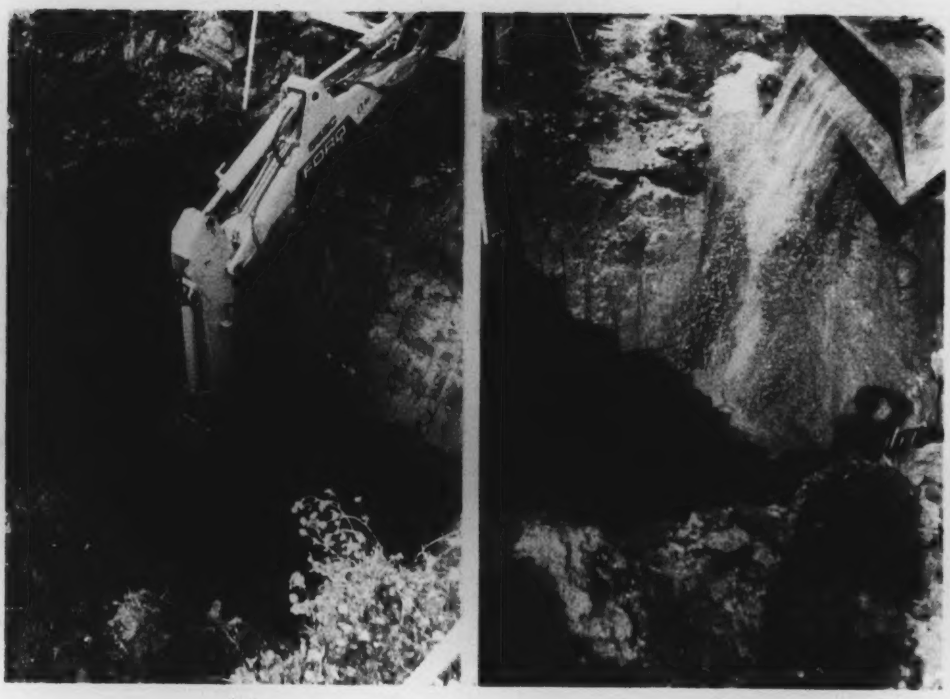

(a) (b)

Figure 5.2 – (a) Excavation of the pit; (b) Filling with sand.

## 5.2 FIRST SERIES OF FIELD TESTS

Two tests were performed during this stage, Test 1 was performed at a maximum depth of 2.2 m, and Test 2 at a maximum depth of 4.6 m. The main goals of this first stage of field work were to test the concept of this new probe, to identify areas of weakness in the probe design that may need improvement, and also to identify the best configuration options needed to perform the HD-PB-CPT test. The major variables examined were:

- with and without a reamer;
- with and without rotation of the reamer, and
- with a different kind of drilling fluid (bentonite, polymer or plain water)

Because the drilling contractor did not have a 10.16 cm (4") diameter reamer available it was not possible to perform a test in a reamed borehole as planned previously.

Drilling fluid was used to stabilize the borehole, cool the drilling bit and lubricate the bit/soil contact. For Test 1, the pilot bore was made using Hydraul-EZ, a bentonite-based drilling fluid manufactured by CETCO (Colloid Environmental Technologies Company). The lubricant property of the drilling fluid may have been one of the reasons for the almost nil friction sleeve resistance recorded in Test 1. To improve friction sleeve resistance, it was decided to perform the pilot bore for Test 2 using no drilling fluid.

Once the pilot bore was completed, prototype 1 was attached to the drill stem and pulled back through the borehole. Figure 5.3 (a) through (d) show the beginning of the penetration process.

Figure 5.3 (d) shows that the hollow shaft allows air or drilling fluid to pass through the probe promoting pressure equilibrium in front of the probe. This feature is important mainly because of the use of the reamer in front of the tool to avoid the development of a vacuum inside the borehole between the reamer and the probe. Despite the fact that a reamer was not used in these first series of tests it was the intention to use one in the future to provide a smoother borehole.

The total time to perform a 50 m long test was about two hours; one hour to bore the pilot hole and another hour to perform the test. This time can be reduced once the operators become more familiar with the boring phase of the process. Because the penetration test was conducted using the same rate of penetration used by a standard CPT, i. e., 2 cm/s, not much can be done to speed this part of the HD-PB-CPT test.

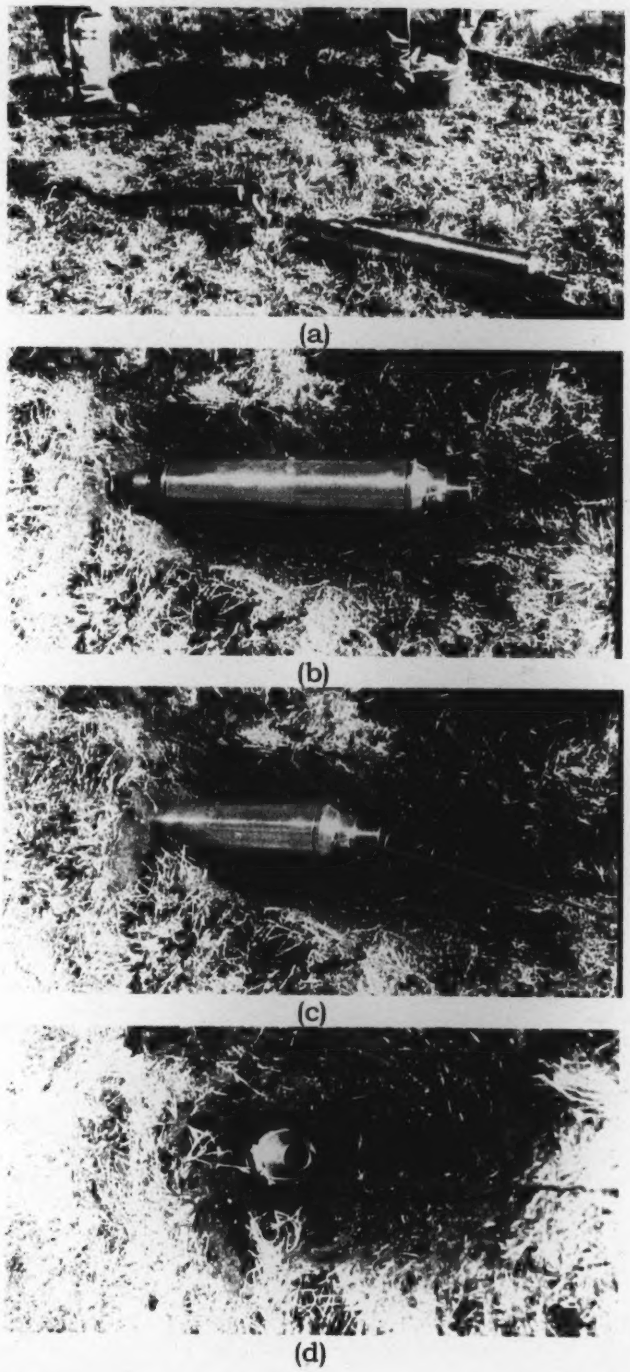

Figure 5.3 - (a) drill stem and probe hook-up; (b) beginning of penetration; (c) continuing penetration, and (d) Rear view of penetration.

### 5.2.1 RESULTS AND DATA ANALYSIS OF TEST 1

Cone resistance, sleeve friction and the friction ratio of Test 1 are presented in Figure 5.4.

Because the borehole was drilled using drilling fluid, the measured sleeve friction and thus the calculated friction ratios were practically zero during the test; nevertheless, cone resistance rendered a very encouraging result. While the probe was in the clay, a more or less constant cone resistance value was obtained, as expected. As soon as the HD-PB-CPT reached the sand pit the tip resistance showed a remarkable drop, then, increased to the same level as before when it exited the sand pit. The reason for the relative drop in tip resistance when the probe reached the sand pit, instead of an increase as usually happens with tip resistance in sands, is due to the very loose state of the sand, as mentioned in section 5.1. Since the clay pit had vertical side walls, it is also possible that arching may have occurred in the sand resulting in a significant decrease in horizontal stresses in the sand thus reduced tip resistance.

Despite measuring essentially no sleeve friction it was possible to easily identify the sand pit position simply from the cone resistance profile. This data shows that the HD-PB-CPT has the potential to identify sand pockets, if not yet in a quantitative way, at least in a qualitative manner.

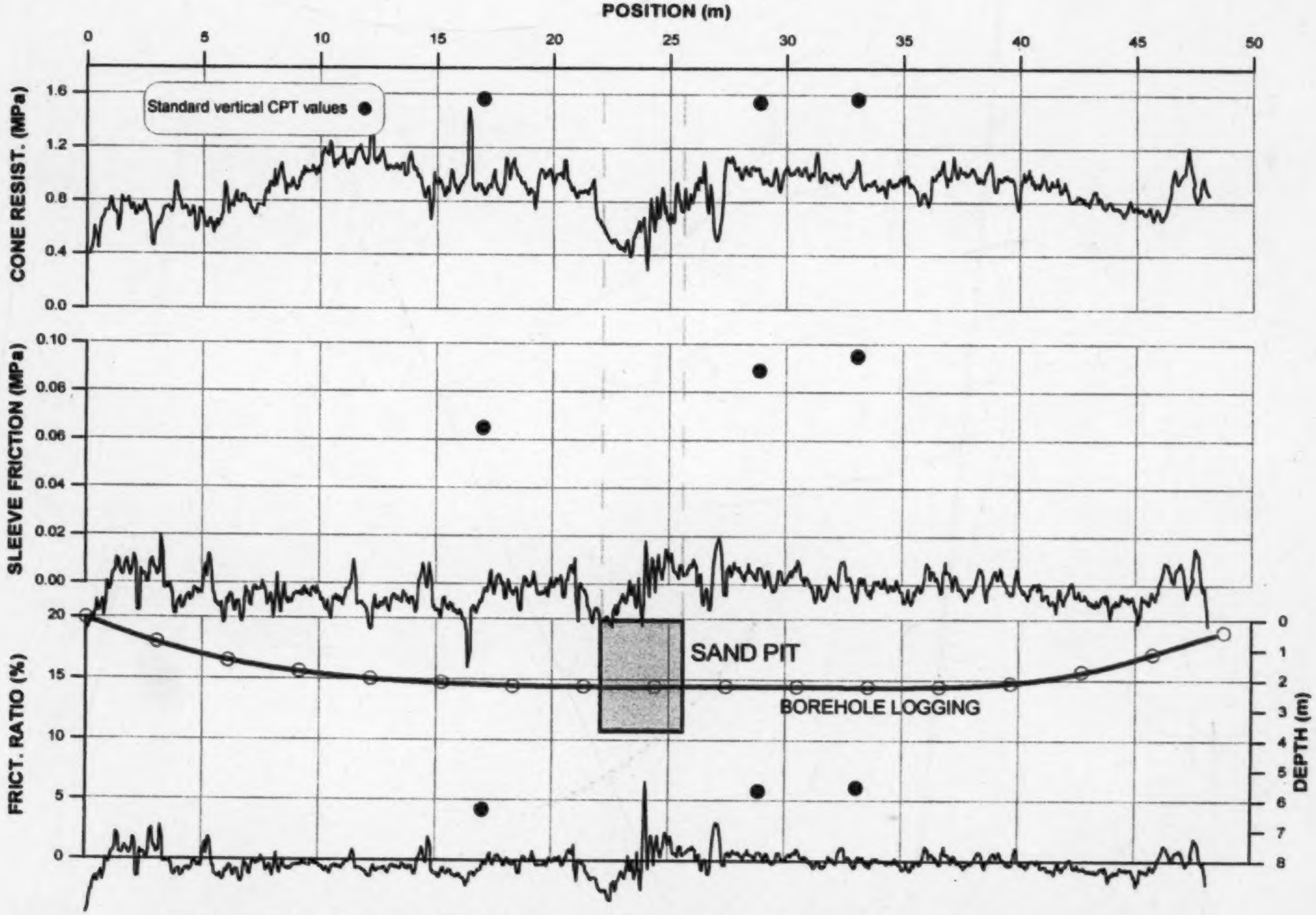

Figure 5.4 – HD-PB-CPT field Test 1 (drilled with a 4" bit and drilling mud).

The black dots on Figure 5.4 indicate standard vertical CPT data, (Appendix 1) performed at the site. The distances where the CPT data (black dots) were plotted were arbitrarily chosen simply for reference; nevertheless the data depth for both tests, CPT and HD-PB-CPT, were the same.

The ground water depth was measured prior to the test and was at 3.04 m below ground level, thus, Test 1 was performed above the ground water.

### 5.2.2 RESULTS AND DATA ANALYSIS OF TEST 2

As mentioned previously, Test 2 pilot hole was drilled dry in order to improve sleeve friction. When boring a dry hole special attention must be paid to the drill bit temperature. High temperature, due to the lack of coolant fluid, will not only damage the drilling bit but also the guidance system that is housed right behind the drilling head. Fortunately, the tracking system allows for the monitoring of the guidance system temperature as the hole is being bored, making it possible to develop a dry pilot hole.

To reach the planned depth (4 m) without having to drill a much longer borehole than the previous one a smaller radius of curvature was used. This made the steering process a little more difficult and the final depth of the pilot hole was 4.6 m instead of 4 m.

Test 2 results are shown in Figure 5.5. This time, the sleeve friction resistance values were significantly higher than those of Test 1, but still lower than those obtained by the standard vertical CPT (black dots on Figure 5.5).

It is interesting to note that the cone resistance of Test 1 was higher than that of Test 2. The borehole for Test 1 was drilled using drilling mud and a formation of a mud cake around the borehole walls might have developed. Mud cake formation can be as thick as 2.5 cm (CMW 1996) promoting in this way a smaller diameter pilot hole. This may have led to higher cone resistance.

Again, Test 2 also shows a noticeable drop in cone resistance values as it reaches the sand pit. Even though the probe passed 1.1 m beneath the sand pit, the reduction in tip resistance may reflect stress relief in the clay due to the sand pit excavation. Additionally, the friction ratio indicated a significant change when the probe passed under the sand pit resulting primarily from the reduced tip resistance. The sleeve friction over this region was approximately the same on average, but more variable.

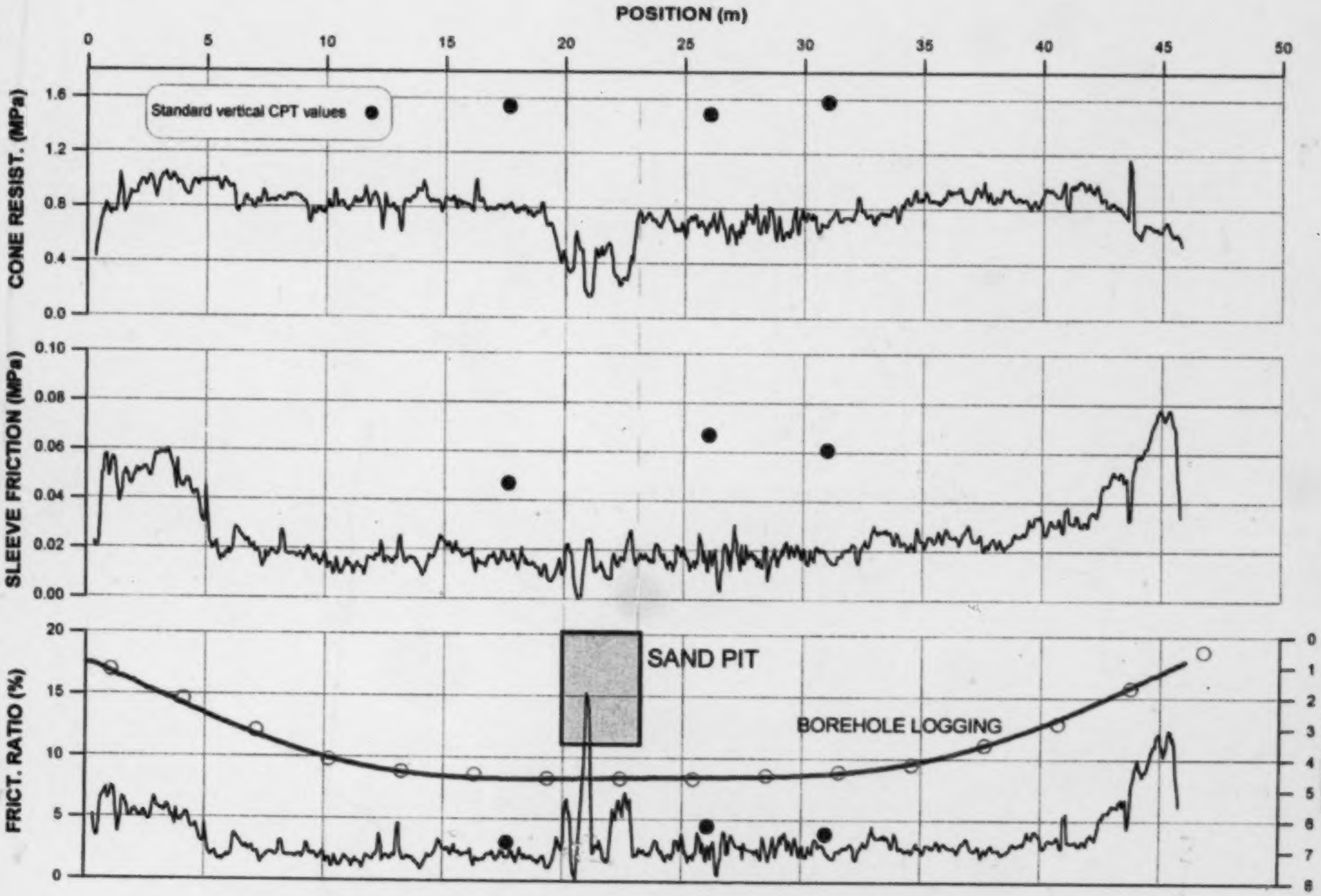

Figure 5.5 – HD-PB-CPT field Test 2 (drilled dry with a 4" bit).

The HD-PB-CPT test will not likely be used at depths greater than 30 m; in this regard the use of normalized data are not really necessary (Robertson 1990). Nevertheless, normalized plots emphasize the borehole curvature effect on the cone resistance values, as can be seen on the normalized plots for Tests 1 and 2, Figure 5.6 and 5.7 respectively. The cone and sleeve friction values are higher as the probe passes through the curved part of the borehole. Because of the significant length of the probe, bending forces are also involved in these curved sections of the test. As the borehole levels out and only a straight pull is in effect, the normalized tip and friction sleeve stresses diminish to constant values.

Figure 5.8 shows the normalized cone resistance versus depth from the CPT performed at the site (Appendix 1). In a given soil deposit cone and sleeve friction resistance usually increases with increasing overburden stress. Normalized cone data are used, therefore, to avoid changing soil classification due to increasing overburden stress when performing a CPT test at great depths. Following that, it was expected that the value of the normalized cone resistance ($Q_c$) from the vertical standard CPT data (black dots) plotted on normalized graphs from Test 1 and 2 would be approximately the same, since both tests were performed in the same type of soil, but it is not. This means that the soil at 2 m depth is slightly different than the soil at 4 m depth. This difference in soil type can be better visualized in the profile shown in Figure 5.8. The upper 2–2.5 m layer has an average $Q_c$ value of approximately 40, $Q_c$ average values then decrease to approximately 20, becoming reasonably constant with depth thereafter.

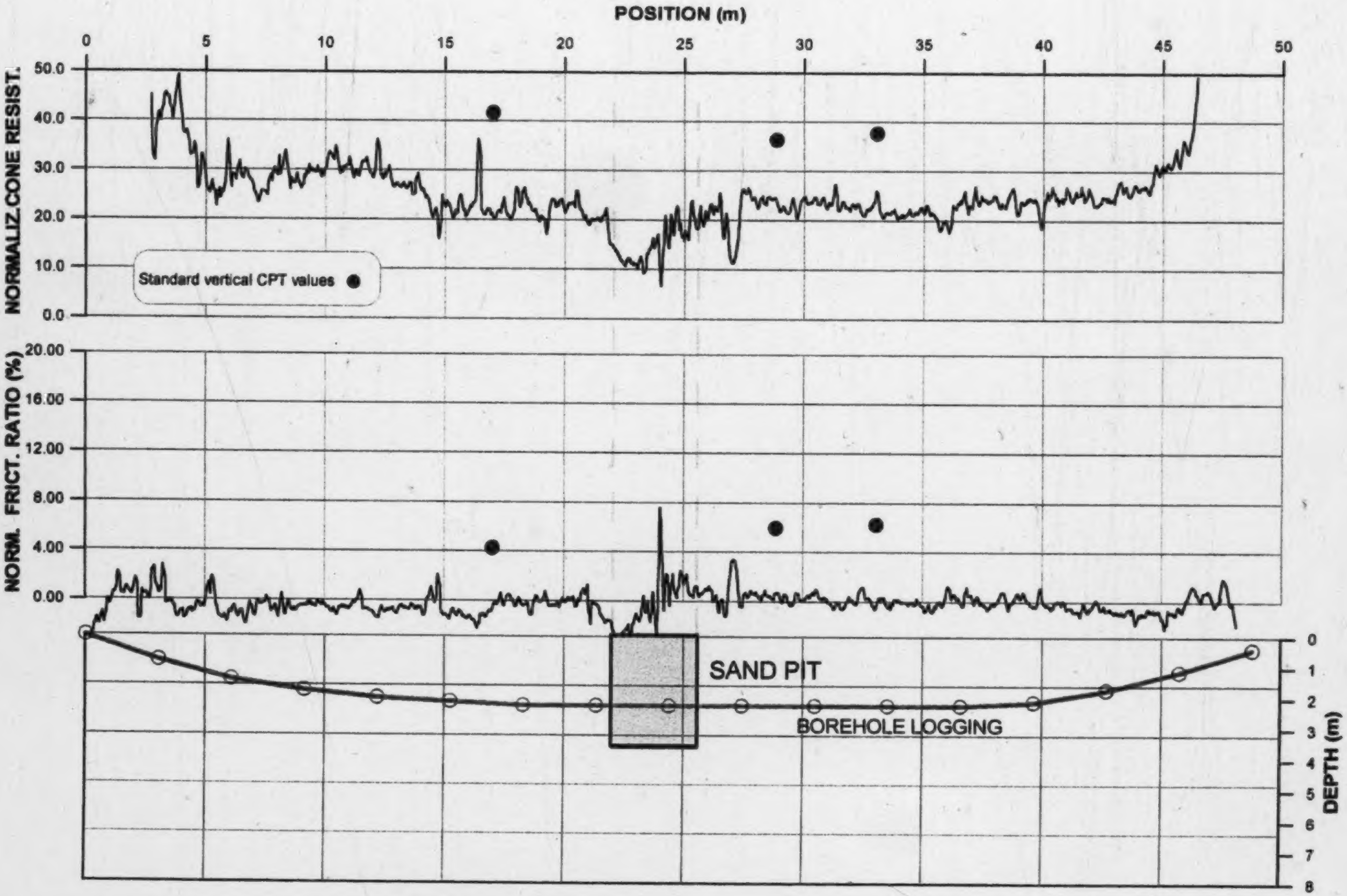

Figure 5.6 – Normalized data from HD-PB-CPT Test 1.

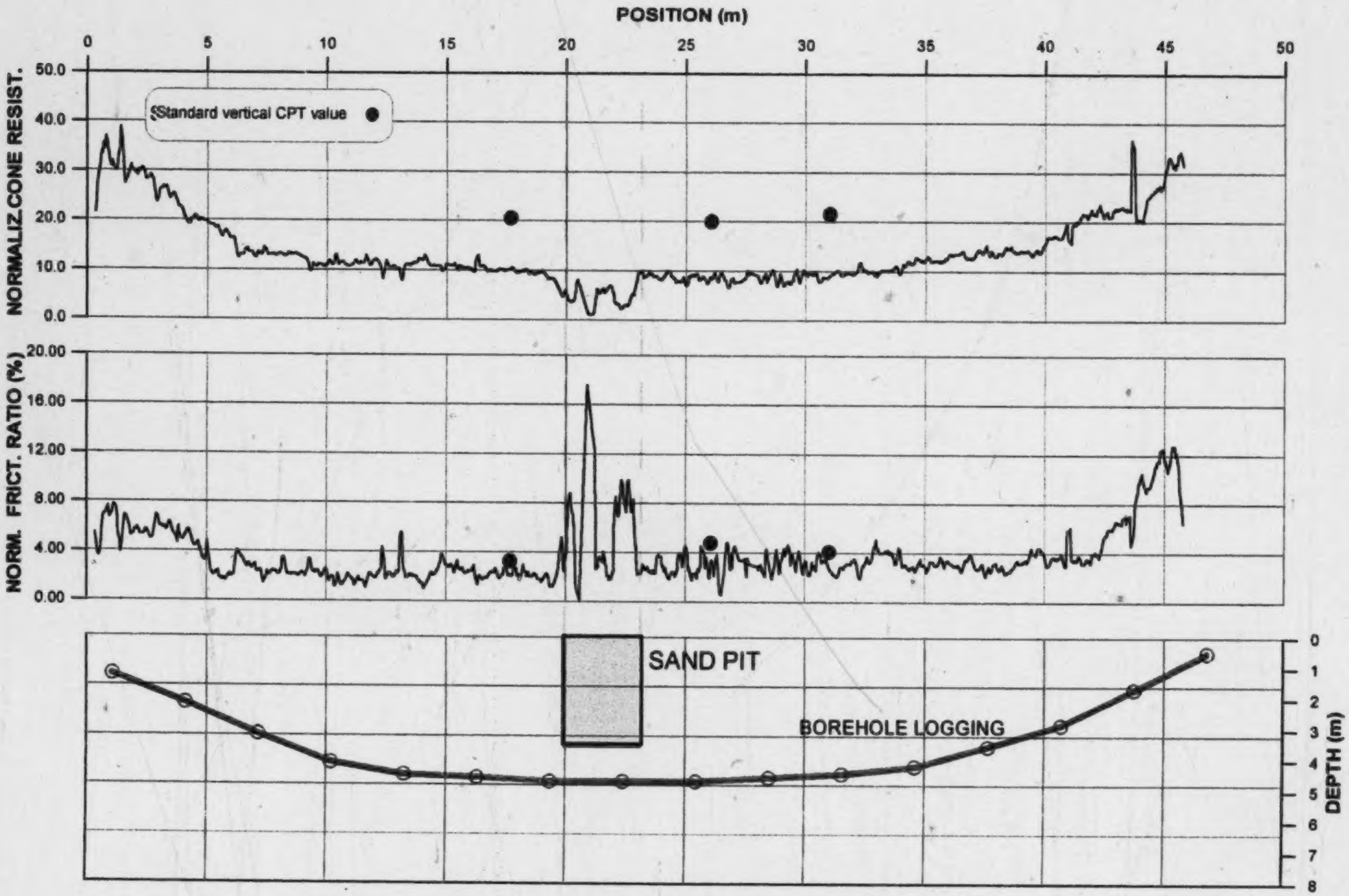

Figure 5.7 - Normalized data from HD-PB-CPT Test 2.

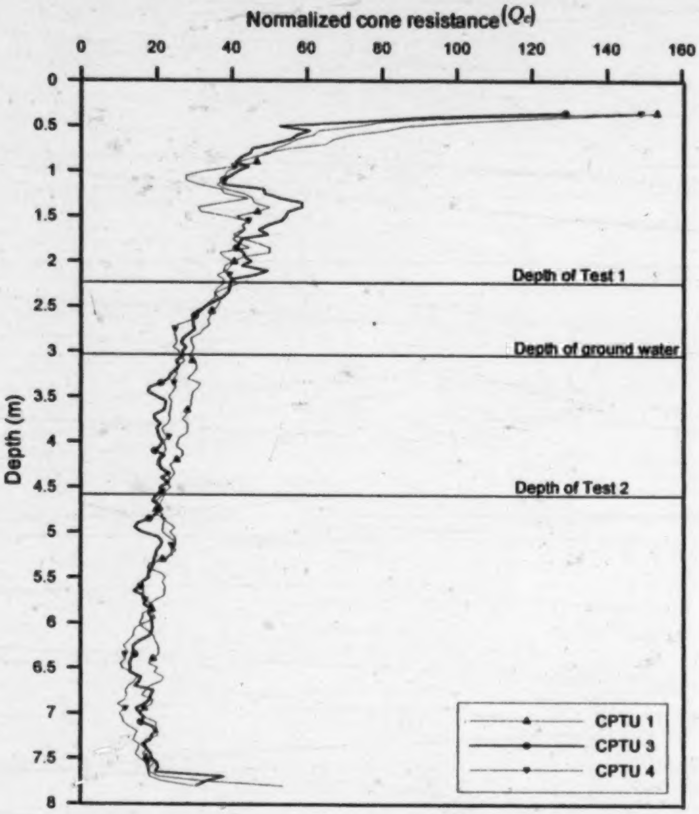

Figure 5.8 Normalized CPT cone resistance versus depth.

To make a comparison between the soil type prediction from the HD-PB-CPT data and from three standard vertical CPT tests (Appendix 1), normalized data of Test 2 were used and plotted into the soil behavior type classification chart (Robertson 1990) as shown in Figure 5.9. To avoid overcrowding the graph only the standard vertical CPT data from the region of interest (1.5 m to 5.5 m in depth), closer to the HD-PB-CPT tests were plotted. The curved sections of Test 2 as well as the data beneath the sand pit were disregarded in this plot.

Despite the HD-PB-CPT having slightly lower values than the standard CPTs, for both cone and friction resistance, both test data fell, more or less, in the same soil zone in the soil behavior type classification chart, that is, silty clay and clayey silt, which is consistent for the Lake Edmonton clays. This indicates that, although there were differences in measured values between the standard vertical CPT data and the HD-PB-CPT results, the resulting soil behavior types using the established CPT method (Robertson 1999) were very similar. Hence the early results using Prototype 1 were encouraging.

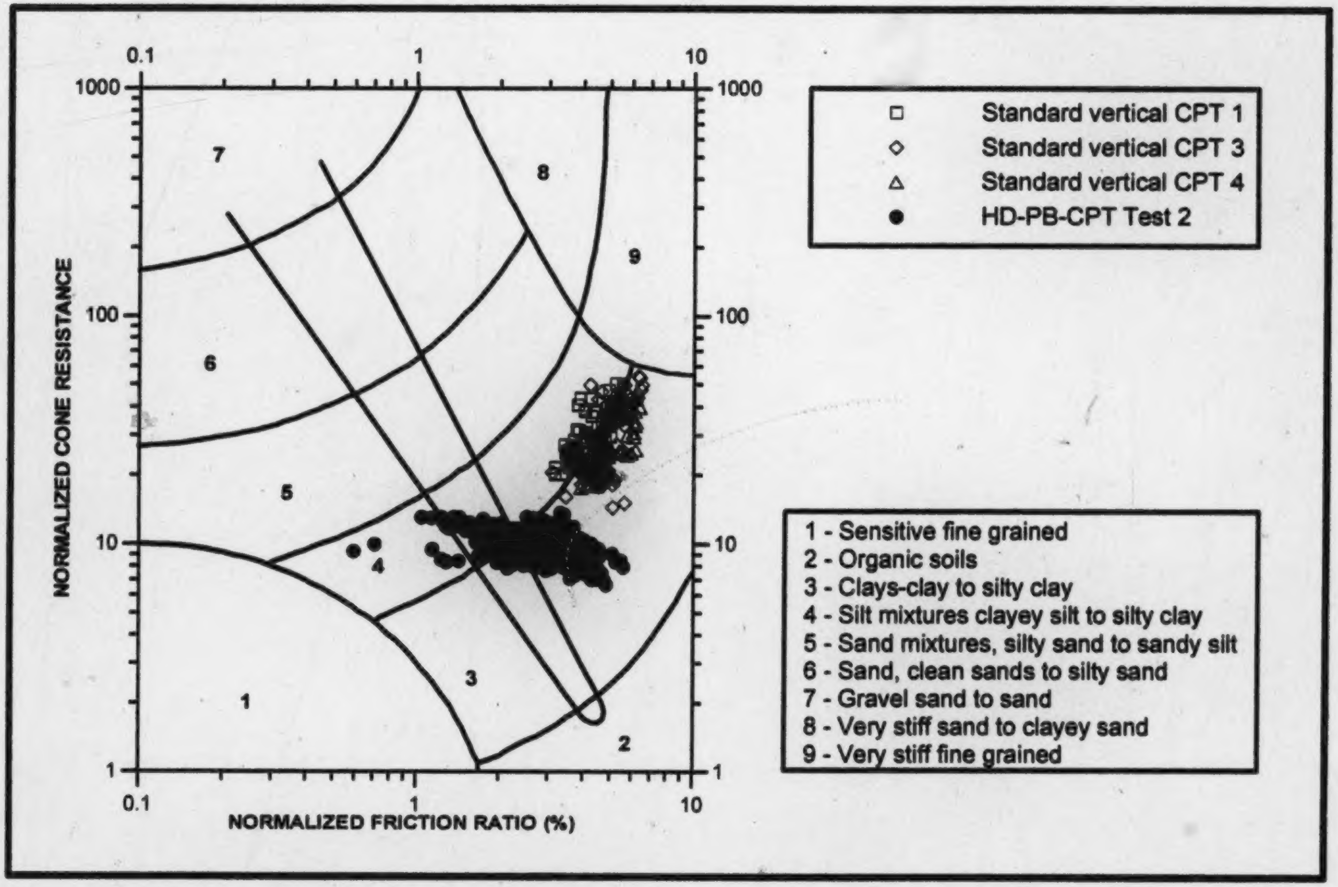

Figure 5.9 –Soil behavior type classification HD-PB-CPT (Test 2) and standard CPT data (modified from Robertson 1990).

## 5.3 SECOND SERIES OF FIELD TESTS

The first series of tests of prototype 1 was not enough to fully define the best way to perform the HD-PB-CPT and to obtain conclusive data about the performance of this new probe. Hence, three more tests were performed at the University of Alberta field laboratory.

To take advantage of the existing sand pit and to avoid interference from the previous tests, these sets of tests were performed at approximately 45 degrees in relation to the former ones, as shown on the sketch in Figure 5.10. The sand pit density was also increased by removing the sand and re-compacting it in layers with the bucket of the backhoe.

To try to improve cone and friction resistance, the drilling bit diameter was reduced to 8.89 cm (3.5") from the 10.16 cm (4") used previously. Furthermore, a special 10.16 cm (4") diameter reamer was built and used in Tests 4 and 5 with the object of obtaining a smoother cylindrical shaped hole. This reamer consisted of a 50 cm long steel pipe with spherical welded end caps (Figure 5.11a and b) that was pulled, without rotation, in front of the probe.

To try to obtain the best possible cylindrical pilot hole an alternative drilling method was used to bore the pilot hole of Test 3. This alternative consisted of drilling a 2 or 3 m section of the borehole, then pulling the drill string backward, with continued rotation of the drilling bit, and finally pushing the string forward again for the next 2 or 3 m of boring. This procedure was intended to deliver a more cylindrical and homogeneous pilot hole. This procedure was only used to drill half of the pilot hole, i.e., from the beginning of the test up to the sand pit; from the sand pit to the end of the test, the pilot hole was drilled in a conventional manner.

Drilling a dry borehole to capture friction sleeve resistance is not a desirable drilling method because the heat generated may jeopardize the guidance system housed behind the drilling bit. Some drilling fluid would have to be used to cool the system, however, for the HD-PB-CPT it is desirable that it does not reduce the friction between soil and probe. To this end, water only was used as a drilling fluid in Tests 3 and 5, but Test 4 still was drilled dry for a better comparison with the results from Test 2.

Following the same procedure as was used in the first series of field tests, these tests were performed at a depth of approximately 2 and 4 meters as shown in the sketch on Figure 5.1. To perform Test 5 the drill rig was moved about 2 m to the south side (Figure 5.10) to avoid interference with the previous two tests (Tests 3 and 4).

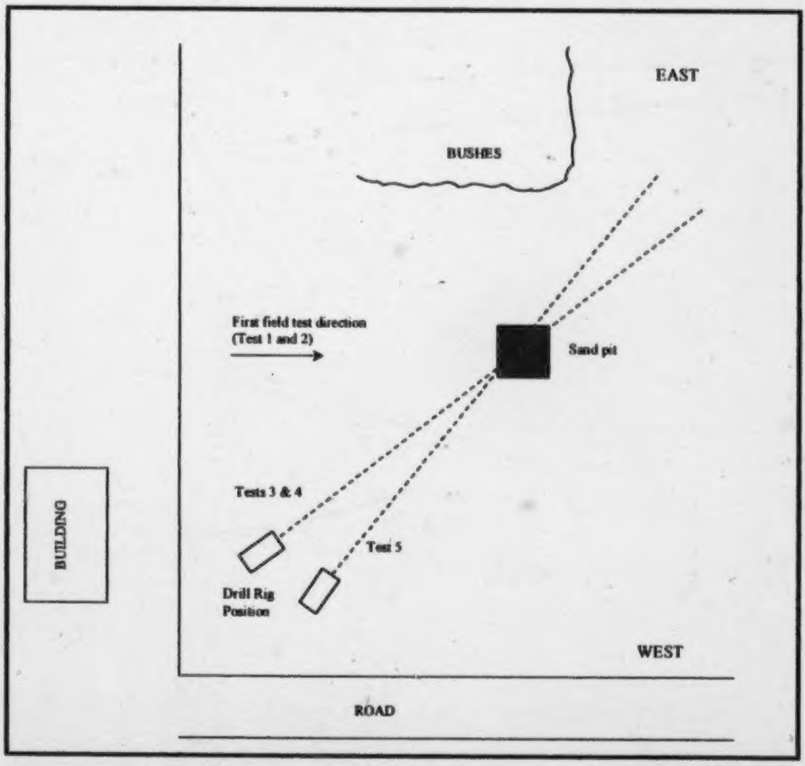
EAST
BUSHES
First field test direction
(Test 1 and 2)
Sand pit
Tests 3 & 4
Test 5
BUILDING
Drill Rig
Position
WEST
ROAD

Figure 5.10 – Directions for the second series of field tests.

(a)

(b)

Figure 5.11 – a) Steel pipe adapted to work as a reamer and b) Test assembly

### 5.3.1 RESULTS AND DATA ANALYSIS OF TEST 3

The results of Test 3 are shown in Figure 5.12, and the normalized data are presented in Figure 5.13.

Despite using water as a drilling fluid the sleeve friction did not show any noticeable reduction compared to the results of Test 2 (Figure 5.5). The cone resistance, however, did show a significant reduction compared with Test 2. Test 3 was, however, performed at a depth of 1.9 m while Test 2 was performed at a depth of 4.6 m, which means lower overburden stresses. The normalized cone resistance of Test 3 (Figure 5.13), however, was only slightly higher than Test 2 (Figure 5.7); but somewhat more erratic. This suggests that water might be a reasonable compromise as a drilling coolant fluid.

With respect to the different drilling technique of multiple-passes during drilling, used in the first half of this bore, it did not produce any significant improvement in tip and sleeve friction resistance; it only increased the test time and, therefore, this option was discarded.

The data in Figure 5.12 and Figure 5.13 shows that it was quite easy to identify the sand pit location. This time, due to the re-compaction of the sand, a significant increase in cone resistance can be seen in Figure 5.12 across the sand pit. The same is not clear for friction ratio, however, which shows a slight drop during penetration through the sand.

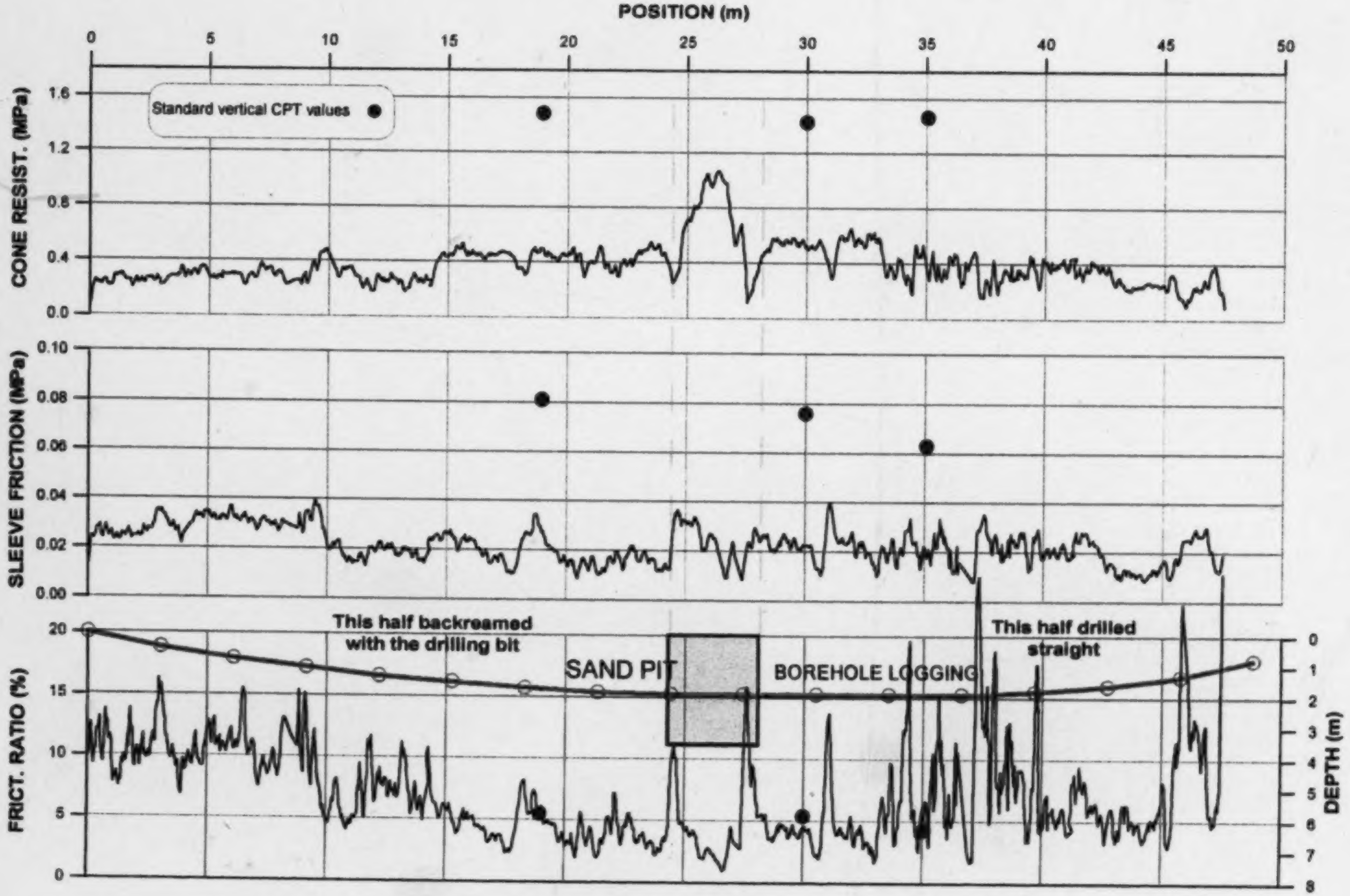

Figure 5.12 – HD-PB-CPT field Test 3 (drilled with a 3.5" bit using water).

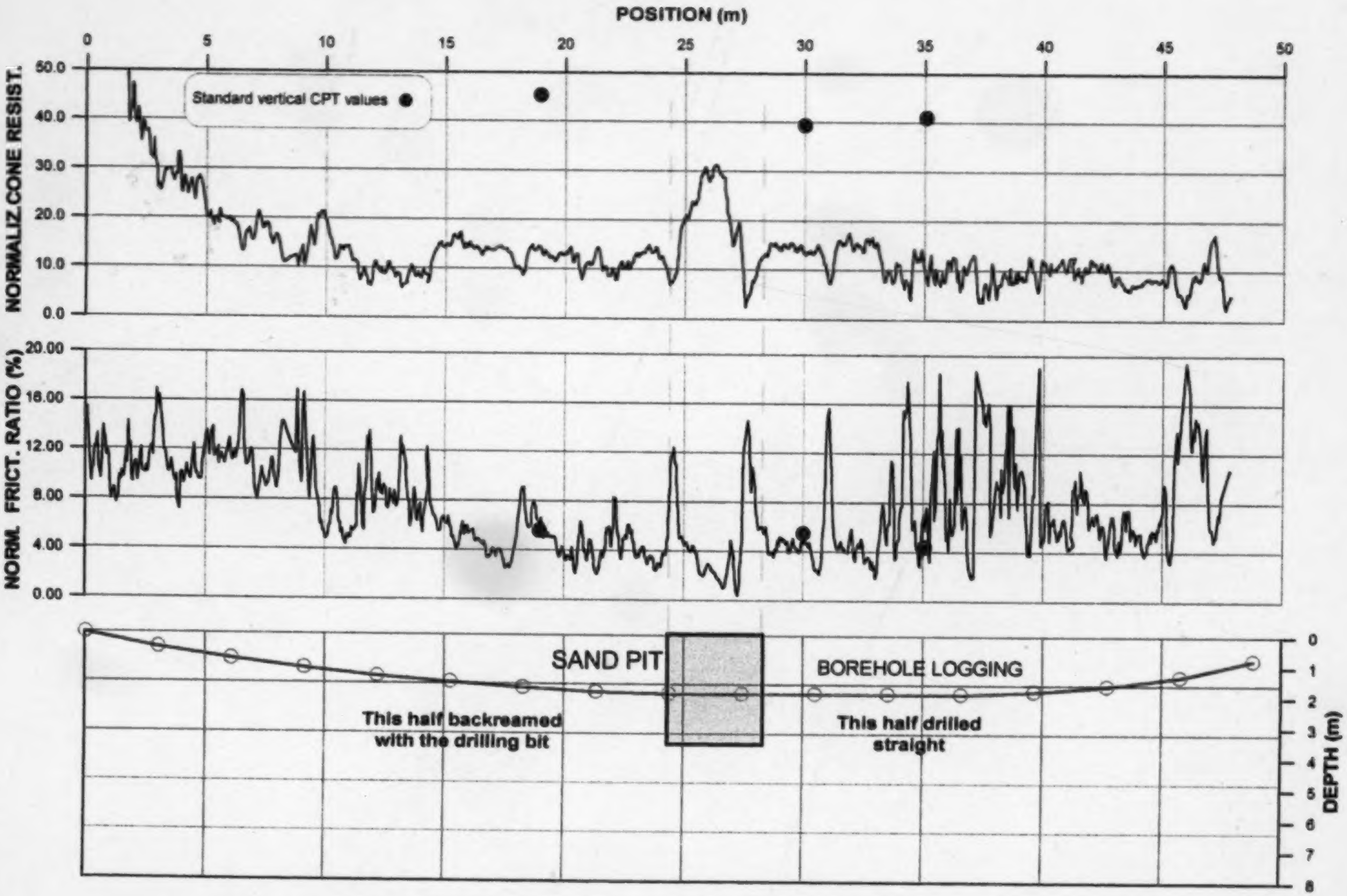

Figure 5.13 – Normalized data from HD-PB-CPT Test 3.

### 5.3.2 RESULTS AND DATA ANALYSIS OF TEST 4

Test 4 was performed in a pilot hole drilled dry with the 8.89 cm (3.5") drill bit. This time, the 10.16 cm (4") diameter reamer was placed ahead of the probe, and the whole assembly was pulled back through the borehole without rotation.

The planned depth for this test was 4 meters; hence a steeper approach angle was used to avoid drilling a long borehole. This brought about a steering problem because the smaller drilling bit (8.89 cm) was not able to properly steer the drilling string in this kind of clay. The resulting depth was 5 m, which made the HD-PB-CPT pass about 1.25 meters below the sand pit. This made the identification of the sand pit location very difficult, which is reasonable because the probe was totally in the clay as it passed beneath the sand pit. However, a slight decrease in cone resistance, possibly due to stress relief, was noticed in the test data shown in Figure 5.14. The normalized data in Figure 5.15, makes it even harder to see any noticeable difference in cone resistance at the region of the sand pit. Nevertheless, this test was the one that provided the closest result to the standard vertical CPT.

The non-normalized cone resistance data for Test 4 was approximately 1.1 MPa, not a significant increase in relation to the other tests. However, the sleeve friction resistance was more or less the same for all tests (i. e. approximately 0.02 MPa), except Test 1, regardless of whether drilling was done with water or not. It seems that the smoother borehole created by using the reamer did not increase tip and friction resistance; however, it appears to have reduced the scatter that was seen in Test 3.

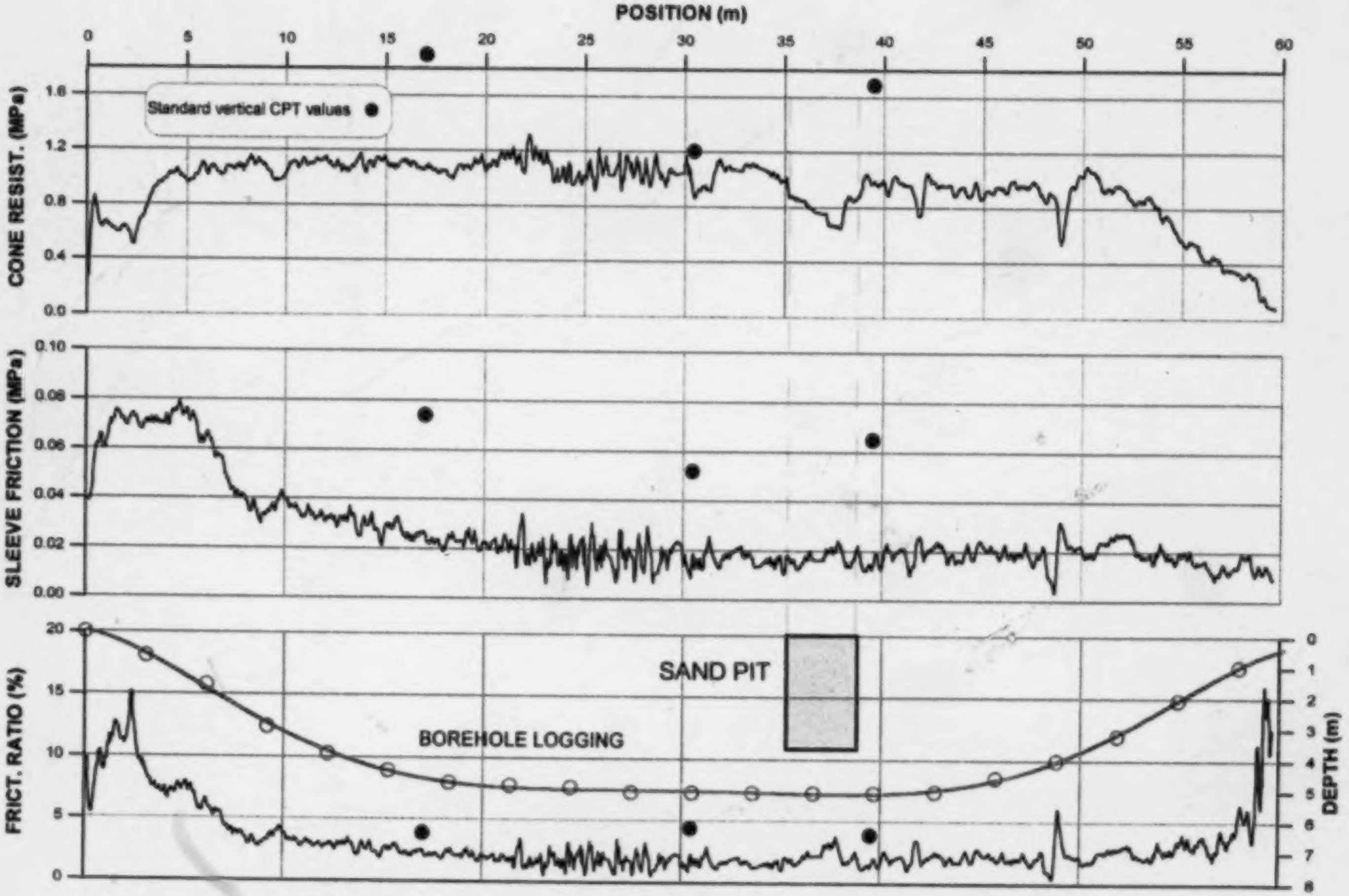

Figure 5.14 - HD-PB-CPT field Test 4 (drilled dry with a 3.5" bit, reamer was used).

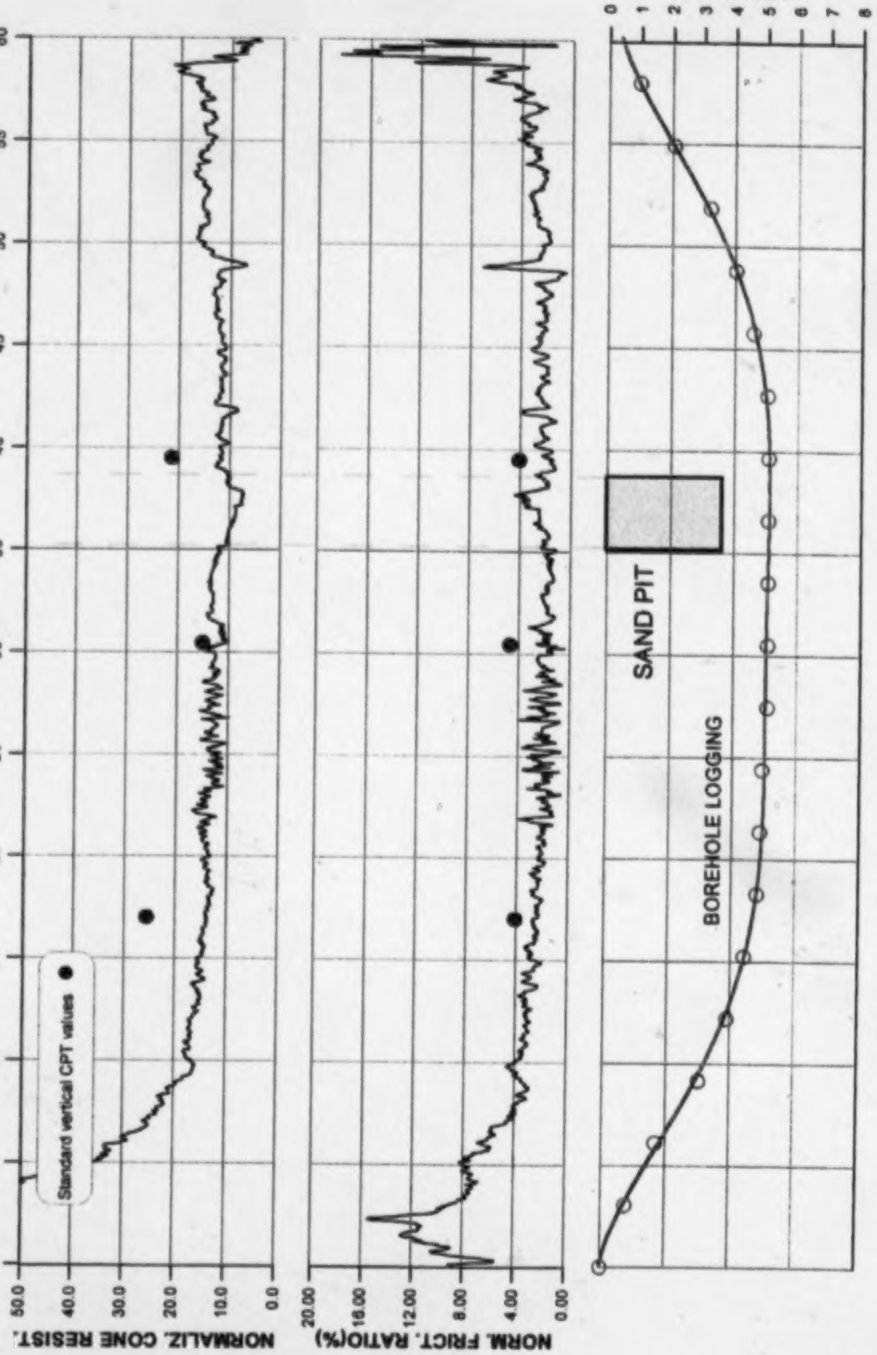

Figure 5.15 - Normalized data from HD-PB-CPT Test 4.

### 5.3.3 RESULTS AND DATA ANALYSIS OF TEST 5

The last test of this series was performed at a depth of 2.7 meters. The pilot hole was bored with a 8.89 cm (3.5") drill bit and water as a drilling fluid and the test was performed using the 10.16 cm (4") diameter reamer. The cone resistance profile (Figure 5.16) shows a clear change in pattern as the HD-PB-CPT reaches the sand pit; the same happens with the friction ratio showing that the probe is able, at least qualitatively, to identify the location of the sand.

The sand pit tip resistance did not increase as it had in Test 3. This result might be due to the variability of the sand re-compaction process that was not able to produce a uniform compaction throughout the entire sand pit, and also to the presence of the hole left behind from the previous test at the same depth (Test 3), or even due to the borehole collapse in the sand.

From the normalized data shown in Figure 5.17, it can be seen that the cone resistance and friction ratio was on average the same value as the previous tests, which indicates that, at least for this kind of soil, the water used during the drilling process does not affect the test result.

The erratic results over the last quarter of the normalized friction ratio, Figure 5.17, happened on the curved section. This makes the interpretation difficult because of the likely bending forces that act on the probe in this section. The erratic data in the curved section of the sounding may also result from the lack of a uniform borehole due to the lack of rotation of the drilling string when the hole is changing direction.

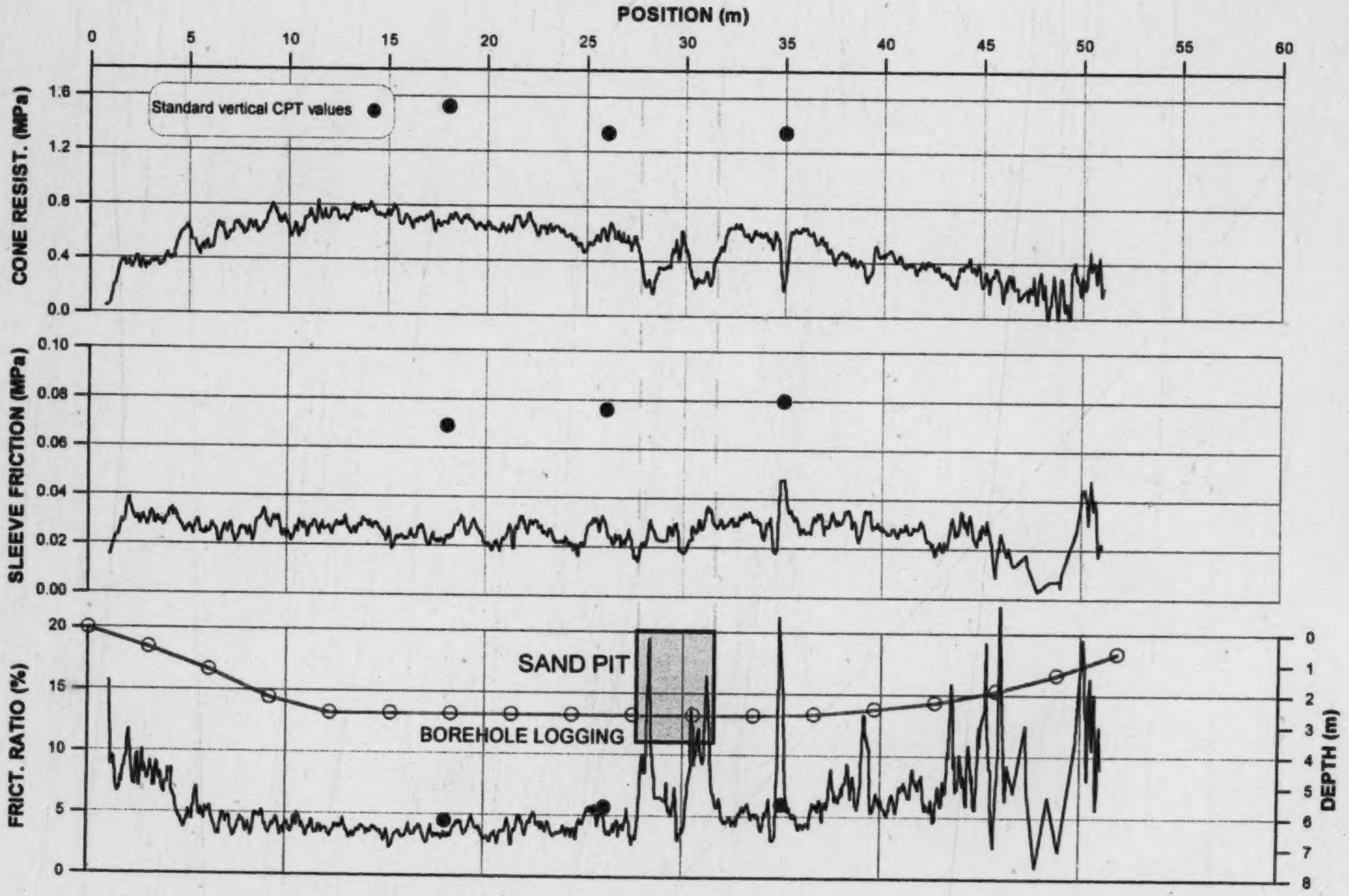

Figure 5.16 - HD-PB-CPT field Test 5 (drilled with a 3.5" bit and water, reamer was used).

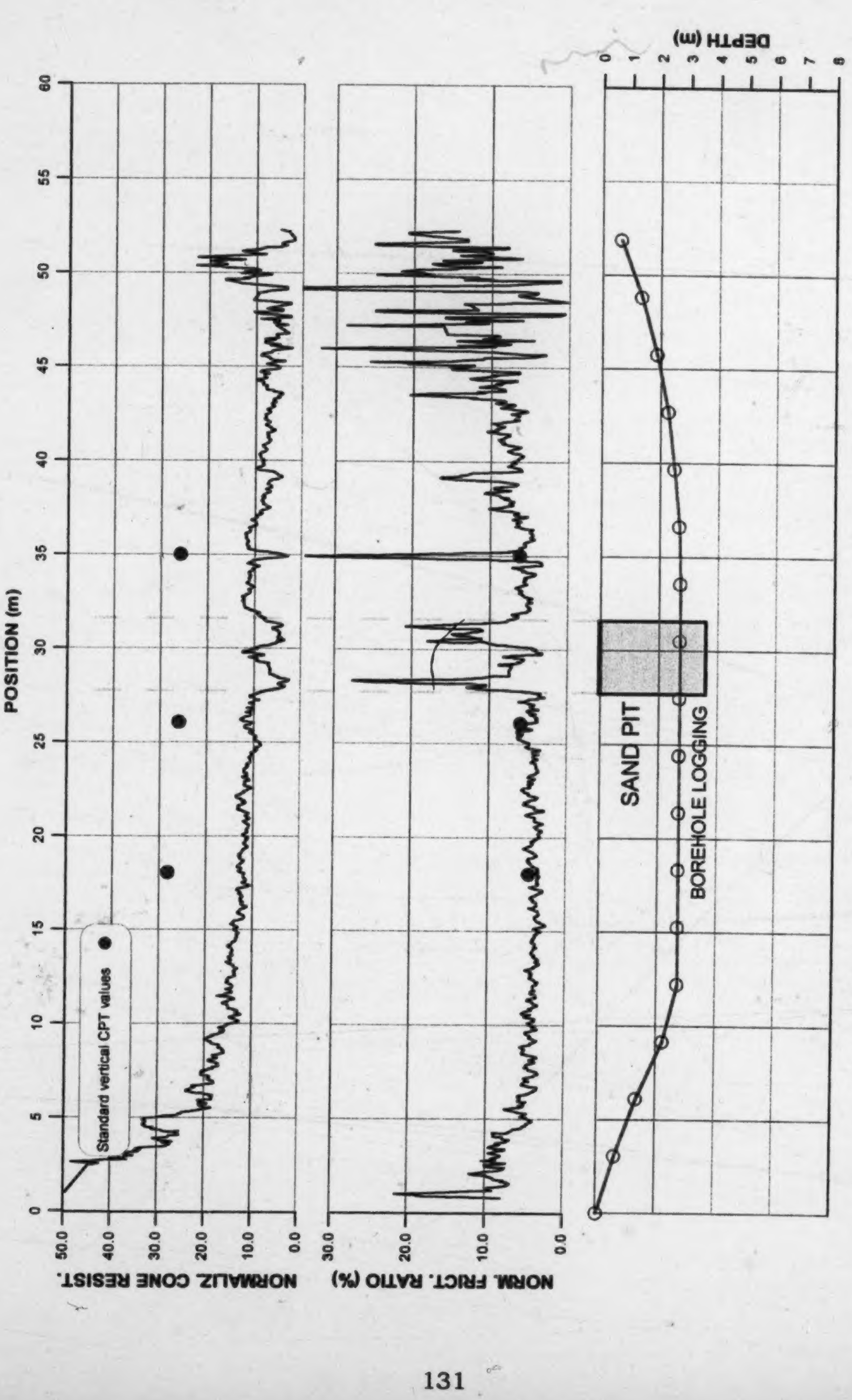

Figure 5.17 - Normalized data from HD-PB-CPT Test 5.

## 5.4 FINAL CONSIDERATIONS

From the different drilling techniques and assembly configurations used to perform the previous tests the following observations were obtained from the prototype 1 field tests:

- cone and friction resistance results of the standard CPT were generally higher than the results obtained by the HD-PB-CPT. Nevertheless, the friction ratio results for both test types were very similar. This suggests that whatever is affecting the HD-PB-CPT cone and friction results is affecting both measurements to the same degree, i.e., maintaining proportionality. This was somewhat different to that found by Broere and van Tol (1998);
- no noticeable increase in resistance (cone and friction) occurred when reducing the drilling bit size from 10.16 cm (4") to 8.89 cm (3.5");
- using the drilling bit to backream the borehole as performed in Test 3, did not provide any beneficial effect, it only increased the drilling time;
- drilling the pilot hole using water as a drilling fluid did not significantly change the cone and friction resistance; and
- the 10.16 cm (4") diameter reamer (steel pipe) in front of the probe (Tests 4 and 5) did not increase the cone and friction resistance, but it reduced the scatter of the data somewhat, mainly on the friction sleeve. However, the two tests performed with the reamer were not sufficient to obtain a definite conclusion in this regard.

Another interesting observation was the large amount of soil that was accumulated in front of the probe at the end of each test (Figure 5.18). Even when the reamer was used, there still was a significant amount of soil accumulation in front of the probe. This accumulation caused the hollowed shaft to clog, limiting the flow of any fluid through the tool. This soil accumulation may also be adversely affecting the cavity expansion process, thus, influencing the results.

There are two possible reasons for this accumulation; the first one is due to the boring process. To be able to steer the borehole, rotation is stopped and the entire drill string is then pushed forward by the drilling rig. This forces the whole assembly to follow the direction of the slanted wedge of the drilling bit. In clays, especially those with a small slanted wedge (8.89 cm), it is necessary to push the drilling string without rotation a long way before the desired correction in direction is achieved. This process creates a borehole with sections that are not cylindrically shaped. When the probe passes through these sections it can accumulate soil in front of it.

The second possible reason is due to soil displacement in the direction of the borehole. Studies from Acar and Tumay (1986), Sagaseta and Houlsby (1988), Teh and Houlsby (1991) and van den Berg (1994) show that for a cone with a 60° apex angle the penetration process creates a compressive plastic yielding of the soil in front of the penetrometer. Because the pilot borehole walls are not confined, the compressive strain that occurs in front of the cone may cause the soil to deform toward the hole, as shown schematically in Figure 5.19. This deformation pattern can cause soil accumulation in the front of the probe and also may be responsible for the lower cone and friction resistance obtained by the HD-PB-CPT tests. Once the soil is able to deform inwards and not outwards as in a regular cavity expansion, some of the stress might be reliefd which would reduce the test results. This issue will be discussed in detail in the next chapter.

PROBE
SOIL ACCUMULATION

Figure 5.18 – View of the soil accumulation in front of the probe after the test.

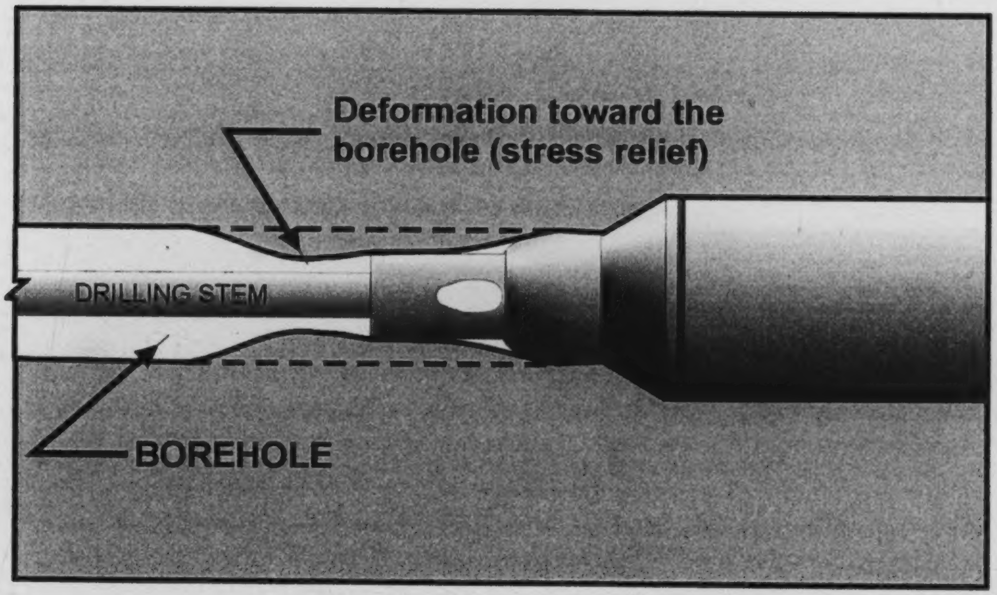
Deformation toward the borehole (stress relief)
DRILLING STEM
BOREHOLE

Figure 5.19 – Possible soil deformation in front of the probe (stress relief).

## 5.5 SUMMARY

Five prototype 1 HD-PB-CPT tests were performed at the University of Alberta field laboratory using different drilling techniques and drilling fluids. The soil at this site is mainly Lake Edmonton clay. To create a well defined contrast between two soils zones, a 3 x 3 x 3.75 m in deep pit was dug and filled with sand intersecting the middle of the test path.

Bentonitic drilling mud was not a good drilling fluid to use in HD-PB-CPT tests because it appeared to reduce the friction sleeve resistance to practically zero. However, water was shown to be effective as drilling fluid, since it provided cooling to the drilling assembly but did not significantly reduce the cone and sleeve friction resistance.

The results of the five tests have shown that the HD-PB-CPT is capable of defining the location of the sand pit.

The lower values of cone and friction resistance obtained by the HD-PB-CPT, in comparison with the standard vertical CPT test, may be a function of stress relief around the cone tip due to the soil being deformed inward toward the borehole instead of outward like in a cavity expansion process.

# CHAPTER 6

# Laboratory Modeling

## 6.1 INTRODUCTION

Several research studies (Baligh 1985; Acar and Tumay 1986; Sagaseta and Houlsby 1988; Teh and Houlsby 1991 and van den Berg 1994) have shown in analytical and laboratory modeling, that for a 60° vertical cone penetration test the soil below the cone tip is subjected predominantly to axial compressive strains. This is illustrated in Figure 6.1 by the strain contours around a 60° penetrometer in clay. In a prebored penetration test, the lack of confinement of the borehole wall may cause the soil ahead of the tip to deform into the borehole when subjected to compressive strains. This could reduce the built-up stress at the tip during penetration as compared to a regular CPT test. This lack of confinement and high compressive strains may also be one of the reasons for the soil accumulation in front of the probe, accounting for the lower cone and sleeve friction resistances obtained by the HD-PB-CPT in comparison with the standard vertical CPT.

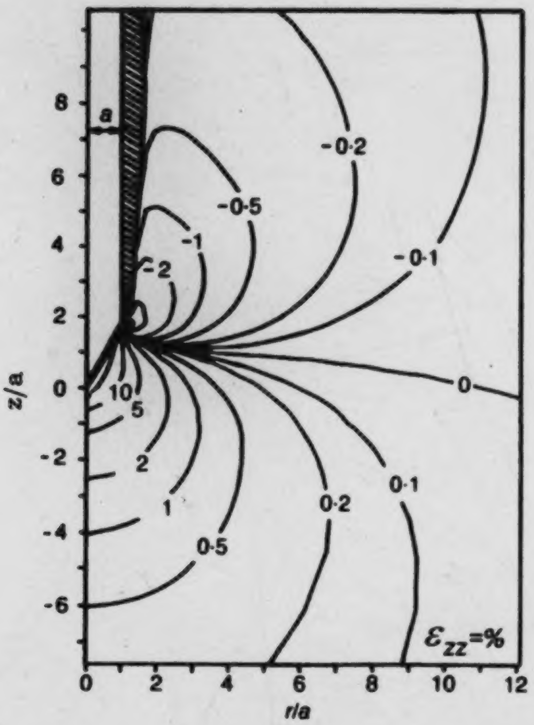

Figure 6.1 – Axial strain contours around a 60° penetrometer. Positive signs are compression strains (modified from Teh and Houlsby 1991).

A series of strain path calculations were carried out by Teh and Houlsby (1991) to show the influence of the cone apex angle ($\beta$) on the resultant soil strains during penetration in clay. They used the same strain invariants $E_1$, $E_2$ and $E_3$ as defined by Baligh (1985):

$$E_1 = \varepsilon_{zz} \qquad [6.1]$$

$$E_2 = \frac{1}{\sqrt{3}}(\varepsilon_{rr} - \varepsilon_{\theta\theta}) \qquad [6.2]$$

$$E_3 = \frac{4}{\sqrt{3}}\varepsilon_{rz} \qquad [6.3]$$

where:

$\varepsilon_{zz}$ = axial strain

$\varepsilon_{rr}$ = radial strain

$\varepsilon_{\theta\theta}$ = circumferential strain

$\varepsilon_{rz}$ = shear strain

$E_1$ represents the strain mode in triaxial compression, $E_2$ corresponds to the strain mode in a pressuremeter test and $E_3$ is the strain mode in a simple shear test. The strain paths shown in Figure 6.2 are for soil elements located initially at a radial distance of one radius from the vertical axis of the cone.

Figure 6.2 shows that increasing the cone angle results in a significant increase in $E_1$ and $E_3$. The axial strains below the cone tip are mainly compressive; however, they are much smaller for the 10° cone than for the 60° cone. According to Bishop et al. (1945), Teh and Houlsby (1991), and Silvestri and Fahmy (1995), the deformation due to the penetration of a very sharp cone is comparable to that predicted by cylindrical cavity expansion. The strain contours below the tip of a 60° cone are close to those predicted by spherical cavity expansion theory.

Acar and Tumay (1986) presented an interesting comparison of octahedral strains in a very soft clay based on analytical solution developed by two penetrometers with different apex angles, one with 18° and the other with 60° (Figure 6.3). By superimposing a borehole boundary with the same cone/borehole diameter ratio used in the HD-PB-CPT into this graph (grey shaded area) and looking at the octahedral strains at the contact cone-borehole wall, the direction of the arrows show that the sharper cone tends to push the soil to the side much more than does the 60° cone.

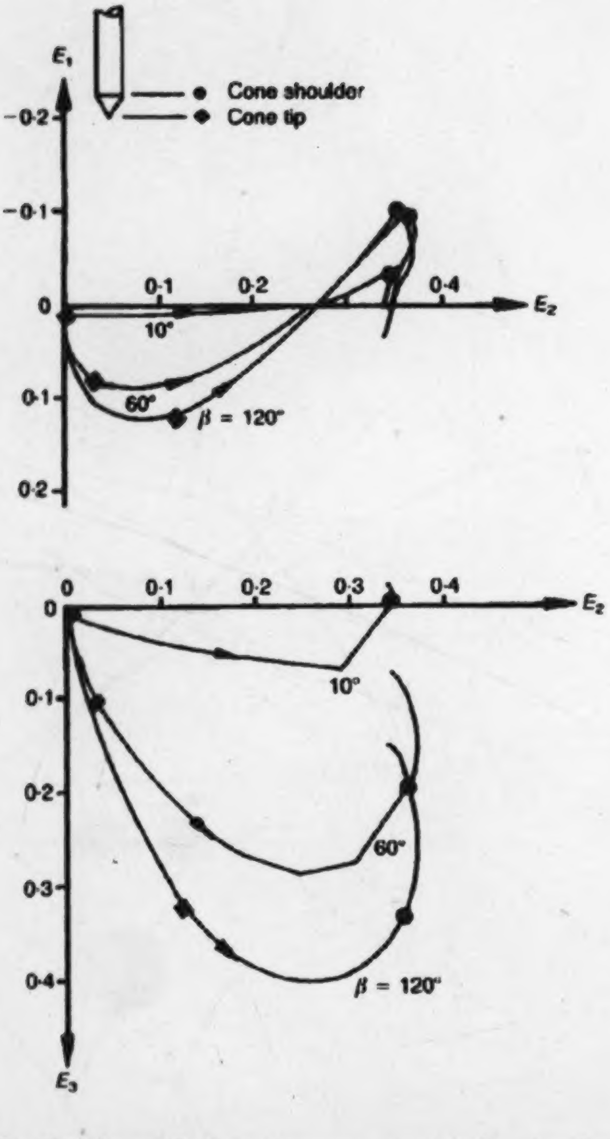

**Figure 6.2 – Strain path due to cone penetration in clay with different apex angles. (modified from Teh and Houlsby 1991)**

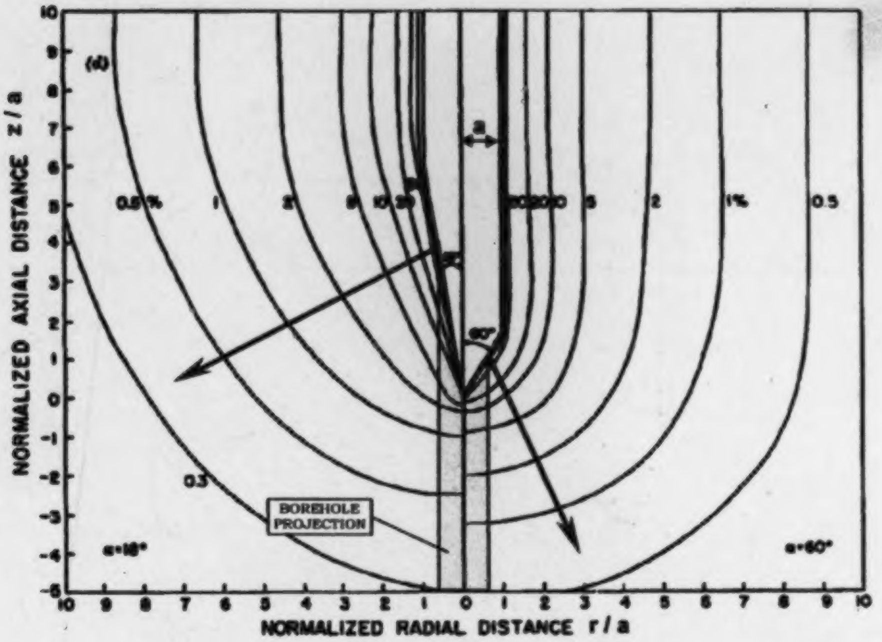

Figure 6.3 – Octahedral strains for 18° and 60° apex angle cones.
(modified from Acar and Tumay 1986)

According to Teh and Houlsby (1991), based on theoretical analysis, the failure zone around a penetrometer may be described by boundaries that divide the soil into two deforming regions, one elastic and the other plastic. They characterized the plastic boundary by means of two parameters: $r_p$, the radial distance of the plastic boundary from the axis of penetration, and $z_p$, the distance between the cone tip and the plastic boundary, measured along the axis of the penetrometer. The variation of these two parameters versus the rigidity index ($I_r$) (defined in section 4.2.3) of the soil is presented in Figure 6.4. From this plot it can be seen that the normalized plastic radius $r_p$ is independent of the cone angle and similar to that of cylindrical cavity expansion, whereas $Z_p$ is affected significantly by the cone angle. Moreover, for a 10° cone and soil's $I_r$ smaller than 100, $Z_p$ is zero. This implies that the soil adjacent to the cone tip may be divided into a plastic and an elastic zone, as shown in Figure 6.5. And for the combination of a very sharp cone with a low $I_r$ (i.e. soft soil), the cone can be said to cut through the soil, with $Z_p = 0$, as shown in Figure 6.5 (b). Whereas, for a more obtuse cone angle the penetration process causes compressive plastic yielding of the soil ahead of the penetrometer, as shown in Figure 6.5 (a).

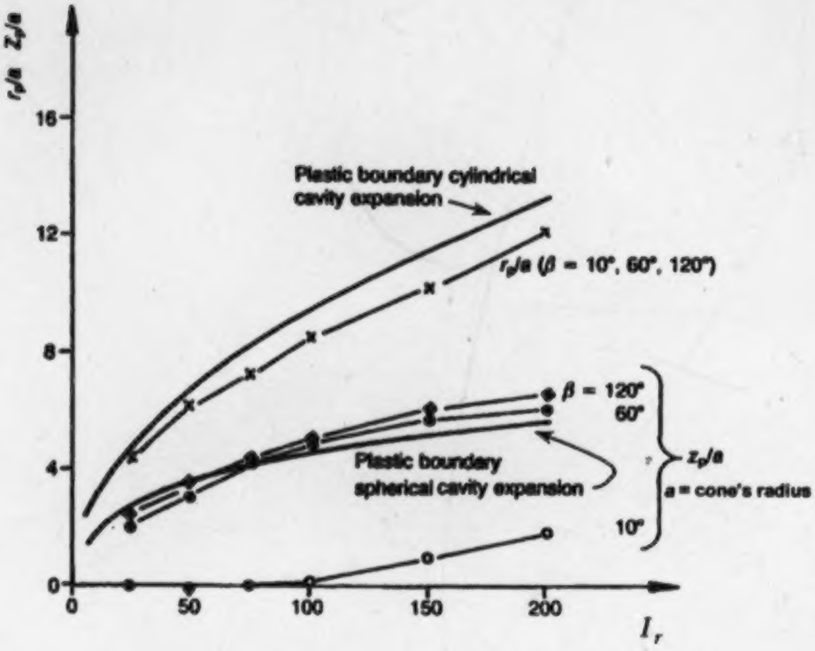

Figure 6.4 – Location of the elasto-plastic boundary in cone penetration (modified from Teh and Houlsby 1991)

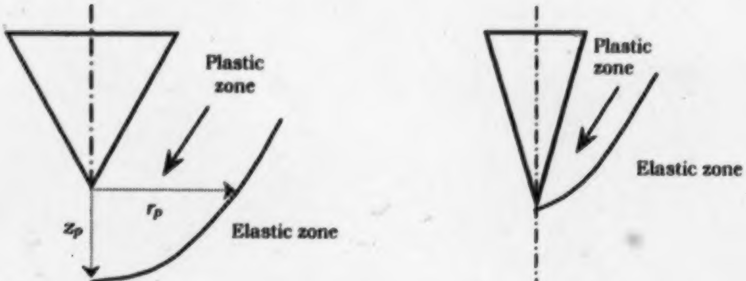

Plastic zone
$r_p$
$z_p$
Elastic zone
Plastic zone
Elastic zone

(a) (b)

Figure 6.5 – Possible plastic zones around a penetrometer: a) for an obtuse cone and b) for a sharp cone and low $I_r$ (modified from Teh and Houlsby 1991).

Applying the above studies to the HD-PB-CPT brought about the idea of reducing the cone angle from its current 60° angle to a sharper one, e.g. 30°. It was thought that this reduction might result in better soil expansion to the sides rather than pushing it into the borehole ahead of the probe. The angle reduction might also increase the stresses around the cone tip and consequently increase the cone and friction resistance closer to that of a standard CPT.

The boundary conditions of a pre-bored CPT test are different from those of a standard CPT test. The deformation patterns therefore, will probably be different from the ones obtained by the previously mentioned authors. Thus, laboratory modeling of a Pre-Bored Cone Penetration Test using smaller scale cones with different apex angles, i.e., one with 60° and the other one with 30°, were carried out to study the soil's deformation pattern during this kind of test. A 30° apex angle cone was chosen because, according to Silvestri and Fahmy (1995), sharp cones that are considered to strain the soil in a manner similar to an expansion of a cylindrical cavity, have apex angles $\beta \leq 30°$. Because of the smaller apex angle the probe would have to be longer. Therefore a 30° apex angle cone could perform well as a sharp cone but would not compromise the probe's length as much, as a 10° cone.

## 6.2 LABORATORY MODELING SET UP

The laboratory modeling followed the same test procedure performed by van den Berg (1994), with some modification. Van den Berg's experiment basically consisted of the consolidation of a homogeneous clay in a test chamber. The chamber was constructed of four (1 m by 0.4 m) hardened glass walls whose thicknesses was 12 mm. The clay was consolidated in the chamber until a certain strength was obtained. A cone was then cut in half lengthwise and was pushed into the clay along the glass wall. A deformation grid plotted on the clay, made it possible to record the soil's deformation pattern during penetration.

The main differences between van den Berg's test and ones performed for this study were that the former performed a full scale cone penetration test while in this study the cone was reduced in size and the penetration was performed in a pre-bored pilot hole. Van den Berg's test used a 3.57 cm diameter cone and a consolidation chamber that had a rectangular shape. The tests for this study used a 2.25 cm diameter cone and a cylindrical consolidation chamber. After consolidation, the chamber was cut in half, lengthwise, and the exposed faces were than covered with an acrylic plate. The full details of the test procedure are given in the next section.

The selection of the cone and borehole diameter was a function of the diameter of the consolidation chamber. It was desired to have a distance from the center of the specimen to the chamber's wall of 10 cone diameters in order to minimize boundary effects (Parkin 1988). A borehole smaller than 1.5 cm on the other hand would have made the observation of the soil's deformation very difficult. Therefore, it was decided to keep the borehole diameter at 1.5 cm. Hence, to obtain a cavity expansion of 50 %, the cone's diameter would have to be 2.25 cm. This would give a distance from the center of the specimen to the chamber's wall of 8.9 cone diameters, which was considered to be acceptable.

### 6.2.1 SAMPLE PREPARATION

The soil used in this experiment was a white kaolinite clay used for pottery work and was acquired from Plainsman Pottery Supply. The Atterberg limits, relative density (former specific gravity) and the laboratory vane undrained shear strength, performed after the test, are presented in Table 6.1.

Table 6.1 – Characteristics of the clay

| | |
|---|---|
| Liquid limit | 43 % |
| Plasticity limit | 25 % |
| Plasticity index | 17 % |
| Relative density (former specific gravity) | 2.64 |
| $S_u$ (average from 32 tests) | 6 kPa |

To obtain a homogeneous clay in the test chamber the kaolinite was mixed with water using a mechanical Hobart mixer, model A-200. The proportion of dry clay to water was 4:2.4 by mass, giving a paste with a water content of approximately 60%, far above the liquid limit. This kind of a slurry paste would make it easier to fill the consolidation chamber and would also minimize any formation of distinctive layers within the sample.

### 6.2.2 CONSOLIDATION CHAMBER

Two consolidation chambers were specially built for this test. They were made with potable water polyvinyl chloride (PVC) pipes that had 400 mm nominal outside diameters and 384 mm inside diameters. Each chamber was cut to a length of 80 cm. The bottom was sealed with a fixed 19 mm (3/4") thick PVC base with a drainage hole that allowed for the seepage of water during consolidation. The top cap was made of the same material and thickness as the PVC base and it had an "O" ring around it which prevented the soil from passing between it and the pipe wall during consolidation.

To allow top drainage during consolidation a 1/4" (6.35 mm) diameter hole was made through the top cap, placed 3 cm off the center, and into which was screwed a small pipe. A detailed diagram of the consolidation chamber is presented in Figure 6.6.

The bottom drainage system was comprised of one sheet of a nonwoven geotextile, Amaco 4508, placed right on top of the PVC base, followed by a 4 cm layer of clean sand, overtopped with four sheets of the same geotextile. Finally a Whatman Chromatography paper filter, Cat. No. 3001917, was placed on top of the geotextile to separate it from the clay. The top drain system was made of one sheet of the Whatman paper filter which was placed on top of the clay followed by three sheets of the geotextile (Figure 6.6).

To accelerate the consolidation process, 14 vertical strips made of the same Whatman paper filter were used as side drains. Each strip had a width of 5 cm and was made by folding the paper filter eight times to increase the filter's thickness. Each end of the side drains overlapped by approximately 5 cm at the top and at the bottom of the specimen, as shown in Figure 6.7.

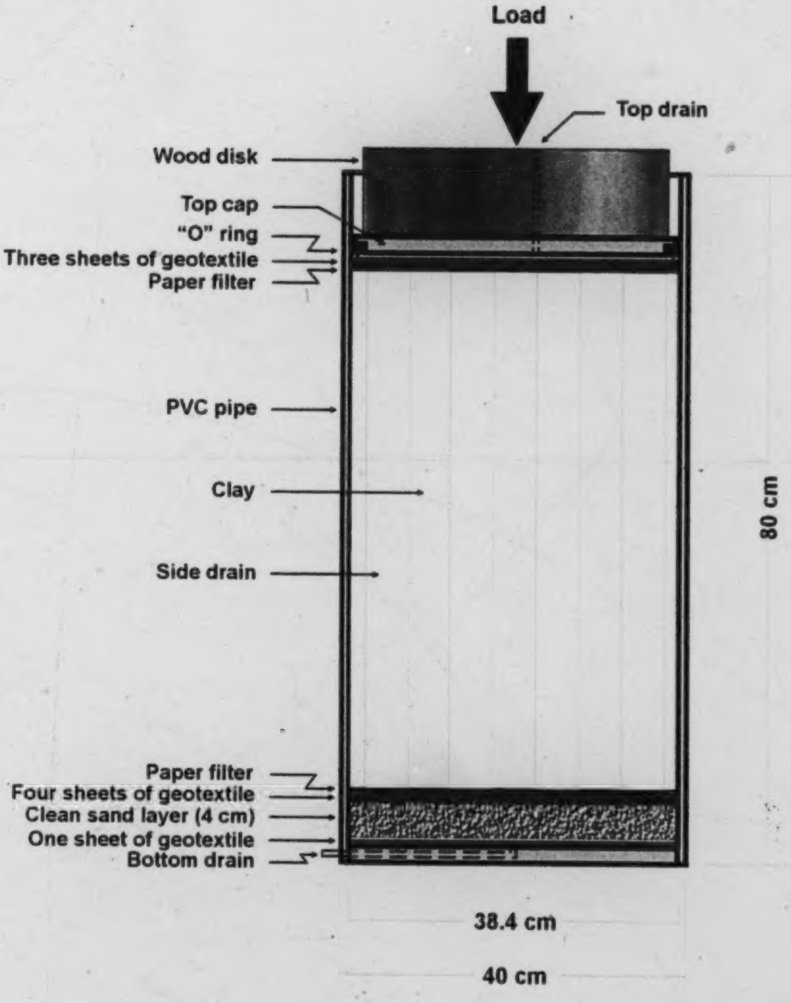
Load
Top drain
Wood disk
Top cap
"O" ring
Three sheets of geotextile
Paper filter
PVC pipe
Clay
Side drain
80 cm
Paper filter
Four sheets of geotextile
Clean sand layer (4 cm)
One sheet of geotextile
Bottom drain
38.4 cm
40 cm

Figure 6.6 – Consolidation chamber diagram

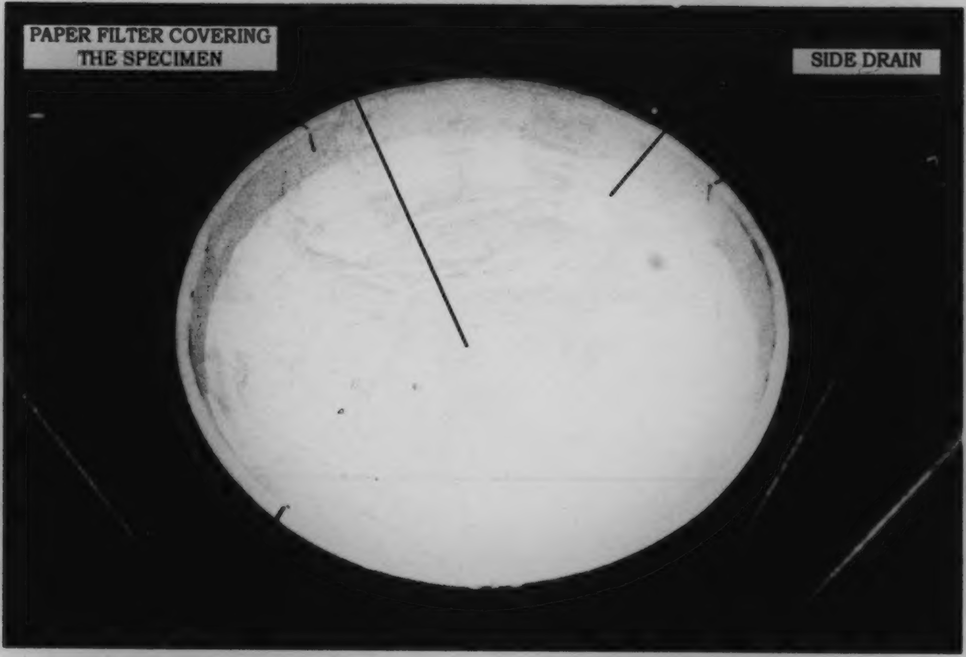

Figure 6.7 – Top view of the consolidation chamber

Each chamber was carefully filled with the clay slurry. To better accommodate the clay inside the chamber and to eliminate voids, the wall of the chamber was often gently tapped with a rubber hammer during filling. The specimens in chambers A and B had a total height before consolidation of 67 cm and 74 cm, respectively.

### 6.2.3 LOAD SYSTEM AND CONSOLIDATION

The loading system was comprised of a steel frame with four 22.2 mm (7/8") diameter threaded rods and two 12 x 2 inch "C" shaped beams. The upper beam had a Bellofram jack with a total load capacity of 19.5 kN. To better distribute the load a solid wood disk 37 cm in diameter and 10 cm thick was placed between the top cap and the

Bellofram's ram. With the help of a magnetic base, a Linear Variable Differential Transformer (LVDT) was fixed on the side of the top beam, and its needle was placed as close as possible to the center of the specimen on the top of the wood disk. Both LVDT's, one from chamber A and the other from chamber B, were connected to a data acquisition system that recorded all the data on a computer. Figure 6.8 shows a general view of the load system and the consolidation chambers.

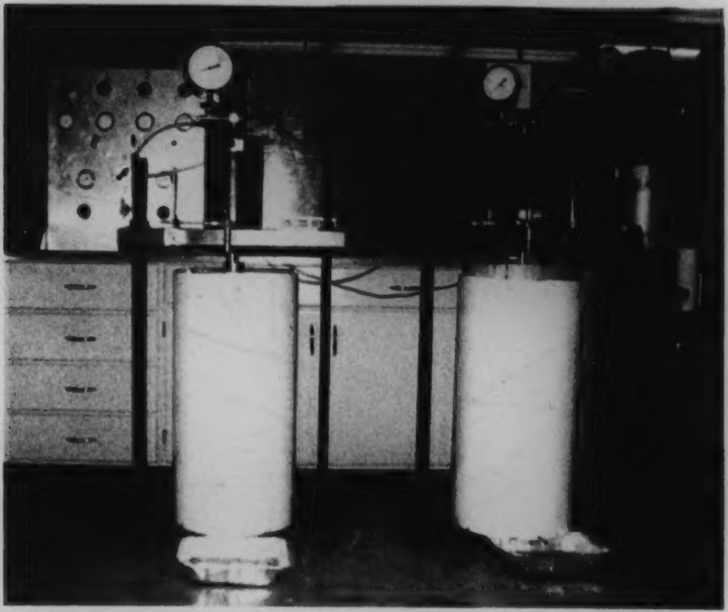

Figure 6.8 – Consolidation load system.

Due to the considerable height of the specimens, the consolidation time lag for each loading stage was expected to be very long, even with the side drains. Therefore, to identify what would be the minimum load necessary to consolidate the soil and bring it to a level of strength high enough to be workable, a smaller trial specimen (20 cm in height and 33 cm in diameter) that would required less time to consolidate was set up and loaded in stages up to a stress of 80 kPa. After the consolidation, laboratory vane tests were performed in this trial specimen. An average undrained shear strength of 8 kPa was obtained. This level of undrained shear strength was considered to have rendered enough stiffness to the specimen allowing it to be handled comfortably.

Based on the information obtained from the trial specimen it was decided to consolidate the test specimens up to the same vertical stress used in the trial specimen, i.e., 80 kPa. It is worth mentioning that despite being loaded with the same vertical stress as the trial specimen the average undrained shear strength measured on the test specimens was 2 kPa lower (see Table 6.1) than the obtained in the trial specimen. The use of side drains may have contributed for this lower undrained shear strength that was mainly measured around the center of the specimens where the pre-bored penetration test was performed.

The vertical loading of the test specimens was performed in stages of 10, 20, 50 and 80 kPa for chamber A, and 5, 10, 20, 50; and 80 kPa for chamber B. The total consolidation time was 30 days for each cell, and the total settlements were 69.1 and 90.3 mm for chambers A and B respectively. Figure 6.9 shows the consolidation curve displacement versus the square root of time for the specimens in chambers A and B.

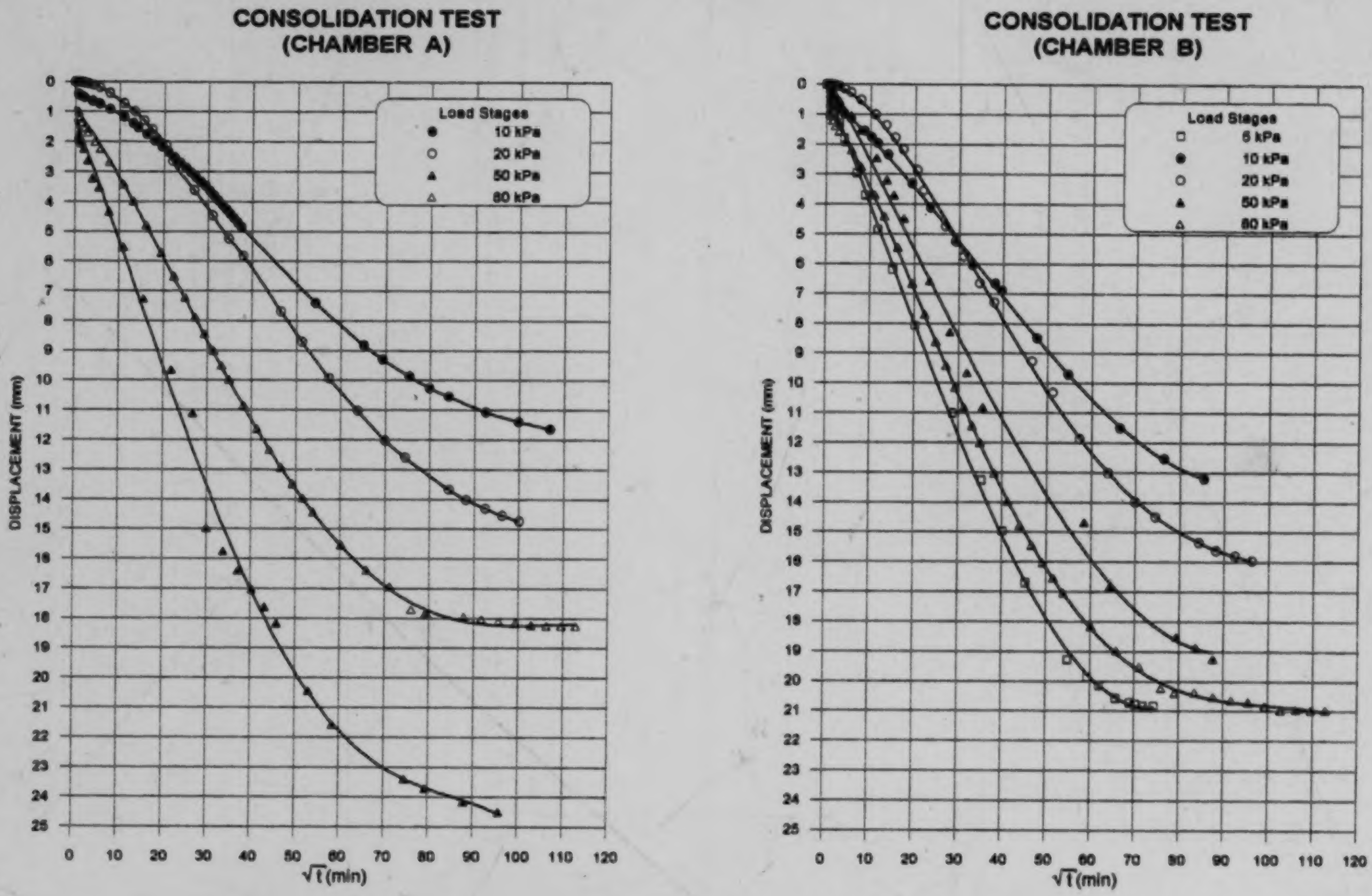

Figure 6.9 – Consolidation curves of specimens from chamber A and B.

### 6.2.4 TEST ASSEMBLY

After the consolidation phase was finished, the top cap was screwed to the pipe wall and the protruding end of the pipe was cut flush with the top cap. Once the specimen was totally confined into its consolidation chamber, the chamber was carefully cut in half as shown in Figure 6.10. After cutting the chamber, the gaps left by the side cuts were filled with small segments of wood with the same thickness as the gaps. After that, the chamber was fastened together around its perimeter with duct tape. This procedure was done in order to minimize any lateral compression to be transferred to the specimen during handling.

Once the PVC chamber was cut, the specimen was then cut in half using a 2 mm diameter wire. Figure 6.11 shows a view of a half specimen after being cut. Except for some small air bubbles, the clay specimen was very homogeneous and had no noticeable layering.

The next step was to prepare the surface and make a 1.5 cm diameter groove lengthwise to simulate the borehole. The cone/borehole diameter ratio was 1.5, i.e., the same as was used in the fieldwork. Using a ruler with a metallic semi-circular disk attached to its center with a diameter of 1.5 cm, it was possible to carefully trim the specimen until the desired shape and depth were achieved (Figure 6.12).

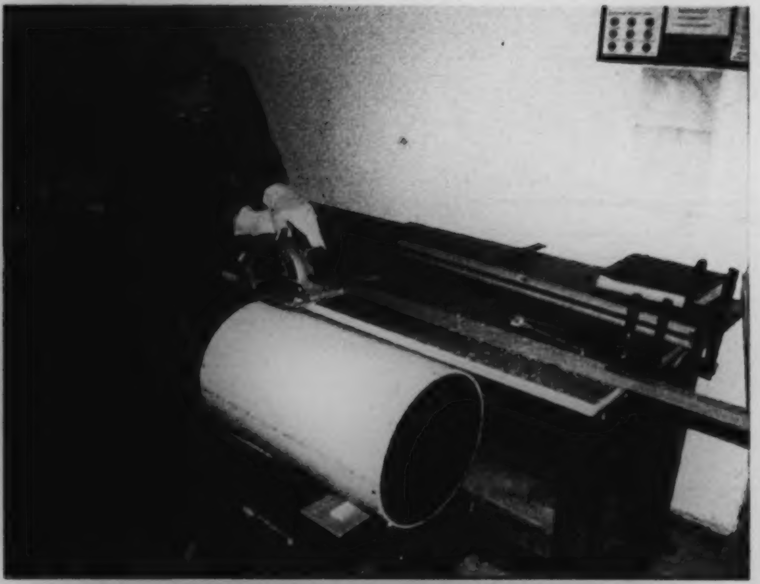

(a)

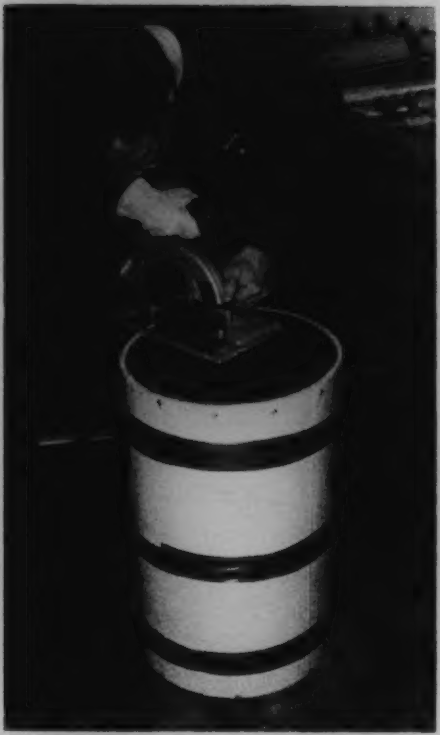

(b)

Figure 6.10 – (a) Chamber's side cut. (b) Chamber's top cut.

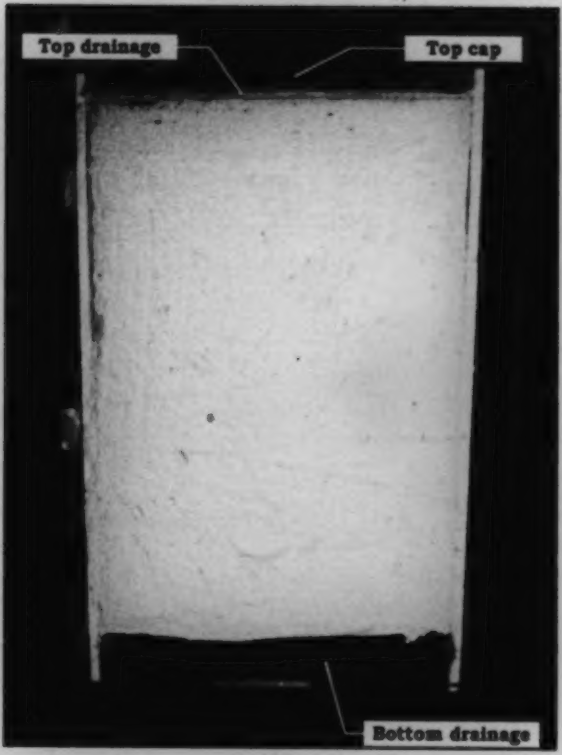

Figure 6.11 – View of a half specimen after being cut.

To record the clay deformation during cone penetration, one centimeter square grid lines were drawn on the clay with dry black paint. An acrylic plate was then placed on top of the specimen and fastened with steel strips. The acrylic surface was greased with glycerin to minimize friction between the plate and the clay during penetration. When the paint contacted the glycerin on the acrylic plate an unexpected small lateral spreading of the lines occurred. This compromised the sharpness of the lines, making the displacement readings more difficult to read and therefore less accurate.

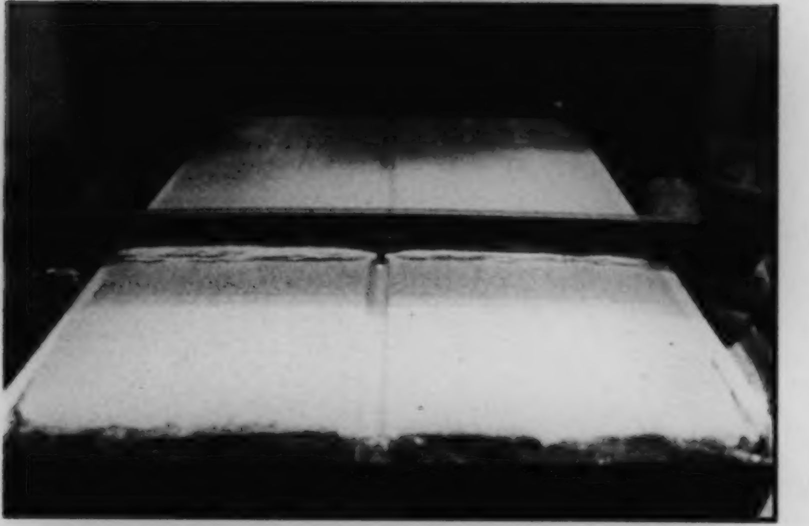

Figure 6.12 – Half pipe preparation (borehole modeling).

The cone was attached to a 6.4 mm diameter rod that slid over a wooden guidance system. The cone was hand pushed at an average rate of around 1.5 mm/s to allow good observation of the deformation pattern. According to Campanella and Robertson (1981) even in clayey silts, penetration is basically undrained down to a penetration rate of around 1 mm/s. Cone penetration resistance is approximately constant for rates varying between 1 and 20 mm/s. Thus, a penetration rate of 1.5 mm/s in a pure clay soil was considered acceptable for the purposes of this study.

Figure 6.13 (a) shows the final test assembly with a view of the cone guidance system. Figure 6.13 (b) shows a closer view of the grid lines and the 60° half cone ready to penetrate the borehole.

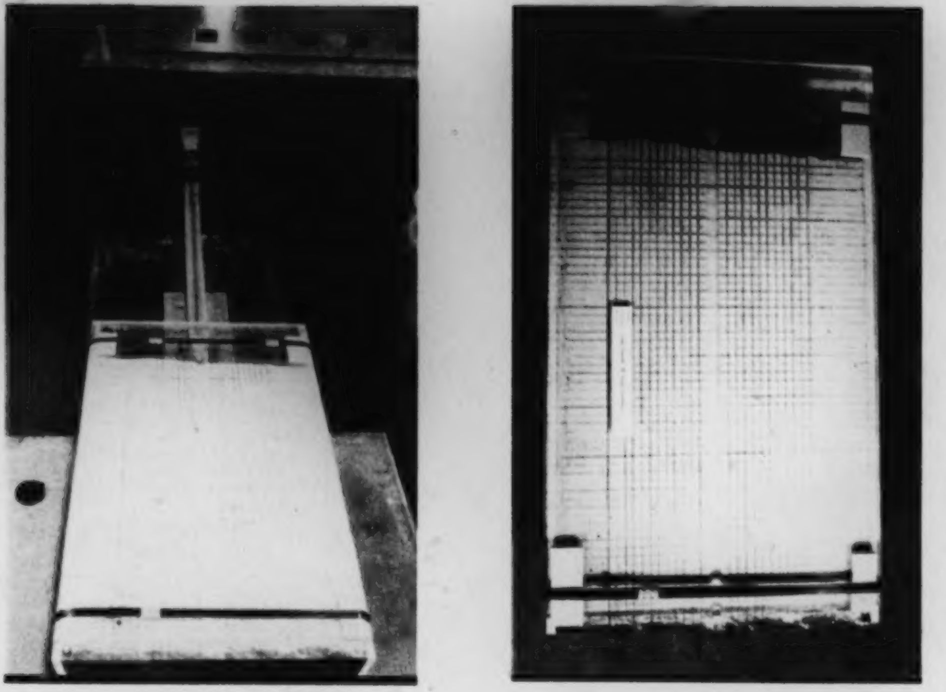

(a) (b)

Figure 6.13 – (a) Final test assembly. (b) Closer view of grid lines and the 60° half cone ready to penetrate the borehole.

## 6.3 PENETRATION TEST

The main purpose of this modeling was to study the deformation pattern of the borehole, to answer the following questions:

- Was the soil being pushed toward the borehole?
- If so, was the soil being accumulated in front of the cone and to what extent?
- Would a sharper cone minimize the effect of this accumulation?

The first test was performed with the 60° apex angle cone, i.e., with the same apex angle as used in a standard CPT and in the previous HD-PB-CPT. Next, the test was repeated in a new clay specimen, but this time with a 30° apex angle cone.

Because the cone tests were performed in a pre-opened hole, the reference for penetration was considered to be the point of contact between borehole wall and cone. This point is the effective point where the cone starts to impose soil deformation. For the 60° cone the reference point for penetration was at 1.3 cm behind the cone's tip, and at 2.8 cm for the 30° cone.

Pictures were taken during the test, to ensure a better analysis of the soil's deformation pattern as well as for strain calculation.

### 6.3.1 60° APEX ANGLE CONE

Right from the beginning of the penetration with the 60° cone, the soil started to displace towards the borehole and accumulate in front of the cone. After the first 2.2 cm of penetration the soil accumulation ahead of the cone was already 1 cm thick. The thickness of this mass of soil remained more or less constant throughout the entire test, varying by 1 to 1.5 cm, as shown in Figure 6.14 (a).

Although the plug of soil in front of the cone was on average about 1.3 cm (0.58 cone diameter) thick, the soil deformation around the cone was in the order of 3.5 cm, i.e., about 1.5 cone diameters. These results are in agreement with the results obtained by van den Berg (1994) for a standard cone test performed in a similar soft clay.

It is interesting to notice in Figure 6.14 (a) and (b) that the soil deformation around the cone's tip is indeed close to a spherical shape and also that the zone of deformation extends well out into the undisturbed soil.

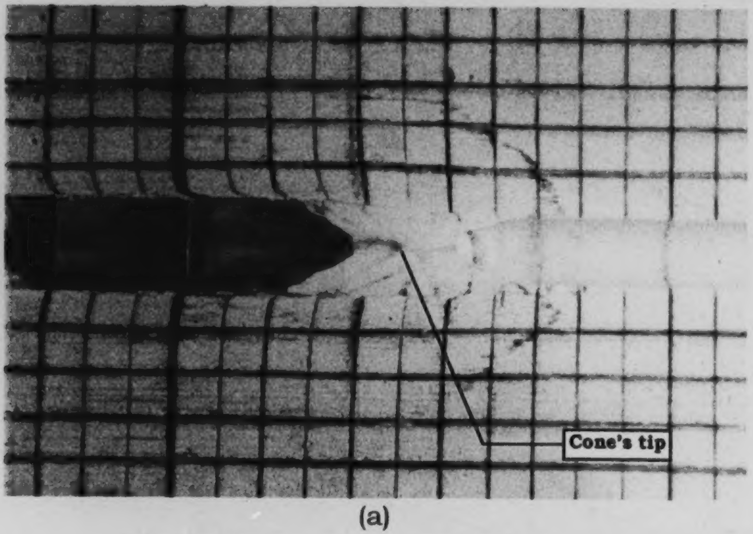

(a)

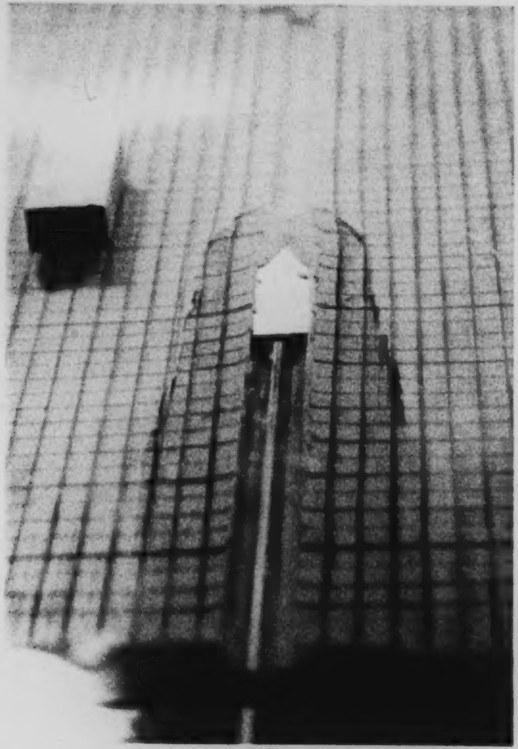

(b)

Figure 6.14– (a) Soil's deformation pattern of a 2.25 cm in diameter cone with an apex angle of 60° being pushed through a 1.5 cm borehole in soft clay. (b) Longitudinal view of penetration.

Octahedral strains ($\gamma_{oct}$) for this penetration test were calculated using Equation 6.4:

$$\gamma_{oct} = \frac{1}{3}[(\varepsilon_{rr} - \varepsilon_{zz})^2 + (\varepsilon_{zz} - \varepsilon_{\theta\theta})^2 + (\varepsilon_{\theta\theta} - \varepsilon_{rr})^2 + 6\varepsilon_{rz}^2]^{1/2} \qquad [6.4]$$

Results were compared with those obtained by Acar and Tumay (1986) from an analytical study based on the flow field around a cone penetrating an inviscid and incompressible medium.

Despite cone penetration not being a plane strain condition, the geometry of the modeling test imposed such condition. Therefore, circumferential strain ($\varepsilon_{\theta\theta}$) was assumed to be zero.

With regards to shear strain calculation, it was easier to measure the diagonal change of the deformed mesh rather than the angular change. Thus, to minimize error of measurement, the shear strain was calculated following the principle of the strain rosette from Equation 6.5.

$$\varepsilon_{zz'} = \frac{\varepsilon_{zz} + \varepsilon_{rr}}{2} + \frac{\varepsilon_{zz} - \varepsilon_{rr}}{2}\cos 2\theta + \varepsilon_{rz}\sin 2\theta \qquad [6.5]$$

where:

$\varepsilon_{zz'}$ = axial strain along the axis z'

$\theta$ = angle between z and z' axis

As explained previously, the edges of the grid lines were not very sharp, which compromised the accuracy of the strain measurements. Therefore, the octahedral strain contours were drawn using the best reasonable fit among the nodes of the octahedral strain mesh, as shown in Figure 6.15 (b). Comparing these contours with the ones obtained by Acar and Tumay (1986), Figure 6.15 (a), it can be seen that they follow, more or less, the same curved trend. However, the strains around the cone's shaft were lower than the ones presented by the previous authors for a standard CPT. Since the cavity expansion for a standard CPT and for a pre-bored CPT are 100 % and 50 %, respectively, larger soil strains are expected to occur in the former test than in the latter. Furthermore, difference in the soil stiffness may also have played a role in the difference of the strain contours. Furthermore, the octahedral strain contours obtained by Acar and Tumay (1986) were based on an analytical solution to the flow field around a cone penetration in a inviscid fluid. Therefore, it does not take into account the material stiffness. According to Tumay et al. (1985) the analytical solution of the flow field will give the first approximation of the strains around cone penetrometers in very soft cohesive soils. This is compatible with the soil consistency used in the pre-bored modeling tests. It is interesting to note that the strain contours of 10 % and 5 % for the pre-bored test were displaced further ahead, by about 0.7 to 0.9 cone diameters respectively, compared to the strain contours obtained by Acar and Tumay (1986). This is a possible reflection of the change in boundary conditions due to the existence of the borehole.

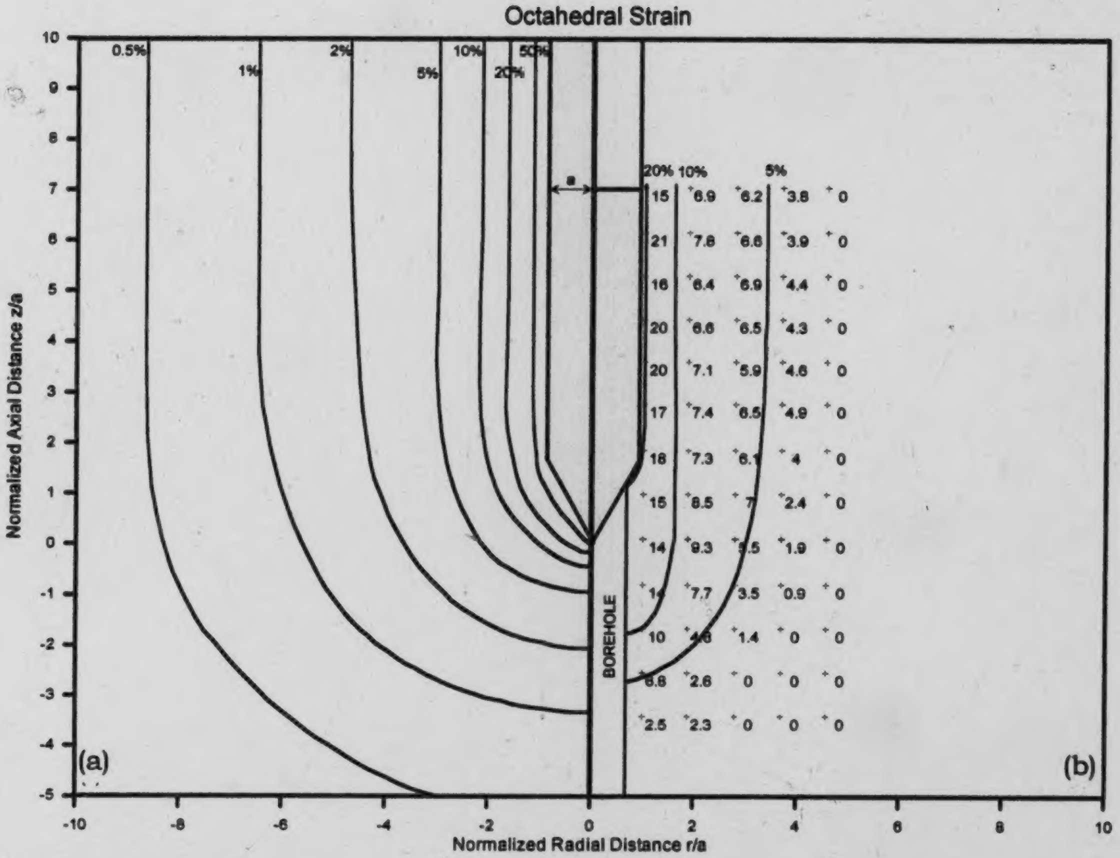

Figure 6.15 – (a) Octahedral strain contours for a standard 60° cone (Acar and Tumay 1986). (b) Octahedral strain contours for a pre-bored 60° cone, and strain mesh with the octahedral strain (%) of each node.

### 6.3.2 30$^{0}$ APEX ANGLE CONE

The modeling test using the 30° cone showed that, despite using a sharper cone, soil still accumulated in front of the cone tip, however, with less intensity. With the 30° cone, the soil started to accumulate after 11.8 cm of penetration (Figure 6.16 a), compared to 2.2 cm of penetration for the 60° cone. The 30° cone test showed an average thickness of soil in front of the cone of only 0.6 cm (Figure 6.16 b), which is approximately half of the thickness of the soil accumulation ahead of the 60° cone's tip.

Furthermore, in looking at the deformed mesh it was possible to observe that the maximum noticeable radial soil deformation for both the 30° and 60° cone was about the same, i. e., approximately 1.5 cone diameters. The maximum noticeable axial deformation, however, was approximately 1.7 and 2.4 cone diameters from the point of contact (soil/cone) for the 30° and 60° cones respectively. This is in agreement with the analytical study of cone penetrations performed by Teh and Houlsby (1991), as shown in Figure 6.4. In other words, the radial distance of the plastic boundary ($r_p$) appear to be independent of the cone angle, whereas the distance between the cone tip and the plastic boundary along the axis of penetration ($z_p$) is significantly influenced by the cone angle, even for a pre-bored cone penetration test.

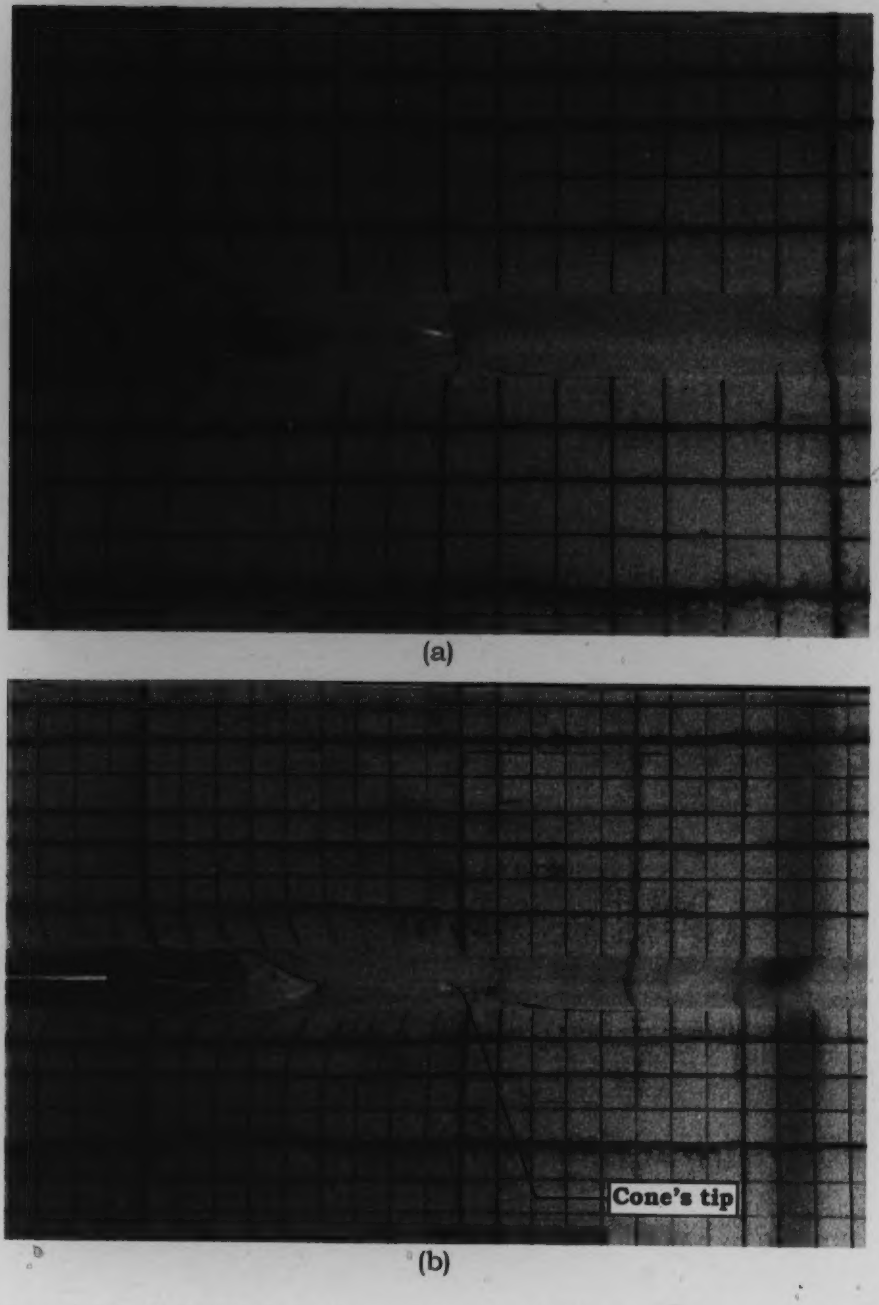

Figure 6.16 – (a) 30° cone penetration, beginning of soil accumulation after 11.8 cm of penetration. (b) After 30 cm of penetration, soil accumulation ahead of the cone's tip was only about 0.6 cm and remains around this magnitude during the whole test.

## 6.4 BOREHOLE CONSTRAINT DEVICE

With the information obtained from the literature and the laboratory scale-model tests carried out for this study, it was decided to design a constraint device that would be placed in front of the cone to prevent the soil from deforming towards the borehole. The goal was to force the soil to expand outward from the borehole, close to a cylindrical cavity expansion.

Two additional scale-model tests were performed using penetrometers that had a cylindrical extension with the same diameter as the borehole in front of their cones. This would allow an analysis of the effectiveness of adding a constraint device to the HD-PB-CPT probe.

### 6.4.1 LENGTH OF THE CONSTRAINT DEVICE

The length of the constraint device was designed based on the data gathered from the previous laboratory scale-model tests. The distance from the soil/cone contact point to the maximum point of noticeable deformation of the borehole ahead of the cone's tip was measured and used as reference to define the constraint device length. These distances were of 2 and 1.8 cone diameters for the 60° and 30° cones, respectively.

As mentioned previously, the distance $z_p$ is a function of the rigidity index ($I_r$). Because the clay used in these modeling tests had a very low undrained shear strength (Table 6.1), the rigidity index was expected to be low. Looking at the chart in Figure 6.4, and from analyzing the shape of the curve for a 60° cone it can be seen that the curve becomes almost asymptotic after $I_r = 200$.

Considering that for the 60° cone modeling test the soil deformation ahead of the contact point was equal to 2 cone diameters,

i. e., $\frac{z_p}{a} = 4$, the rigidity index for the tested clay will be equal to around 75, according to the chart in Figure 6.4. For stiffer soils, $I_r$ = 200, the value of $\frac{z_p}{a}$ from the chart, will be equal to 5.6 (2.8 cone diameters). For soil with higher $I_r$ it can be expected that $\frac{z_p}{a}$ will not increase much due to the asymptotic shape of the curve. For the modeling test, it was decided that a constraint device of 2.5 cone diameters long would be sufficient to overcome the deformed zone. Figure 6.17 shows the diagram of the penetrometers used in these modeling tests.

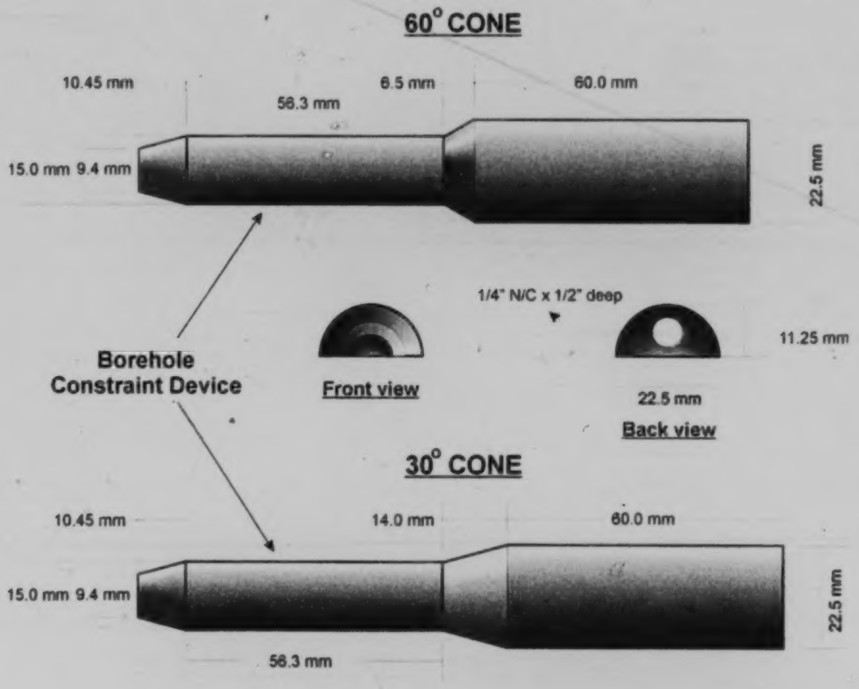
60° CONE
10.45 mm
56.3 mm
6.5 mm
60.0 mm
15.0 mm 9.4 mm
22.5 mm
1/4" N/C x 1/2" deep
11.25 mm
Borehole
Constraint Device
Front view
22.5 mm
Back view
30° CONE
10.45 mm
14.0 mm
60.0 mm
15.0 mm 9.4 mm
22.5 mm
56.3 mm

Figure 6.17 – Diagram of the penetrometers, with the constraint device used in the modeling test.

### 6.4.2 ANALYSIS OF THE RESULTS

Figure 6.18 (a) and (b) show the deformation patterns obtained from the modeling tests with the borehole constraint devices, for the 60° and 30° cones respectively.

To highlight the borehole boundary a (red) line was drawn on top of the acrylic plate aligned with the borehole edges.

Unfortunately due to a misalignment between the 60° cone axis and the borehole's axis, the soil on the top of Figure 6.18 (a) was less strained than the soil on the bottom. This misalignment resulted in a soil accumulation in front of the probe. This soil accumulation was not due to soil deformation from the cone, but rather from the tip of the constraint device that had been scraping the bottom edge of the borehole since the beginning of the test. By observing the bottom edge of the borehole it can be seen that the bottom edge of the constraint device is below the borehole boundary (red line), introducing some distortion to the mesh in this region. On the other hand, the mesh at the top edge of the borehole, in the region of the constraint device, presents little or no distortion, showing that the borehole constraint device appears to be holding the soil in place.

With regard to the 30° cone in Figure 6.18 (b), better alignment was obtained. It can be seen that a sharper cone aids in the centralization of the probe. As a consequence, a more symmetrical deformation pattern was obtained and no soil accumulation in front of the probe occurred during the whole test. Figure 6.18 (b) clearly shows a wave of plastic soil deformation that moves ahead of the conical section of the probe reaching to about the first third of the constraint device. In observing the mesh around this region it can be seen that the mesh between the conical part of the probe and the leading edge of the plastic deformation zone had little or no deformation toward the borehole. This absence of deformation illustrates that the borehole constraint device works reasonably well in preventing the soil from being displaced towards the borehole.

In spite of the misalignment of the 60° cone test, an attempt to calculate the octahedral strain was made using the deformed mesh from the top part of the picture in Figure 6.18 (a) and Equation 6.4. A comparison of these octahedral strains and those obtain by Acar and Tumay (1986) is shown in Figure 6.19. As previously stated, the same problems regarding the accuracy of the strain measurements were also encountered here. It is worth noting that the octahedral strain contours presented by Acar and Tumay (1986) were only for cone penetrations with apex angles of 60° and 18°. Therefore, it was not possible to compare their results with those obtained from the laboratory modeling test with the 30° apex angle cone performed in this study.

The misalignment of the test is reflected in the lower strains that were obtained, compared to the previous ones using 60° cone modeling without the constraint device (see Figure 6.15). Despite the lower strain values it is interesting to note that the octahedral strain contours are now much closer in shape to those obtained by Acar and Tumay (1986) as shown in Figure 6.19. The constraint device did not allow the soil to move towards the borehole making the deformation pattern more similar to a standard cone penetration test.

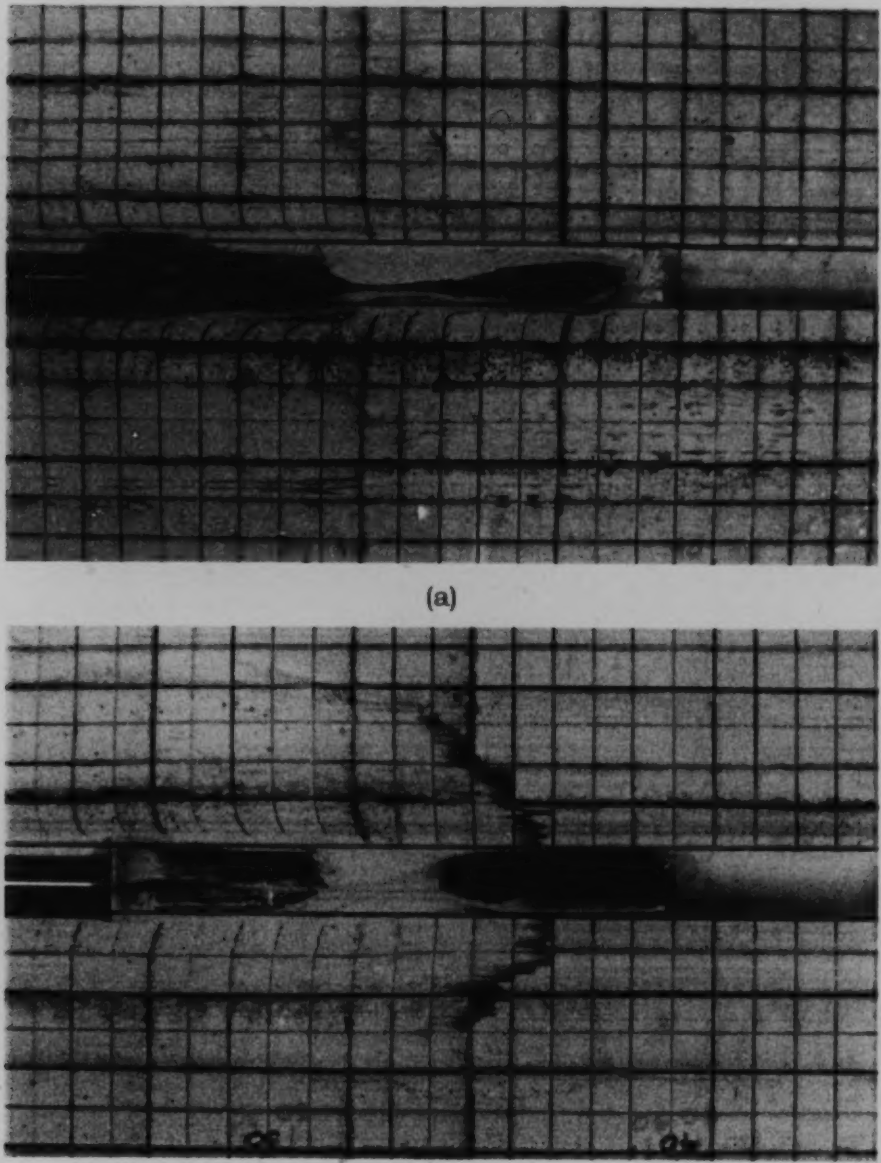

(a)

(b)

Figure 6.18 – (a) Deformation pattern of the 60º cone with the borehole constraint device. (b) Deformation pattern of the 30º cone with the borehole constraint device.

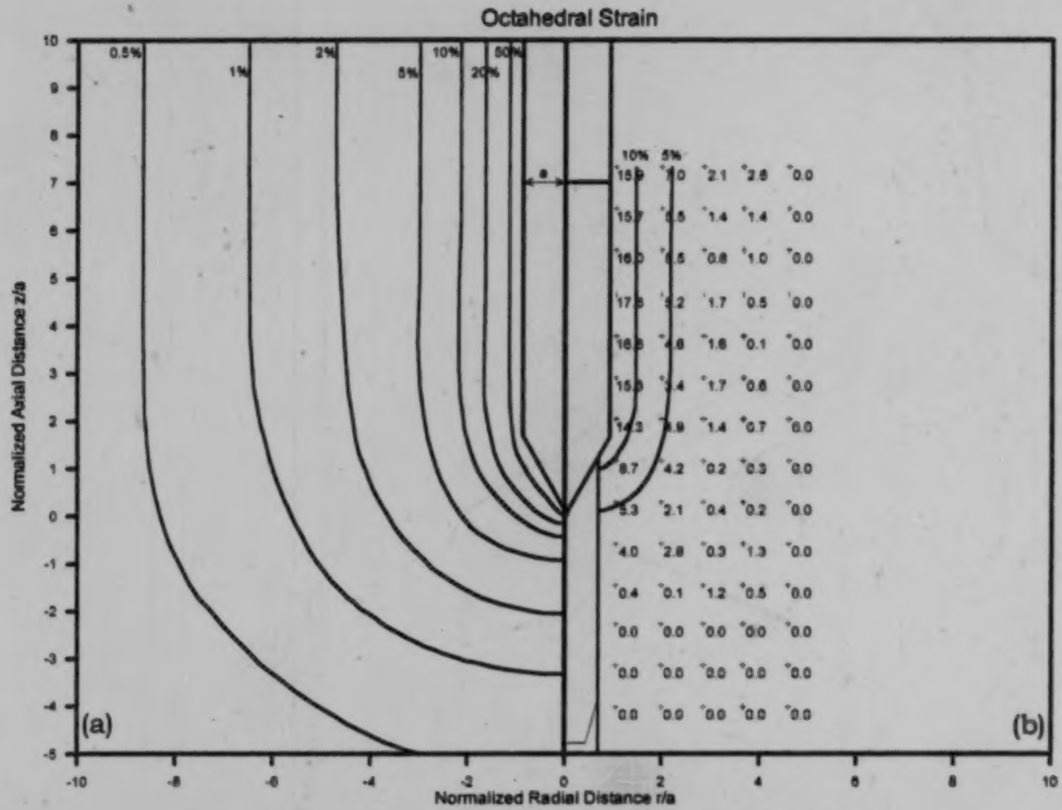

Figure 6.19 – (a) Octahedral strain contours for a standard 60° cone (Acar and Tumay, 1986). (b) Octahedral strain contours for a pre-bored 60° cone with borehole constraint device, and strain mesh with the octahedral strain (%) of each node.

## 6.5 SUMMARY

To better understand the borehole deformation pattern of a pre-bored penetration test, four small-scale laboratory model tests were performed in soft kaolinite clay specimens consolidated in stages up to 80 kPa in a 80 cm high by 40 cm in diameter PVC chamber. After consolidation, the chamber was split in half and assembled for the test.

The cone and borehole diameters were 2.25 and 1.5 cm respectively, which implies a cavity expansion of 50 %.

The first two tests were performed using cones with apex angles of 60° and 30°, respectively.

During the 60° cone penetration the soil ahead of the cone was almost immediately pushed towards the borehole creating an average soil accumulation in front of the cone tip of about 0.58 cone diameters. The accumulated soil thickness ahead of the cone remained more or less constant during the whole penetration test.

For the 30° cone, soil accumulation started to occur after 5.24 cone diameters of penetration, and in smaller amounts (0.27 cone diameter) when compared with the soil accumulation from the 60° cone test.

To avoid or minimize soil accumulation in front of the cone tip, a device 2.5 cone diameters in length, with the same diameter as the borehole, was placed in front of both cones. The purpose of this device was to constrain the borehole deformation in front of the probe.

Two more sets of laboratory modeling tests were performed using these newly shaped probes with the constraint devices.

Octahedral strain contours plotted for the 60° cone with the constraint device showed that the shape of the curves were closer to those of a standard cone penetration tests.

The 30° cone with the constraint device showed that a sharper cone renders a better probe centralization into the borehole.

These model test results show that placing a borehole constraint device ahead of the HD-PB-CPT might enhance the probe's cone and friction sleeve resistance by bringing the soil's deformation pattern closer to those produced by a standard cone penetration test. The development of a HD-PB-CPT prototype 2, with the improvements suggested by these test results is presented in Chapter 8.

# CHAPTER 7

# Soil Electrical Resistivity Measurement for Environmental Application

## 7.1 INTRODUCTION

As previously mentioned in Chapter 1, the HD-PB-CPT has potential for environmental site investigation. Its ability of logging a borehole in a horizontal direction makes the HD-PB-CPT especially attractive when searching for DNAPLs contamination as explained in Chapter 1.

There are several environmental sensors that could easily be installed in the probe to allow it to search for soil contamination plumes or pools. However, the electrical resistivity measurement is the most appealing one due to its relatively simple equipment requirements and its broad application. It was decided, therefore, to add an electrical resistivity module to the HD-PB-CPT. This chapter provides information about soil electrical resistivity measurement principles and its application in environmental site investigation. The implementation of the electrical resistivity module to the HD-PB-CPT is discussed in detail in Chapter 8.

## 7.2 A BRIEF BACKGROUND

Electrical resistivity (and its reciprocal conductivity) measurements have been used for many years in the field of soil science to measure soluble salts dissolved in water. The United States Salinity Laboratory Staff (1954) has actually recorded the use of these measurements since 1897. This technology has long been applied by geophysicists in mining and petroleum exploration (Hvorslev 1949), using surface or downhole methods, mainly for the purposes of estimating in-situ porosity and density of geological formations to determine reservoir characteristics (Archie 1942). Surface electrical resistivity methods have also been used for many years in the exploration of sand and gravel deposits (Wilcox 1942; Hvorslev 1949).

With the increasing concern for groundwater contamination, researchers began applying this old but powerful technology to track contamination plumes, not only for inorganic compounds, which cause a drop in soil resistivity, but also for free phase organic compounds, which cause an increase in soil resistivity. For the resistivity method to work, there must be resistivity contrasts in the subsurface. The successful application of surface and downhole geophysical soil resistivity measurements for the delineation of contaminant plumes has been reported by Cartwright and McComas (1968); Hackbarth (1971); Stollar and Roux (1975); Greenhouse and Slaine (1983); Schneider and Greenhouse (1992).

According to Lunne et al. (1997) the electrical resistivity cone penetration test (RCPT) has been used since the mid 1970s in Holland especially for estimation of sand density (van de Graaf and Zuidberg 1985). The attraction of using the RCPT is that it utilizes electrodes that are in full contact with the soil whereas resistivity probes deployed in mud filled boreholes do not always have good contact with the soil. Surface methods generally require at least a 5 to 10% electrical resistivity contrast to be successful. The resistivity measurement resolution of a RCPT, however is 1%, and it has the added advantage of being able to assist the in identification of soil lithology changes as well (Weemees 1990).

Because of its ability to detect both inorganic and organic groundwater contamination, the use of the RCPT for environmental applications is rapidly increasing. Some examples of environmental applications of RCPTs for screening groundwater contamination are presented in section 7.3.

## 7.3 ELECTRICAL RESISTIVITY (CONDUCTIVITY) MEASUREMENT PRINCIPLE

### 7.3.1 PROPAGATION OF ELECTRIC CURRENT

There are three ways to propagate an electric current. The most common and well known way is through electronic (ohmic) conduction, which consists of the transfer of a charge as a result of the flow of free electrons in materials such as metals. A second is dielectric conduction which occurs in poor conductors or insulatoing material, and which has very few or no charge carriers. When an external time varying electrical field is applied to such materials it creates dielectric polarization, i. e., the atomic electrons are displaced slightly with respect to their nuclei and this slight relative separation of negative and positive charges produces a current known as the displacement current (Telford et al. 1990).

The last and most significant type of current flow for soil bulk resistivity measurement is electrolytic conduction. In electrolytic conduction, currents are carried by ions, i. e., by molecules having an excess or deficiency of electrons; this represents an actual transport of material that may result in chemical transformation (Telford et al. 1990).

Soil particles are usually poor conductors, hence, in saturated soils, the dominant mechanism of electric transfer charges is electrolytic conduction. Therefore, bulk resistivity is predominantly controlled by the electrical resistivity of the pore fluid. Because of this dependence, any change in pore fluid resistivity can strongly affect the bulk soil resistivity.

### 7.3.2 METHODS USED TO MEASURED SOIL ELECTRICAL RESISTIVITY (CONDUCTIVITY)

The two most common methods used to determine soil electrical resistivity are the electromagnetic method and the galvanic method.

The electromagnetic method induces currents into the ground. In other words, it uses a time varying electromagnetic field, generated by a transmitter, which upon penetrating the ground, induces a voltage which causes a current to flow within a conducting subsurface, requiring no physical contact. Galvanic methods, on the other hand, always require the injection of a current into the ground by means of electrodes (CCME 1994). This latter method is the one that was adapted for use in the resistivity cone penetration test (RCPT) because of its lower cost and its less complex equipment requirements, which makes it less susceptible to malfunction during operation.

### 7.3.3 PRINCIPLES AND UNITS

The electrical properties of soil that quantify its ability to let current flow through it is better expressed in terms of electrical resistivity ($\rho$) rather than resistance ($R$), because resistance is not a material property, whereas resistivity is.

According to Halliday and Resnick (1988), resistivity is defined by Equation 7.1 as:

$$\rho = \frac{E}{J} \qquad [7.1]$$

Where:

$E$ = Electrical field (volt per meter), and

$J$ = Current density (ampere per square meter)

Resistance can be defined as a function of the distance $L$ between two electrodes; the cross-section area $A$ of the material between these electrodes, i.e., the conductor), and the proportionality constant known as the electrical resistivity $\rho$, the value of which depends on the nature of the conductor. Therefore, resistance can be expressed by Equation 7.2:

$$R = \rho \frac{L}{A} \qquad [7.2]$$

If $R$ is measured in ohm, $L$ in m, and $A$ in m$^2$, the unit of $\rho$ is ohm·m.

By measuring the soil resistance $R$ it is possible to obtain $\rho$ by multiplying $R$ by the ratio $A/L$, known as the geometry correction factor, which is usually determined by conducting a calibration test. Assuming that the soil is a homogeneous isotropic medium, that the electrodes work as perfect conductors, and that the current supply source is also perfect, the geometry correction factor $A/L$ will be constant and will sometimes be represented as a calibration factor $K$ (Weemees 1990; Everard 1995; Lunne et al. 1997). This calibration factor can be deduced from direct calibration tests such as those shown in Chapter 8.

The reciprocal of resistivity ($\rho$) is conductivity ($\sigma$). The dimension of $\sigma$ can be expressed as (ohm·m)$^{-1}$ or (ohm·cm)$^{-1}$. In the past the reciprocal of "ohm" was expressed as "mho", thus the unit for $\sigma$ was often represented as mho/cm. Because mho/cm usually rendered a very small number, it was common practice to use mmho/cm as a unit for the electrical conductivity of soils. Presently, the "Système International d'unités" (SI) unit for $\sigma$ is S/m where S stands for Siemens, and 1 Siemen is equal 1 ampere/volt (Wolt 1994).

Technical literature often presents $\sigma$ units as being expressed as dS/m. This unit is used because 1 dS/m is equal to 1 mmho/cm (the unit used in the past), hence, dS/m is a very convenient unit to use when handling old data.

Typical values for soil bulk resistivity (conductivity) as well as pore fluid resistivity (conductivity) for geoenvironmental applications are presented in Table 7.1. As shown in this table, the range of soil bulk conductivity (resistivity) values is very large, meaning that at times it is more convenient to express $\sigma$ as μS/cm rather than dS/m. Conversion from conductivity to resistivity can easily be performed according to Equation 7.3:

$$\sigma\,(\mu S/cm) = 10000/\rho\,(ohm \cdot m) \qquad [7.3]$$

Soils with high concentrations of total dissolved solids (TDS) (inorganic contaminants) yield low bulk resistivity. It is more suitable to express data in terms of electrical conductivity because $\sigma$ increases as the TDS increases, thus simplifying the interpretation. For soils with high concentrations of high resistivity contaminants (organic contaminants), which yield high bulk resistance, electrical resistivity measurements are more appropriate. Both ways of expressing the soil's ability to conduct a current are widely represented in technical literature, with their use being dependent on their convenience.

Table 7.1 – Typical resistivity and conductivity values for bulk soil mixtures and pore fluids (modified from Campanella et al. 1994b and Lunne et al. 1997).

| Material type | Bulk resistivity (ohm·m) | Fluid resistivity (ohm·m) | Bulk conductivity (μS/cm) | Fluid conductivity (μS/cm) |
|---|---|---|---|---|
| Sea water | - | 0.2 | - | 50 000 |
| Drinking water | - | > 15 | - | < 665 |
| Clays | 1 - 100 | - | 100 - 10 000 | - |
| Alluvium and sands (non-marine) | 10 - 800 | - | 12 - 1 000 | - |
| Oil sands | 4 - 800 | - | 12 – 2 500 | - |
| Mine tailing sand with acid drainage leachate | 1 - 40 | 2 – 27 | 250 - 10 000 | 370 – 5 000 |
| Mine tailing sand without acid drainage leachate | 70 – 100 | 15 – 50 | 100 - 145 | 200 - 665 |
| Typical landfill leachate | 1 – 30 | 0.5 – 10 | 330 – 10 000 | 1 000 – 20 000 |
| Industrial site – inorganic contaminants in sand | 0.5 – 1.5 | 0.3 – 0.5 | 6 500 – 20 000 | 20 000–33 000 |
| Industrial site – organic contaminants in sand | 125 | - | 80 | - |
| Coal gas plant contam. soil | 200 – 300 | - | 33 -50 | - |
| Wood waste | 300 – 600 | - | 33 – 66 | - |
| 100% Ethylene Dichloride (ED) | - | 20 400 | - | 0.5 |
| 50% ED and 50% water in sand | 700 | - | 14 | - |
| 17% ED and 83% water in sand | 275 | - | 36 | - |

## 7.4 RESISTIVITY CONE PENETRATION TEST (RCPT) FOR ENVIRONMENTAL APPLICATIONS

RCPTs have been used successfully in a variety of different groundwater contamination sites such as at: brine disposal pond leakages (Horsnell 1988); waste disposal sites (Zuidberg et al. 1988); organic solvent (DNAPL) spill sites (Woeller et al. 1991); hydrocarbon (jet fuel) spill sites (Strutynsky et al. 1992); sites where inorganic compounds such as sulphates, chlorides and phosphates have contaminated soils (Campanella et al. 1994a); and creosote sites (Campanella et al. 1994b; Okoye et al. 1995).

Soil electrical resistivity is a function of the soil matrix, i. e., the soil particles and their arrangement and the pore fluid; therefore, it is usually referred to as bulk resistivity ($\rho$) (Urich 1981; Okoye et al. 1995). In saturated soils, bulk resistivity is predominantly controlled by the electrical resistivity of pore fluids. Thus, if a pore fluid resistivity change occurs, due to some kind of contamination, a resistivity probe can measure the contrast in resistivity readings and map the extent of the contamination. However, resistivity is also a function (though to a lesser degree) of soil particles and their arrangement, i. e., grain type, mineralogy, porosity, and tortuosity, among others (Urich 1981). In general, clayey soils have a lower resistivity than sandy soils because clay minerals usually have higher water content and high cation exchange capacity (CEC); the higher the CEC the lower the resistivity (Campanella and Weemees 1990; Okoye et al. 1995).

When a pore fluid resistivity is constant, i.e., when no change in pore fluid occurs, bulk resistivity measurements become excellent tools for the detection of sand pockets in clayey mediums. But if the goal is to detect changes in pore fluid resistivity, because of contamination, it would be important that the resistivity probe be capable of tracking soil lithology changes as well. This is where the RCPT plays an important role since it is able to provide information about resistivity and lithology changes.

For a visual representation of the ability of the RCPT to detect groundwater contamination, Figures 7.1 to 7.3 show examples of RCPT resistivity (conductivity) profiles performed on sites with different types of contaminant.

Figure 7.1(a) and (b) show two RCPTs conductivity profiles conducted at a waste disposal site, of inorganic compounds, from a contaminated and a non-contaminated area, respectively (Zuidberg et al. 1988). The results from Figure 7.1 (a) clearly show relatively high values of conductivity within the sand layer, which are due to the high TDS content in the groundwater. Figure 7.1(b) on the other hand shows a much lower and more constant value of conductivity for the same but non-contaminated groundwater.

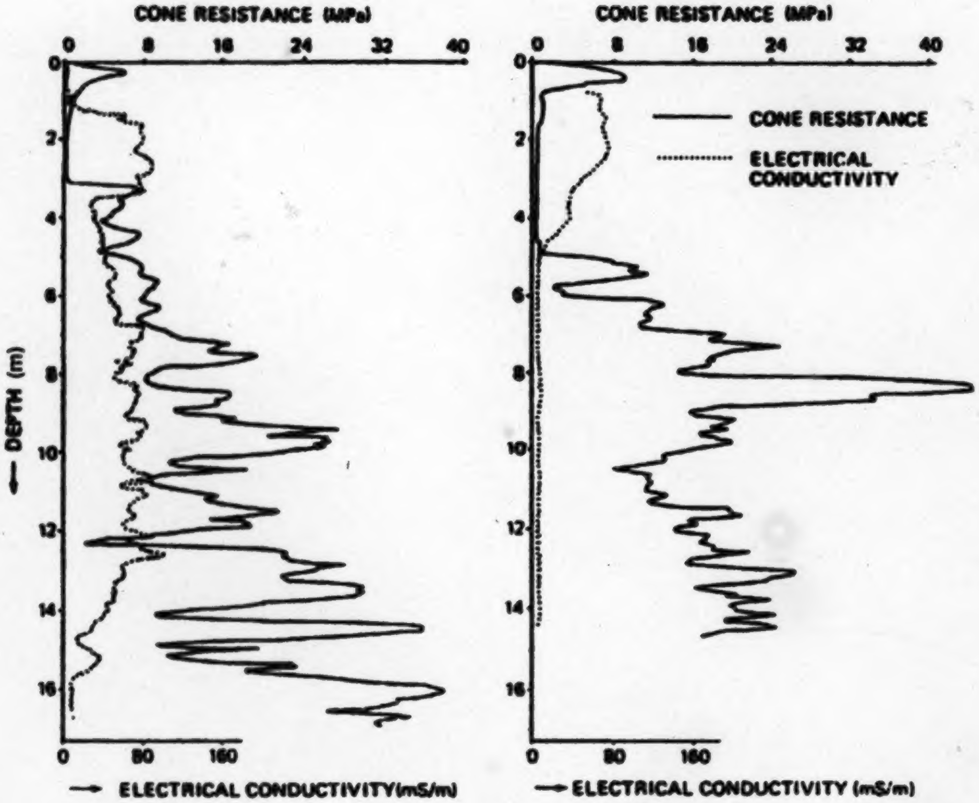

(a) (b)

Figure 7.1 – RCPT from a waste disposal (inorganic compound) site: (a) high conductivity for a contaminated area and (b) low conductivity for a non-contaminated area (modified from Zuidberg et al. 1988).

Woeller et al. (1991) present an interesting series of RCPT tests performed at a DNAPL contaminated site, reproduced in Figure 7.2. The first resistivity profile is from an area not affected by the DNAPL spill. The other three tests were performed in an area affected by the DNAPL spill. The tests start from the spill zone and are performed at 100 m intervals downgradient. The contaminated zone can be seen clearly due to its higher bulk resistivity (approximately 100 ohm·m) compared to the lower bulk resistivity (20 ohm·m) of the non-contaminated area. It is interesting to note there is an increase in depth of the contamination with the increasing distance from the contamination source, reflecting the tendency of DNAPL contamination to sink in groundwater.

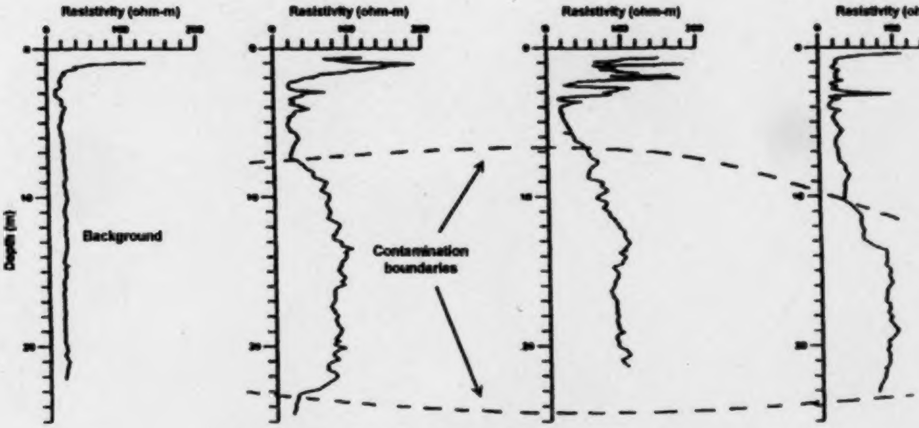

Figure 7.2 – RCPT of a DNAPL spill site
(modified from Woeller et al. 1991).

Figure 7.3 shows a RCPT test from a creosote contaminated site (Campanella et al. 1994b). The dark area indicates the increase in bulk resistivity, due to the presence of contamination. The spikes in the bulk resistivity profile, at depths of 15 to 19 m indicate the presence of free phase product, whose existence was confirmed by monitoring well samples.

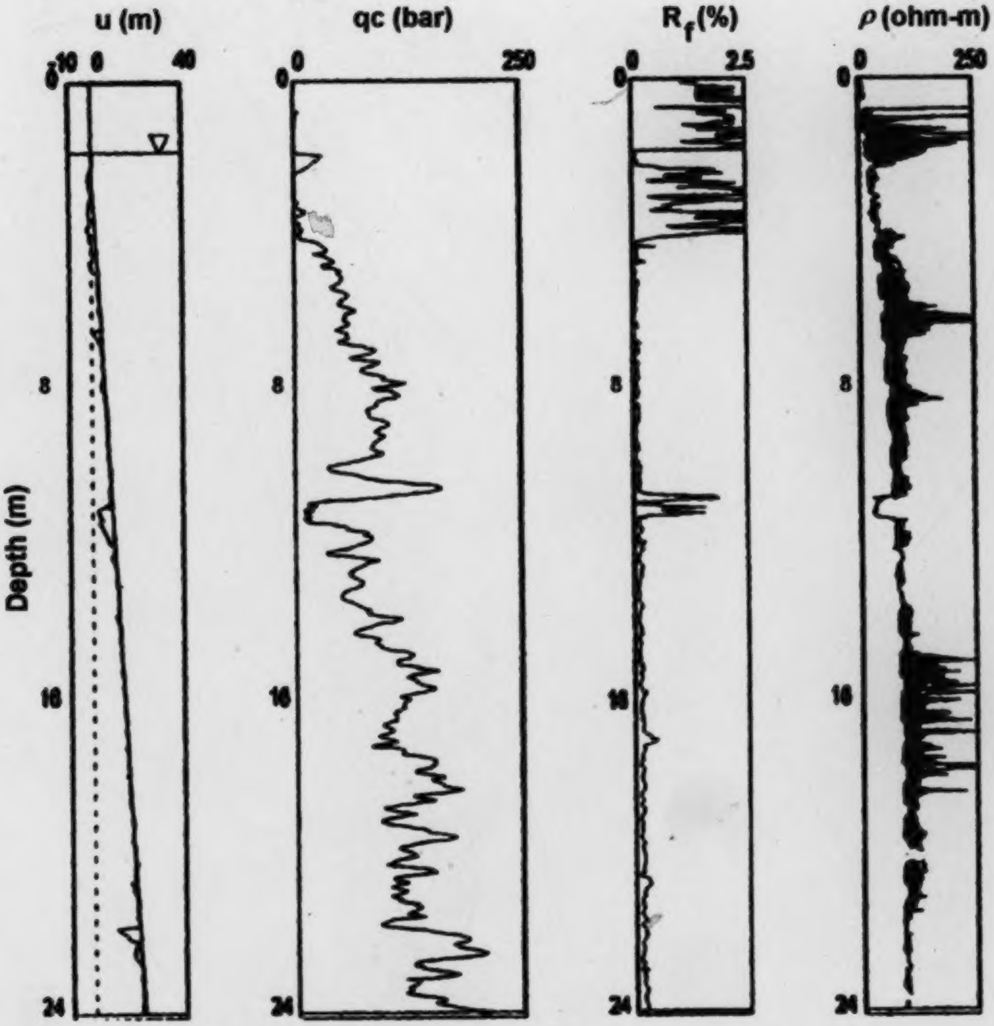

Figure 7.3 – RCPT profile from a creosote contaminated site (modified from Campanella et al. 1994b).

The above examples show that when underground bulk resistivity contrasts exist and it is possible to obtain a good background value for comparison, soil bulk resistivity measurements can be a valid instrument for screening soil contamination.

## 7.5 SUMMARY

Despite soil electrical resistivity (conductivity) measurement being a mature technology, its use for tracking groundwater contamination in geoenvironmental practice is relatively new. Its use is growing quickly as professionals gain experience in its use and interpretation.

Because an electrical current flow in a saturated soil occurs predominantly by electrolytic conduction, soil electrical resistivity is mainly controlled by pore fluid resistivity. Therefore, any change in pore fluid resistivity can strongly affect the soil bulk resistivity. The presence of inorganic contaminants in groundwater will typically decrease its soil bulk resistivity, whereas organic contaminants will tend to increase its soil bulk resistivity.

Nevertheless, soil bulk resistivity is also a function of the soil particles and their arrangement. Clayey soils have high cation exchange capacity which usually present lower resistivity measurements than sandy soils. In this context, it is important, when screening for groundwater contamination, that the resistivity probe also be capable of identifying soil lithology. Consequently, the use of a Resistivity Cone Penetration Test (RCPT) is gaining in popularity because it is one of the best logging tools for the identification of soil stratigraphy and for independently measuring soil bulk resistivity.

RCPTs have been used successfully for screening groundwater contamination produce by a variety of different contaminants such as: brine spills, landfill leachates, jet fuel spills, creosotes, sulphates, chlorides and phosphates.

A resistivity module similar to the one used in a standard RCPT can be easily incorporated into the HD-PB-CPT and used not only for screening groundwater contamination, but also to improve its ability to identify sand pockets in clayey mediums.

# CHAPTER 8

# Horizontal Directional Pre-Bored Resistivity Cone Penetration Test HD-PB-RCPT (Prototype 2 Development)

## 8.1 INTRODUCTION

The Prototype 1 cone resistance results from Chapter 5 have shown that it was possible to distinguish the presence of a sand pit in a clay medium. On the other hand, the results from the friction sleeve indicated a poor contrast between these two soil types. Furthermore, the cone and friction sleeve values were lower than those obtained by the standard vertical CPTs. These contrasting results showed a need to modify prototype 1 to improve its results.

The laboratory modeling tests from Chapter 6 have shown that a cone with a 30° apex angle pushes the soil ahead of the cone more in a sideways direction than does a 60° cone, resulting in improved borehole (cavity) expansion. It also has been shown that placing a cylindrical constraint device in front of the probe with the same diameter as the borehole would restrain the soil, forcing it to expand outwards. This device might also reduce the stress relief around the probe promoting an increase in cone and friction resistance results from the HD-PB-CPT test.

Based on the information gathered from the laboratory modeling test, changes were made to the HD-PB-CPT design to develop prototype 2. This new version of the HD-PB-CPT has the capability of performing the test with either a 60° or a 30° apex angle cone tip. The objective of performing the test with two different cone tips was to see which one would give a better $q_c$ result. The model tests have shown that the 30° cone performed better in the expansion of the borehole, and should therefore, improve cone resistance. On the other hand, Silvestri and Fahmy (1995) indicated that for a vertical cone penetration, $q_c$ steadily increases for increasing values of the apex angle above 30°. Bishop et al. (1945) have shown that the pressure required to expand a cylindrical cavity is slightly lower than the pressure required to expand a spherical cavity. Despite the better performance of the 30° cone in the laboratory model tests in expanding the borehole, it was possible that the $q_c$ value obtained by this sharper cone would be less than that from a standard 60° vertical CPT. Hence, it was decided to build prototype 2, capable of using both cone tips and to field test both tips.

The bullet shaped device in front of prototype 1 was replaced by the constraint device in prototype 2. The constraint device was similar to the bullet except that it was longer.

Prototype 2 also had an electrical resistivity module (ERM) incorporated into its design making the probe capable of measuring soil bulk resistivity (Chapter 7). Because of its ability to measure soil electrical resistivity, prototype 2 was called the Horizontal Directional Pre-Bored Resistivity Cone Penetration Test (HD-PB-RCPT).

The ERM will allow prototype 2 to detect possible contamination plumes and pools, and also it will improve the probe's capability to locate sand pockets embedded in a clay medium due to the contrast in bulk resistivity that is usually presented by these two types of soil.

The following sections will describe in detail the design and construction of the HD-PB-RCPT, with special attention given to the development of the electrical resistivity module.

## 8.2 MODIFICATIONS TO IMPROVE CONE AND FRICTION SLEEVE RESULTS

All the parts used to build prototype 1 were used to build prototype 2, i.e., load cells, friction sleeve, connection tool, and the 60° cone tip. Some modifications had to be made at the back of the probe for the ERM.

Based on the analysis described in section 6.4.1, it was determined that the length of the constraint device should be 2.8 probe diameters when performing the test with the 60° cone and 2.5 probe diameters when using the 30° cone.

To accommodate these changes a new hollowed shaft was built, not only to accommodate the length of the constraint device but also to accommodate the ERM at the back of the probe.

This new shaft was built with alloyed steel AISI 4140; the same class of steel that was used to build the previous shaft. The constraint device, for the 30° cone, was incorporated into the new shaft. A separated piece of steel, 5 cm in length, was made to reach the required length of the constraint device when performing the test with the 60° cone tip, as shown in Figure 8.1(a).

To reduce the weight of the shaft, the constraint device was made from a 10.16 cm (4") diameter steel pipe that was slid onto the shaft and had its ends fastened to the shaft's wall leaving an air gap between the two parts. Detailed drawings of the design of the HD-PB-RCPT are presented in Appendix 4.

The 30° apex angle cone tip was built of the same stainless steel as the previous 60° cone and it also had two sets of "O" rings to protect the load cells against groundwater. Sketches of the HD-PB-RCPT with the two different apex angle tips are shown in Figure 8.1(a) and (b). A picture of the probe assembled with the 30° cone and data acquisition cable is presented in Figure 8.2.

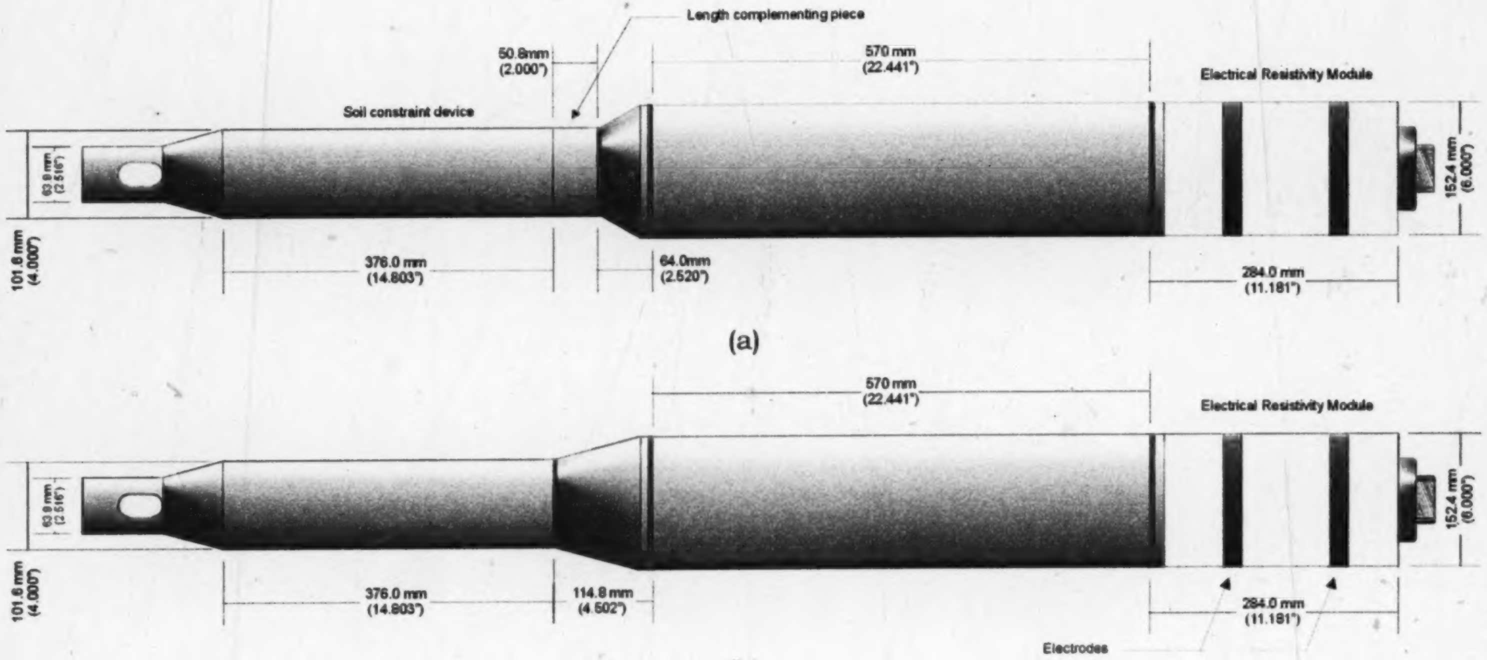
Length complementing piece
50.8mm (2.000")
570 mm (22.441")
Electrical Resistivity Module
Soil constraint device
63.9 mm (2.516")
152.4 mm (6.000")
101.6 mm (4.000")
376.0 mm (14.803")
64.0mm (2.520")
284.0 mm (11.181")
570 mm (22.441")
Electrical Resistivity Module
63.9 mm (2.516")
152.4 mm (6.000")
101.6 mm (4.000")
376.0 mm (14.803")
114.8 mm (4.502")
284.0 mm (11.181")
Electrodes

(a)

(b)

Figure 8.1 – HD-PB-RCPT (a) with a 60º apex angle cone tip and (b) with a 30º.

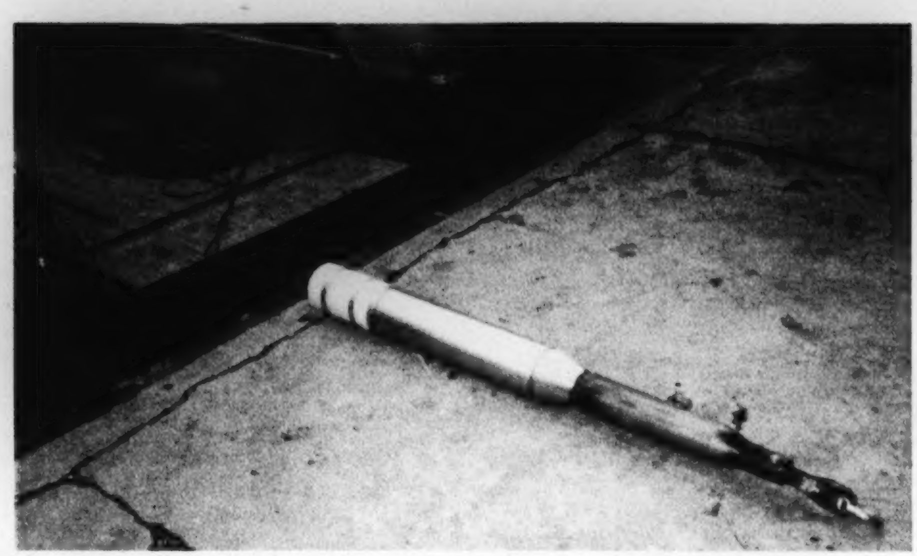

Figure 8.2 – HD-PB-RCPT assembled with the 30° cone

## 8.3 ELECTRICAL RESISTIVITY MODULE (ERM)

A comprehensive study into the development and construction of an electrical resistivity CPT was carried out by Weemees (1990). The ERM for the HD-PB-RCPT was built based on information and research conducted for this study and others such as Woeller et al. (1991), Kokan (1992), Everard (1994) and Lunne et al. (1997).

### 8.3.1 EXCITATION SOURCE AND RESISTIVITY CALCULATION

As explained in Chapter 7, the transfer of electrical charge in saturated soil occurs mainly through electrolytic conduction; therefore, there is a potential for the electrodes to become polarized. Polarization is the buildup of ions at the electrodes which produces an impedance in series with that of the surrounding soil (Weemees 1990). To avoid electrode polarization an alternate current excitation source at a frequency of 1000 Hz is commonly used for measurement of soil electrical resistivity. At this frequency the ions do not have time to accumulate at the electrodes reducing the potential for polarization.

A Kenwood Function Generator FG-272 was used as an excitation source for the HD-PB-RCPT. This generator has frequency variation capability from 0.2 Hz to 2 MHz and maximum amplitude output of 10 volts. Unfortunately this wave generator was not capable of delivering a constant current source; as the medium electrical resistance changes the voltage and the current of the complete system change as well. This made the data acquisition more complex. In order to obtain the soil electrical resistance it was necessary not only to measure the system output voltage, but also the current; the data acquisition card was not capable of directly measuring current. To overcome this, the current was measured indirectly by placing a constant value (32.5 Ω) wire wound resistor in series in the circuit, as shown in Figure 8.3. This made it possible to measure the voltage across this resistor and by applying Ohm's law, the circuit current was calculated at each reading. Once the circuit current was known the soil resistance was calculated by dividing the circuit output voltage by the current. Finally, the soil bulk resistivity was obtained by multiplying the soil's electrical resistance by the calibration factor previously explained in section 7.3.3.

All the alternating voltage measurements were automatically converted to root mean square (RMS) voltages by the data acquisition card. RMS voltage can be defined as the effective voltage applied, i. e., it is the value of alternating voltage that produces the same heating effect as would be produced by an equal value of direct voltage (Graf 1978).

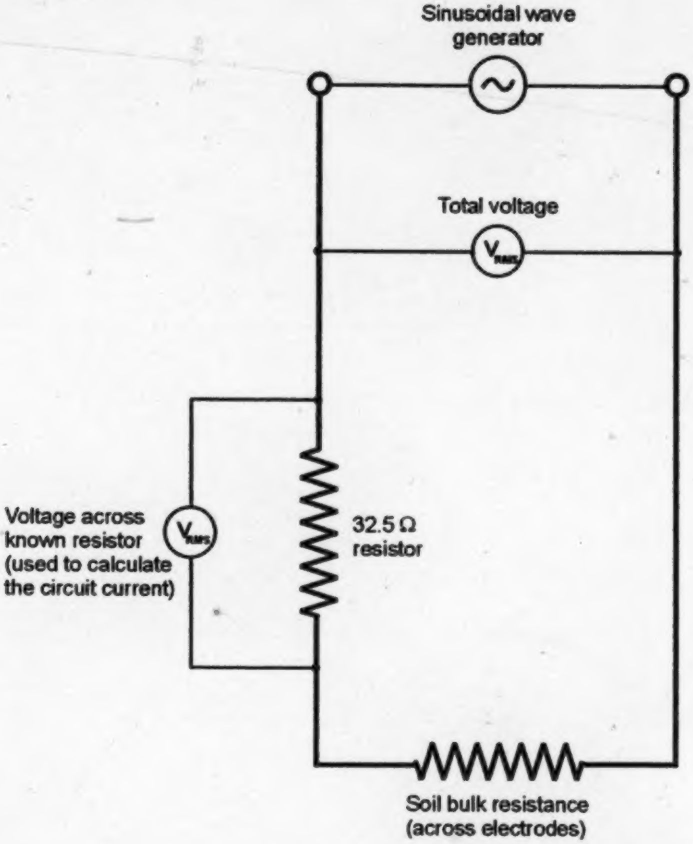
Sinusoidal wave generator
Total voltage
V RMS
Voltage across known resistor (used to calculate the circuit current)
V RMS
32.5 Ω resistor
Soil bulk resistance (across electrodes)

Figure 8.3 – HD-PB-RCPT ERM circuit.

### 8.3.2 NUMBER OF ELECTRODES

Electrode polarization is a function of current; therefore, by using a four electrode configuration probe electrode polarization can be minimized. In this kind of configuration the outermost electrodes apply the current and inner electrodes are used to measure the voltage output. Because the circuit that measures the voltage has high impedance the current passing through the electrodes is very small hence reducing polarization effects. The advantage of such a configuration is that it can be operated at low frequencies without polarizing the electrodes. However, manufacturing the probe is more cumbersome. Furthermore, because electrical resistivity penetration measurement is a function of electrode spacing, the farther apart the electrodes are placed, the deeper will be the penetration of the electrical field into the soil. To have a representative amount of soil tested it is best to have the electrodes spaced as far apart as possible. By using a four electrode array configuration and placing them sufficiently far apart to be able to measure the resistivity of a considerable amount of soil, the probe's length would have been adversely compromised.

Studies conducted by Weemees (1990) have shown that a two electrode array could be employed successfully when adequate excitation frequency is used. Figure 8.4 shows the influence of polarization on the resistivity measurement as a function of frequency for a two and a four electrode configuration probe. The measured resistivity is normalized against the resistivity measured at 1000 Hz. The graph clearly shows that for a four electrode array, the resistivity measurements are independent of frequency. Conversely a two electrode system is greatly affected by frequency. Nevertheless, as the frequency approaches 1000 Hz, the polarization effects on the two electrode array are reduced to insignificant levels. Therefore, it was decided to build the HD-PB-RCPT ERM with a two electrode array operating at a frequency of 1000 Hz.

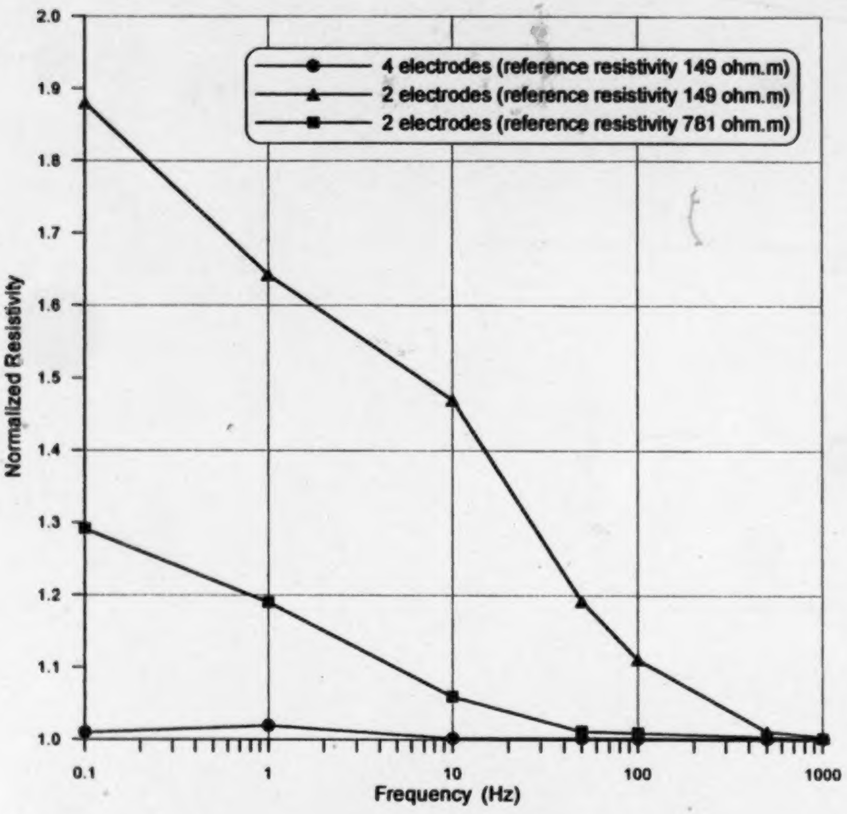

Figure 8.4 – Effect of polarization in a two and four electrodes configuration probe (modified from Weemees 1990).

### 8.3.3 ERM AND DATA ACQUISITION SYSTEM DESCRIPTION

The electrical resistivity module was placed on the back end of the probe as shown in Figure 8.1. It consisted of a two electrode configuration module; each electrode had a width of 2 cm and they were spaced 12 cm apart, center to center.

The body of the ERM was made with Delrin, an acetal resin, which is a crystalline plastic made by the polymerization of formaldehyde (DuPont 2000a). This material has electrical conductivity smaller than $10^{-12}$ S/m (DuPont 2000b) which makes it a good electrical insulator (Keller 1982). It also has excellent mechanical properties and it is not difficult to machine. In addition Delrin has been used successfully in the past to build a similar electrical resistivity module for a standard CPTU (Woeller et al. 1991). This particular module was totally independent of the rest of the probe, i.e., it had its own data acquisition cable so the test could be carried out with or without the ERM. Details of the module's design are presented in Appendix 4.

The same data acquisition system used for prototype 1 was used for prototype 2. The LabView program used to control and monitor the test was modified to be able to log the new data. The front panel (Figure 4.20), displayed on the laptop screen, was also modified to include a profile of resistivity versus penetration distance. Having four profiles on a laptop screen made the readability of the profiles difficult. It was decided to make the friction sleeve profile interchangeable with the resistivity profile; i.e., by toggling a button it was possible to switch from one profile to the other during the test. The most useful piece of information for soil classification from a CPT test are the cone resistance and the friction ratio. Hiding the friction sleeve resistance profile in the background did not pose any problems for the interpretation of the results during the test.

### 8.3.4 ERM CALIBRATION

The ERM measures the soil resistance, and a conversion from resistance to resistivity is made by means of a calibration factor (*K*) obtained from laboratory calibration tests.

The calibration test for the HD-PB-RCPT was performed in a large tank (237cm long, 63 cm in width and 90 cm deep) filled with tap water. The HD-PB-RCPT was then immersed in the water as shown in Figure 8.5. The probe had a clearance from the tank's walls, the bottom, as well as from the water surface level of at least 1.5 probe's diameter.

Despite the small distance between the probe and the tank's boundaries, studies made by Yeung and Akhtar (1995) of the boundary effects of a calibration chamber on electrical resistivity measurements have shown that the influence of boundary effects on the value of *K* decrease as the ratio of the distance between electrodes ($d_e$) to diameter of the probe ($d_c$) decrease. This can be better visualized in the chart shown in Figure 8. 6. Because of the large diameter of the HD-PB-RCPT the ratio $d_e/d_c$ was very small (0.8). Since the graph in Figure 8. 6 shows, the curve for $\frac{d_e}{d_c}=2$ is already quite flat it can be assumed that for smaller $d_e/d_c$ ratios the curve would be even flatter. Hence, the influence of the boundaries of the tank in the calibration test were neglected.

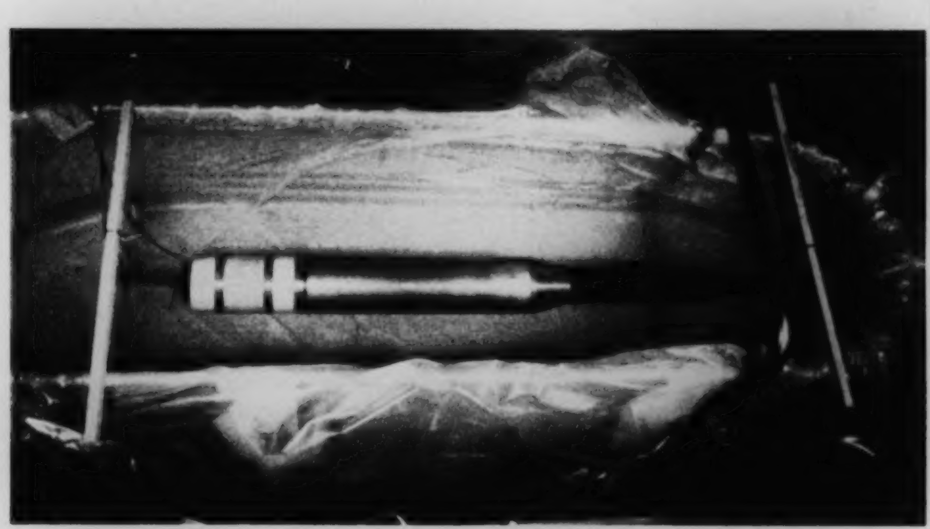

Figure 8.5 – Electrical resistivity calibration tank.

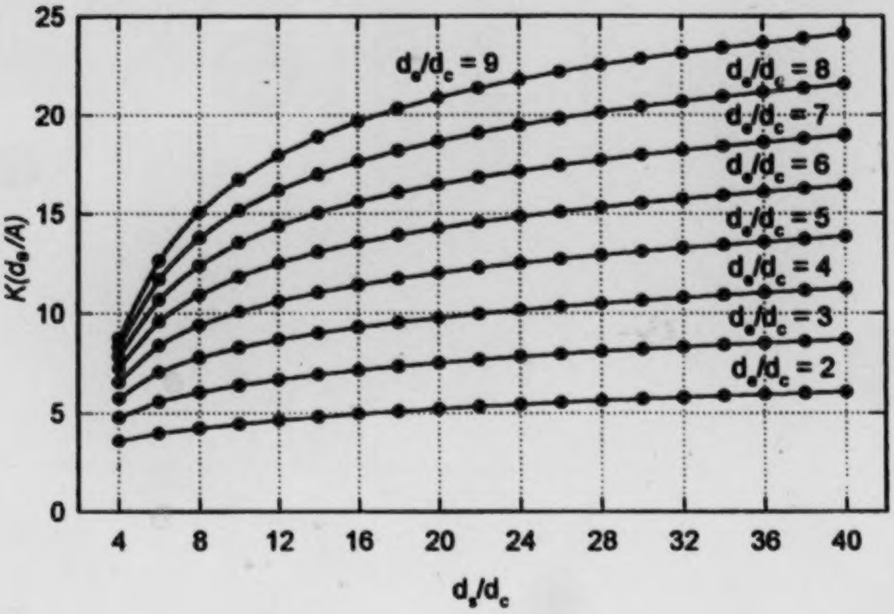

Figure 8. 6 – Influence in *K* value as a function of $d_s/d_c$ and $d_e/d_c$ (modified from Yeung and Akhtar 1995). $d_e$ = distance between electrodes; $d_c$ = probe's diameter; $d_s$ = chamber's diameter and *A* = probe's cross section area.

The medium (water) resistivity was changed incrementally by adding salt. At each new electrolyte concentration, the solution resistance was measured by the HD-PB-RCPT and the resistivity was measured using a portable conductivity/resistivity meter (Oakton WD-37607). This portable conductivity/resistivity meter also measured the solution temperature and automatically corrected the resistivity to a reference temperature of 25°C.

The portable conductivity/resistivity meter was calibrated in reference solutions of potassium chloride (KCl) at concentrations of 1, 0.1, 0.01 and 0.001 normality, and prepared according to the ASTM (1995b) standard test method D 1125.

The value of resistance and resistivity for each electrolyte concentration was then plotted on a chart (Figure 8.7). The relationship between these parameters is usually close to a straight line as shown in Figure 8.7 and *K* is the angular coefficient of this line, as shown in the Equation 8.1.

$$\rho = \overbrace{0.2827}^{K} R - 11.79 \qquad [8.1]$$

where:

$\rho$ = resistivity

$R$ = resistance

$K$ = calibration factor

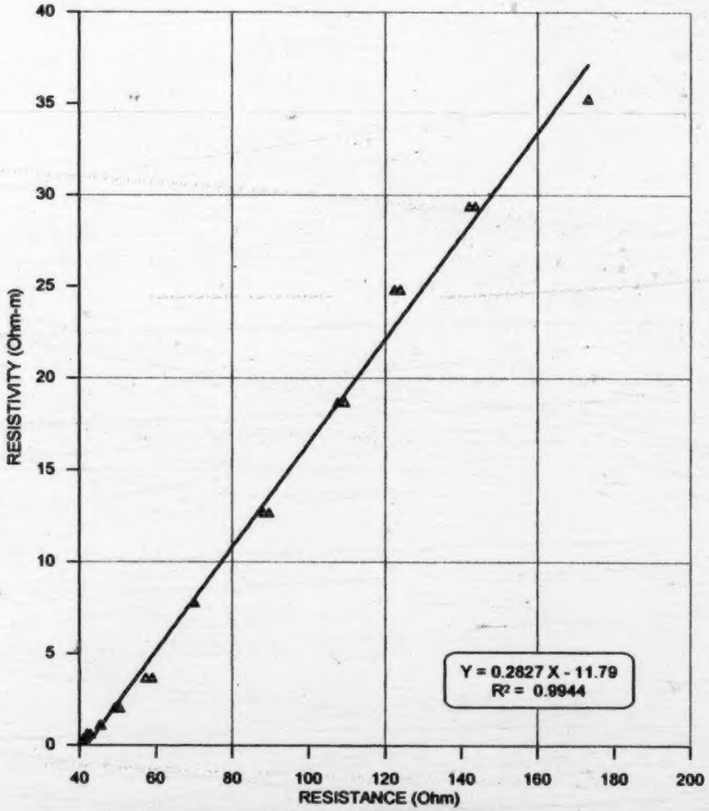

Figure 8.7 – Electrical Resistivity Module calibration curve.

The resistivity of an electrolyte solution is a function of temperature because the acceleration of ions in an electrolytic conduction is reduced by viscous drag (Carr 1982; Keller 1982; Campanella and Weemees 1990; Yeung and Akhtar 1995). Hence, if temperature increases, viscosity will decrease, decreasing resistivity. Therefore, when measuring resistivity, it is important to measure the temperature as well, so the value of the resistivity can be corrected to a reference temperature, such as 25° C for instance.

When using the HD-PB-RCPT test in particular, what was being sought was not the true value of soil bulk resistivity, but rather the contrast in resistivity. Thus measuring temperature to correct the resistivity value was not necessary. Nevertheless, if it is desired to use the probe to measure the formation factor (*F*), a temperature sensor should be installed in the probe.

The formation factor, originally defined by Archie (1942), is the ratio of the soil bulk resistivity to the porewater resistivity. Usually the porewater resistivity is measured with a different instrument than the one used to measured soil bulk resistivity. In this case it is imperative to have both resistivity measurements referenced to the same temperature.

Once the calibration factor *K* was obtained, its value was put into the LabView program which than automatically did the conversion from measured resistance (Ohm) into resistivity (Ohm·m) and plotted the results as resistivity versus penetration distance on the laptop screen. After this calibration, prototype 2 was ready to be field tested.

## 8.4 SUMMARY

In an attempt to improve cone and friction sleeve results, a second prototype of the HD-PB-CPT was built. The main modifications were the addition of a soil constraint device in front of the probe and a new 30° apex angle cone.

The intent behind these modifications was to improve the borehole (cavity) expansion. Laboratory modeling tests showed that the 30° cone pushes the soil more to the sides than the 60° cone, and that the constraint device did not allow the soil in front of the probe to deform towards the borehole forcing it to expand outward. This might increase the state of stress around the probe during penetration and consequently increase cone and friction sleeve values.

Another improvement to prototype 2 was the addition of an Electrical Resistivity Module (ERM). The ERM not only enables the probe to profile for soil contamination by means of contrast measurements in soil bulk resistivity, but also improves the capability of the probe to identify sand lenses in a clay medium. Due to their higher cation exchange capacity, clayey soils usually have lower electrical resistivity than sandy soils. The ERM, therefore, provides a good aid for tracking soil lithology changes.

Because of its ability to measure soil resistivity, prototype 2 was named the Horizontal Directional Pre-Bored Resistivity Cone Penetration Test (HD-PB-RCPT).

# CHAPTER 9

# Prototype 2 – Field Tests

## 9.1 INTRODUCTION

The field testing program for prototype 2 was designed so no new variables were introduced except for the changes in the probe design. The HD-PB-RCPT was therefore field tested at the same site as prototype 1 was tested (in November of 1999).

Analogous to the prototype 1 field tests, two sets of tests were performed along the same alignment, but at different depths (2 and 4 meters) (Figure 5.2). A new pit was dug 3.5 m in width, 4.5 m in length and 4.5 m in depth and filled with sand. However, this time the sandpit was excavated to a greater depth to have all the tests pass through the sandpit. The sand was placed into the pit in layers with each layer compacted with the backhoe bucket.

Because a small time lag would occur from the time of construction of the sandpit to the time of the field tests, there was likely no time for pore pressure equalization in the sandpit. To minimize this problem the sandpit was filled with water with the help of four 2" diameter pipes that were placed in the sandpit during construction. Three of these pipes had their ends placed close to the bottom of the pit while the other placed, at the center of the pit, had its end placed at a half depth.

Operational problems did not permit the performance of these tests with the same drill rig contractor used in the previous field tests. A new contractor, Commercial Trenching Ltd., was contacted and agreed to do the field tests of the HD-PB-RCPT.

Commercial Trenching operates with Ditch Witch HDD rigs. The closest available rig to the Vermeer D24x40 Navigator used previously, was the Ditch Witch JT1720. Like the Vermeer D24x40, this rig is capable of drilling a 10.16 cm (4") diameter borehole, but has a pullback force capability of only 75.6 kN (17000 lbs.), 30.3 kN lower than the Vermeer rig. Nevertheless, the results from the previous field tests showed that it would not be a problem for the rig to pull the probe through the Lake Edmonton clay formation at the University of Alberta field laboratory.

To assure a borehole diameter no larger than 10.16 cm (4"), all the boreholes for prototype 2 field tests were drilled using an 8.89 cm (3.5") drill bit. The pilot holes were also drilled using water as a drilling fluid.

Figure 9.1, Figure 9.2 (a) and (b) show views of the HDD rig Ditch Witch JT 1720 used to pull the probe, the beginning of the test when the HD-PB-RCPT was hooked-up to the drill stem, and the start of the penetration, respectively.

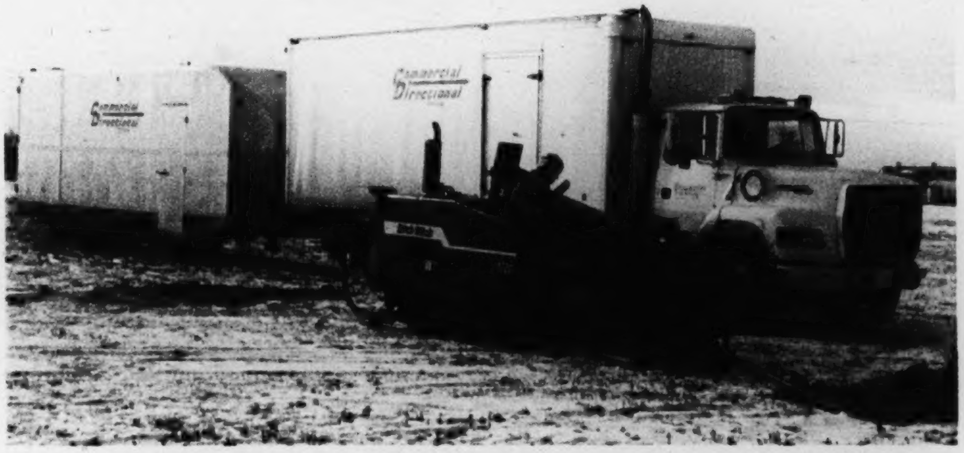

Figure 9.1 – HDD drill rig Ditch Witch JT 1720.

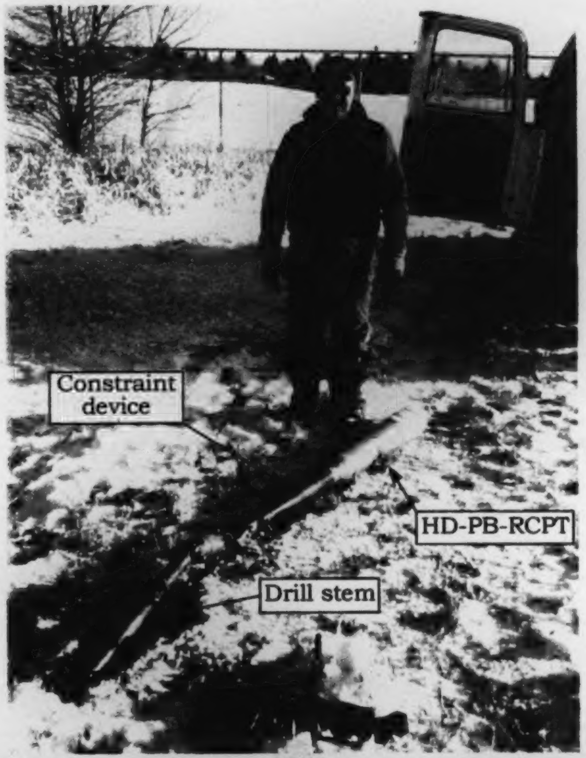

Constraint device
HD-PB-RCPT
Drill stem

(a)

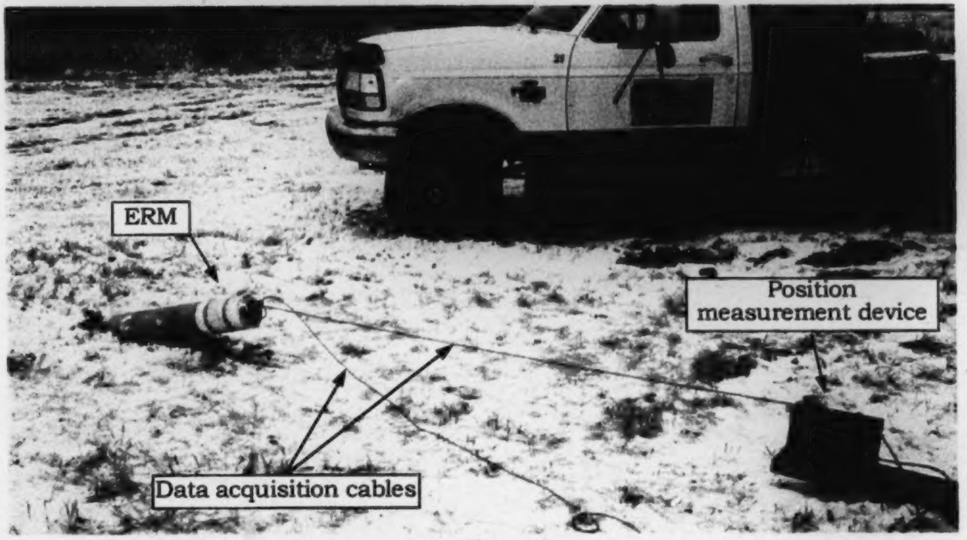

ERM
Position measurement device
Data acquisition cables

(b)

Figure 9.2 – (a) Drill stem and HD-PB-RCPT hook-up and (b) beginning of penetration.

The initial plan for the field work was to perform only four HD-PB-RCPT tests, two tests using the 60° cone and two tests with the 30° cone each at a depth of 2 and 4 meters. These four tests were expected to provide sufficient information regarding the performance of the constraint device and the efficiency of a sharper cone to improve borehole expansion. Constraint device efficiency was analyzed by comparing the results from prototype 1 with the results from prototype 2 using the 60° cone. A comparison of results between prototype 2 tests with the 60° cone and the 30° cone would render information with respect to the efficiency of a sharper cone.

The ERM was used in all four tests. Because the ERM is located at the back of the probe, any changes made in the front of the probe were not expected to affect the electrical resistivity measurements. Four electrical resistivity profiles were, therefore, considered sufficient to evaluate the performance of the ERM.

Unfortunately, a problem occurred with the data acquisition system making the data for cone and friction sleeve resistance completely spurious and useless. The results from the electrical resistivity measurements, however, were very good. After taking the probe back to the laboratory and fixing the above mentioned problem, a second series of tests were carried out, in January of 2000.

The next section will discuss the results for both series of tests. The first series had the problematic cone and friction sleeve results; the second series was completed after fixing the problem.

## 9.2 FIRST SERIES OF HD-PB-RCPT TESTS (November, 1999)

Cone and friction sleeve results from these tests were jeopardized due to a malfunction of the DC adapter used to deliver the excitation voltage to the load cells. The DC adapter was not able to deliver the required 9 volts to the amplifiers. Unfortunately, all attempts to detect the source of the problem in the field were unsuccessful. Nevertheless, the results obtained from the electrical resistivity measurement tests were very successful. Because the ERM works with an independent AC excitation source, the malfunctioned DC adapter had no influence on the electrical resistivity measurements.

### 9.2.1 HD-PB-RCPT TESTS WITH THE 60° APEX ANGLE CONE

The first HD-PB-RCPT test was performed using the 60° apex cone at a depth of 2 meters (Test 6). The test was performed in an east-west direction and had a total length of 60 meters. The total time needed to open the 60 m long pilot hole was 33 minutes and the test itself was performed in 70 minutes. Adding 10 minutes to hook-up the probe to the drilling rods, the total time to perform a 60 m borehole log was 113 minutes.

Test 6 results presented in Figure 9.3 show that the cone, friction sleeve, and friction ratio data results are so scattered they are essentially meaningless. Some cone data had negative values. On the other hand, the electrical resistivity data present a smooth clear result. When the ERM was outside the borehole the resistivity is very high (infinite). As the probe entered the borehole and the electrodes come into contact with the soil the resistivity dropped suddenly until it reached a stable and constant value in the clay of around 8 ohm·m. As the HD-PB-RCPT reached the sand pit the resistivity values jump to greater than 40 ohm·m returning to 8 ohm·m as the probe moved into the clay again. Some electrical resistivity spikes can be seen at 44, 53, 56 and 58 meters of penetration. The reasons for the spikes are difficult to identify without complementary investigation, but probably their cause is due to the presence of small sand lenses or pockets in the clay medium.

A second test (Test 7) was also conducted using the 60° cone, but at a depth of 4.2 m. To obtain a reasonably straight section of the test before and after the sandpit at this depth, a longer pilot hole was drilled, with a total length of 70 meters.

The results from Test 7 are presented in Figure 9.4. Like Test 6, the data results for cone, friction sleeve, and friction ratio were useless. The electrical resistivity results, however, were again very consistent with the previous test, showing that the ERM has a very good repeatability. It is interesting to note that at the left side of the sand pit there are no spikes in the resistivity data, whereas at the right side both tests presented a few spikes. This contrast indicates that the soil formation at the left of the sandpit side appears to be more homogenous than the soil formation at the right side.

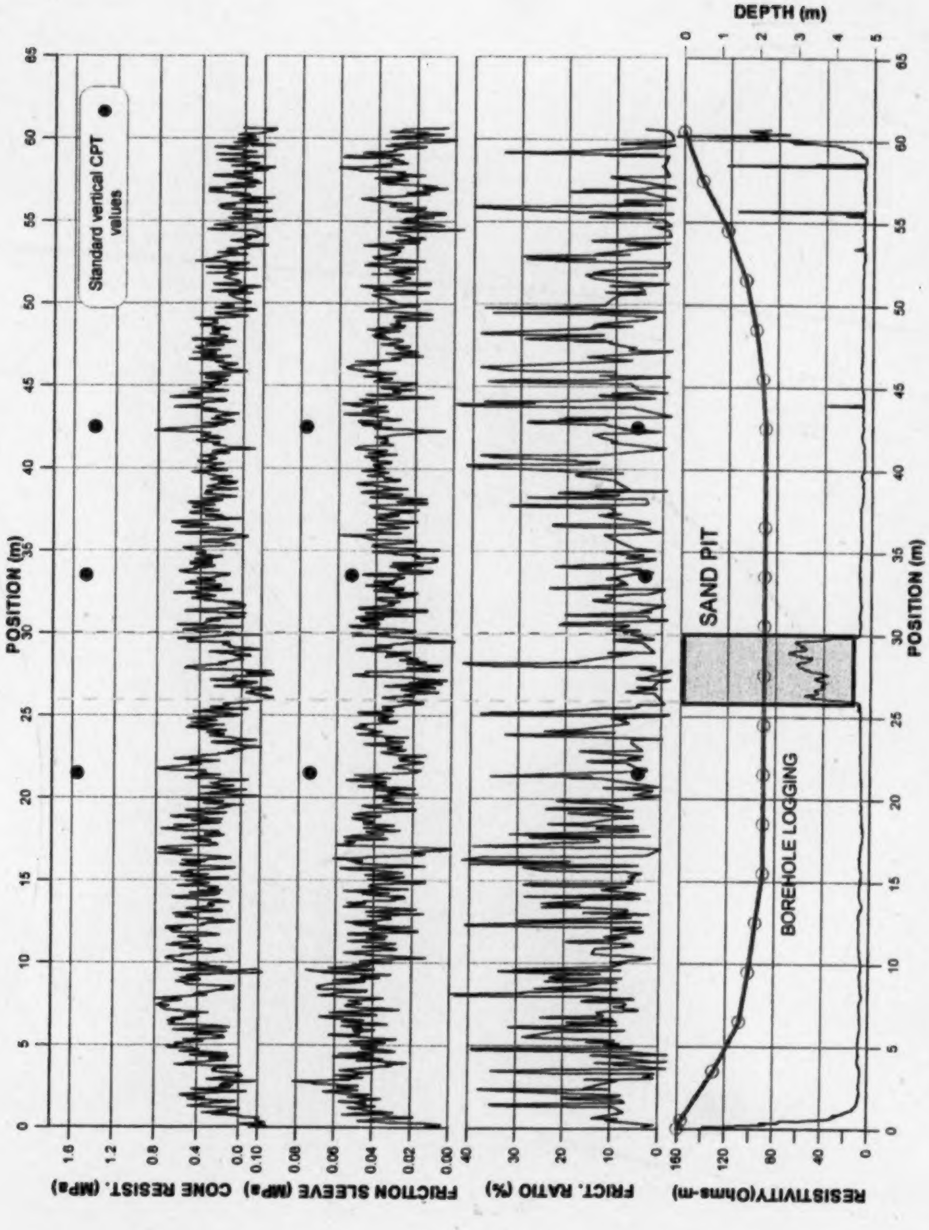

Figure 9.3 – HD-PB-RCPT Test 6 with the 60° apex angle cone.

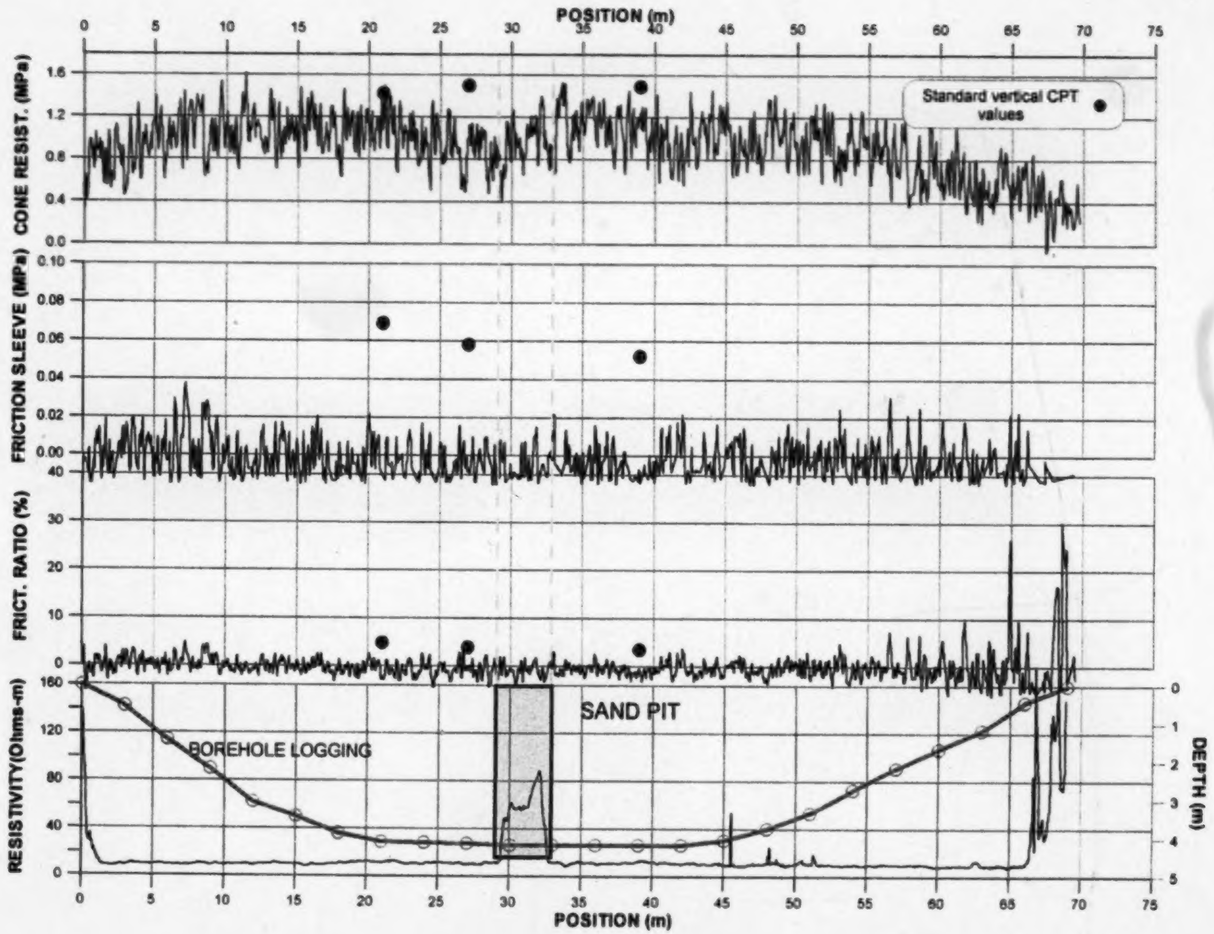

Figure 9.4 – HD-PB-RCPT Test 7 with the 60° apex angle cone.

### 9.2.2 HD-PB-RCPT TESTS WITH THE 30° APEX ANGLE CONE

After performing both of the previous tests, the HDD rig was repositioned to perform the next two tests in a north-south direction across the sandpit. The HD-PB-RCPT cone tip was replaced with a 30° apex angle cone and tests 8 and 9 were performed at depths of 2 and 4 meters, respectively.

The results from Test 8 and Test 9 are shown in Figure 9.5 and 9.6, respectively. This time, the cone and friction sleeve results were a little better than for Tests 6 and 7, but still showed a lot of scattering.

It is interesting to note at this point that despite the scattered results of the cone resistance data of Test 9 (Figure 9.6) they show a significant drop in value as the probe reached the sandpit and nearly constant value of approximately 0.4 MPa when the probe was in the clay. Friction sleeve data in this same profile was at an average constant value of around 0.035MPa while the HD-PB-RCPT was in the clay; however, there is no noticeable change in friction values when the probe passed through the sandpit.

Despite the unreliable cone and friction sleeve results the electrical resistivity results from both tests (8 and 9), once again, were very good, showing a clear picture of the sandpit location and also the good repeatability of the bulk electrical resistivity test.

There are a few spikes in resistivity at the left side of the sandpit for both tests, probably caused by small embedded sand lenses in the clay medium. At the right side, on the other hand, there are a significant number of spikes in the data, concentrated around the same region in both tests. Because the test depths were 2 meters apart the reason for these spikes may be other than the presence of sand lenses. Further research into the past use of this site indicated that very close to the area where the concentration of spikes occurred, screw pile testing took place in 1998 at 3.05 to 5.18 meters in depth (Zhang 1999). The soil disturbance introduced by the screw pile tests could have caused the spikes in the electrical resistivity data. It is interesting to note that the test at 4 meters depth (Test 9) had fewer spikes than the 2 meter test (Test 8). In the area of the screw piles tests, the piles extended to a maximum depth of 5.18 m. Hence, there may have been slightly less disturbance at depth of 4 m (Test 9). Unfortunately, the precise location of the screw pile tests were not known due to the absence of a fixed point of reference.

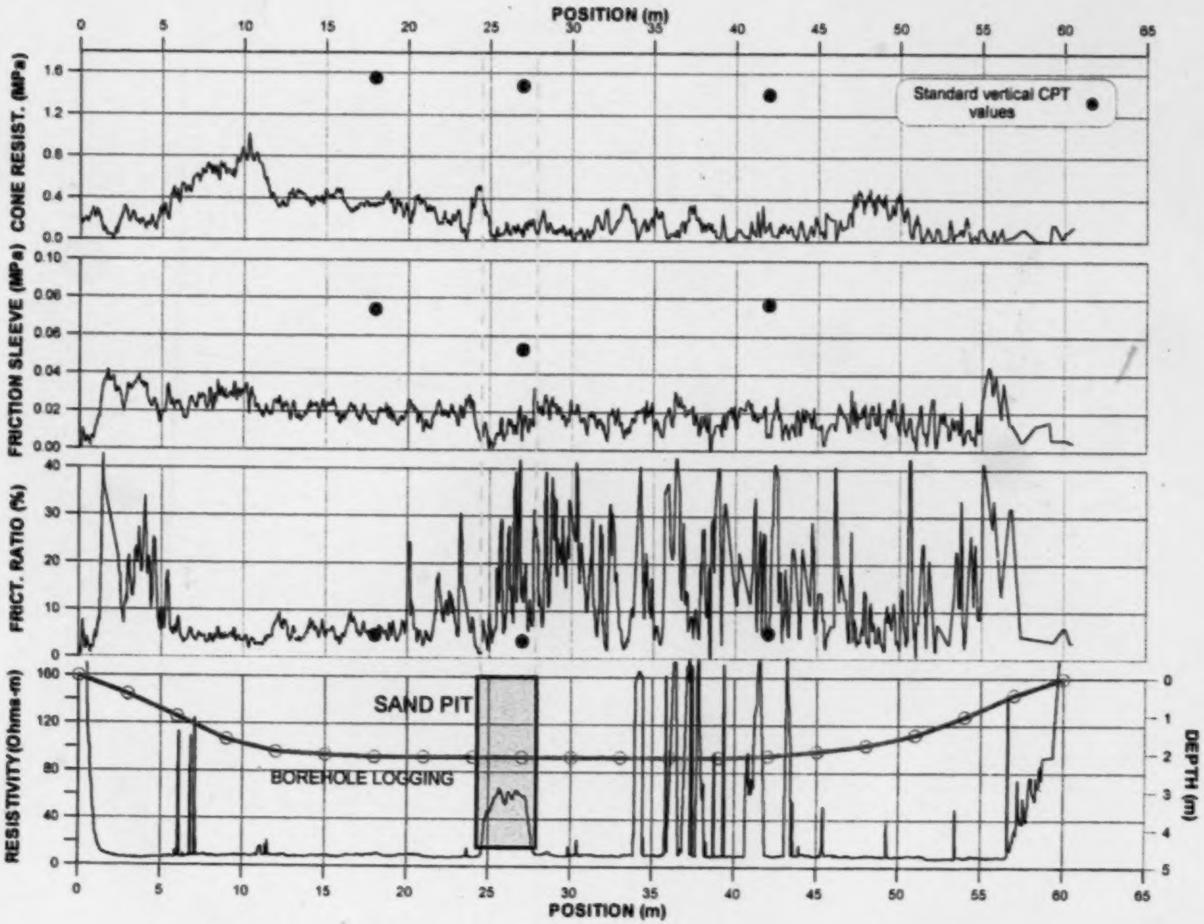

Figure 9.5 - HD-PB-RCPT Test 8 with the 30° apex angle cone.

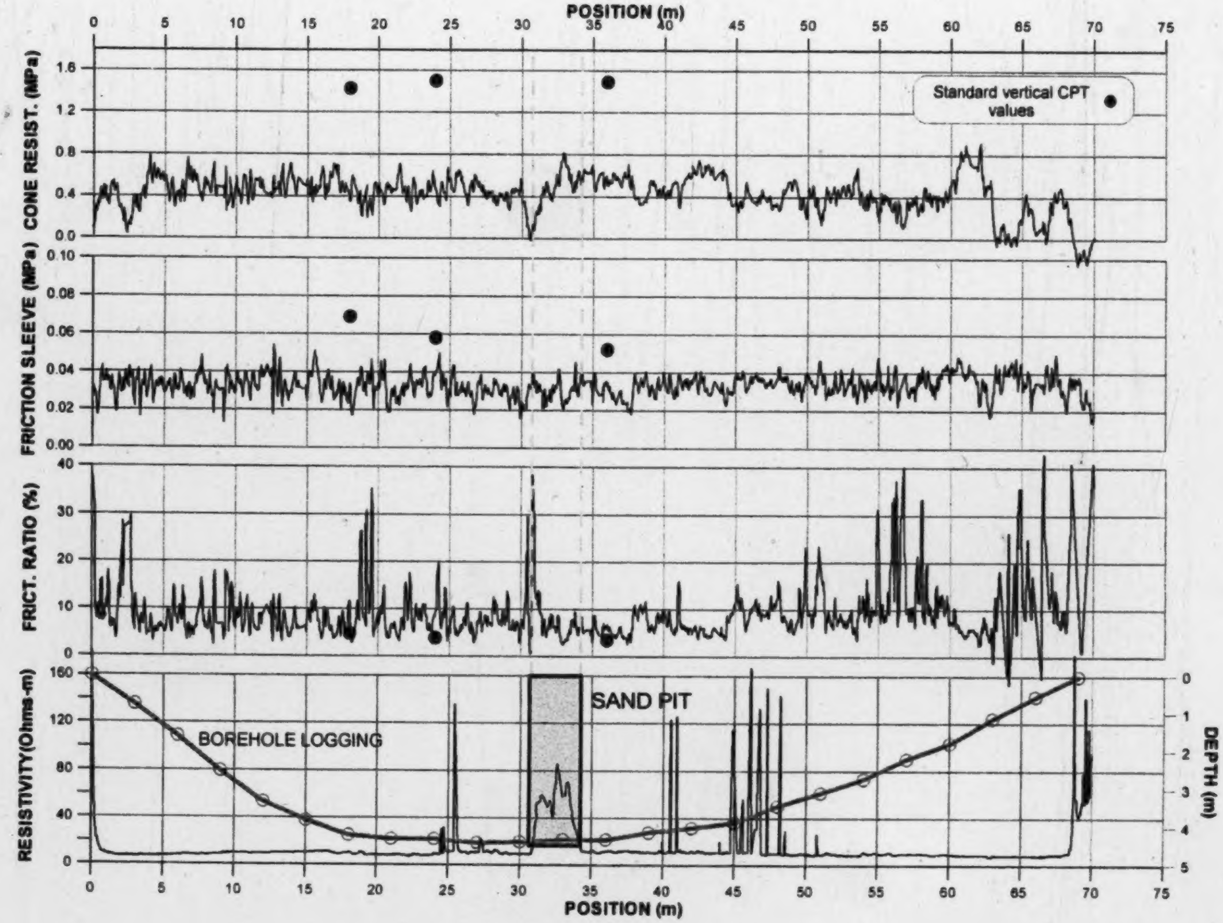

Figure 9.6 - HD-PB-RCPT Test 9 with the 30° apex angle cone.

## 9.3 SECOND SERIES OF HD-PB-RCPT TESTS (January, 2000)

When the prototype 2 probe was taken back into the geotechnical instrumentation laboratory, the DC adapter was replaced and the load cells were recalibrated. The new calibration plots (Figure 9.7) show that with the new DC adapter the load cell output results were stable and of good quality, similar to the previous calibration results (Figure 4.17).

After the probe was repaired a second series of tests were performed in January of 2000 in the same manner as the first series. Four tests were performed, two for each apex angle cone, and at depths of 2 and 4 meters. To utilize the existing sandpit and to avoid interception with the previous test paths, the second series of field tests were performed in a NE-SW and a SE-NW direction using the 60° and 30° cones respectively.

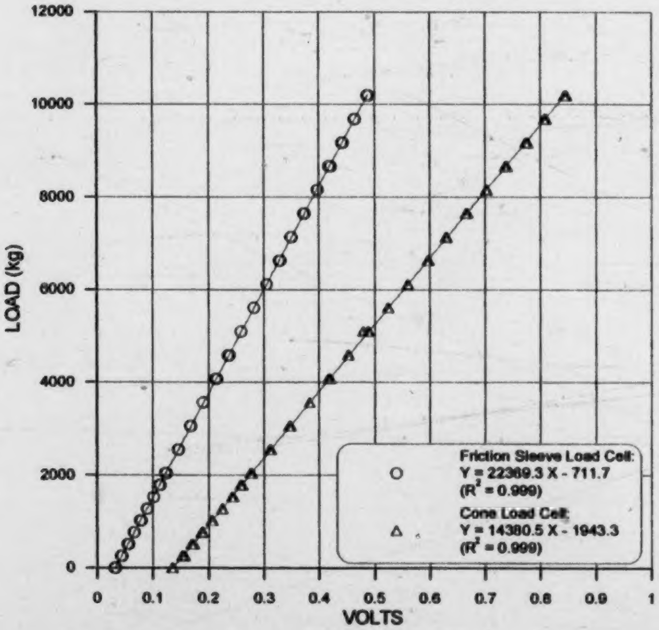

Figure 9.7 – Load cell calibration curves using the new DC adapter.

### 9.3.1 HD-PB-RCPT TESTS WITH THE 60$^0$ APEX ANGLE CONE

Figure 9.8 shows the results of HD-PB-RCPT Test 10 using the 60° cone at a depth of 2 meters. After the first 2 m of penetration, the connection between the probe and the drill stem broke. Since the depth of the probe was only 60 cm it was excavated re-connected and the test proceeded.

The cone resistance results followed the same trend as for prototype 1, with a more or less constant value as the probe passed through the clay and a significant decrease in cone resistance through the sand pit. Once the probe exited the sand pit the cone resistance increased again to the same level as before. The friction sleeve results still did not show a clear change in value as the probe passed through the sand pit. Nevertheless, the friction ratio presented a significant change in value in the sand pit location, as a reflection from the drop in cone resistance.

Electrical resistivity measurements continued to illustrate a clear picture of the sand pit location. However, within the sand pit the resistivity measurements were more erratic. This behavior may have been the result of soil disturbance generated during the previous tests. It is interesting to note the increase in bulk electrical resistivity from 2 to 5 meters (horizontal position); where a pit was opened to re-connect the HD-PB-RCPT to the drilling stem.

Figure 9.9 shows the normalized data from Test 10 and it follows a similar pattern as the non-normalized data shown in Figure 9.8, i.e., normalized cone resistance decrease as the probe reaches the sand pit and increases again when it exits. However, the change in normalized friction ratio within the sand pit was not as significant as seen in the non-normalized plot.

The results from Test 11 are presented in Figure 9.10 and the normalized results in Figure 9.11; this test was performed in the same way as Test 10 but at a depth of 4 meters. By looking only at cone and friction sleeve results (Figure 9.10) it was not possible to definitely locate the sand pit. A slight decrease in cone resistance can be noted at the beginning of the sand pit. If the position of the sand pit were not previously known, however, it would have been very difficult to have located its position using only the cone and friction sleeve results. However, the normalized cone resistance result rendered more uniform data as the probe went through the clay, making it easier to notice a slight contrast in reading at the sand pit location, as shown in Figure 9.11. The electrical resistivity result, on the other hand, shows a clear and precise location for the sand pit.

From the results of Test's 10 and 11 the constraint device did not appear to increase the cone and friction sleeve results. To better visualize the influence of the constraint device in improving cone and friction results, data from the tests performed with prototype 1 were plotted on the soil behavior type classification chart based on normalized data (Robertson 1990), shown in Figure 9.12. The data from prototype 2 (Tests 10 and 11) were then plotted on the same chart for comparison in Figure 9.13. To facilitate the interpretation of the results neither the curved end segments nor the sand pit section of the tests were plotted.

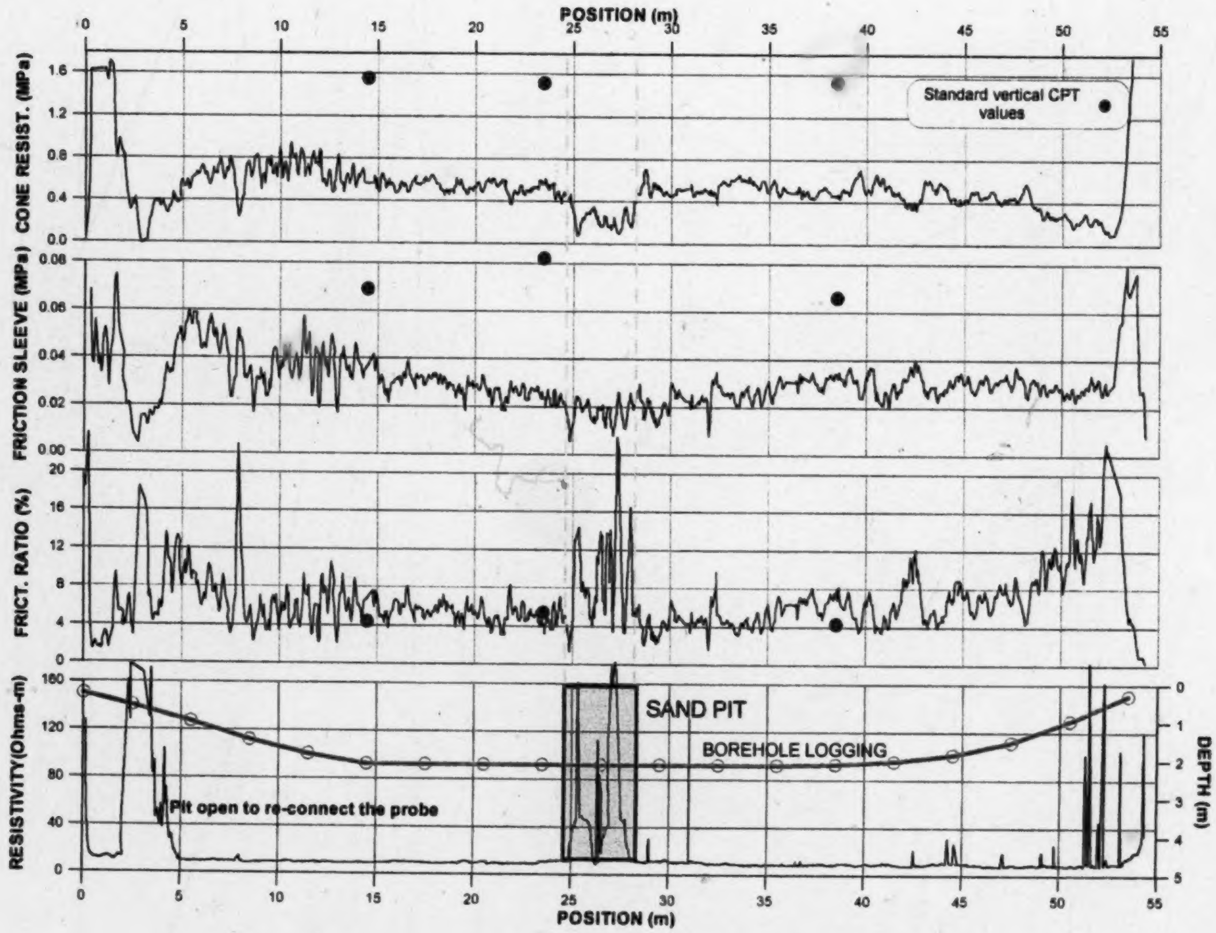

Figure 9.8 – HD-PB-RCPT Test 10, with 60° apex angle cone.

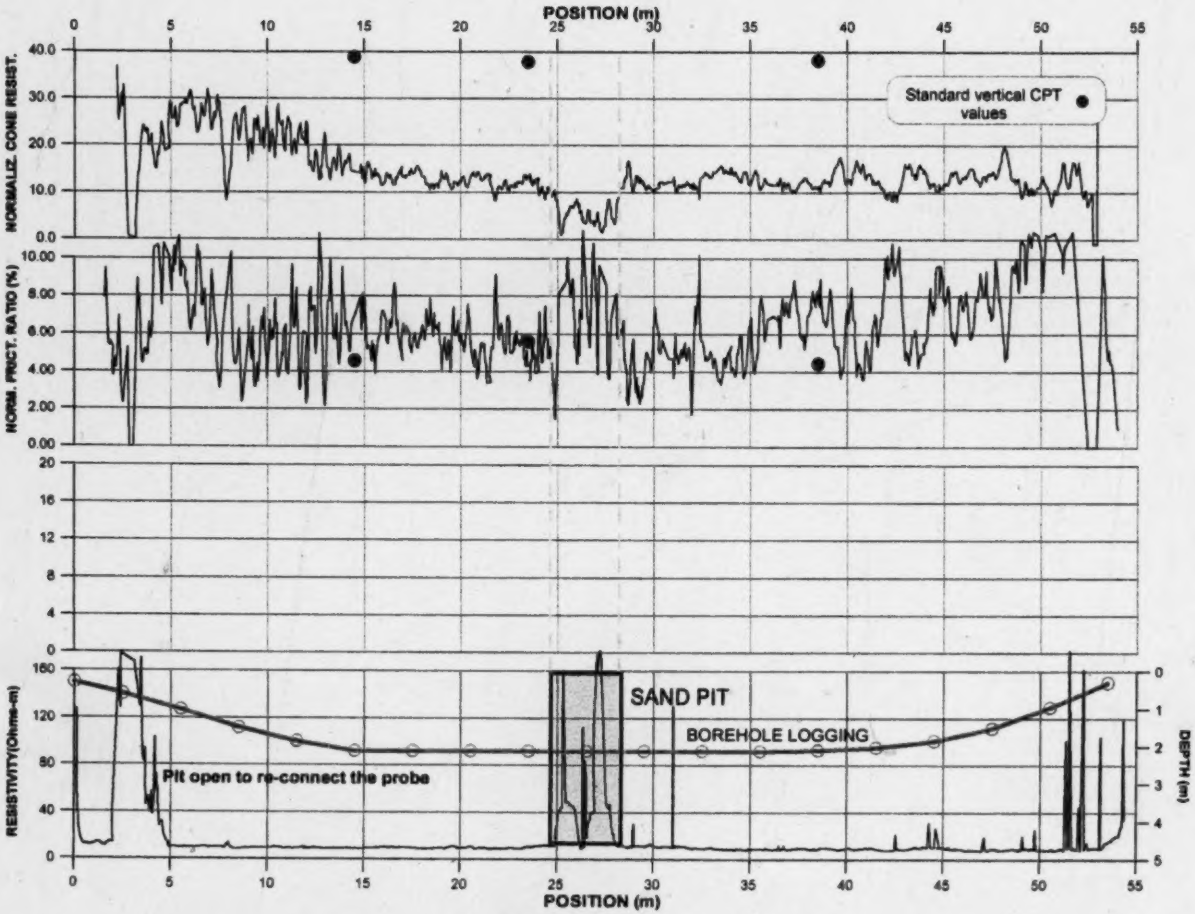

Figure 9.9 – HD-PB-RCPT Test 10, with 60° apex angle cone, normalized data.

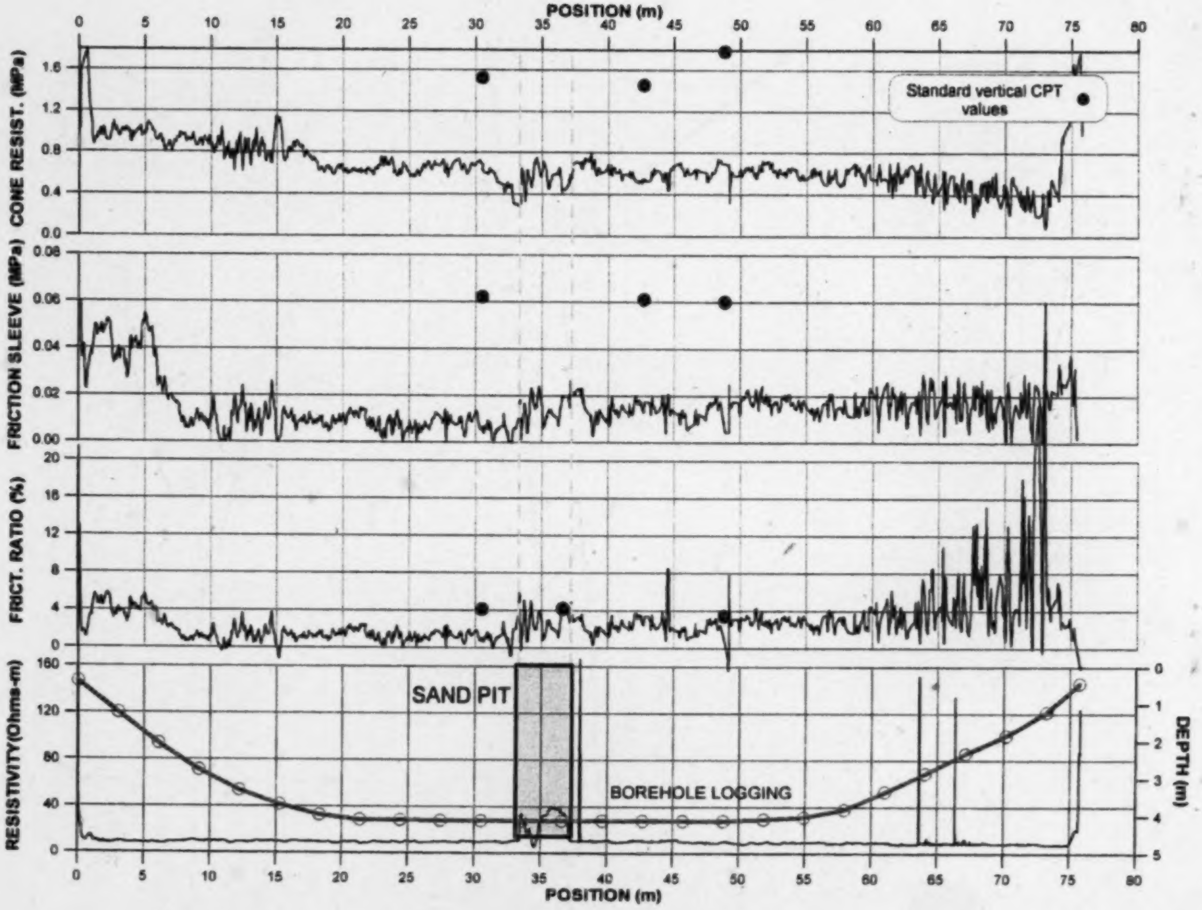

Figure 9.10 - HD-PB-RCPT Test 11, with 60º apex angle cone.

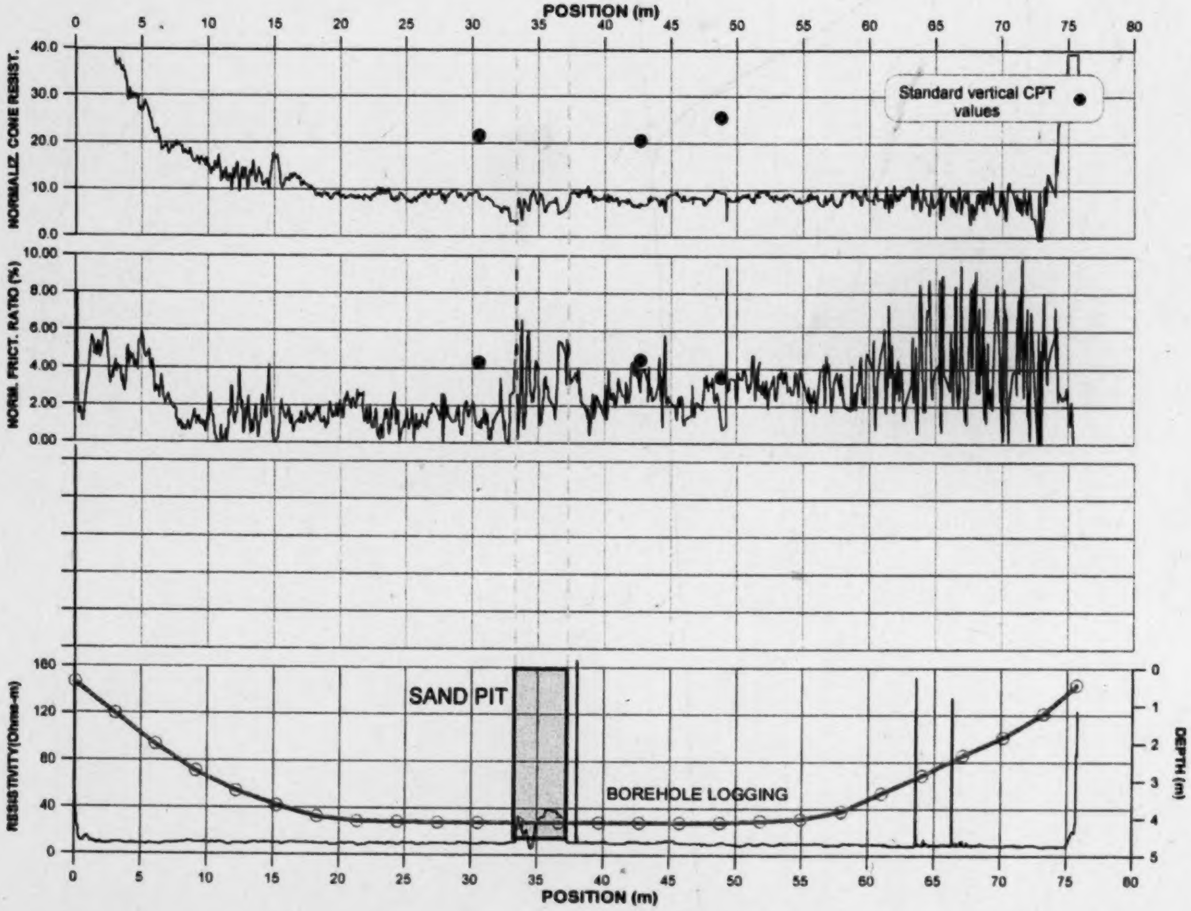

Figure 9.11 - HD-PB-RCPT Test 11, with 60° apex angle cone, normalized data.

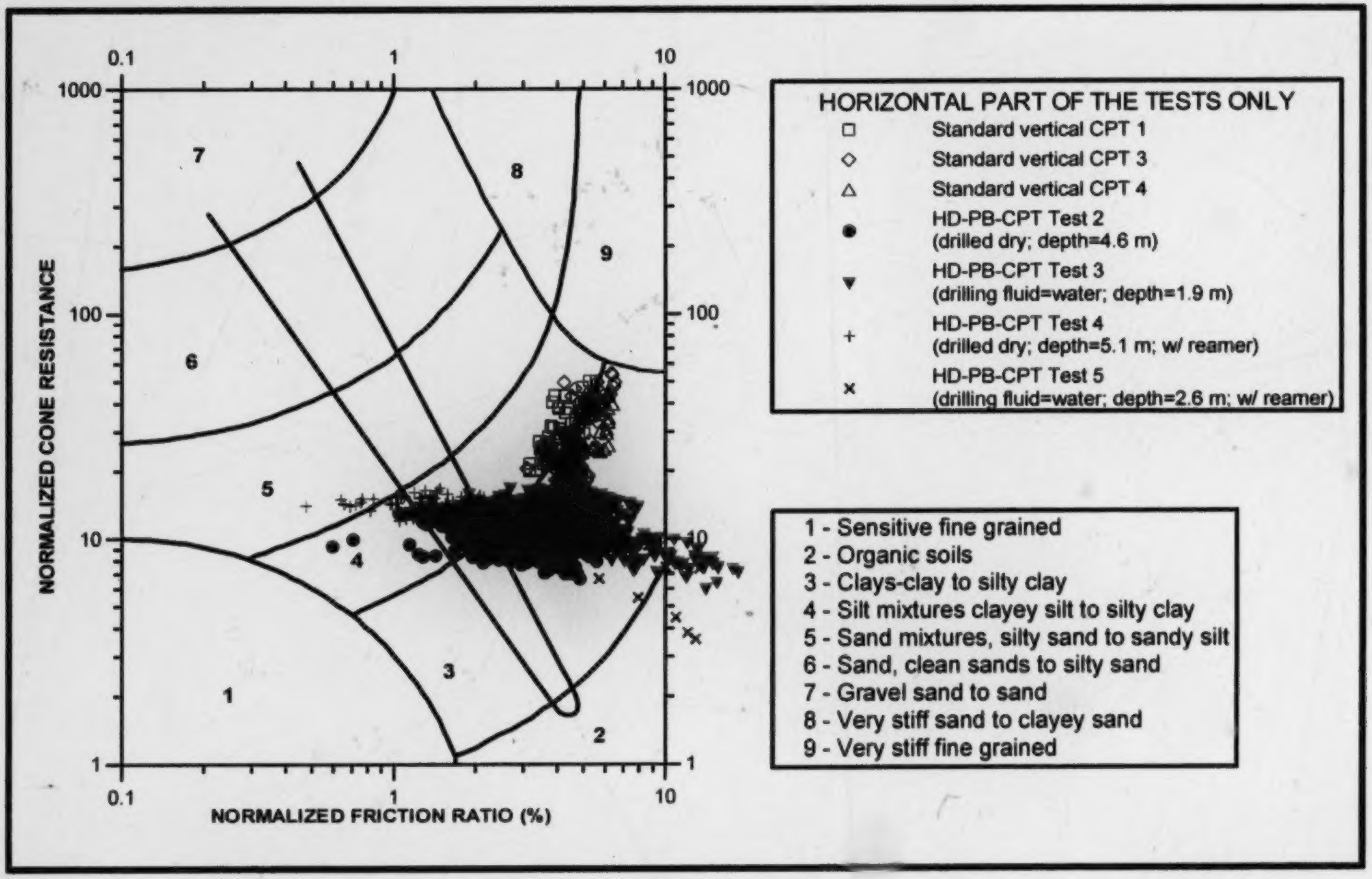

Figure 9.12 – Soil Behavior type classification chart, results from prototype 1 Tests, except Test 1 (modified from Robertson, 1990).

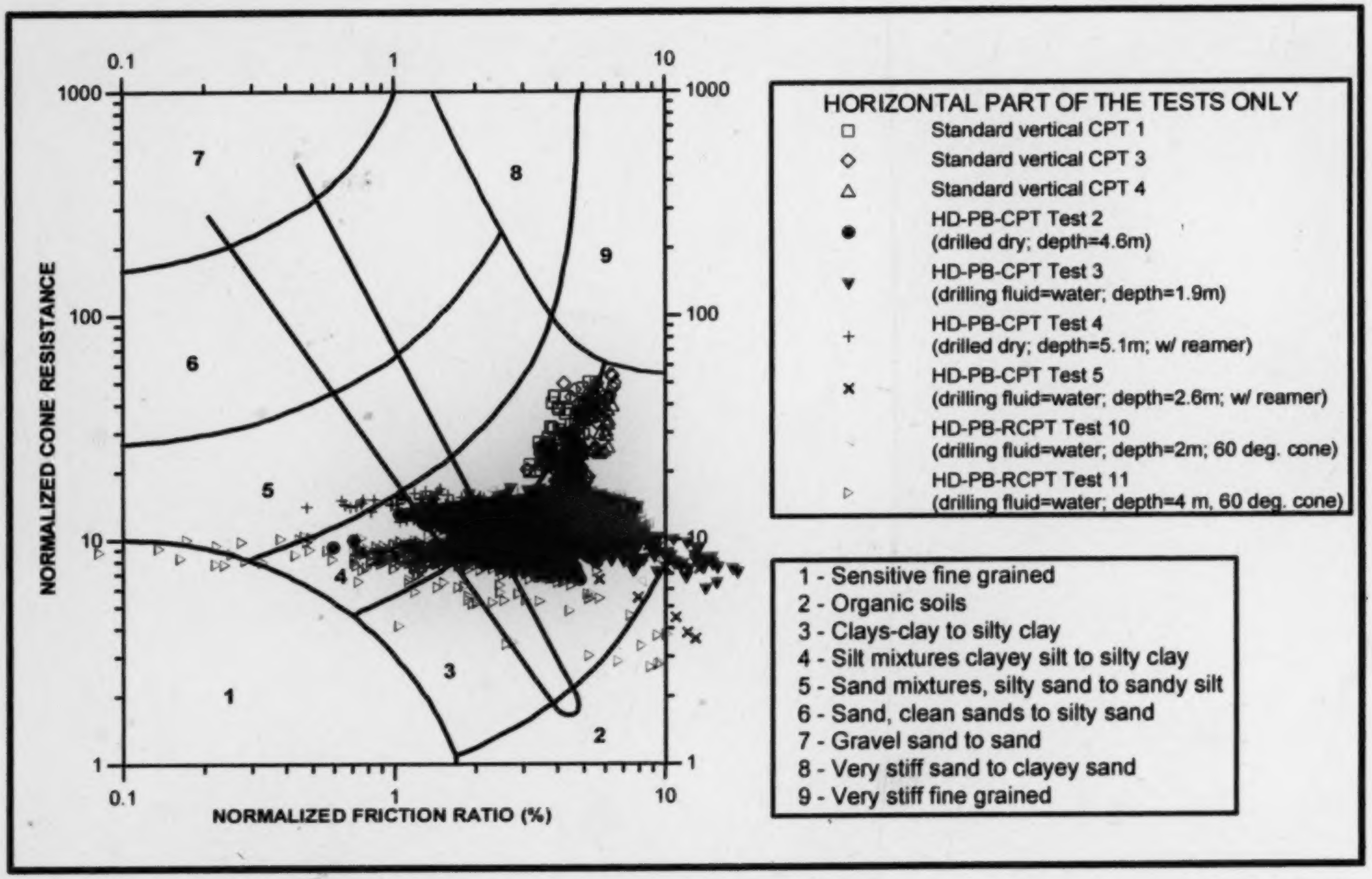

Figure 9.13 - Soil Behavior type classification chart, results from prototype 1 Tests, except Test 1 and prototype 2 Tests 10 and 11(modified from Robertson, 1990).

The normalized results shown in Figure 9.13 show that Test 10 data essentially overlap Test 3 (prototype 1) data, which are those that had the highest normalized cone and friction ratio results compared to all previous tests. Test 3 data have shown a reasonable match with the standard vertical CPT data, though this data is concentrated mainly on the lower boundary of the standard vertical CPTs swarm. Test 3 data also had a significant amount of unusually high normalized friction ratio that caused some data to be plotted off the chart, something that did not happen in Test 10.

At first glance the constraint device appears to have improved the test results, at least to some degree. But the results from Test 11 show no improvement in the data and in fact show an increase in scatter. These results were evidence that the constraint device did not work as expected.

### 9.3.2 HD-PB-RCPT TESTS WITH THE 30° APEX ANGLE CONE

The HD-PB-RCPT tests using the 30° apex angle cone were performed in a SE-NW direction. Like the other tests in this series the pilot hole was drilled using an 8.89 cm (3.5") drilling bit with only water used as a drilling fluid. Two tests were performed with the 30° cone, Test 12, at a depth of 4 meters and Test 13, at a depth of 2 meters.

During the execution of Test 12 two significant incidents occurred. The first occurred during the drilling of the pilot hole. The drilling company was unfortunately accustomed to working with Imperial units, while the information regarding the pilot hole depth and length had been given to them in metric units. The track system operator, however, decided to work in metric instead of the imperial units he was comfortable with. After boring the first 10 meters, the operator, instead of pushing the imperial to metric conversion button on the track system device, pushed the calibration button by mistake, causing the whole system to lose its calibration. The drill stem had to be retrieved to the surface and the track system device recalibrated. The drilling stem was then pushed back to about 10 meters, through the already existing borehole, and only at that point was the drilling restarted. It is worth mentioning that the first 10 meters of drilling is equivalent to the last 10 meters of HD-PB-RCPT testing.

The second incident occurred during the actual HD-PB-RCPT test phase. The usual standard HDD operation procedure is to enlarge the pilot hole through a process of back-reaming, which is always made by rotating the reamer while pulling it back. The rig operator was used to rotating the drilling assembly while pulling it back. After changing the fourth rod at a test position of 12 meters and about to restart pulling the HD-PB-RCPT probe, the rig operator mistakenly started rotating the rods. This rotation process, however, broke the connection between probe and drilling stem. A three meter deep pit then had to be opened in order to reestablish the connection.

The results and the normalized data results of Test 12 are presented in Figure 9.14 and Figure 9.15, respectively. There are data missing from the penetration position of 12 to 19 meters due to the pit having been opened in order to reestablish a probe connection. A significant drop in cone resistance can be seen at the penetration position of 60 meters, which is the same point where the tracking system device lost its calibration. When the rods were again pushed through the existing borehole after recalibration, an oversized hole was likely created. This oversizing caused a drop in cone resistance because of the smaller soil contact area. It is worth noting here the existence of negative cone resistance values, which show that the load cell's electrical system was not as stable as was expected.

By observing both non-normalized and normalized results of cone and friction resistance from Test 12 it was not possible to identify the location of the sand pit. The results also show that the sharper cone did not improve the data as expected.

For the first time the electrical resistivity data were extremely variable. The data show consistently high spikes in resistivity all along the test path. It is interesting to note, though, that the lower boundaries of the spikes are extremely consistent and never drop below 8-10 ohm·m This value of soil bulk resistivity is the same value obtained for the clay from the other HD-PB-RCPT tests. As the probe reached the sand, the lower spike boundaries increase to a level of around 40 ohm·m, which is the same resistivity level registered for the sand from the previous tests. By connecting the points from the lower spike boundaries a result similar to that of previous tests is obtained, shown by the shaded area in Figure 9.14. It looks as though electrical noise of some kind was affecting the reading. Unfortunately it was not possible to identify the source of this noise in the field.

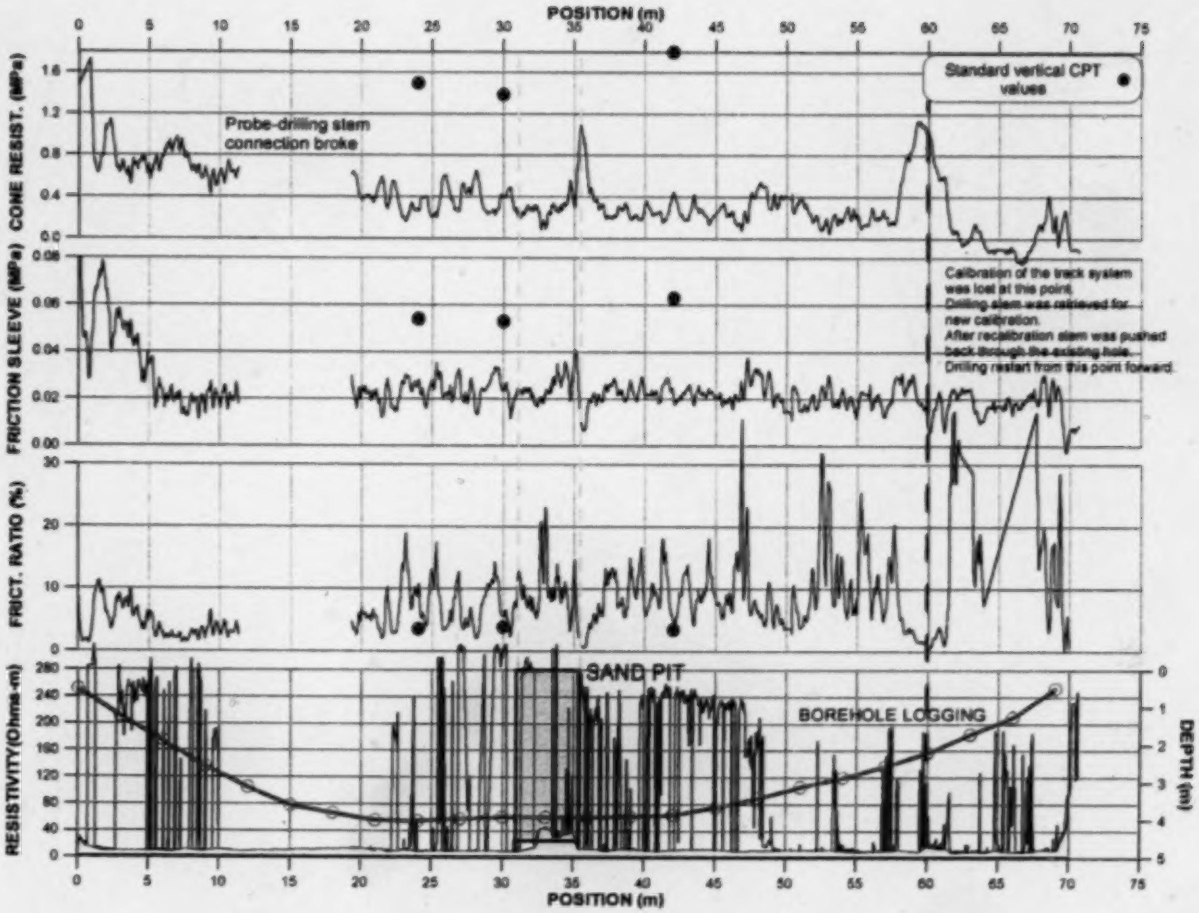

Figure 9.14 - HD-PB-RCPT Test 12, with 30° apex angle cone.

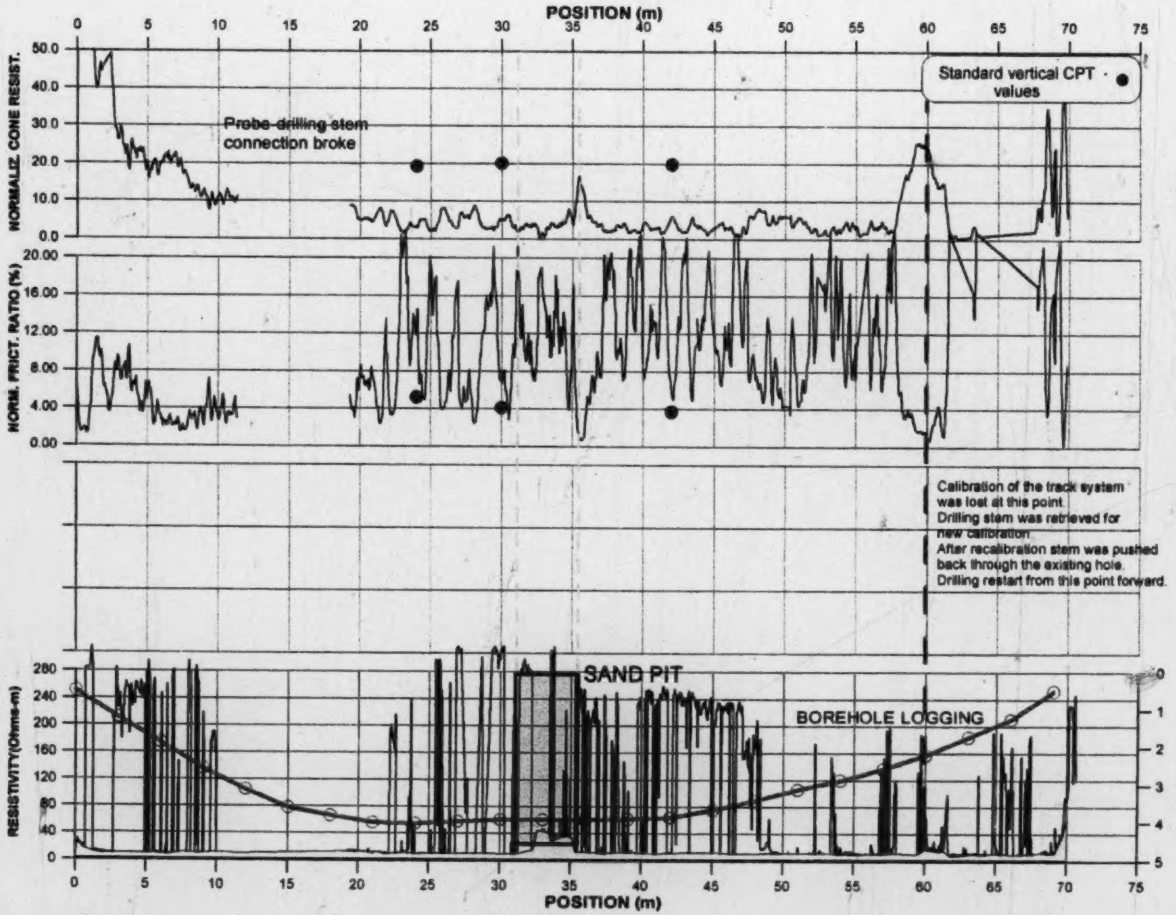

Figure 9.15 - HD-PB-RCPT Test 12, with 30° apex angle cone, normalized data.

Test 13, the second test of this series and the last HD-PB-RCPT field test, was performed to a depth of 2 meters. The pit opened to reconnect the probe during Test 12 was at the same alignment as Test 13, which means the test commenced at a depth of 2 m, as shown in Figure 9.16 (a) through (d). There is no curved section at the beginning of this test, since it already starts at the desired depth of 2 m. The HD-PB-RCPT was placed at the bottom of the pit where it was connected to the drilling stem (Figure 9.16a). Test 13 results are shown in Figure 9.17 and normalized results are shown in Figure 9.18.

A slight drop in cone resistance was noted at the position of the sand pit as well as a drop in friction sleeve resistance. Some friction sleeve data also showed a negative value. At low load levels the electrical instability of the load cells increases. Because the friction load cell is of the subtractive type, it is difficult to obtain a perfect match between the cone resistance measured by the cone load cell and by the friction load cell. Therefore, when low friction sleeve values are measured, some negative values may result from the subtraction operation.

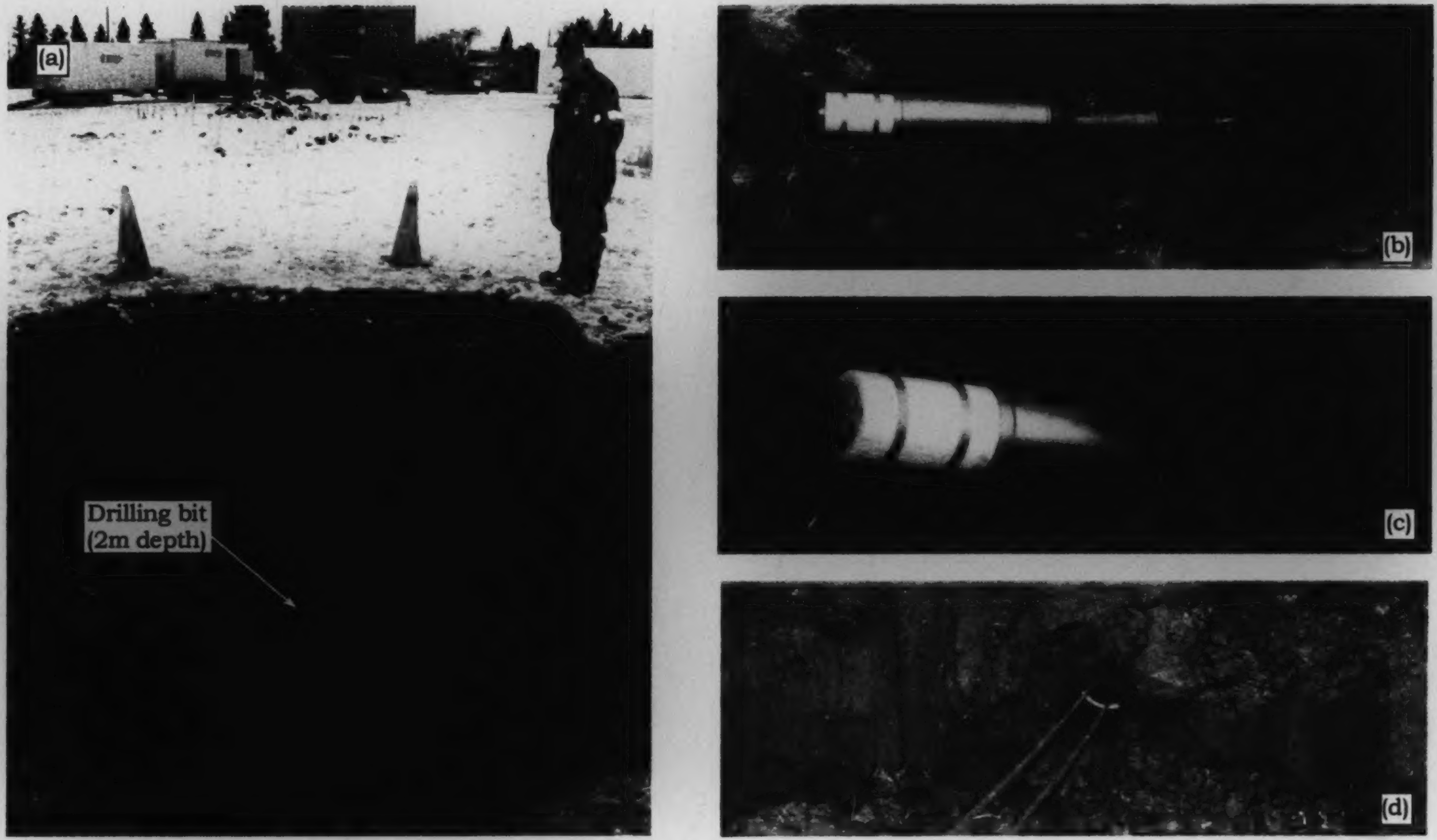
(a)
Drilling bit
(2m depth)
(b)
(c)
(d)

Figure 9.16 – (a) arrival of the drilling bit; (b) connection of the probe; (c) penetration and (d) probe completely inside the soil.

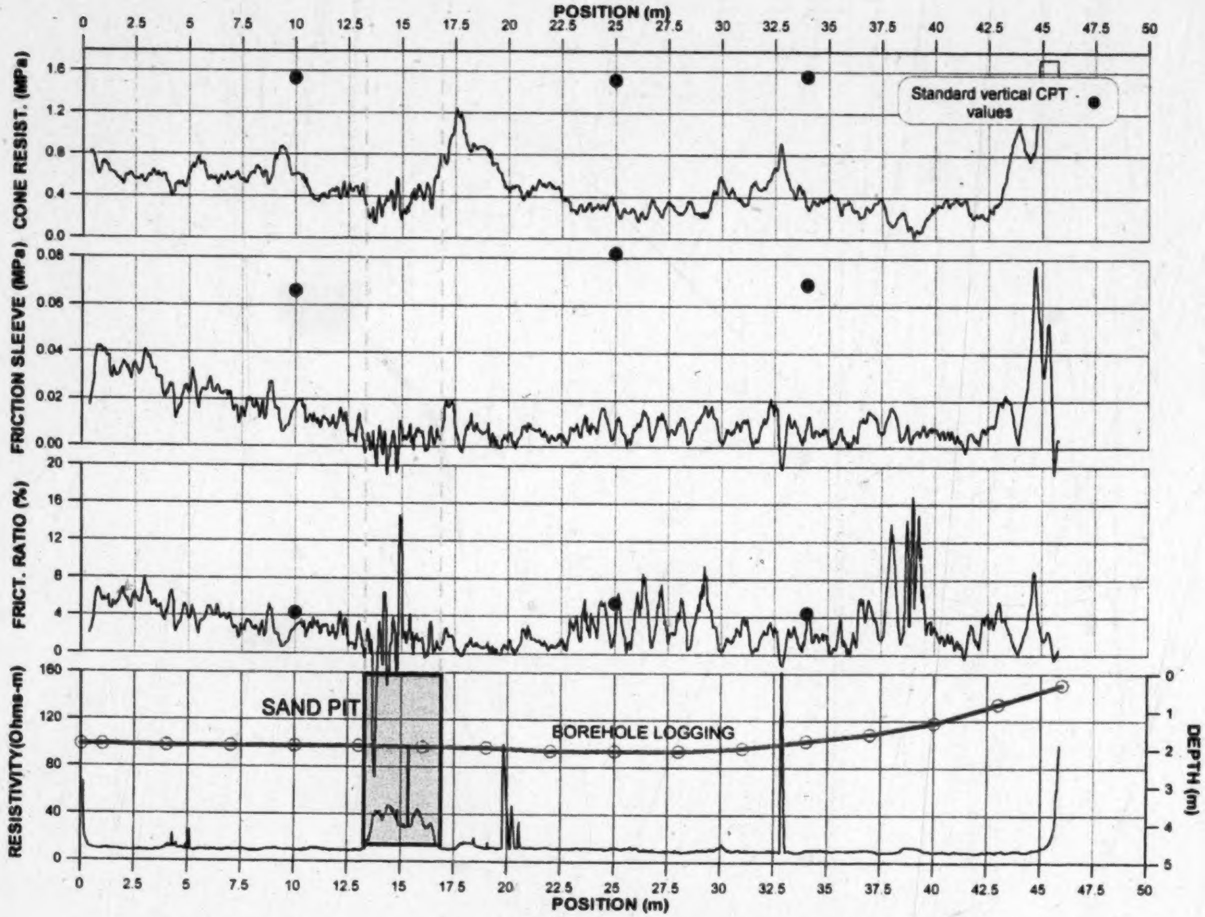

Figure 9.17 - HD-PB-RCPT Test 13, with 30° apex angle cone.

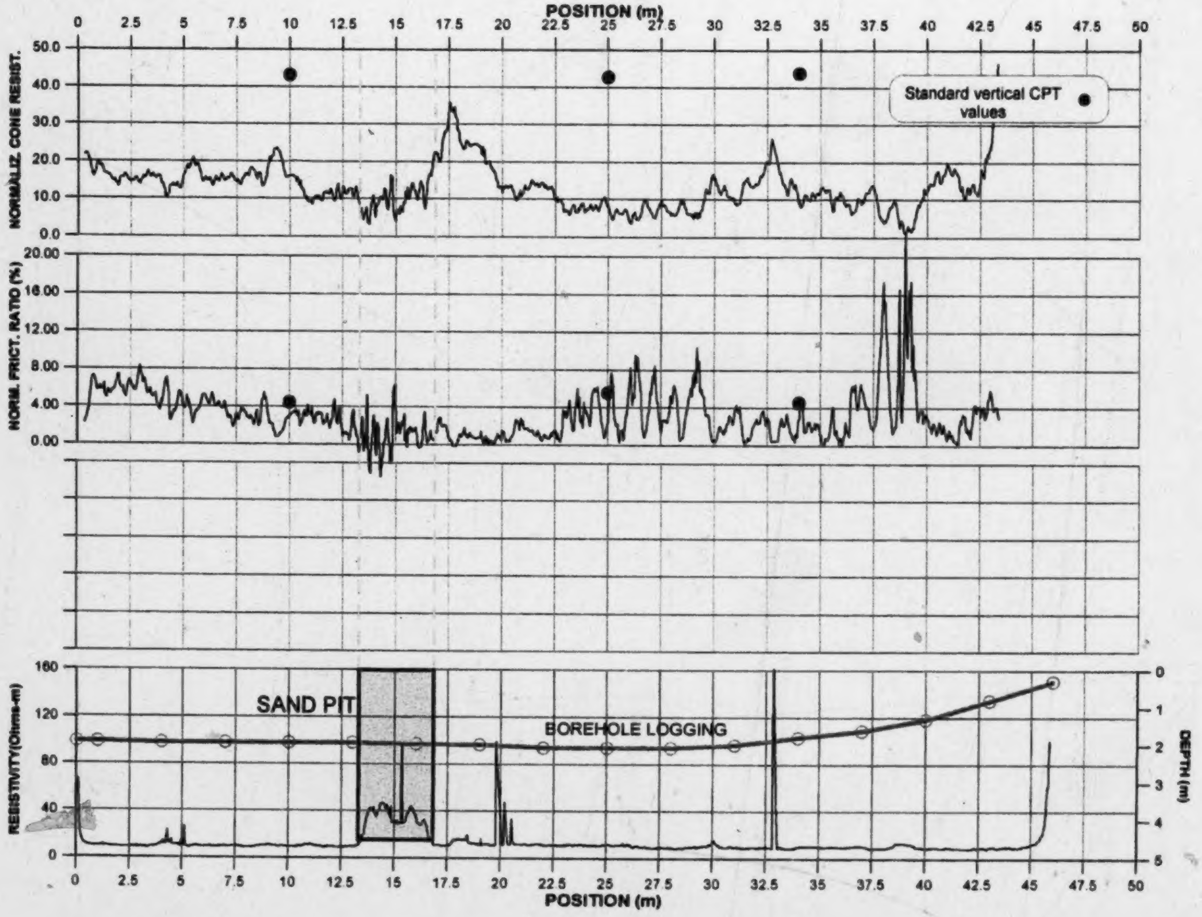

Figure 9.18 - HD-PB-RCPT Test 13, with 30° apex angle cone, normalized data.

Contrary to Test 12, the electrical resistivity results from Test 13 (Figure 9.17) were once again very clear, leaving no doubt about the sand pit location. Like previous tests some distinctive spikes in electrical resistivity can be seen along the test path; here they appear at test positions of 5, 20 and 33 meters.

## 9.4 COMPLEMENTARY DATA ANALYSIS

### 9.4.1 AVERAGE VALUES AND STANDARD DEVIATION

The results from Tests 12 and 13, Figure 9.14 and Figure 9.17 respectively, show that the sharper cone did not increase cone or friction resistance. To better compare the performance of prototype 2, Table 9.1 shows the average and the standard deviation values of normalized cone and friction sleeve resistance obtained from all HD-PB-CPT and HD-PB-RCPT tests. The data from the curved parts of the tests as well as from the sand pit sections were disregarded. For comparison, the average and standard deviation results from the standard vertical CPT tests performed by Conetec are also included in the table.

Table 9.1 – Data comparison between the HD-PB-CPT and HD-PB-RCPT tests. Only the horizontal sections of the tests were considered. The sand pit section was not included.

| **Tests** | | **Remarks** | ***$NQ_t$*** | | ***$NF_s$ (%)*** | |
|---|---|---|---|---|---|---|
| | | | **Average** | **Std. dev.** | **Average** | **Std. dev.** |
| **SOIL ZONE BETWEEN 1.5 AND 2.5 METERS DEPTH** | | | | | | |
| **Std vertical CPT** | Conetec 1 | Considered depth – 1.5 to 2.5 m | 40.8 | 4.6 | 4.7 | 0.5 |
| | Conetec 3 | Considered depth – 1.5 to 2.5 m | 43.5 | 5.6 | 5.6 | 0.6 |
| | Conetec 4 | Considered depth – 1.5 to 2.5 m | 39.4 | 3.3 | 5.7 | 0.4 |
| | Conetec 6 | Considered depth – 1.5 to 2.5 m | 40.8 | 5.6 | 5.9 | 1.0 |
| **HD-PB-CPT** | Test 3 | Drilled using water | 12.6 | 2.5 | 5.4 | 2.7 |
| | Test 5 | Drilled using water. Reamer was used in this test | 11.5 | 1.6 | 4.7 | 1.3 |
| **HD-PB-RCPT** | Test 10 | Drilled using water, 60 deg. cone | 12.6 | 1.7 | 5.7 | 1.4 |
| | Test 13 | Drilled using water, 30 deg. cone | 14.0 | 5.8 | 3.2 | 2.0 |
| **SOIL ZONE BETWEEN 4 AND 5 METERS DEPTH** | | | | | | |
| **Std vertical CPT** | Conetec 1 | Considered depth – 4 to 5 m | 23.4 | 2.1 | 3.8 | 0.5 |
| | Conetec 3 | Considered depth – 4 to 5 m | 20.1 | 2.4 | 4.5 | 0.6 |
| | Conetec 4 | Considered depth – 4 to 5 m | 21.7 | 1.0 | 4.3 | 0.3 |
| **HD-PB-CPT** | Test 2 | Drilled dry | 10.0 | 1.4 | 2.7 | 0.84 |
| | Test 4 | Drilled dry. Reamer was used in this test. | 13.0 | 1.2 | 1.9 | 0.6 |
| **HD-PB-RCPT** | Test 11 | Drilled using water, 60 deg. cone | 8.2 | 1.2 | 2.4 | 1.3 |
| | Test 12 | Drilled using water, 30 deg. cone | 4.3 | 2.3 | 10.6 | 5.5 |

***$NQ_t$*** = Normalized cone resistance and ***$NF_s$*** = Normalized friction ratio.

The normalized standard CPT cone resistance profiles presented in Figures 5.8 show that at the depths where the pre-bored tests were performed, the normalized cone resistance value for the upper 2.3 m depth is approximately 41 and decreases to approximately 22 below the 3.5 m depth and becomes reasonably constant thereafter. This is an indication of two different soil behavior type zones, which coincide with the zones where the shallower and the deeper prototype tests were performed. Therefore, to better compare the results, the normalized average and standard deviations presented in Table 9.1 are divided in these two distinguished zones, i.e., from 1.5 to 2.5 m and from 4 to 5 m; which are the two soil regions where the horizontal pre-bored tests were performed during this study.

The data in Table 9.1 show that in the upper soil zone, normalized cone resistances *($NQ_t$)* for the standard CPT were approximately 3 times higher than the pre-bored test results, and about 2.4 times higher in the lower soil zone. The highest $NQ_t$ value for the pre-bored tests was from Test 13 (HD-PB-RCPT with the 30° cone); however, this test also had the highest standard deviation. This result suggests that the constraint device and the sharper cone did improve the cone resistance results. The data from the second HD-PB-RCPT with the 30° cone, on the other hand, rendered the lowest $NQ_t$ value from all the pre-bored tests. It is well known from the work of Bishop et al. (1945) and Vesic (1972) that the limit pressure obtained from spherical cavity expansion theory is higher than the one obtained from cylindrical cavity expansion. It was expected was that the sharper cone would push the soil more sideways instead of forward improving the borehole expansion, consequently increasing cone resistance. It was expected that the improvement in the borehole expansion would outweigh the reduction in cone bearing promoted by the use of a sharper cone that would bring the soil deformation pattern more closely to the expansion of a cylindrical cavity rather that a spherical cavity. However, this tradeoff seems not to have occurred or at least it is not as evident as it was expected to be. Furthermore, two sets of test cannot be considered sufficient for a final conclusion of the effectiveness of a sharper cone in improving the HD-PB-RCPT data.

The $NQ_t$ and standard deviation values from Tests 10 and 11 (60° cone with the constraint device) are approximately the same as the Tests performed without the constraint device. This suggests that the constraint device did not work as expected. However, like the tests on the sharper cone, more tests would have to be performed before a final conclusion could be drawn.

Table 9.1 shows that a better match between vertical CPT and HD-PB-CPT was obtained for the normalized friction ratio ($NF_s$). This was, however, due to the lower value of both, cone and friction resistance from the pre-bored tests, which causes friction ratio to be more or less the same as the standard vertical cone.

Table 9.2 shows the average values for cone and friction resistance as well as the average force acting on the cone load cell and on the friction sleeve load cell during each Test. The load cell type used in prototype 1 and 2 were of the subtractive kind; therefore, the friction sleeve load cell forces shown in Table 9.2 is the sum of both, the cone and the friction sleeve forces. However, the value of friction sleeve resistance ($f_s$) shown in Table 9.2 was calculated based on the force acting exclusively on the friction sleeve, i.e., the force obtained by subtracting the force acting on the cone load cell from the force acting on the friction sleeve load cell.

The force values shown in Table 9.2 are all less than 16 % of the load cell capacity of 100 kN, designed to withstand high pulling forces to pull the probe through deposits of dense sand. However, the soil deposits where the probes were tested were firm to stiff clay, hence the load cells were being loaded only at the lower end of their capacity where they are less accurate. This may have promoted a significant contribution to the scatter and inconsistency of the data results, especially for the HD-PB-RCPT, which load cells were less stable (Figure 9.7) than the load cells used in the HD-PB-CPT (Figure 4.17). From the available load calibration data from the HD-PB-RCPT it was possible to estimate a resolution of –4% to +7% for the load range between 5.00 to 7.50 kN and above 15.00 kN load the load cell resolution was approximately ± 1%. Ideally, two sets of load cells should have been built, one for low strength and one for high strength, like often is the case in a standard CPT test when testing very soft deposits. However, time and budged constraints did not allow for the construction of two sets of load cells.

Table 9.2 – Average cone and friction sleeve resistance and average force acting on the cone load cell and on the friction sleeve load cell.

| Tests | | Remarks | Average | | Average | |
|---|---|---|---|---|---|---|
| | | | $q_c$ (MPa) | Load cell force | $f_s$ (MPa) | Load cell force (kN) |
| **SOIL ZONE BETWEEN 1.5 AND 2.5 METERS** | | | | | | |
| **HD-FB-CPT** | Test 3 | Drilled using water | 0.4572 | 4.633 kN<br>(472 kg) | 0.0201 | 10.118 kN<br>(1031 kg) |
| | Test 5 | Drilled using water. Reamer was used in this test | 0.6357 | 6.442 kN<br>(657 kg) | 0.0264 | 13.647 kN<br>(1391 kg) |
| **HD-FB-RCPT** | Test 10 | Drilled using water, 60 deg. cone | 0.5301 | 5.372 kN<br>(548 kg) | 0.0273 | 12.822 kN<br>(1307 kg) |
| | Test 13 | Drilled using water, 30 deg. cone | 0.5271 | 5.342 kN<br>(546 kg) | 0.0143 | 9.244 kN<br>(942 kg) |
| **SOIL ZONE BETWEEN 4 AND 5 METERS** | | | | | | |
| **HD-FB-CPT** | Test 2 | Drilled dry | 0.7755 | 7.859 kN<br>(801 kg) | 0.0182 | 12.826 kN<br>(1307 kg) |
| | Test 4 | Drilled dry. Reamer was used in this test. | 1.0655 | 10.798 kN<br>(1101 kg) | 0.0180 | 15.710 kN<br>(1601 kg) |
| **HD-FB-RCPT** | Test 11 | Drilled using water, 60 deg. cone | 0.6163 | 6.246 kN<br>(637 kg) | 0.0122 | 9.575 kN<br>(976 kg) |
| | Test 12 | Drilled using water, 30 deg. cone | 0.3558 | 3.606 kN<br>(368 kg) | 0.0230 | 9.883 kN<br>(1007 kg) |

### 9.4.2 STANDARD CONE AND PRE-BORED CONE RESISTANCE RELATIONSHIP

Cavity expansion theory approach is often used in theoretical analysis of cone penetration (Yu and Michell 1998). Spherical cavity expansion theory is normally used to obtain an analytical solution for cone penetration test (Lunne et al. 1997) and cylindrical cavity expansion approach is used in the interpretation of pressuremeter tests (Baguelin et al. 1978). Due to the geometry of a pre-bored cone penetration test it is expected that the cone resistance will be somewhat between the limit pressure of a spherical and a cylindrical cavity expansion. Vesic (1972) presented the following Equations 9.1 and 9.2 as the general solution for the problem of a spherical and a cylindrical cavity expansion, respectively, in an ideal soil with friction angle equal to zero.

$$p_{l_s} = \frac{4}{3} S_u \left[ ln \frac{E}{2(1+v)S_u} + 1 \right] + p_0 \qquad [9.1]$$

$$p_{l_c} = S_u \left[ ln \frac{E}{2(1+v)S_u} + 1 \right] + p_0 \qquad [9.2]$$

where:

$p_{l_s}$ and $p_{l_c}$ = spherical and a cylindrical cavity expansion limit pressures respectively;

$S_u$ = undrained shear strength;

$E$ = Young's modulus;

$v$ = Poisson's ratio

$p_o$ = effective overburden stress

Therefore, the spherical and cylindrical cavity expansion ratio for shallow depth can be expressed approximately by Equation 9.3:

$$\frac{p_{l_s}}{p_{l_c}} = \frac{4}{3} \text{ or } p_{l_s} = 1.33 p_{l_c} \qquad [9.3]$$

Increasing the average normalized cone resistance (Table 9.1) by 33%, as indicated by Equation 9.3, render results closer but still lower than the results obtained by the standard vertical CPT. Furthermore, the pre-bored test cannot be assumed to be a perfect cylindrical cavity expansion; therefore, it is expected that the correction factor would be somewhat smaller than 1.33.

Another relationship that can be considered was established by Van Wieringen (1982) between cone resistance and limit pressure ($p_l$) from pressuremeter tests. Van Wieringen (1982) assumed the failure mechanism shown in Figure 9.19. According to Van Wieringen (1982) a kinematic mechanism of deformation is admissible if the internal rate of dissipation of energy is equal to the rate at which external forces create work, i.e., the failure mechanism is kinematically admissible if all velocity boundary conditions are satisfied.

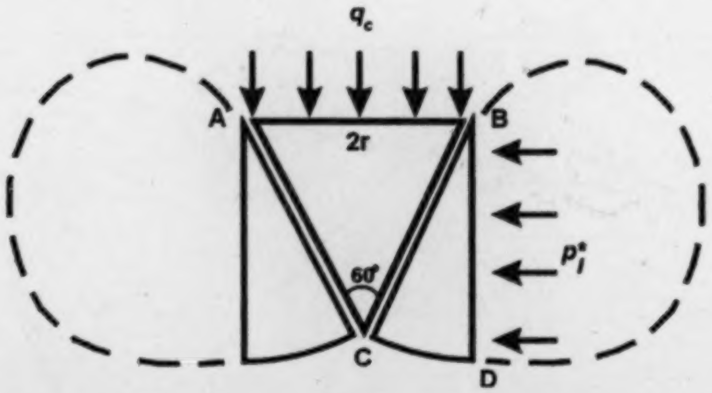

Figure 9.19 – Model of cone penetration into a perfectly plastic medium (modified from Van Wieringen 1982).

The external pushing force acting in the area AB gives the virtual velocity $V_1$. The shear force acting in the conical surface BC has a velocity $V_2$. Velocity $V_1$ equals the vertical component of $V_2$. Along the slip surface CD there is another shear force at velocity $V_3$; this tangential velocity $V_3$ is perpendicular to BC and BD. On the cylindrical surface BD acts a resisting force moving at a velocity $V_4$. The balance of rate of energy is given by Equation 9.4.

$$q_c \pi r^2 V_1 = S_u 2\pi r^2 V_2 + S_u \pi r^2 \frac{\pi}{3} V_3 + p_l^* 4\pi r^2 V_4 \qquad [9.4]$$

where:

$r$ = cone radius

$p_l^*$ = corrected limit pressure (described below)

The failure mechanism developed by cone penetration is assumed to be somewhere between a cylindrical and a spherical cavity expansion. A material shape factor is therefore introduced to correct the pressuremeter limit pressure $p_l$, as shown by Equation 9.5:

$$p_l^* = s p_l \qquad [9.5]$$

where:

$s$ = shape factor (for cohesive soil, $s = 1.25$)

As noted by Van Wieringen (1982), several correlation studies in The Netherlands have shown that Equation 9.6 represents a good approximation between undrained shear strength and cone resistance, at shallow depth.

$$q_c = 15\, S_u \qquad [9.6]$$

Finally, the relationship shown in Equation 9.7, between cone resistance and pressuremeter limit pressure can be found by combining Equations, 9.4, 9.5 and 9.6.

$$q_c = 3\,p_l \qquad [9.7]$$

Figure 9.20 shows the ratio of cone resistance and pressuremeter limit pressure distribution for 170 measurements on clay (Van Wieringen 1982). From this graph it can be seen that the ratio of 3 from Equation 9.7 fits the data results well.

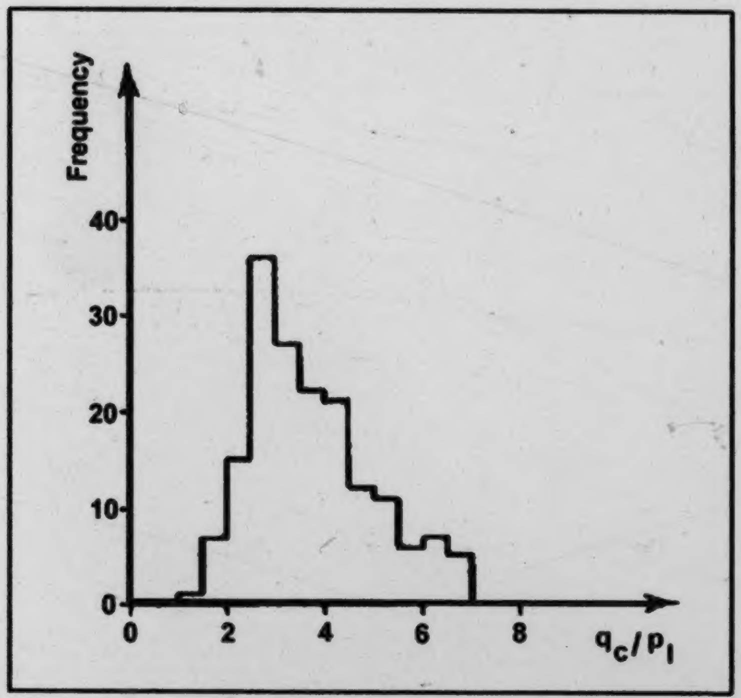

Figure 9.20 – Frequency distribution of cone resistance/limit pressure ratio from 170 measurements on clay (modified from Van Wieringen 1982).

Following the same methodology as Van Wieringe (1982) a possible lower bound solution may be obtained by assuming the failure mechanism shown in Figure 9.21, the balance of rate of energy for probe/borehole diameter ratio of 1.5 is given by Equation 9.8 (see Appendix 5 for derivation).

$$q_{c_{PB}} \pi r^2 V_1 = S_u \frac{10}{9} \pi r^2 V_2 + S_u \frac{5}{9} \pi r^2 \frac{\pi}{3} V_3 + p_l^* \frac{4}{3} \pi r^2 V_4 \qquad [9.8]$$

where:

$q_{c_{PB}}$ = cone resistance from a pre-bored penetration test.

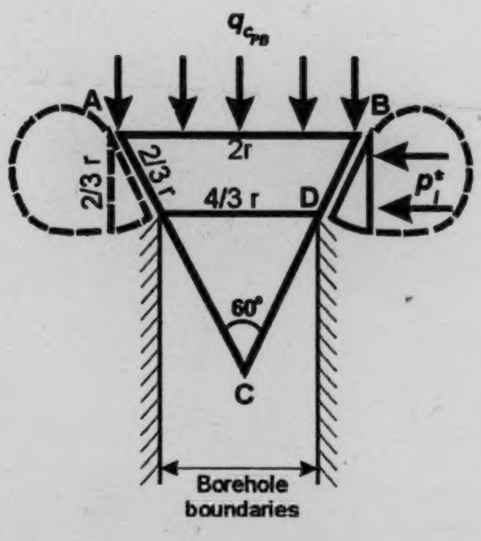

Figure 9.21 – Model of a pre-bored cone penetration into a perfectly plastic medium

The undrained shear strength for Lake Edmonton clay at the depth of the tests is shown to be approximately 100 kPa in Figure 4.8. The average pre-bored cone resistance for the clay obtained from the HD-PB-CPT and HD-PB-RCPT tests with the 60° apex angle cone, was

0.68 MPa. Using Equation 9.6, a cone factor of 7 is obtained, thus for pre-bored test Equation 9.9 is obtained.

$$q_c = 7\, S_u \qquad [9.9]$$

Assuming also that the pre-bored test is closer to a cylindrical than a spherical cavity expansion the shape factor *s* from Equation 9.5 can be assumed to be 1.3 as shown in Equation 9.10. This value is in between the 1.25 assumed by Van Wieringen (1982) and 1.33 from Equation 9.3, therefore:

$$p_l^* = 1.3 p_l \qquad [9.10]$$

The relationship in Equation 9.11 can be obtained for the pre-bored cone penetration test by combining Equations 9.8, 9.9 and 9.10.

$$q_{c_{PB}} = 1.06 p_l \qquad [9.11]$$

The relationship between cone resistance from a pre-bored test and a standard CPT can be obtained by combining Equation 9.7 and 9.11, as shown by Equation 9.12.

$$q_c = 2.8 q_{c_{PB}} \qquad [9.12]$$

Table 9.3 shows the results of the normalized cone resistance for 60° apex angle cone with the correction factor of 2.8. The factored results are closer to the standard vertical CPT. However, the results of the upper soil zone are slightly lower than the CPT reference, and the results of the lower soil zone are higher. As more horizontal pre-bored test data becomes available a better correction factor can be developed, which will allow the use of HD-PB-CPT data in existing soil classification charts developed for CPT, until there are enough data for the development of a specific HD-PB-CPT soil classification chart.

To be possible to use exiting classification charts with a factored *$NQ_t$* the friction sleeve results have to be also factored. However, defining a factor number for friction sleeve requires a better quality data set. Friction sleeve results have to be improved to allow for an evaluation of a correction factor.

Table 9.3 – Factored normalized cone resistance.

| **Tests** | | **Remarks** | **Factored $NQ_t$ (Average)** |
|---|---|---|---|
| **SOIL ZONE BETWEEN 1.5 AND 2.5 METERS DEPTH** | | | |
| **Std vertical CPT** | Conetec 1 | Considered depth – 1.5 to 2.5 m | 40.8 |
| | Conetec 3 | Considered depth – 1.5 to 2.5 m | 43.5 |
| | Conetec 4 | Considered depth – 1.5 to 2.5 m | 39.4 |
| | Conetec 6 | Considered depth – 1.5 to 2.5 m | 40.8 |
| **HD-PB-CPT** | Test 3 | Drilled using water | 37.1 |
| | Test 5 | Drilled using water. Reamer was used in this test | 34.1 |
| **HD-PB-RCPT** | Test 10 | Drilled using water, 60° cone | 37.0 |
| **SOIL ZONE BETWEEN 4 AND 5 METERS DEPTH** | | | |
| **Std vertical CPT** | Conetec 1 | Considered depth – 4 to 5 m | 23.4 |
| | Conetec 3 | Considered depth – 4 to 5 m | 20.1 |
| | Conetec 4 | Considered depth – 4 to 5 m | 21.7 |
| **HD-PB-CPT** | Test 2 | Drilled dry | 30.3 |
| | Test 4 | Drilled dry. Reamer was used in this test. | 38.6 |
| **HD-PB-RCPT** | Test 11 | Drilled using water, 60° cone | 25.0 |

It worth mentioning that because no standard CPT test was carried on in the sand pit there were no available data for comparison and analysis with the HD-PB-CPT results.

## 9.5 SUMMARY

A total of eight field tests of the HD-PB-RCPT prototype 2 were performed at the University of Alberta field laboratory. Because the main soil formation at this site is Lake Edmonton clay, a sand pit was built on the test pathway to allow a clear contrast between two different soil types, in the same way that it was performed for prototype 1 field tests.

The first four sets of tests did not permit a good evaluation of prototype 2 performance due to a problem with the DC adapter, which provides the excitation voltage to the load cell strain gages. Cone and friction resistance results from these tests were totally spurious and unreliable. Electrical resistivity results, on the other hand, were very good, indicating that the Electrical Resistivity Module (ERM) was working properly. It also aided in improving the identification of soil lithology changes.

After correcting the problem with the DC adapter, a second series of four tests were performed at the same site. Two tests were performed using a 60° apex angle cone also at depths of 2 and 4 meters. The same procedure was repeated for two more tests using a 30° apex angle cone.

The electrical resistivity results from this second series of tests were also very good, showing a clear and precise sand pit localization. The only exception was in the results of Test 12, which appears to have been affected by some kind of electrical noise thus resulting in the spurious electrical resistivity measurements.

The cone and friction sleeve results from the 60° apex angle cone tests did not provide evidence that the constraint device was able to improve the data, as had been expected. Similarly, the 30° cone results did not improve borehole expansion as desired and cone resistance results from these tests were even lower than the results from the probe using the 60° cone. However, the load cells may have had too high a capacity for the tested clay, thus making them inaccurate at the low load levels experienced in the field tests. This in part, caused the scatter and inconsistency of the results compromising data analysis

A tentative correlation between the standard cone resistance and a pre-bored cone resistance was developed based on Van Wieringen's (1982) approach. This correlation showed that it is likely possible to develop a correction factor that would allow using the HD-PB-CPT results with existing soil behavior type classification charts. However, extensive field tests in different type of soils would be necessary to validate this approach. Alternatively, when extensive data from horizontal pre-bored cone penetration test became available new soil classification charts could be specially developed.

# CHAPTER 10

## Summary and Conclusions

### 10.1 INTRODUCTION

The main goal of this research was to evaluate the feasibility of using CPT technology to develop a probe for logging HDD boreholes for geotechnical and geoenvironmental applications. Two prototypes were designed, built and field tested in a lacustrine clayey soil, the Lake Edmonton clay formation.

The field test results were encouraging. They showed that this new technology is indeed feasible and could be a useful tool for geotechnical and geoenvironmental site investigation especially in situations where conventional vertical logging is not possible or considered unproductive.

The test results have shown that the prototypes were able to produce profiles similar to those of a conventional CPT. Prototype 2, which had the addition of the Electrical Resistivity Module, greatly enhanced the probe's ability to identify soil lithology changes. Further research and field testing, however, in different soil conditions and with higher sensitivity load cells is necessary to improve the probe design and the data.

## 10.2 CONCLUSIONS

The field test results obtained from the HD-PB-CPT and HD-PB-RCPT were encouraging. They showed that CPT technology can be applied to horizontal directionally drilled boreholes to obtain soil lithology and probably soil contamination information as well. Cone resistance and electrical resistivity measurements have shown good capability in detecting soil changes. Electrical resistivity rendered an especially good ability to detect bulk electrical resistivity contrast.

The data acquisition system worked very well. It plotted all the data in real time on a computer screen in four different graphs for: cone resistance, friction resistance, friction ratio and electrical resistivity versus probe position. The ability to show the test results in real time facilitates the on site decision making process.

However, before this new technology reachs its commercialization stage further research is required to improve some aspects of this new site characterization tool.

Nevertheless, it is the author's opinion that in its present form, the HD-PB-RCPT is ready to locate sand pockets embedded in clayey mediums. And it is also ready to screen soil contamination where high contrast in electrical resistivity is expected, such as in contamination sites with high levels of total dissolved solids or large volumes of free phase hydrocarbons

The addition of an ultra violet induced fluorescence (UVIF) sensor to the probe would greatly improve its ability to detect hydrocarbons. UVIF technology coupled with CPTs to screen for hydrocarbon contamination is widely used. Therefore, there is no reason the incorporation of a UVIF sensor into the HD-PB-CPT should not work as well as did the addition of the electrical resistivity module. The UVIF sensor would make the HD-PB-CPT a very powerful tool for geoenvironmental site investigation.

Finally, Dr. Ralph Peck's (2000) Cross Canada Lecture 2000 very cleverly summarizes the whole challenge and the issues surrounding geotechnical/geoenvironmental site investigation in one phrase:

*"Site Investigation: Expect the Unexpected"*

This statement implies that geological formations can be so complex that it does not matter how thorough one does the site investigation there will always be surprises. It is the author's hope therefore that this new probe will provide valuable contribution to the work of geotechnical/geoenvironmental engineers in their endeavors to discover what nature is hiding from them.

## 10.3 FURTHER RESEARCH

### 10.3.1 DEVELOPMENT OF A SPECIAL REAMER

Disregarding the tests that had problems with the DC adapter (Tests 6, 7, 8 and 9); the tests performed with the 30° cone (Tests 12 and 13); and the ones for which the probe passed beneath the sand pit (Tests 2 and 4); all other tests (Tests 3, 5 and 10) except one (Test 12), showed a clear change in cone resistance when the probe reached the sand pit. Even the tests for which the probe passed beneath the sand pit (Tests 2 and 4) presented a noticeable drop in cone resistance. This drop was thought to be due to a possible stress relief that occurred beneath the sand pit as a result of its excavation. The drop in cone resistance was not as clear in Test 4 as it was in Test 2 because the former test passed through the soil at greater depth beneath the sand pit than did the latter.

Nevertheless, in order to use the HD-PB-RCPT data for soil behavior type classification purposes, cone and friction resistance have to be improved. A worthwhile means to enhance the data would be to create a better quality pilot hole.

The pilot hole drilling process creates sections of a non-cylindrical borehole that will affect the quality of the data. In other words, while the drilling bit is rotating it creates a more uniform cylindrical borehole section. When the rotation is stopped, however, and pushed forward to correct the borehole direction, it creates a non-cylindrical section as shown in Figure 10.1. As the probe passes through these non-cylindrical sections, soil accumulation occurs in front of the probe. This soil accumulation may be affecting the cavity expansion process and consequently the data quality as well. The soil constraint device was not efficient in preventing this kind of soil accumulation. This device was designed to constrain soil deformation arising from cone penetration i.e., from the sides and not from the front of the probe. Consequently, a significant amount of soil was accumulated in front of the probe as shown in Figure 10.2. To obtain a better quality borehole a special reamer with the same diameter as the drilling bit should be developed. The prime function of this reamer would be not to enlarge the borehole as it is normally used to, but to clean and develop a smooth and homogenous cylindrical borehole throughout the length of the pilot hole. A better quality pilot hole should reduce scattered data, and improve test data, as well as test repeatability thus facilitating analysis of the results.

A reamer like device, which was pulled straight and without any rotation, was used in Tests 4 and 5. This device was nothing more than a steel pipe of four inches in diameter (Figure 5.13a) whose effectiveness in cleaning the borehole was questionable. Nevertheless the highest cone resistance data were obtained from these two tests for the same drilling condition i.e., drilled using water or drilled dry.

The use of a rotating reamer might introduce some new problems such as unwanted noise in the data readings due to the reamer rotation and the swivel between the reamer and the probe could not work properly causing the rotation of the probe damaging the electrical cable. However, these variables could easily be tested in a simulated laboratory setting before being tested in the field.

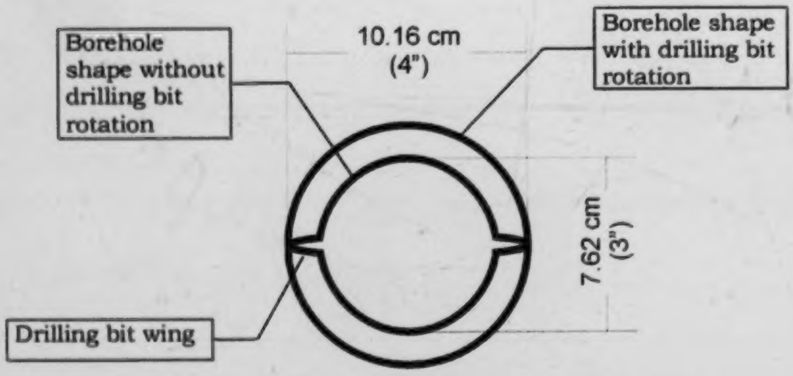
Borehole shape without drilling bit rotation
10.16 cm
(4")
Borehole shape with drilling bit rotation
7.62 cm
(3")
Drilling bit wing

Figure 10.1 – Difference in borehole shape.

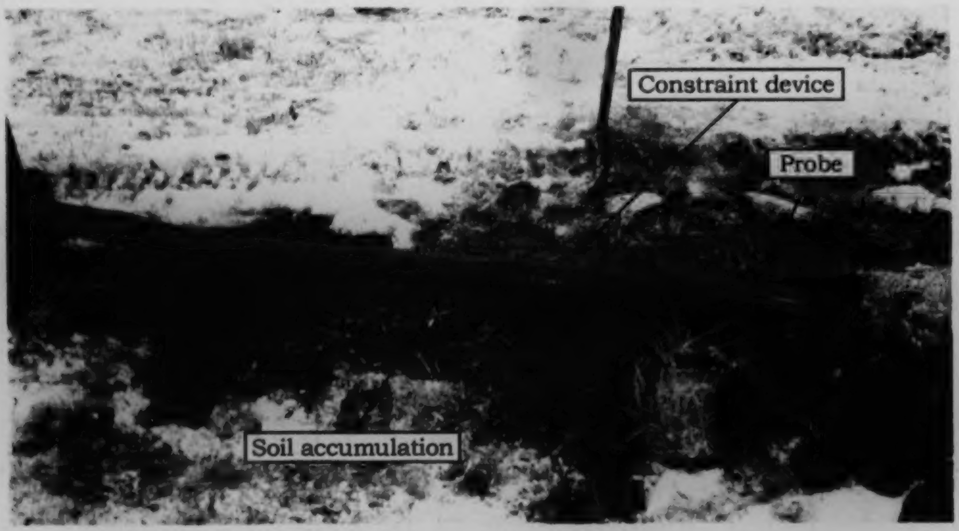
Constraint device
Probe
Soil accumulation

Figure 10.2 – Soil accumulation in front of the HD-PB-RCPT.

## 10.3.2 PORE PRESSURE MEASUREMENT

Since the 1970's pore pressure probes have been developed and successfully used for in situ soil characterization (Janbu and Senneset 1974; Schmertmann 1974; Torstensson 1975; Wissa et al. 1975). Currently, pore pressure measurement is a standard procedure in cone penetration tests; the difference in cost does not justify performing a CPT test without measuring pore water pressure.

During penetration in a saturated soil medium the measured pore pressure is the result of the sum of the hydrostatic or equilibrium pore pressure ($u_o$) and the excess pore pressure ($\Delta u$) generated by the penetration of the cone into the soil. The value of $\Delta u$ is a function of the soil permeability and mechanical characteristics (Bruzzi and Battaglio 1987). In general, for sands where the failure mechanism is drained, the generated excess pore pressure is zero or very small, whereas for clays where the failure mechanism is undrained, $\Delta u$ is large. Figure 10.3 shows a typical pore pressure measurement versus depth profile for a layered soil system. The position of the sand layer can easily be identified by the sudden drop in $\Delta u$.

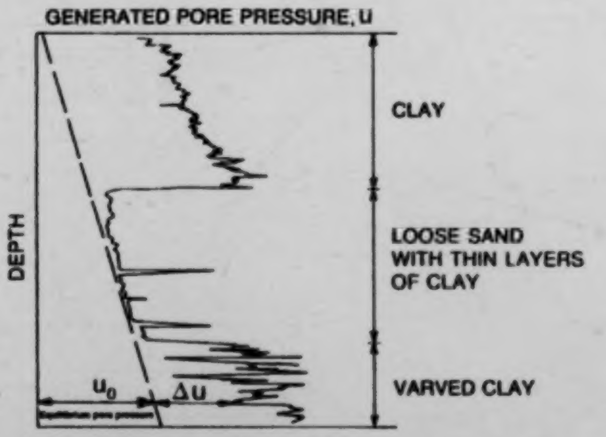

Figure 10.3 – Example of pore pressure versus depth diagram during penetration (modified from Torstensson 1975).

Pore pressure measurements are very useful data that could greatly enhance the capability of HD-PB-RCPTs identifying soil lithology changes, as shown in Figure 10.3. An interesting future research project would be to install a pore pressure transducer into the HD-PB-RCPT to record pore pressure during the test and to compare these results with those obtained by a standard vertical CPTU. An attempt to obtain soil classification by using existing soil behavior type classification charts based only on the cone resistance and pore pressure, such as those proposed by Jones and Rust (1982), Robertson et al. (1986) and Robertson (1990) could also be made. If the final result is satisfactory, the attempt to improve sleeve friction results may no longer be necessary. The HD-PB-RCPT results could be analyzed based only on cone resistance, pore pressure and electrical resistivity data.

### 10.3.3 ENVIRONMENTAL SENSORS

In principle, all environmental sensors normally used in electrical piezocone, as discussed in Chapter 3, could be easily adapted for the HD-PB-CPT. Following the example of the electrical resistivity module (HD-PB-RCPT), there is no apparent reason for them not to work as efficiently. Among these sensors the most appealing one for environmental applications is the ultra violet induced fluorescence (UVIF), because the most common ground contamination is by hydrocarbons, and the UVIF has a great ability to detect hydrocarbons.

A future line of research that should be conducted is to install a UVIF unit into the HD-PB-CPT and field test a contaminated site. Once the HD-PB-CPT has a fully operational UVIF unit it will become a very useful tool to detect surface and subsurface fuel storage tank leakage.

## 10.4 FINAL CONSIDERATIONS

When developing a new tool for site characterization such as the HD-PB-RCPT a question that comes to mind is cost. Will the cost of performing an HD-PB-RCPT test be competitive with the cost of traditional site investigation technology?

The best way to assess this issue is by comparing the price of performing a standard vertical CPT test and an HD-PB-RCPT. According to ConeTec (2000) the cost of a CPT test runs on average around CAN$26.00/m or CAN$8.00/ft. According to Commercial Trenching (2000), to perform an HD-PB-RCPT the cost would be no less than CAN$350.00/h, for only the drilling. To that must be added the hourly cost of a technician for the probe operation and the use of the probe, which could be estimated at approximately CAN$80.00/hour.

A cost comparison can be made for the situation presented in Figure 1.5. Eighteen CPT tests with an average depth of 10 m were performed to delineate the boundary of a brine contamination plume. The same result may have been achieved by performing 4 HD-PB-RCPT tests with a total estimated test length of 501 meters. During a 10 hour shift it is feasible to perform a HD-PB-RCPT test 167 m long. Thus, it will take 30 hours to perform the 501 m test at a total cost of CAN$ 12,900 (including HDD and probe operation cost). To that, still has to be added the cost of two or so standard vertical CPT to define the contamination depth. Therefore, the final cost for the HD-PB-RCPT would be CAN$ 13,420. The cost to perform the 18 standard vertical CPT would be CAN$ 4,680.

The cost of the HD-PB-RCPT test is, therefore, 2.9 times higher than for the standard vertical CPT. However, the CPT provides no information beneath the contamination source (i.e., brine disposal pond), whereas, the HD-PB-RCPT does. Furthermore, as explained in Chapter 1, some times site investigations using vertical logging tools are not feasible. Similarly, in geoenvironmental investigations, when searching for DNAPLs, vertical probing could even aggravate the soil contamination scenario which could significantly increase the remediation cost or even make the clean up impossible. For those special situations, the higher cost of the HD-PB-RCPT may be insignificant compared to its overall benefit. Furthermore, as competition among HDD contractors increase as does familiarity with this new technology, the price of the test will be expected to decrease making its use more attractive even for routine site investigation applications.

# References

Acar, Y. B. and Tumay, M. T. 1986. Strain Field Around Cones in Steady Penetration. Journal of Geotechnical Engineering - ASCE. February, vol. 112, No. 2. pp. 207-213.

Allouche, E. N., Ariaratnam, S. T and Lueke, J. S. 1998a. A Survey of Current Horizontal Directional Drilling Practices in Canada and the United States. Department of Civil and Environmental Engineering, University of Alberta, Edmonton, Alberta, Canada. CEM Technical Report TT-98/03. p. 69.

Allouche, E. N., Biggar, K. W., Ariaratnam, S. T. and Mah, J. W. 1998b. Application of horizontal directional drilling for contaminated site characterization. Proceedings of The First International Conference on Site Characterization –ISC' 98 – Geotechnical Site Characterization. Atlanta, Georgia, USA. A. A. Balkema, Rotterdam. April, vol 1, pp. 341-346.

Archie, G. E. 1942. The electrical Resistivity Log as an Aid in Determining Some Reservoir Characteristics. Transactions of the American Institute of Mining and Metallurgical Engineers. Petroleum Development and Technology, Petroleum Division. Vol. 146, pp. 54-61

Ariaratnam, S. T., Allouche, E. N. and Biggar, K. W. 2000. Testing of a new generation horizontal soil sampler. Canadian Geotechnical Journal, February, vol. 37, No. 1, pp 259–263.

ASME. 1953. Screw Thread Manual, A Shop and Drafting Room Abridgment of the American-Unified Standard for Screw Threads and Their Gages. Published by The American Society of Mechanical Engineers – ASME. p.62

ASTM. 1994. Standard Method for Deep, Quasi-Static, Cone and Friction-Cone Penetration Tests of Soil, D 3441-94 American Society for Testing and Materials (ASTM). pp 348-354.

ASTM. 1995a. Standard Testing Method for Performing Electronic Cone and Piezocone Penetration Testing of Soils, D 5778-95. American Society for Testing and Materials (ASTM). pp. 576–593.

ASTM. 1995b. Standard Test Method for Electrical Conductivity and Resistivity of Water, D 1125. American Society of Testing and Materials (ASTM). pp. 88-94.

Baldi, G. Bellotti, R. Ghionna, V. Jamiolkowski, M. J. and Pasqualini, E. 1982. Design parameters for sands from CPT. Proceeding of the Second European Symposium on Penetration Testing –ESOP II. Amsterdam, May 24-27. Vol. 2, pp. 425-432.

Baldi, G. Bellotti, R. Ghionna, V. Jamiolkowski, M. J. and Pasqualini, E. 1986. Interpretation of CPTs and CPTUs; 2nd part: drained penetration of sands. Proceedings of the Fourth International Geotechnical Seminar, Singapore. pp. 143-156.

Baligh, M. M. 1985. Strain Path Method. Journal of Geotechnical Engineering-ASCE. September, vol. 111, No. 9. pp. 1108 – 1136.

Baguelin, F., Jézéquel, J. H. and Shields, D. H. 1978. The pressuremeter and Foundation Engineering. Series on Rock and Soil Mechanics. Trans Tech Publications, Germany. First Edition. p.617.

Barentsen, P. 1936. Short Description of a Field-Testing Method with Sounding Apparatus. Proceedings of the International Conference on Soil Mechanics and Foundation Engineering. Graduate School of Engineering, Harvard University, Cambridge, Massachusetts. Jun. 22 – 26. Vol. I, pp. 7 – 10.

Bishop, R. F., Hill, R. and Mott, M. F. 1945. The Theory of Indentation and Hardness Tests. Proceedings of the Physical Society. Vol. 57, part 3, No 321, pp. 147-159.

Bhanot, K. L. 1968. Behaviour of scaled and full-length cast-in-place concrete piles. Ph.D. thesis, University of Alberta, Edmonton, AB, Canada. p. 336.

Bratton, W. L., Bratton, J. L. And Shinn, J. D. 1995. Direct Penetration Technology for Geochnical and Environmental Site Characterization. Proceeding of the Special Conference Geoenvironmental 2000, Characterization, Containment, Remediation, and Performance in Environmental Geotechnics. Geotechnical Engineering Division and Environmental Engineering Division of the American Society of Civil

Engineers – ASCE. Geotechnical Special Publication No. 46. New Orleans, Louisiana. Volume 1, pp. 105-166.

Broere, W. and van Tol, A. F. 1998. Horizontal Cone Penetration Testing. Proceedings of The First International Conference on Site Characterization – ISC' 98 – Geotechnical Site Characterization. Atlanta, Georgia, USA. A. A. Balkema, Rotterdam. April, vol 2, pp. 989-994.

Broms, B. B. and Flodin, N. 1988. History of soil penetration testing. Proceedings of the International Symposium on Penetration Testing, ISOPT-1. Orlando, Florida. Balkema, Rotterdam. Volume 1, pp. 157-220.

Bruzzi, D. and Battaglio, M. 1987. Pore pressure measurements during cone penetration tests. ISMES Publication, Bergamo, Italy. p. 201.

Campanella, R. G., Davies, M. P., Boyd, J. L. and Everard, J. L. 1994a. In-situ testing methods for groundwater contamination studies. Proceedings of the Symposium on Developments in Geotechnical Engineering. A. A. Balkema, Rotterdam. Bangkok, Thailand. January. pp. 371-379.

Campanella, R. G., Davies, M. P., Boyd, J. L. and Everard, J. L. 1994b. Geoenvironmental Subsurface Site Characterization Using In-Situ Soil Testing Methods. Proceedings of the First International Congress on Environmental Geotechnics. Edmonton, Alberta, Canada. July. pp. 153-159.

Campanella, R. G. and Kokan, M. J. 1993. A New Approach to Measuring Dilatancy in Saturated Sands. Geotechnical Testing Journal – ASTM. December, vol. 16, No. 4, pp. 485-495.

Campanella, R. G. and Robertson, P. K. 1981. Applied Cone Research. Proceeding of the Symposium on Cone Penetration Testing and Experience, Geotechnical Engineering Division - ASCE, St. Louis, MI, New York, pp. 343-362.

Campanella, R. G. and Robertson, P. K. 1984. A seismic cone penetrometer to measure engineering properties of soil. Proceeding of the 54th Annual International Meeting Society of Exploration Geophysicists, Atlanta.

Campanella, R. and Weemees, I. 1990. Development and use of an electrical resistivity cone for groundwater contamination studies. Canadian Geotechnical Journal. October, vol. 27, No. 5, pp. 557-567.

Carr, C. 1982. Handbook on Soil Resistivity Surveying. Center for American Archeology Press. Evanston, Illinois, USA. p.676.

Carter, J. P., Booker, J. R. and Yeung, S. K. 1986. Cavity Expansion in Cohesive Frictional Soils. Geotechnique, vol. 36, No. 3, pp. 349–358.

Cartwright, K. and McComas, M. R. 1968. Geophysical Surveys in the Vicinity of Sanitary Landfills in Northeastern Illinois. Ground Water, journal of the Technical Division National Water Well Association. Vol. 6, No.5, pp. 23–30.

CCME, Canadian Council of Ministers of the Environmental. 1994. Subsurface Assessment Handbook for Contaminated Sites. Report CCME EPC-NCSRP-48E, March. p. 293.

CCME, Canadian Council of Ministers of the Environmental 1999. Canadian Environmental Quality Guidelines. Volume 1.

CMW – The Charles Machine Works, Inc. 1996. The Green Book – Horizontal Directional Drilling Systems: A New Dimension for Remediation. Perry, Oklahoma. Publication number CMW-950. p.154.

Cohen, M. and Allouche, E. N. 1998. Introduction to Horizontal Sampling and Logging. Proceedings of the Nait Field Demonstration and Symposium – Environmental Applications of Horizontal Directional Drilling Technology. Edmonton, Alberta, Canada. April. pp. 47-55.

Commercial Trenching. 2000. Personal communication. Commercial Trenching Ltd. 4770-74 Ave, Edmonton, Alberta, Canada. T6H 2H6.

ConTec Investigation Ltd. 1989. Presentation and interpretation of CPT data: Lutose creek cover. Technical Report prepared for the Canadian National Railways, Calgary, Alberta, Canada.

ConTec Investigation Ltd. 2000. Personal communication. Vancouver, British Columbia, Canada.

de Rutier, J. 1982. The static cone penetration test. State-of-the-art-report. Proceeding of the Second European Symposium on Penetration Testing ESOPT II. Amsterdam. A. A. Balkema, Rotterdam. May 24-27. pp. 389-405.

DOE, U.S. Department of Energy. 1993. Drilling Sideways – A Review of Horizontal Well Technology and Its Domestic Application. Energy Information Administration – EIA Technical Report DOE/EIA-TR-0565. Washington, DC. April. p. 25.

DOE – U.S. Department of Energy. 1996. Cone Penetrometer – Innovative Technology Summary Report. DOE/EM-0309. April. p.17.

DuPont 2000a. Delrin acetal resin. DuPont Engineering Polymers. Web site http://www.dupont.com /enggpolymers/americas/delrin.html.

DuPont 2000b. Product and Properties Guide. Delrin acetal resin, Delrin P performance acetal resin and Delrin "Eleven Series" acetal resin. DuPont Engineering Polymers. p. 22.

Eisenstein, Z. 1999. Solution for Urban Tunneling. Talk at the 31st Annual General Meeting of the Geotechnical Society of Edmonton - GSE. Edmonton, Alberta, Canada. May 5th.

Eisenstein, Z. and Sorensen, K. L. 1986. Tunnelling for the South LRT Extension in Edmonton, Alberta. Canadian Tunnelling Canadien. An annual publication of the Tunnelling Association of Canada. pp. 19-30.

Eisenstein, Z. and Sorensen, K. L. 1987. Complex geology accommodated en route. The International Journal of Underground Works – Tunnels & Tunnelling. November, pp. 45–50.

EPA 1998. Geophysical Techniques to Locate DNAPLs: Profiles of Federal Funded Project. U.S. Environmental Protection Agency. EPA 542-R-98-020, December. p. 26

Everard, J. L. 1995. Characterization of Hydrocarbon Contaminated Site Using In-Situ Methods. M.A.Sc. thesis, department of Civil Engineering, The University of British Columbia. Vancouver, British Columbia, Canada. p.121.

Ferreira, R. S. 1992. Interpretation of Pressuremeter Tests Using a Curve Fitting Technique. Ph.D. thesis, Department of Civil and Environmental Engineering, University of Alberta. Edmonton, Alberta, Canada. p. 232.

Fetter. C. W. 1993. Contaminant Hydrogeology. Macmillan Publishing Company, New York. p.458.

Graf, R. F. 1978. Modern Dictionary of Electronics. Howard W. Sams & Co. Inc. Indianapolis, Indiana, USA. Fifth edition. p.832.

Greenhouse, J. P., and Slaine, D. D. 1983. The use of reconnaissance electromagnetic methods to map contaminant migration. Ground Water Monitoring Review. Vol. 3, NO. 2, pp.47–59.

Greenhouse, J. P., Gudjurgis, P. and Slaine, D. 1997. Applications of Geophysics in Environmental Investigations. The Engineering Geophysical Society – EEGS. p.150.

Haas, J. And Forney, R. 1995. Simple approaches to sensing in the subsurface environment. Environmental Monitoring and Hazardous Waste Site Remediation. The International Society for Optical Engineering. Vol. 2504, pp. 54-58.

Hackbarth, D. A. 1971. Field Study of Subsurface Spent Sulfite Liquor Movement Using Earth Resistivity Measurements. Ground Water, journal of the Technical Division National Water Well Association. Vol. 9, No.3, pp.11-16.

Halliday, D. and Resnick, R. 1988. Fundamentals of Physics. Third edition, John Wiley & Sons Inc. p. 977.

Head, K. H. 1988. Manual of soil laboratory testing. Pentech Press Limited. Volume 2: Permeability, Shear Strength and Compressibility Test. p.747.

Horsnell, M. R. 1988. The use of cone penetration testing to obtain environmental data. Proceedings of the geotechnology conference Penetration Testing in the UK, organized by the Institue of Civil Engineers. Bermingham, UK, Thomas Telford, London. July. pp.289-294.

Houlsby, G. T. and Hitchman, R. 1988. Calibration chamber tests of a cone penetrometer in sand. Geotechnique, vol. 38, No. 1, pp. 33–44.

Hvorslev, M. J. 1949. Subsurface Exploration and Sampling of Soil for Civil Engineering Purpose. Report on a research project of the American Society of Civil Engineers – ASCE. Edited and printed by Water Experiment Station, Vicksburg, Mississippi. November, p. 521.

ISSMFE. 1989. International Reference Test Procedure (IRTP) for Cone Penetration Test. Report of the International Society of Soil Mechanics and Foundation Engineering (ISSMFE) Technical Committee on Penetration Testing of Soil – TC 16, with Reference to Test Procedures, Swedish Geotechnical Institute, Linkõping, Sweden. Information 7, pp. 6–16.

Janbu, N. and Senneset, K. 1974. Effective stress interpretation of in situ static penetration tests. Proceedings of the European Symposium on Penetration Testing, ESOPT, Stockholm. Volume 2-2, pp. 181-193.

Jones, G. A. and Rust, E. 1982. Piezometer penetration testing. Proceedings of the Second European Symposium on Penetration Testing, ESOPT II. Amsterdam. A. A. Balkema, Rotterdam. May 24-27. pp. 607-613.

Kaback, D. And Oakley, D. 1996. Horizontal Environmental Wells in the United States: A Catalogue. Colorado Center for Environmental Management. April. p. 32.

Keller, G. V. 1982. Electrical properties of rocks and minerals. In R.S. Carmichael (ed.) Handbook of Physical Properties of Rocks (Chapter 2). CRC press, Boca Raton, Florida, USA. Vol. 1, pp. 217-293.

Kokan, M. J. 1992. Dilatancy Characterization of Sands Using the Resistivity Cone Penetration Test. M.A.Sc. thesis, department of Civil Engineering, The University of British Columbia. Vancouver, British Columbia, Canada. p.140.

Kramer, S. R., McDonald W. J. and Thomson, J. C. 1992. An Introduction to Trenchless Technology. Published by Chapman and Hall, New York, NY. p. 223.

LabVIEW 1998. LabVIEW user manual. National Instruments Corporation. Austin, Texa, USA. p. 504.

Ladanyi, B. 1994. Some unconventional field testing methods for earth materials. Proceedings of the Symposium on Developments in Geotechnical Engineering. Bangkok, Thailand. A. A. Balkema, Rotterdam, Brookfield. January, pp. 95–100.

Lunne, T., Robertson, P. K. and Powell, J. J. M. 1997. Cone Penetration Testing in Geotechnical Practice. Published by Blackie Academic and Professional, an imprint of Chapman & Hall. p.312.

Matheson, D. S. 1970. A tunnel roof failure in till. Canadian Geotechnical Journal. Vol. 7, No. 3, pp. 313–317.

May, R. W. and Thomson, S. 1978. The geology and geotechnical properties of till and related deposits in the Edmonton, Alberta, area. Canadian Geotechnical Journal. Vol. 15, No. 3, pp. 362–370.

Miran J. and Briaud, J. L. 1990. The Cone Penetration Test. Civil Engineering Department, Texas A & M University, College Station, Texas, USA. August. p.144.

Meigh, A. C. 1987. Cone Penetration Testing, methods and interpretation. CIRIA Ground Engineering Report: In-situ Testing. Butterworths. p.141.

Nielsen, B. 1997. Site Characterization Using Horizontal Boring/Drilling Technology. Technology summary sheet of The U.S. Air Force Research Laboratory, Material and Manufacturing Directorate, Airbase and Environmental Technology Division (AFRL/MLQ). pp.1.

Nielsen, B., Johnson, S., Gates, T., Olhoeft, G. and Grimm. B. 1997. Dense Non-Aqueous Phase Liquid (DNAPL) Cleanup Starts with Detection. Technology summary sheet of The U.S. Air Force Research Laboratory, Material and Manufacturing Directorate, Airbase and Environmental Technology Division (AFRL/MLQ). pp.1.

Oberg, E., Jones, F. D., and Horton, H. L. 1989. Machinery's Handbook 23rd edition. Industrial Press Inc. New York. p. 2511.

Okoye, C. N.; Cotton, T. R. and O'Meara, D. 1995. Application of Resistivity Cone Penetration Testing for Qualitative Delineation of Creosote Contamination in Saturated Soils. Geoenvironment 2000, Characterization, Containment, Remediation and Performance in Environmental Geotechnics. ASCE Geotechnical Special Publication No. 46. Vol. 1, pp. 151–166.

Pankow, J. F. and Cherry, J. A. 1996. Dense Chlorinated Solvents and other DNAPLs in Groundwater: History, Behavior, and Remediation. Waterloo Press. p. 522.

Palmer, A. C. 1972. Undrained Plane Strain Expansion of a Cylindrical Cavity: A Simple Interpretation of the Pressuremeter Test. Geotechnique vol. 22, No. 3, pp. 451–457.

Parmentier, P. P. and Klemovich, R. M. 1996. A New Direction in remediation. Civil Engineering. April. pp.55-57.

Peck, R. 2000. Site Investigation: Expect the Unexpected. 2000 Cross Canada Lecture of the Canadian Geotechnical Society. The Geotechnical Society of Edmonton. November 16. Edmonton, Alberta, Canada.

Robertson, P. K. 1986. In situ testing and its application to foundation engineering. Canadian Geotechnical Journal. June, vol. 23, pp.573-594.

Robertson, P. K. 1990. Soil classification using the cone penetration test. Canadian Geotechnical Journal. June, vol. 27, No. 1. pp.151-158.

Robertson, P. K. 1998. Cone Penetration Testing Geotechnical Application Guide. Produced by ConeTec Inc. and Gregg In Situ Inc. Second edition, October. p.52.

Robertson, P. K. and Campanella, R. G. 1983a. Interpretation of cone penetration tests. Part I: Sand. Canadian Geotechnical Journal. Vol. 20, No. 4, pp. 718-733.

Robertson, P. K. and Campanella, R. G. 1983b. Interpretation of cone penetration tests. Part II: Clay. Canadian Geotechnical Journal. Vol. 20, No. 4, pp. 734-745.

Robertson, P. K. and Campanella, R. G. 1988. Guidelines for geotechnical design using CPT and CPTU. University of British Columbia, Vancouver, Department of Civil Engineering, Soil Mechanics Series No. 120. February. p. 192.

Robertson, P. K., Campanella, R. G., Gillespie, D. and Greig, J. 1986. Use of piezometer cone data. Proceedings of In Situ' 86, Special Conference sponsored by the Geotechnical Engineering Division of the American Society of Civil Engineers - ASCE. Geotechical Special Publication No. 6. Virginia, Blacksburg. pp. 1263-1280.

Robertson, P. K., Campanella, R. G., Gillespie, D. and Rice, A. 1986. Seismec CPT to Measured In Situ Shear Wave Velocity. Journal of Geotechnical Engineering, Geotechnical Engineering Division of the American Society of Civil Engineers – ASCE. August, vol. 112, No. 8, pp. 791-803.

Robertson, P. K., Sully, J. P., Woeller, D. J., Lunne, T., Powell, J. J. M. and Gillespie, D. G. 1992. Estimating coefficient of consolidation from piezocone tests. Canadian Geotechnical Journal, Vol. 29, No. 4, pp. 551-557.

Robertson, P. K., Lunne, T. and Powell, J. J. M. 1998. Geo-environmental application of penetration testing. Proceedings of the First International Conference on Site Characterization – ISC '98 – Geotechnical Site Characterization. Atlanta, Georgia, USA. A. A. Balkema, Rotterdam. April, vol 1, pp. 35-48.

Sagaseta, C. and Houlsby, G. T. 1988. Elastic incompressible flow around and infinite cone. Proceedings of 1st International Symposium on Penetration Testing. Orlando, vol. 2. pp. 933-938.

Sanglerat, G. 1972. The Penetrometer and Soil Exploration. Interpretation of penetration diagrams – theory and practice. Elsevier Publishing Company. p.464.

Schmertmann, J. H. 1974. Penetration pore pressure effects on quasi-static cone bearing, $q_c$. Proceedings of the European Symposium on Penetration Testing, ESOPT, Stockholm. Volume 2-2, pp. 345-351.

Schmertmann, J. H. 1978. Guidelines for cone penetration test. Performance and Design. U. S. Department of Transportation – Federal Highway Administration. FHWA-TS-78-209. p. 145.

Schneider, G. W. and Greenhouse, J. P. 1992. Geophysical detection of perchloroethylene in a sandy aquifer using resistivity and nuclear logging techniques. Symposium on Application of Geophysics to Engineering and Environmental Problems, Oakbrook, IL, April 26-29. pp. 619-628

Silvestri, V. and Fahmy, Y. 1995. Influence of Apex Angle on Cone Penetration Factors in Clay. Geotechnical Testing Journal – ASTM. September, vol. 18, No. 3. pp. 315-323.

Stollar, R. L. and Roux, P. 1975. Earth Resistivity Surveys – A Method for Defining Ground-Water Contamination. Ground Water, journal of the Technical Division National Water Well Association. Vol. 13, No.2, pp.145-150.

Strutynsky, A. I., Sandiford, R. E. and Cavaliere, D. 1992. Use of Piezometric Cone Penetration Testing with Electrical Conductivity Measurements (CPTU-EC) for the Detection of Hydrocarbon Contamination in Saturated Granular Soils. Current Practices in Ground Water and Vadose Zone Investigation. ASTM STP 1118. pp. 169-182.

Swedish Geotechnical Society. 1992. Recommended Standard for Cone Penetration Tests. SGF-Report 1:93E. June 15. p.27.

Teh, C. I. and Houlsby, G. T. 1991. An analytical study of the cone penetration test in clay. Geotechnique. March, vol. 41, No. 1. pp. 17-34.

Telford, W. M., Geldart, L. P. and Sheriff, R. E. 1990. Applied Geophysics. Cambridge University Press second edition. p. 770.

Torstensson, B. A. 1975. Pore Pressure Sounding Instrument. Proceeding of the Conference on In Situ Measurement of Soil Properties. Special Conference of the Geotechnical Engineering Division, ASCE. Raleigh, North Carolina. June 1-4. Volume II, pp. 48-54.

Tumay, M. T., Acar, Y. B., Cekirge, M. H and Ramesh, N. 1985. Flow Field Around Cones in Steady Penetration. Journal of Geotechnical Engineering – ASCE. February, vol. 111, pp. 193-204.

Tweedie, R. W.; Branco, P. J.; Eisenstein, Z.; and Heise, R. A. 1992. Ground Control During Construction of the Edmonton SLRT Twin Tunnels. Canadian Tunnelling Canadien. An annual publication of the Tunnelling Association of Canada. pp. 141-155.

Unite States Salinity Laboratory Staff. 1954. Diagnosis and Improvement of Saline and Alkali Soils. United State Department of Agriculture handbook No. 60. p.160

Urich, D. W. 1981. Electrical Resistivity-Hydraulic Conductivity Relationships in Glacial Outwash Aquifers. Water Resources Research. October, vol. 17, No. 5. pp 1401-1408.

van de Graaf, H.C. and Zuidberg. 1985. Field Investigation. The Netherlands Commemorative Volume. 11th International Conference on Soil Mechanics and Foundation. San Francisco, USA, August 12-18. pp.29-44.

van den Berg, P. 1994. Analysis of soil penetration. Delft University Press, The Netherlands. p. 175.

Van Ree, C. C. D. F. and Olie, J. J. 1993. The development of in situ measurement techniques by means of CPT-equipment in the Netherlands. Field Screening Methods for Hazardous Waste and Toxic Chemicals. Vol. 1, pp. 296-303.

Vermeer, 1998. Underground Equipment Catalogue. Vermeer Manufacturing Company. p. 18.

van Wieringen, J. B. M. 1982. Relating cone resistance and pressuremeter test results. Proceeding of the Second European Symposium on Penetration Testing, ESOPT II, Amsterdam. A. A. Balkema, Rotterdam. May 24-27, vol. 2, pp. 951-955.

Vesic, A. S. 1972. Expansion of cavities in infinite soil mass. Soil Mechanics and Foundations Division – ASCE 98: pp. 265-289.

Weemees, I. A. 1990. Development of an Electrical Resistivity Cone for Groundwater Contamination Studies. M.A.Sc. thesis, Department of Civil Engineering, The University of British Columbia. Vancouver, British Columbia, Canada. p. 77.

Wilcox, S. W. 1942. The electrical Resistivity Log as an Aid in Determining Some Reservoir Characteristics. Transactions of the American Institute of Mining and Metallurgical Engineers. Petroleum Development and Technology, Petroleum Division. Discussion, Vol. 146, pp. 61-62.

Wissa, A. E. Z., Martin, R. T. and Garlanger, J. E. 1975. The Piezometer Probe. Proceeding of the Conference on In Situ Measurement of Soil Properties. Special Conference of the Geotechnical Engineering Division, ASCE. Raleigh, North Carolina. June 1-4. Volume I, pp. 536-545.

Woeller, D. J., Weemees, I, Kokan, M., Jolly, G. and Robertson, P. K. 1991. Penetration Testing for Groundwater Contaminants. Geotechnical Engineering Congress. ASCE Geotechnical Special Publication No. 27. Vol. 1 pp. 77-87.

Wolt, J. D. 1994. Soil Solution Chemistry Application to Environmental Science and Agriculture. Edited by John Wiley & Sons, Inc. p. 345.

Yeung, A. T. and Akhtar, A. S. 1995. Numerical analysis of boundary effects on calibration chamber on electrical resistivity measurements. Proceedings of the International Symposium on Cone Penetration Testing - CPT'95. Linköping, Sweden, October 4-5. Vol. 2, pp. 123-128.

Yu, H. S. and Mitchell, J. K. 1998. Analysis of Cone Resistance: Review Methods. Journal of Geotechnical and Geoenvironmental Engineering - ASCE. February. Vol. 124, No. 2, pp.140-148.

Zhang, D. J. Y. 1999. Predicting Capacity of Helical Screw Piles in Alberta Soils. M.Sc. thesis, Department of Civil and Environmental Engineering, University of Alberta, Edmonton, AB, Canada. p. 304.

Zuidberg, H. M., ten Hoope, J. and Geise, J. M. 1988. Advances in in-situ measurements. Second International Symposium on Field Measurements in Geomechanics. Balkema, Rotterdam. Vol. 1, pp.279–291.

# APPENDIX 1

## CPTU PROFILES

## (UNIVERSITY OF ALBERTA FIELD LABORATORY)

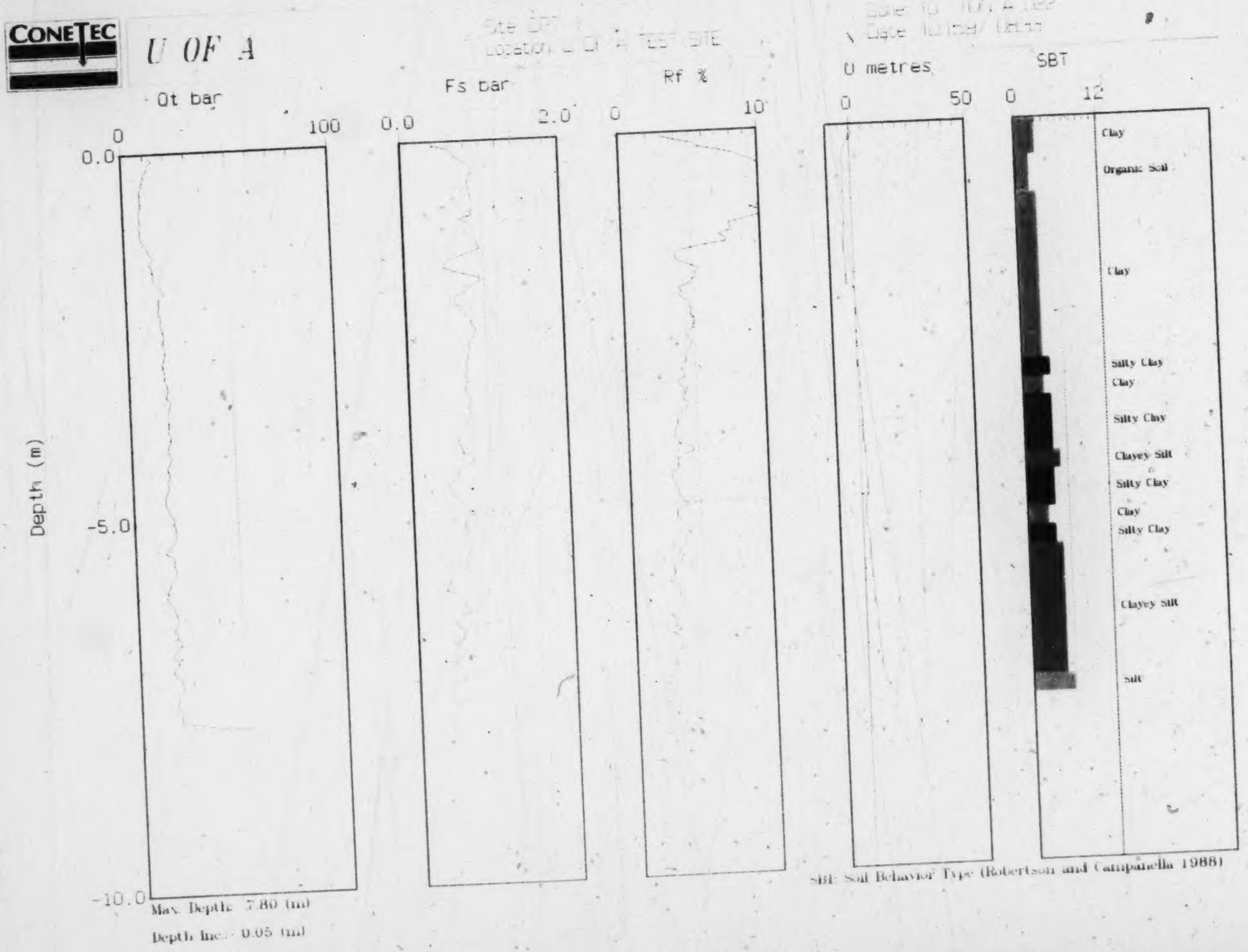

SBT: Soil Behavior Type (Robertson and Campanella 1988)

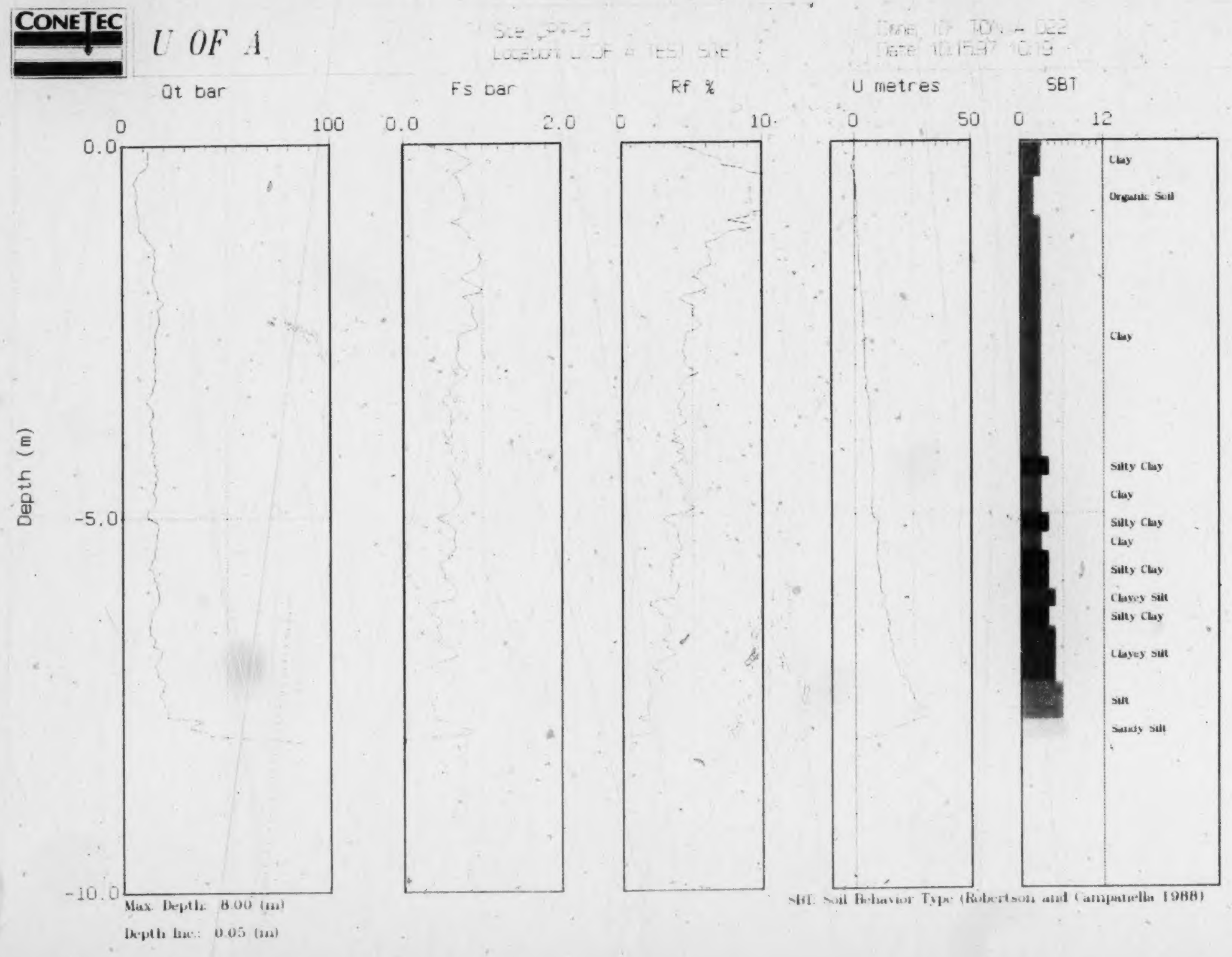CONETEC
U OF A
Site CPT-3
Location U OF A TEST SITE
Cone ID TON - 022
Date 10:15:97 10:19
Qt bar
0
100
Fs bar
0.0
2.0
Rf %
0
10
U metres
0
50
SBT
0
12
0.0
-5.0
-10.0
Depth (m)
Clay
Organic Soil
Clay
Silty Clay
Clay
Silty Clay
Clay
Silty Clay
Clayey Silt
Silty Clay
Clayey Silt
Silt
Sandy Silt
Max. Depth: 8.00 (m)
Depth Inc.: 0.05 (m)
SBT: Soil Behavior Type (Robertson and Campanella 1988)

CONETEC

*U OF A*

Site: CPT-4
Location: U OF A TEST SITE

Cone ID: [illegible] A 022
Date: 10/[illegible]

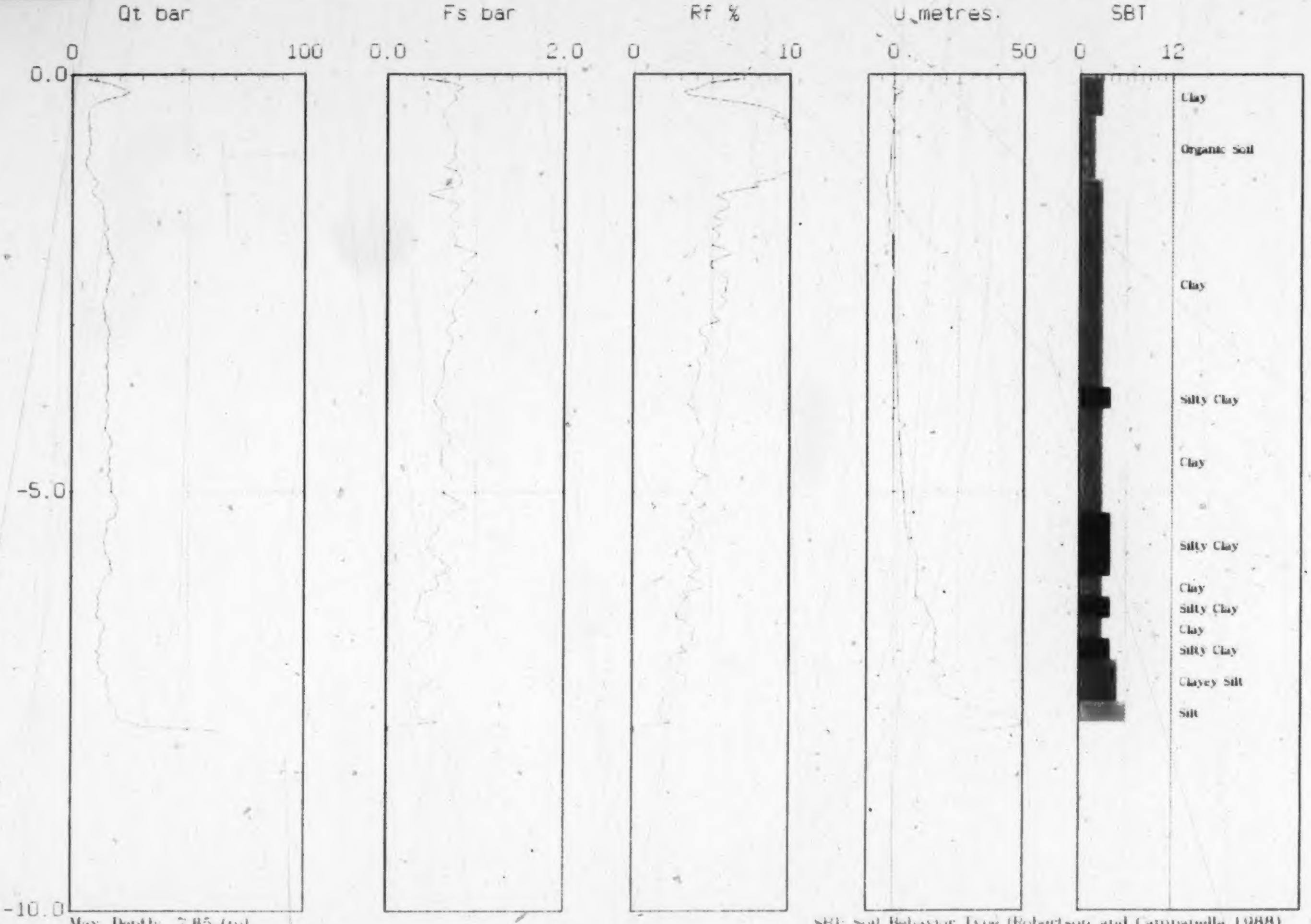

Max. Depth: 7.85 (m)

Depth Inc.: 0.05 (m)

SBT: Soil Behavior Type (Robertson and Campanella 1988)

**U OF A**

Site: CPT GENERATOR
Location: U OF A TEST SITE

Cone: 10 TON A 022
Date: 10:15:97 10:04

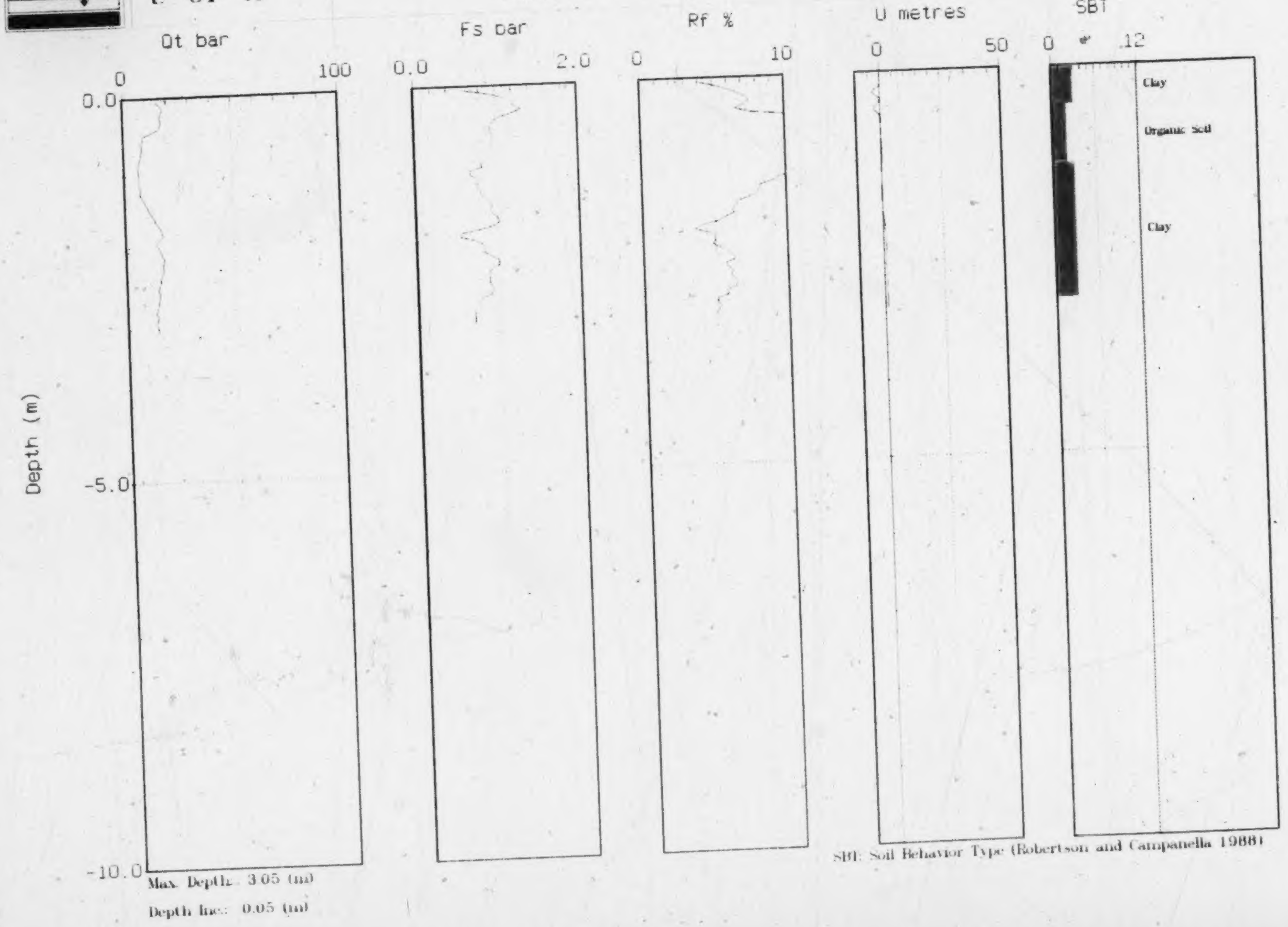

Max. Depth: 3.05 (m)
Depth Inc.: 0.05 (m)

SBT: Soil Behavior Type (Robertson and Campanella 1988)

# APPENDIX 2

## LABORATORY INDEX TESTS

## LAKE EDMONTON CLAY

| | |
|---|---|
| Liquid Limit (%) | 73 |
| Plastic Limit (%) | 32 |
| Plastic Index (%) | 41 |
| Natural moisture content (%) | 32.6 |
| Relative density, former specific gravity ($G_s$) | 2.68 |

## SAND

| | |
|---|---|
| Min. density ($g/cm^3$) | 1.527 |
| Max. void ratio | 0.72 |
| Max. density ($g/cm^3$) | 1.822 |
| Min. Void ratio | 0.44 |
| Relative density, former specific gravity ($G_s$) | 2.61 |

**Lake Edmonton clay**

## GRAIN SIZE DISTRIBUTION

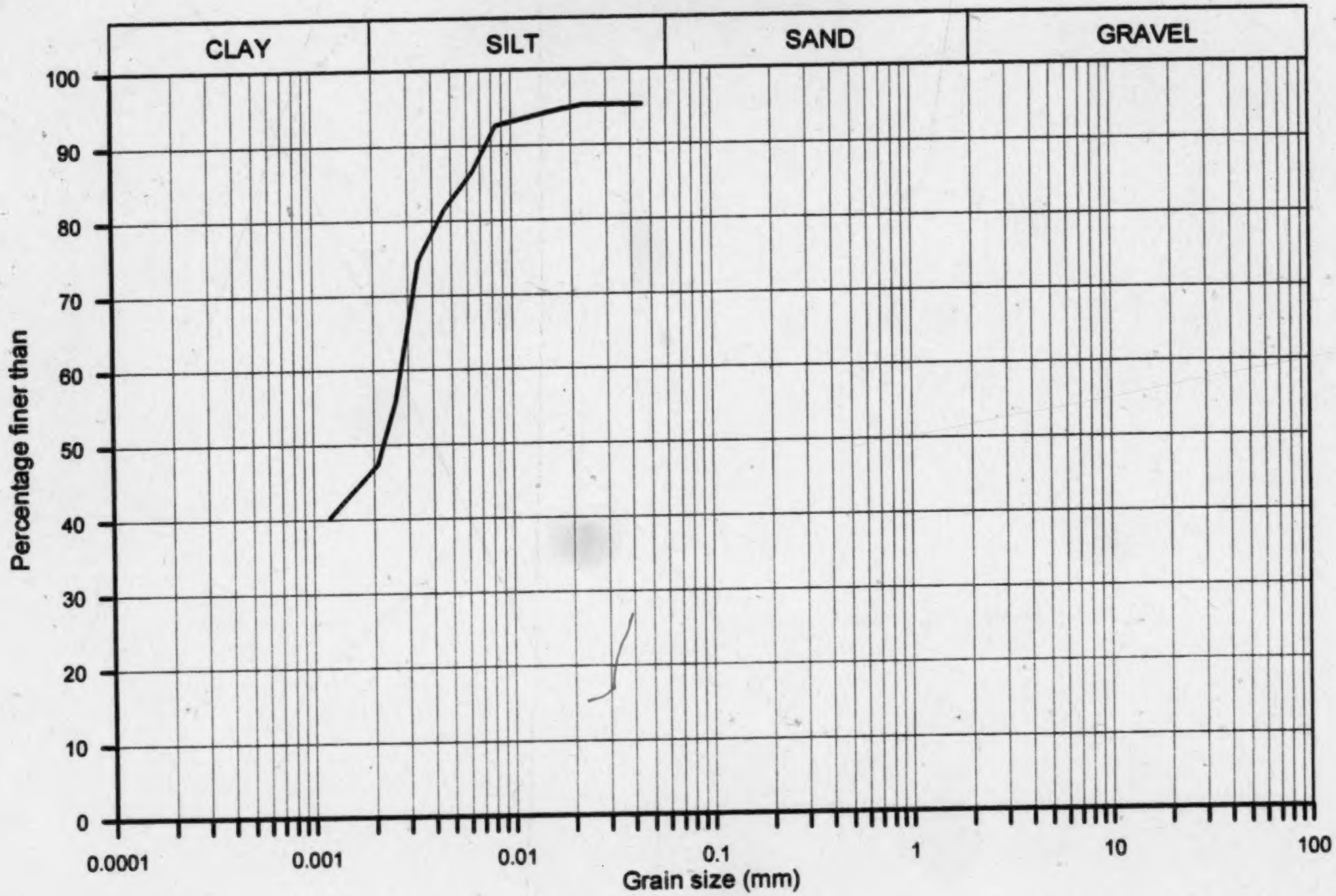

**Sand**

## GRAIN SIZE DISTRIBUTION

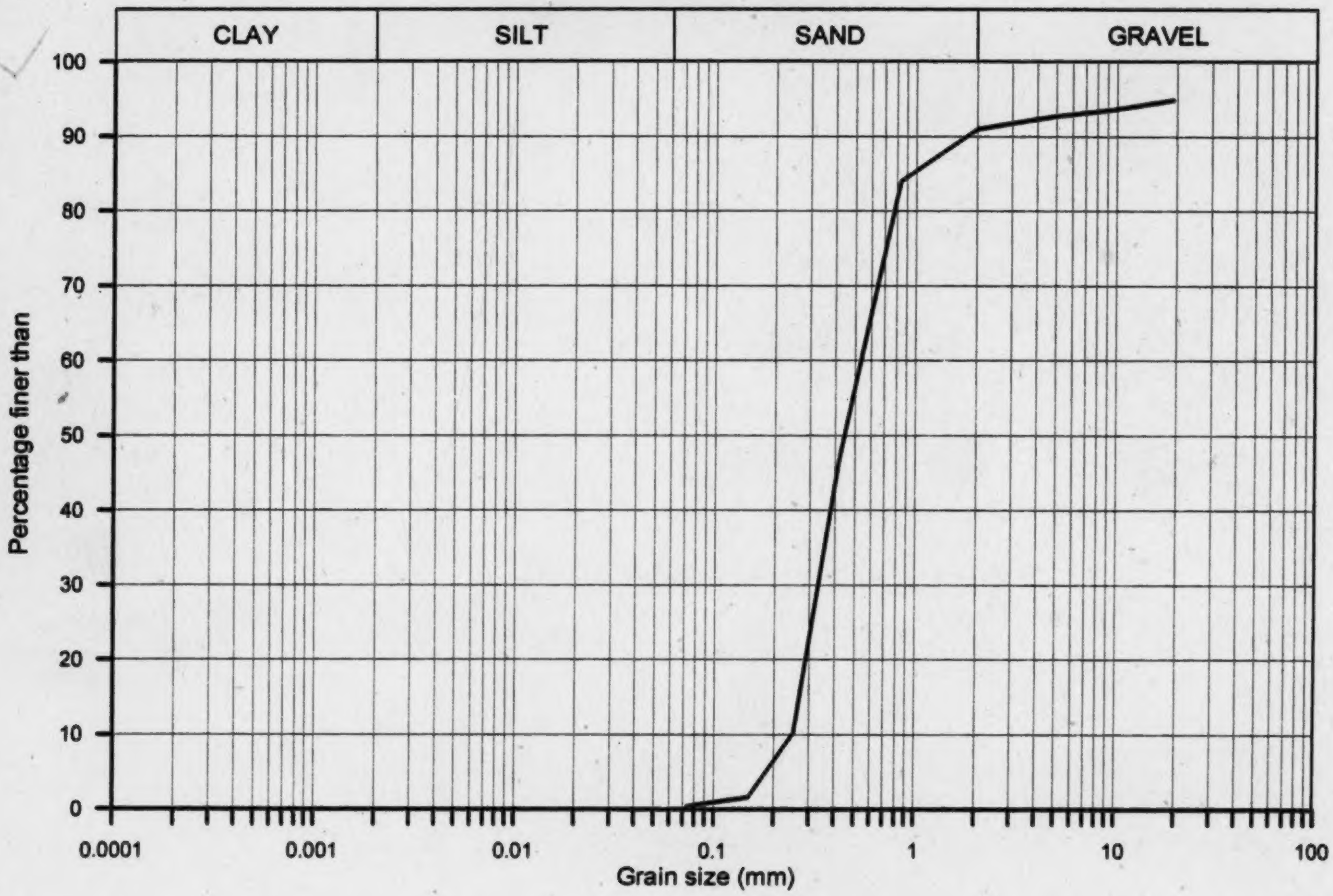

# APPENDIX 3

## HD-PB-CPT DRAWINGS

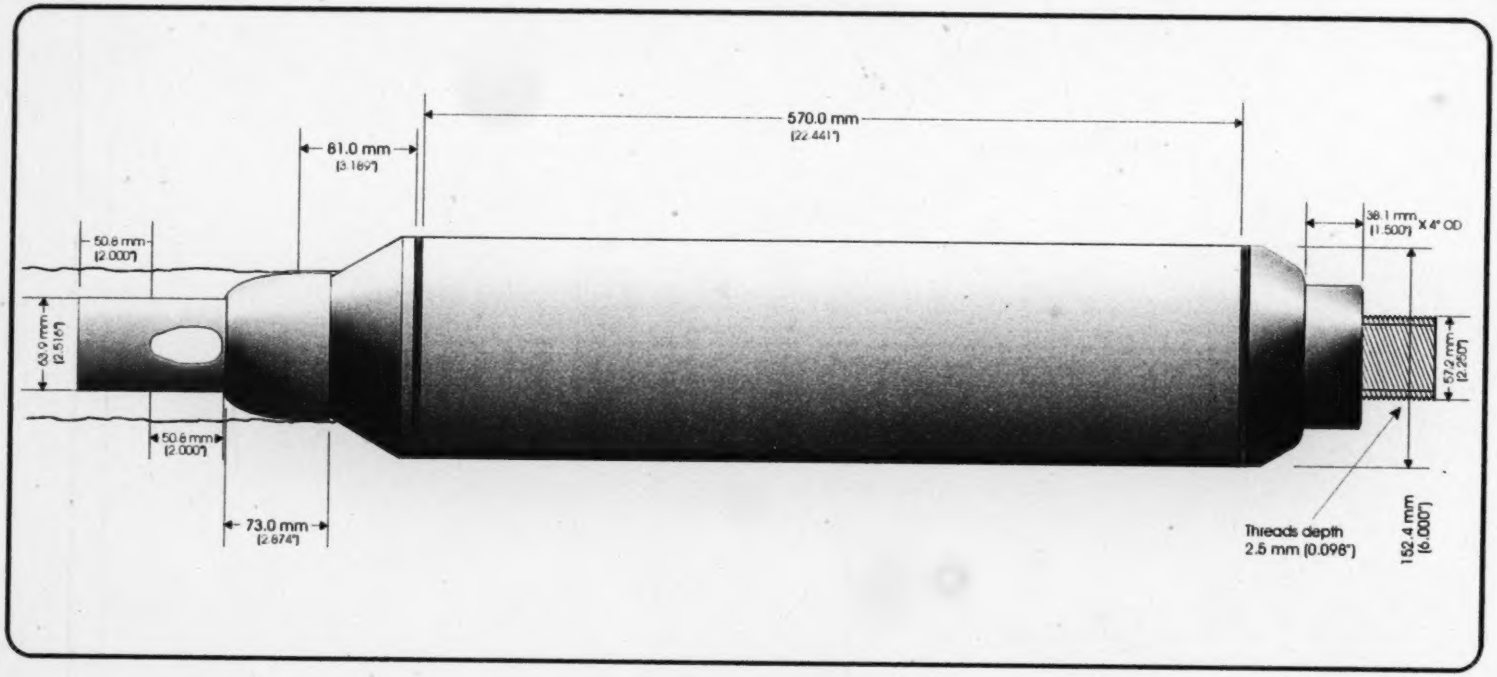
570.0 mm [22.441"]
81.0 mm [3.169"]
50.8 mm [2.000"]
63.9 mm [2.516"]
50.8 mm [2.000"]
73.0 mm [2.874"]
38.1 mm [1.500"] X 4" OD
57.2 mm [2.250"]
152.4 mm [6.000"]
Threads depth
2.5 mm [0.098"]

**HD-PB-CPT**

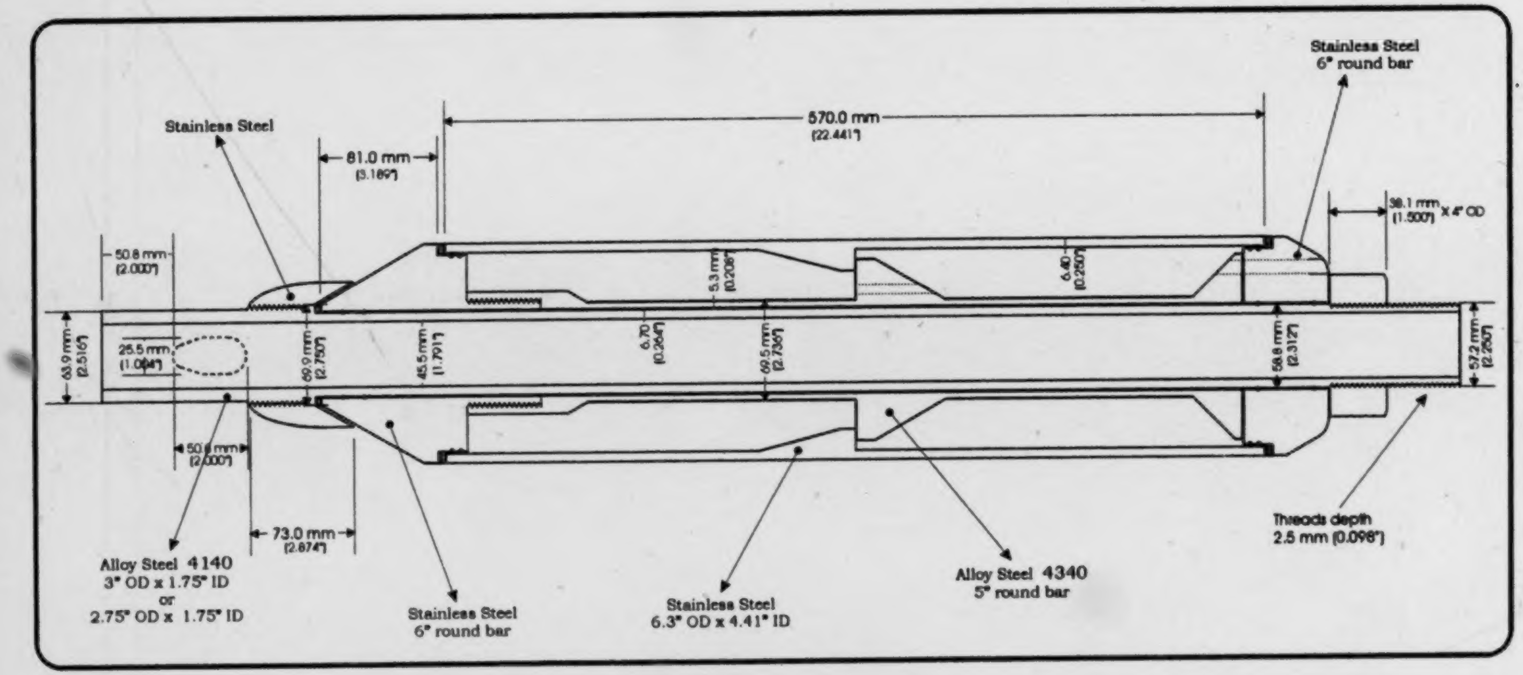
Stainless Steel
81.0 mm (3.189")
570.0 mm (22.441")
Stainless Steel 6" round bar
38.1 mm (1.500") X 4" OD
50.8 mm (2.000")
5.3 mm (0.208")
6.40 (0.250")
63.9 mm (2.516")
25.5 mm (1.004")
69.9 mm (2.750")
45.5 mm (1.791")
6.70 (0.264")
69.5 mm (2.736")
58.8 mm (2.312")
57.2 mm (2.250")
50.8 mm (2.000")
73.0 mm (2.874")
Alloy Steel 4140 3" OD x 1.75" ID or 2.75" OD x 1.75" ID
Stainless Steel 6" round bar
Stainless Steel 6.3" OD x 4.41" ID
Alloy Steel 4340 5" round bar
Threads depth 2.5 mm (0.098")

**HD-PB-CPT INSIDE VIEW**

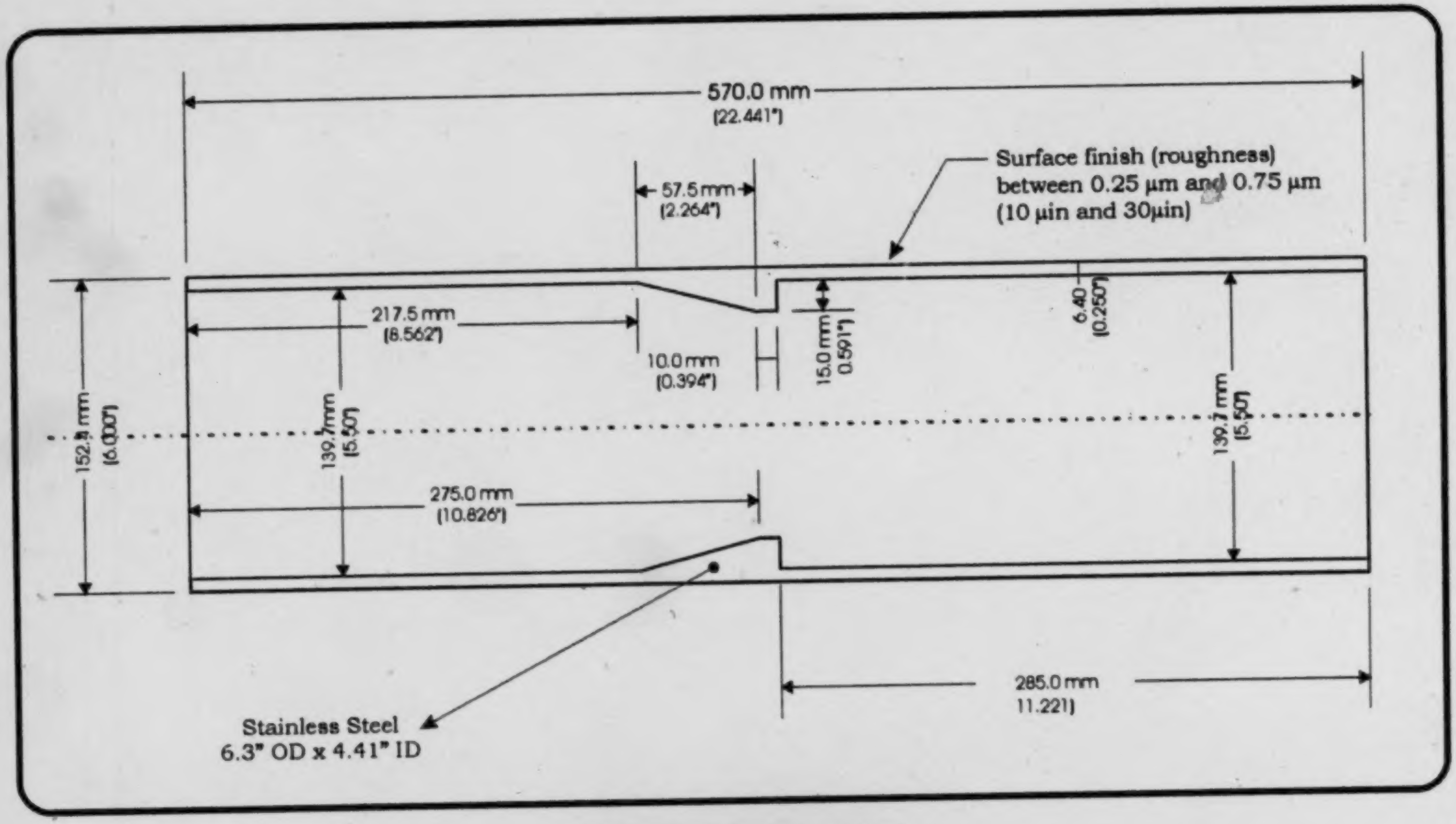
570.0 mm
(22.441")
Surface finish (roughness)
between 0.25 µm and 0.75 µm
(10 µin and 30µin)
57.5 mm
(2.264")
217.5 mm
(8.562")
10.0 mm
(0.394")
15.0 mm
0.591")
6.40
(0.250")
152.4 mm
(6.000")
139.7 mm
(5.50")
275.0 mm
(10.826")
139.7 mm
(5.50")
285.0 mm
11.221)
Stainless Steel
6.3" OD x 4.41" ID

FRICTION SLEEVE

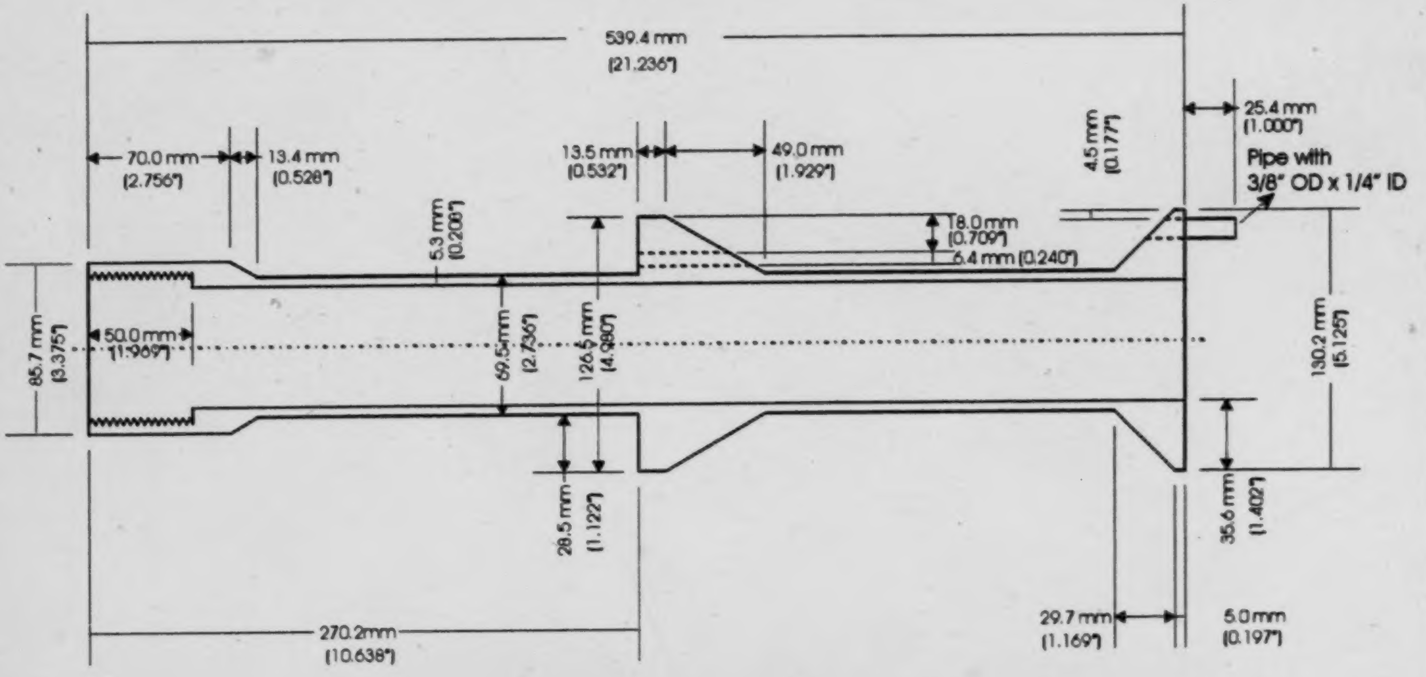
539.4 mm
(21.236")
25.4 mm
(1.000")
Pipe with
3/8" OD x 1/4" ID
70.0 mm
(2.756")
13.4 mm
(0.528")
13.5 mm
(0.532")
49.0 mm
(1.929")
4.5 mm
(0.177")
18.0 mm
(0.709")
6.4 mm (0.240")
5.3 mm
(0.208")
85.7 mm
(3.375")
50.0 mm
(1.969")
69.5 mm
(2.736")
126.5 mm
(4.980")
130.2 mm
(5.125")
28.5 mm
(1.122")
35.6 mm
(1.402")
270.2 mm
(10.638")
29.7 mm
(1.169")
5.0 mm
(0.197")

SUBTRACTIVE TYPE LOAD CELL

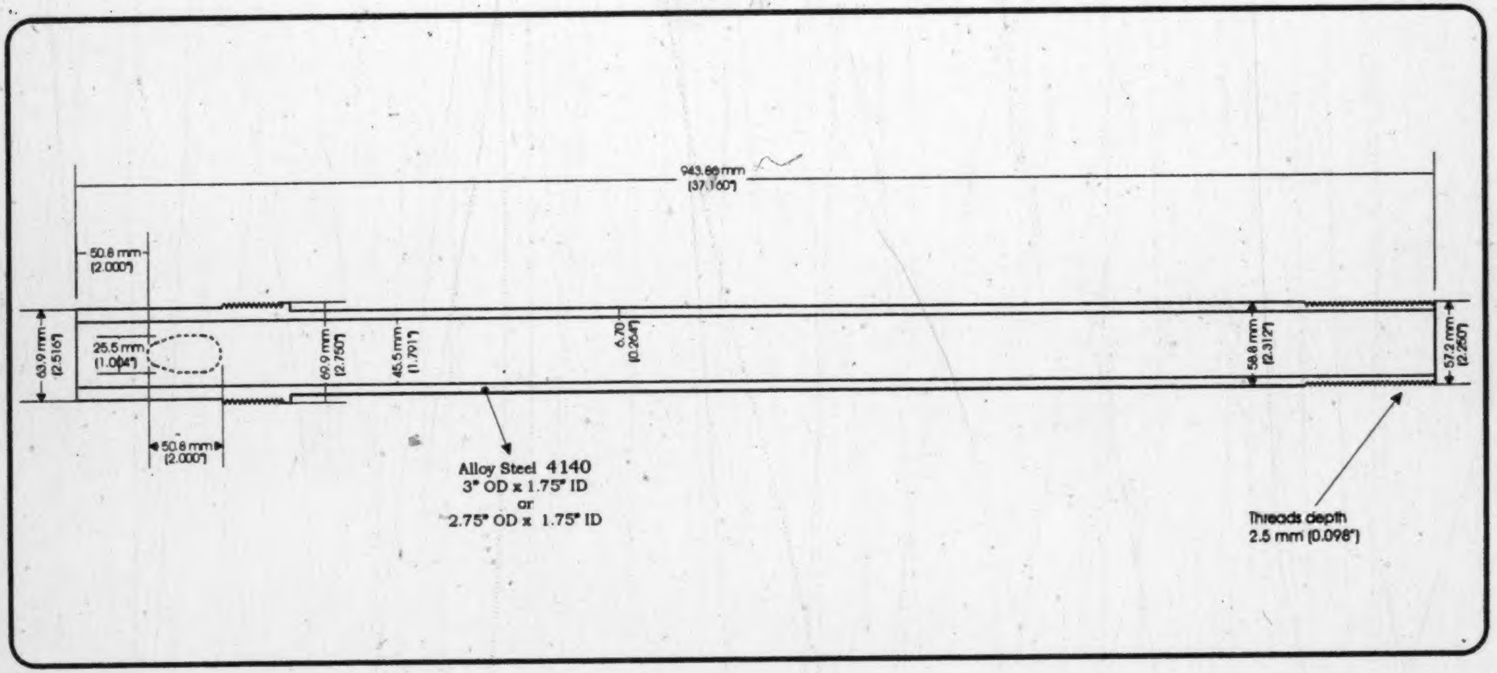
943.86 mm
(37.160")
50.8 mm
(2.000")
63.9 mm
(2.516")
25.5 mm
(1.004")
50.8 mm
(2.000")
69.9 mm
(2.750")
45.5 mm
(1.791")
6.70
(0.264")
58.8 mm
(2.312")
57.2 mm
(2.250")
Alloy Steel 4140
3" OD x 1.75" ID
or
2.75" OD x 1.75" ID
Threads depth
2.5 mm (0.098")

INTERNAL SHAFT

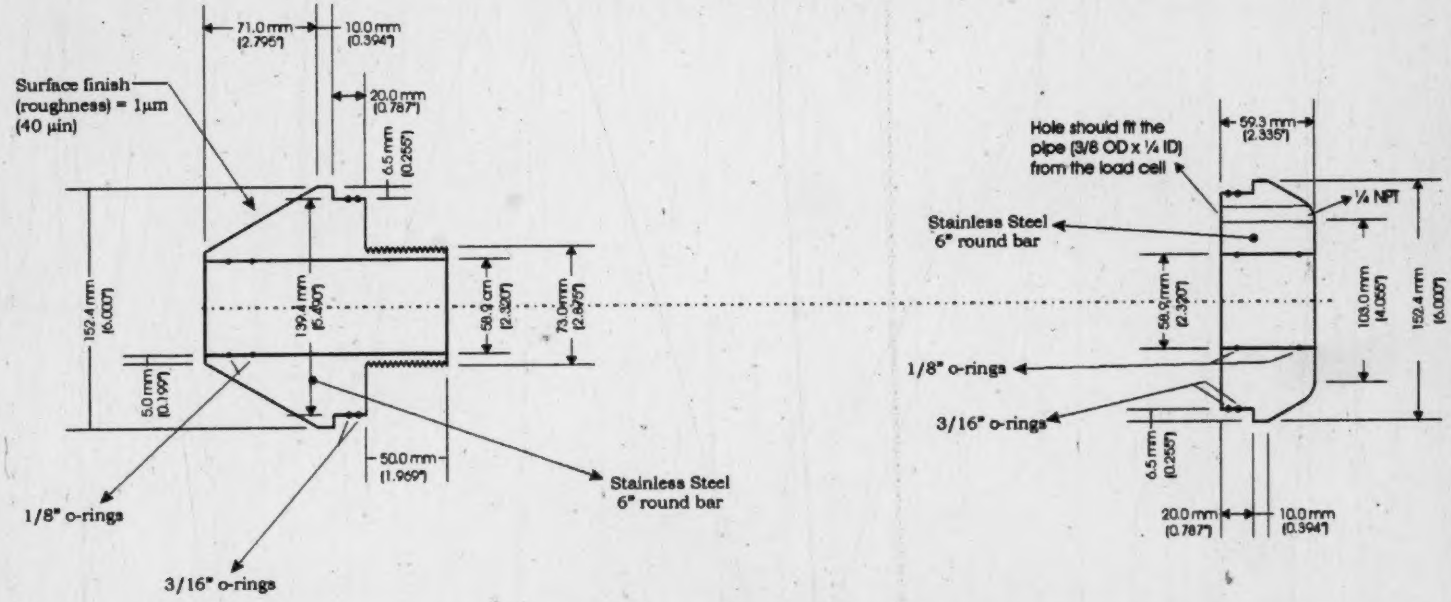
71.0 mm (2.795")
10.0 mm (0.394")
20.0 mm (0.787")
6.5 mm (0.256")
Surface finish (roughness) = 1μm (40 μin)
152.4 mm (6.000")
5.0 mm (0.197")
139.4 mm (5.490")
58.9 cm (2.320")
73.0 mm (2.875")
50.0 mm (1.969")
1/8" o-rings
3/16" o-rings
Stainless Steel 6" round bar
Hole should fit the pipe (3/8 OD x ¼ ID) from the load cell
59.3 mm (2.335")
¼ NPT
Stainless Steel 6" round bar
58.9 mm (2.320")
103.0 mm (4.055")
152.4 mm (6.000")
1/8" o-rings
3/16" o-rings
6.5 mm (0.256")
20.0 mm (0.787")
10.0 mm (0.394")

CONE TIP AND TAIL

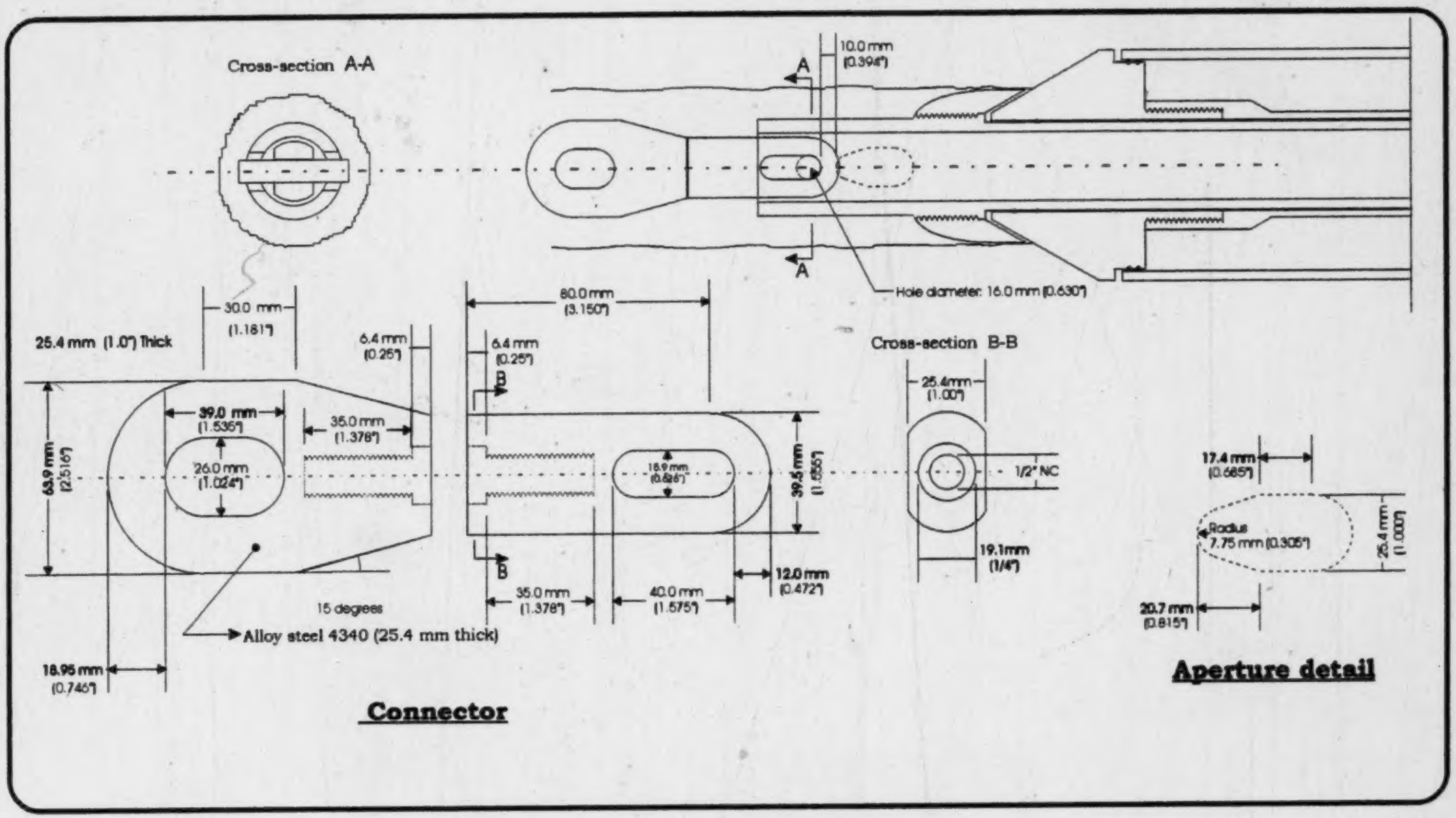
Cross-section A-A
A
A
10.0 mm
(0.394")
Hole diameter: 16.0 mm (0.630")
30.0 mm
(1.181")
25.4 mm (1.0") Thick
6.4 mm
(0.25")
80.0 mm
(3.150")
6.4 mm
(0.25")
B
B
39.0 mm
(1.536")
35.0 mm
(1.378")
26.0 mm
(1.024")
63.9 mm
(2.516")
18.9 mm
(0.626")
39.5 mm
(1.555")
15 degrees
Alloy steel 4340 (25.4 mm thick)
35.0 mm
(1.378")
40.0 mm
(1.575")
12.0 mm
(0.472")
18.95 mm
(0.746")
Connector
Cross-section B-B
25.4mm
(1.00")
1/2" NC
19.1mm
(1/4")
17.4 mm
(0.685")
Radius
7.75 mm (0.305")
25.4 mm
(1.000")
20.7 mm
(0.815")
Aperture detail

## CONNECTION SYSTEM

# APPENDIX 4

## HD-PB-RCPT DRAWINGS

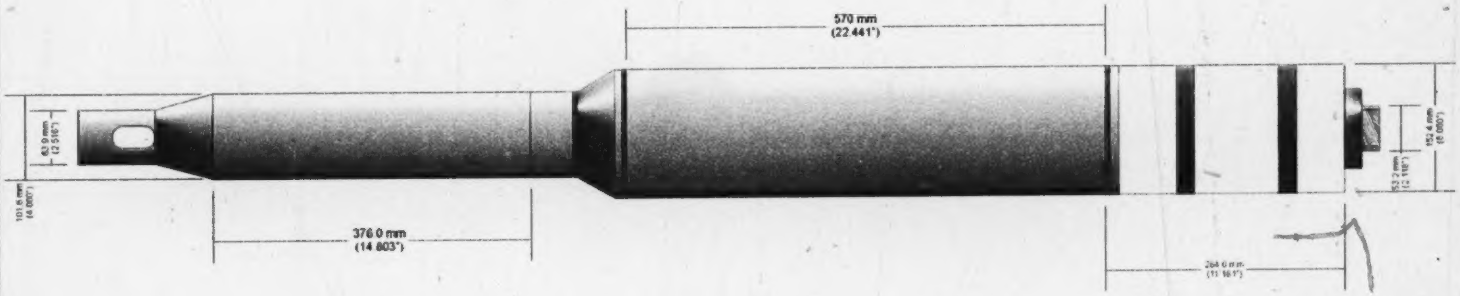
570 mm
(22.441")
376.0 mm
(14.803")
284.0 mm
(11.181")
63.9 mm
(2.516")
101.6 mm
(4.000")
53.2 mm
(2.118")
152.4 mm
(6.000")

**HD-PB-RCPT (60° CONE)**

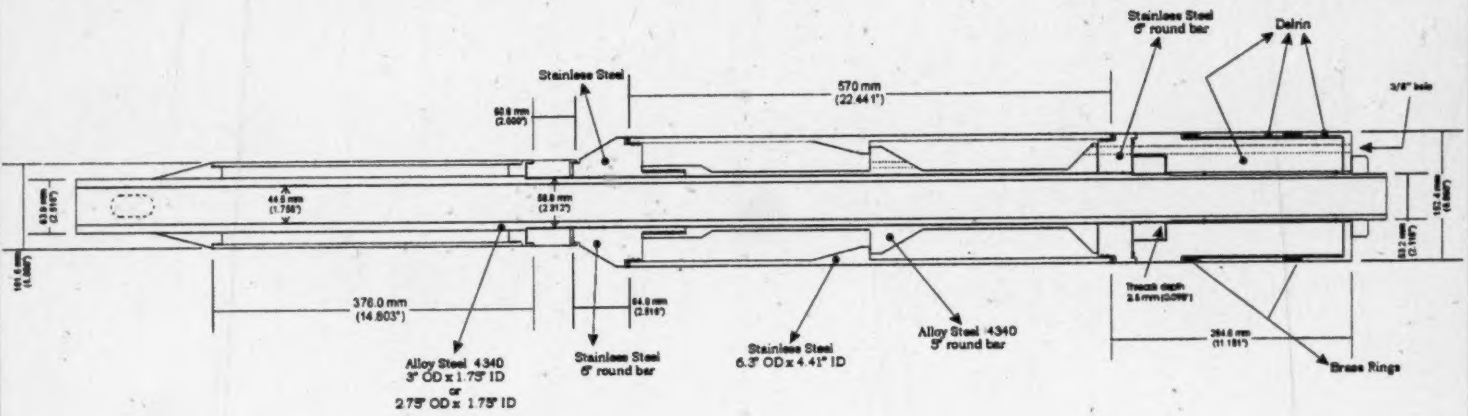
Stainless Steel
6" round bar
Delrin
3/8" hole
Stainless Steel
570 mm
(22.441")
50.8 mm
(2.000")
63.9 mm
(2.515")
44.5 mm
(1.750")
58.8 mm
(2.312")
101.6 mm
(4.000")
152.4 mm
(6.000")
53.7 mm
(2.115")
376.0 mm
(14.803")
64.0 mm
(2.519")
Track depth
2.5 mm (0.098")
284.0 mm
(11.181")
Alloy Steel 4340
3" OD x 1.75" ID
or
2.75" OD x 1.75" ID
Stainless Steel
6" round bar
Stainless Steel
6.3" OD x 4.41" ID
Alloy Steel 4340
5" round bar
Brass Rings

**HD-PB-RCPT INSIDE VIEW (60° CONE)**

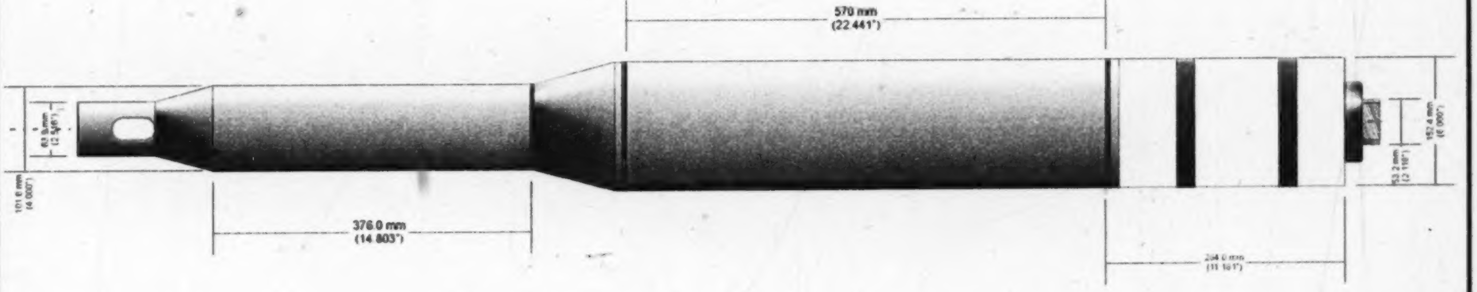
570 mm
(22.441")
376.0 mm
(14.803")
284.0 mm
(11.181")
101.6 mm
(4.000")
63.5 mm
(2.500")
152.4 mm
(6.000")
53.2 mm
(2.118")

HD-PB-RCPT (30° CONE)

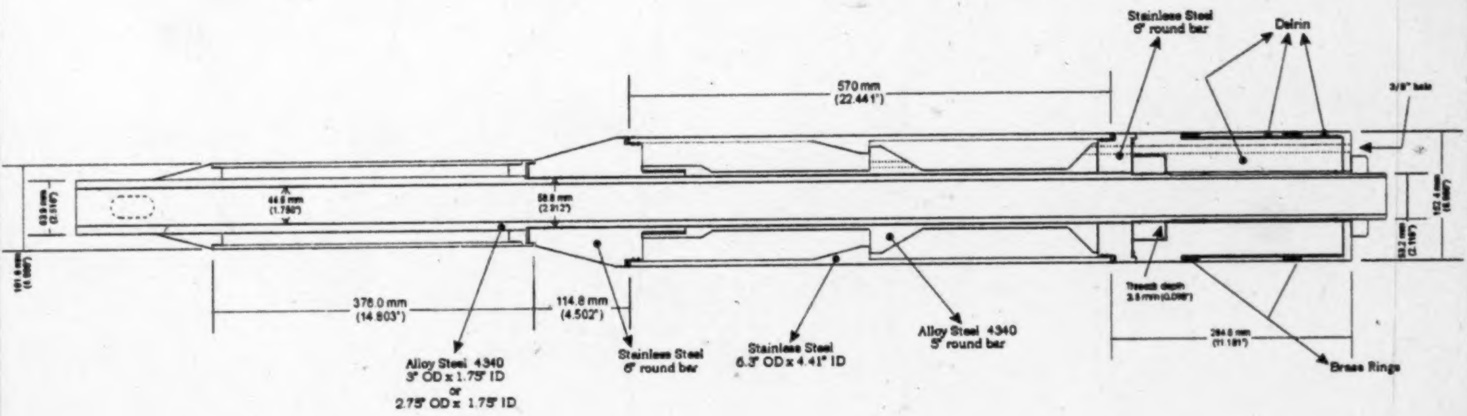

Stainless Steel 6" round bar
Delrin
3/8" hole
570 mm (22.441")
63.9 mm (2.515")
101.6 mm (4.000")
44.5 mm (1.750")
58.8 mm (2.312")
152.4 mm (6.000")
53.2 mm (2.114")
Trench depth 3.8 mm (0.098")
376.0 mm (14.803")
114.8 mm (4.502")
284.0 mm (11.181")
Alloy Steel 4340 3" OD x 1.75" ID or 2.75" OD x 1.75" ID
Stainless Steel 6" round bar
Stainless Steel 6.3" OD x 4.41" ID
Alloy Steel 4340 5" round bar
Brass Rings

## HD-PB-RCPT INSIDE VIEW (30° CONE)

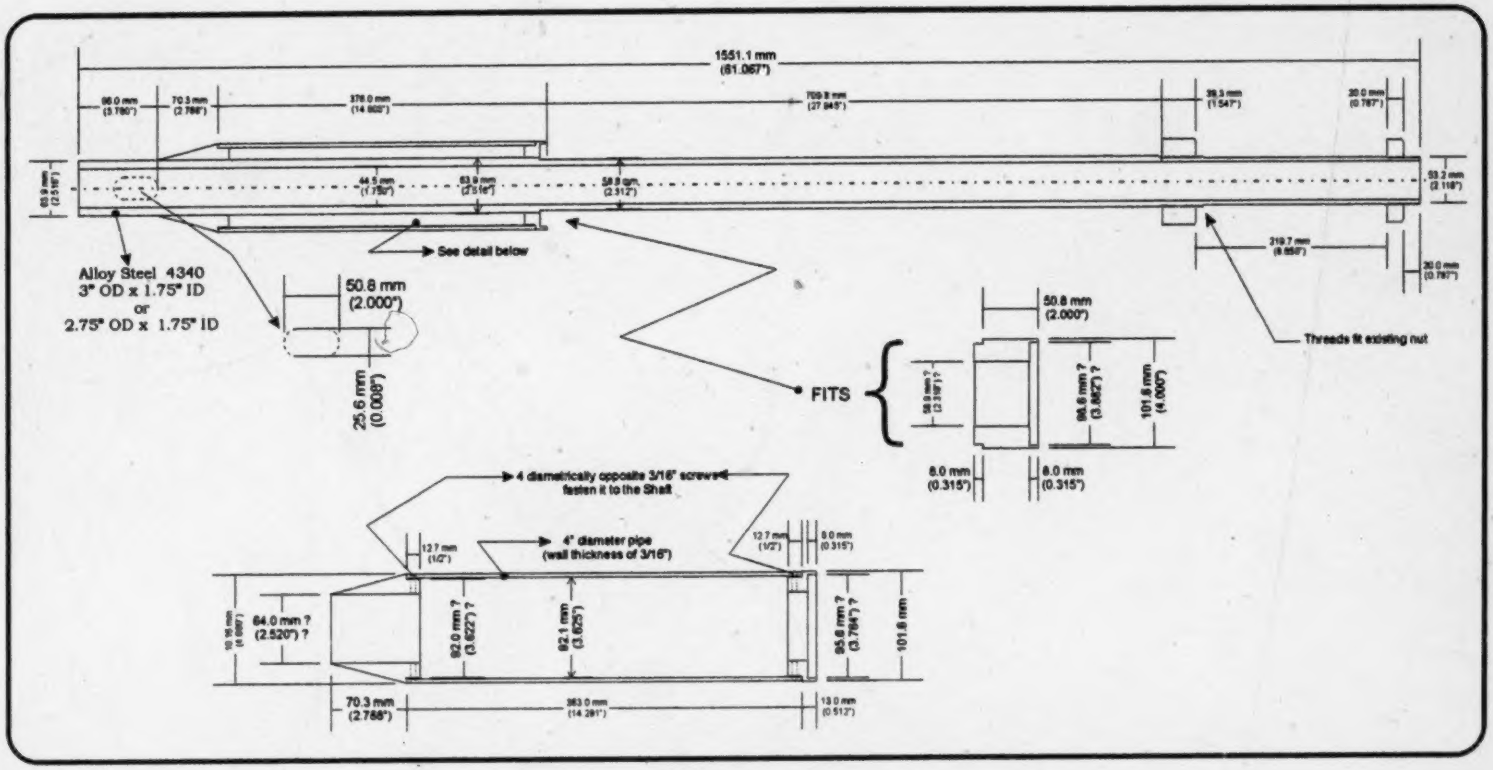
1551.1 mm (61.067")
96.0 mm (3.780")
70.3 mm (2.768")
376.0 mm (14.803")
709.8 mm (27.945")
39.3 mm (1.547")
20.0 mm (0.787")
63.9 mm (2.516")
44.5 mm (1.750")
63.9 mm (2.516")
58.8 mm (2.312")
53.2 mm (2.118")
219.7 mm (8.650")
20.0 mm (0.787")
See detail below
Threads fit existing nut
Alloy Steel 4340
3" OD x 1.75" ID
or
2.75" OD x 1.75" ID
50.8 mm (2.000")
25.6 mm (0.008")
FITS
50.8 mm (2.000")
58.9 mm ? (2.319") ?
98.6 mm ? (3.882") ?
101.6 mm (4.000")
8.0 mm (0.315")
8.0 mm (0.315")
4 diametrically opposite 3/16" screws fasten it to the Shaft
4" diameter pipe (wall thickness of 3/16")
12.7 mm (1/2")
12.7 mm (1/2")
8.0 mm (0.315")
10.16 mm (4.000")
64.0 mm ? (2.520") ?
92.0 mm ? (3.622") ?
92.1 mm (3.625")
95.6 mm ? (3.764") ?
101.6 mm
70.3 mm (2.768")
363.0 mm (14.291")
13.0 mm (0.512")

# HD-PB-RCPT INTERNAL SHAFT

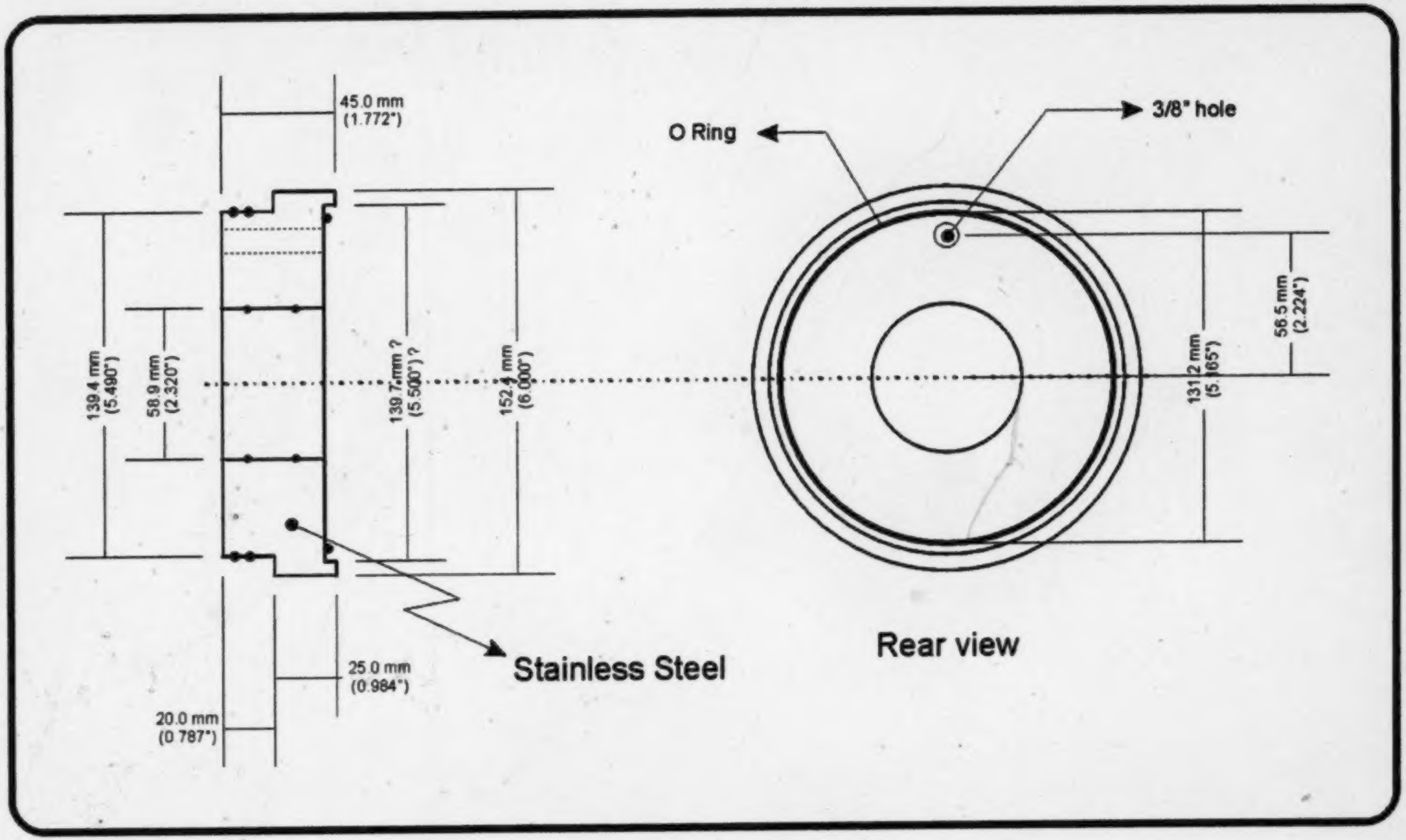
45.0 mm
(1.772")
O Ring
3/8" hole
139.4 mm
(5.490")
58.9 mm
(2.320")
139.7 mm ?
(5.500") ?
152.4 mm
(6.000")
131.2 mm
(5.165")
56.5 mm
(2.224")
25.0 mm
(0.984")
20.0 mm
(0.787")
Stainless Steel
Rear view

**HD-PB-RCPT (TAIL)**

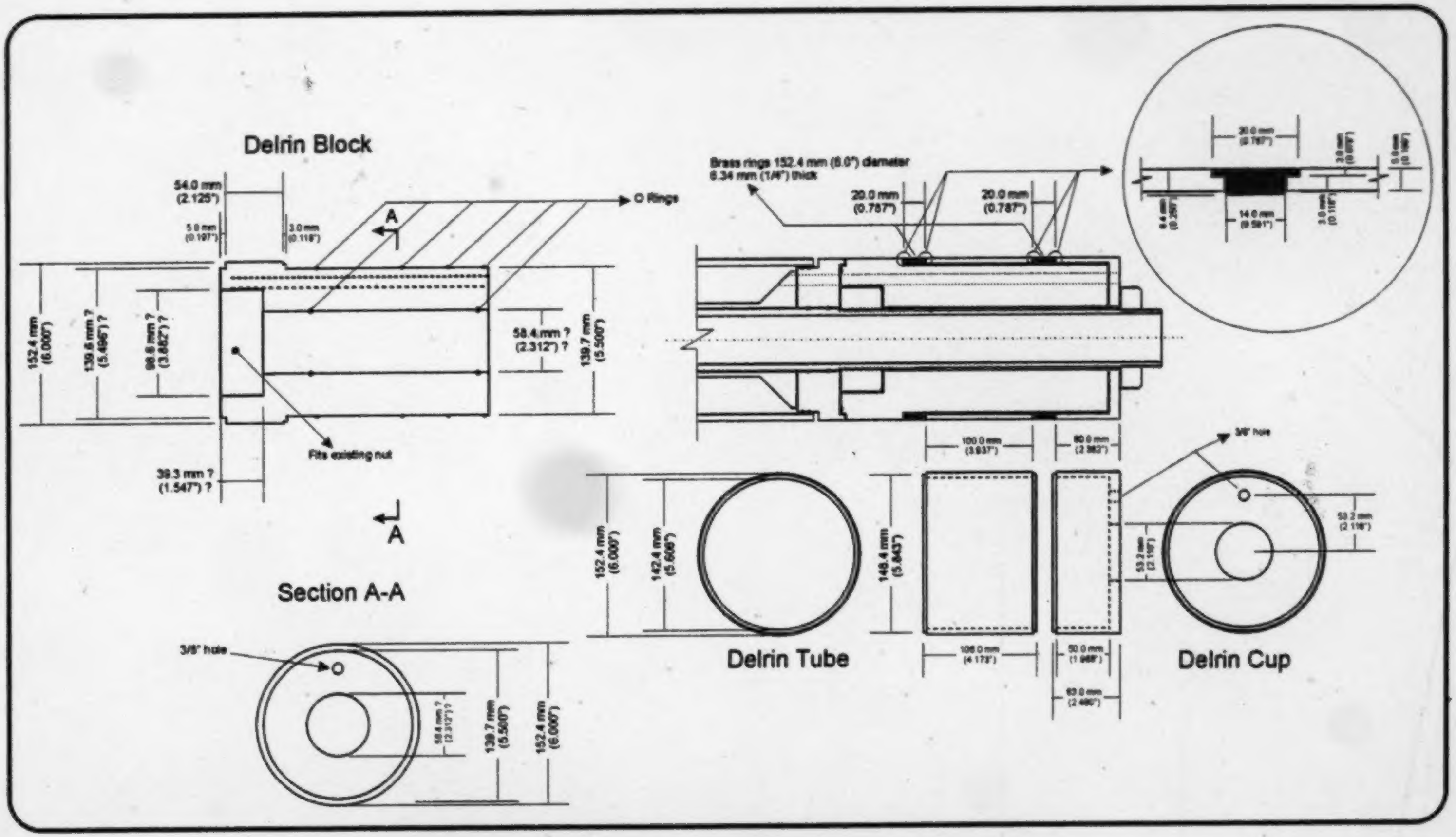
Delrin Block
54.0 mm (2.125")
5.0 mm (0.197")
3.0 mm (0.118")
A
O Rings
152.4 mm (6.000")
139.6 mm ? (5.496") ?
98.6 mm ? (3.882") ?
58.4 mm ? (2.312") ?
139.7 mm (5.500")
Fits existing nut
39.3 mm ? (1.547") ?
A
Section A-A
3/8" hole
58.4 mm ? (2.312") ?
139.7 mm (5.500")
152.4 mm (6.000")
Brass rings 152.4 mm (6.0") diameter 6.34 mm (1/4") thick
20.0 mm (0.787")
20.0 mm (0.787")
20.0 mm (0.787")
14.0 mm (0.551")
6.4 mm (0.250")
3.0 mm (0.118")
2.0 mm (0.079")
5.0 mm (0.197")
100.0 mm (3.937")
60.0 mm (2.362")
3/8" hole
152.4 mm (6.000")
142.4 mm (5.606")
148.4 mm (5.843")
53.2 mm (2.116")
53.2 mm (2.116")
Delrin Tube
106.0 mm (4.173")
50.0 mm (1.968")
63.0 mm (2.480")
Delrin Cup

**ELECTRICAL RESISTIVITY MODULE**

# APPENDIX 5

## EQUATIONS DEVELOPMENT

- Van Wieriengen 1982 – Relating cone resistance and pressuremeter test results.

$$q_c \pi r^2 V_1 = S_u 2\pi r^2 V_2 + S_u \pi r^2 \frac{\pi}{3} V_3 + p_l^* 4\pi r^2 V_4 \qquad [9.4]$$

where:

$V_1 \cos 60^\circ = V_3$

$V_1 \cos 30^\circ = V_2$

$V_3 = V_4$

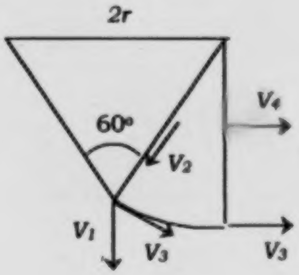
2r
$V_4$
60°
$V_2$
$V_1$
$V_3$
$V_3$

Therefore:

$$V_4 = V_3 = \frac{V_1}{2}$$

$$V_2 = \frac{\sqrt{3}}{2} V_1$$

Combining the Equation of $V_2$, $V_3$ and $V_4$, as well as Eq. [9.5] and [9.6] in Eq. [9.4]:

Brings to Eq. [9.7] ⟶ $q_c = 3p_l$

- For the pre-bored cone penetration test

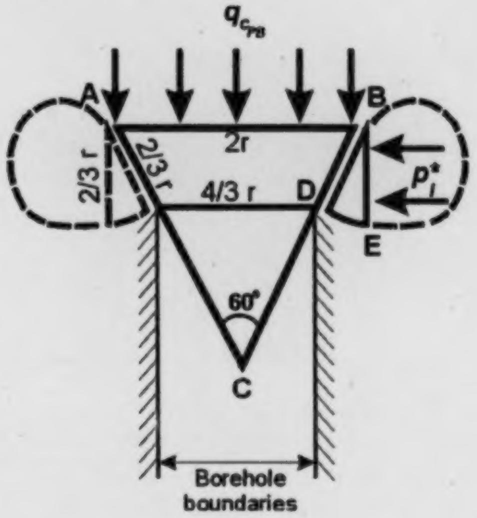
$q_{c_{PB}}$
A
B
2r
2/3 r
2/3 r
4/3 r
D
$p_l^*$
E
60°
C
Borehole boundaries

Area BD:

$$A_{BD} = \pi(\frac{1}{2}\frac{4}{3}r + \frac{1}{2}2r)\frac{2}{3}r$$

$$A_{BD} \quad A = \frac{1}{2} \quad A_{BD} = \frac{10}{9}\pi r^2$$

Area DE:

$$A_{DE} = \pi(\frac{1}{2}\frac{4}{3}r + \frac{1}{2}2r)\frac{2}{3}r\frac{\pi}{6}$$

$$A_{DE} = \frac{5}{9}\pi r^2 \frac{\pi}{3}$$

Area BE:

$$A_{BE} = 2\pi r\frac{2}{3}r$$

$$A_{BE} = 2\pi r\frac{2}{3}r$$

$$A_{BE} = \frac{4}{3}\pi r^2$$

The balance of rate of energy will be:

$$q_{c_{PB}}\pi r^2 V_1 = S_u \frac{10}{9}\pi r^2 V_2 + S_u \frac{5}{9}\pi r^2 \frac{\pi}{3} V_3 + p_l^{*} \frac{4}{3}\pi r^2 V_4 \qquad [9.8]$$

By combining Equation 9.8, 9.9 and 9.10 and substituing $V_2$, $V_3$ and $V_4$

Brings to Eq [9.11] ⟶ $q_{c_{PB}} = 1.06\,p_l$